

**Integrated Process Modeling and Data Analytics for Optimizing Polyolefin
Manufacturing**

Niket Sharma

Dissertation submitted to the faculty of the Virginia Polytechnic Institute and State
University in partial fulfillment of the requirements for the degree of

Doctor of Philosophy
In
Chemical Engineering

Y.A. Liu, Chair
Donald G. Baird
Richey M. Davis
Hongliang Xin

Oct 26, 2021
Blacksburg, Virginia

Keywords: polyolefins, polymers, process modeling, machine learning, data analytics,
hybrid machine learning, science-guided machine learning

Integrated Process Modeling and Data Analytics for Optimizing Polyolefin Manufacturing

Niket Sharma

ABSTRACT

Polyolefins are one of the most widely used commodity polymers with applications in films, packaging and automotive industry. The modeling of polymerization processes producing polyolefins, including high-density polyethylene (HDPE), polypropylene (PP), and linear low-density polyethylene (LLDPE) using Ziegler-Natta catalysts with multiple active sites, is a complex and challenging task. In our study, we integrate process modeling and data analytics for improving and optimizing polyolefin manufacturing processes.

Most of the current literature on polyolefin modeling does not consider all of the commercially important production targets when quantifying the relevant polymerization reactions and their kinetic parameters based on measurable plant data. We develop an effective methodology to estimate kinetic parameters that have the most significant impacts on specific production targets, and to develop the kinetics using all commercially important production targets validated over industrial polyolefin processes. We showcase the utility of dynamic models for efficient grade transition in polyolefin processes. We also use the dynamic models for inferential control of polymer processes. Thus, we showcase the methodology for making first-principle polyolefin process models which are scientifically consistent, but tend to be less accurate due to many modeling assumptions in a complex system.

Data analytics and machine learning (ML) have been applied in the chemical process industry for accurate predictions for data-based soft sensors and process monitoring/control. Specifically, for polymer processes, they are very useful since the polymer quality measurements like polymer melt index, molecular weight etc. are usually less frequent compared to the continuous process variable measurements. We showcase the use of predictive machine learning models like neural networks for predicting polymer quality indicators and demonstrate the utility of causal models like partial least squares to study the causal effect of the process parameters on the polymer quality variables. ML models produce accurate results can over-fit the data and also produce scientifically inconsistent results beyond the operating data range. Thus, it is growingly important to develop hybrid models combining data-based ML models and first-principle models.

We present a broad perspective of hybrid process modeling and optimization combining the scientific knowledge and data analytics in bioprocessing and chemical engineering with a science-guided machine learning (SGML) approach and not just the direct combinations of first-principle and ML models. We present a detailed review of scientific literature relating to the hybrid SGML approach, and propose a systematic classification of hybrid SGML models according to their methodology and objective. We identify the themes and methodologies which have not been explored much in chemical engineering applications, like the use of scientific knowledge to help improve the ML model architecture and learning process for more scientifically consistent solutions. We apply these hybrid SGML techniques to industrial polyolefin processes such as inverse modeling, science guided loss and many others which have not been applied previously to such polymer applications.

**Integrated Process Modeling and Data Analytics for Optimizing Polyolefin
Manufacturing**
Niket Sharma

GENERAL AUDIENCE ABSTRACT

Almost everything we see around us from furniture, electronics to bottles, cars, etc. are made fully or partially from plastic polymers. The two most popular polymers which comprise almost two-thirds of polymer production globally are polyethylene (PE) and polypropylene (PP), collectively known as polyolefins. Hence, the optimization of polyolefin manufacturing processes with the aid of simulation models is critical and profitable for chemical industry. Modeling of a chemical/polymer process is helpful for process-scale up, product quality estimation/monitoring and new process development. For making a good simulation model, we need to validate the predictions with actual industrial data.

Polyolefin process has complex reaction kinetics with multiple parameters that need to be estimated to accurately match the industrial process. We have developed a novel strategy for estimating the kinetics for the model, including the reaction chemistry and the polymer quality information validating with industrial process. Thus, we have developed a science-based model which includes the knowledge of reaction kinetics, thermodynamics, heat and mass balance for the polyolefin process. The science-based model is scientifically consistent, but may not be very accurate due to many model assumptions. Therefore, for applications requiring very high accuracy predicting any polymer quality targets such as melt index (MI), density, data-based techniques might be more appropriate.

Recently, we may have heard a lot about artificial intelligence (AI) and machine learning (ML) the basic principle behind these methods is to making the model learn from data for prediction. The process data that are measured in a chemical/polymer plant can be utilized for data analysis. We can build ML models to predict polymer targets like MI as a function of the input process variables. The ML model predictions are very accurate in the process operating range of the dataset on which the model is learned, but outside the prediction range, they may tend to give scientifically inconsistent results. Thus, there is a need to combine the data-based models and scientific models.

In our research, we showcase novel approaches to integrate the science-based models and the data-based ML methodology which we term as the hybrid science-guided machine learning methods (SGML). The hybrid SGML methods applied to polyolefin processes yield not only accurate, but scientifically consistent predictions which can be used for polyolefin process optimization for applications like process development and quality monitoring.

Dedication

I dedicate my PhD dissertation to my parents, mother, Mrs. Rekha Sharma and father, Mr. Raj Kumar Sharma without their love and support this would not have been possible.

Acknowledgement

I would like to express my heartfelt gratitude to my PhD advisor, Prof. Y.A. Liu for his guidance throughout my PhD journey. I am obliged that he gave me this opportunity to pursue research and shared his technical knowledge, writing skills and professional engagement in the last four years of my studies. His guidance made me industry ready.

Besides my advisor I would like to express my sincerest appreciation my entire PhD committee: Prof. Richey M. Davis, Prof. Donald Baird and Prof. Hongliang Xin for their help, guidance, support and availability throughout this journey. I am also grateful to Aspen Technology and PetroChina for supporting the Center of Excellence in Process System Engineering at Virginia Tech.

In this section I would like to acknowledge those who played a key role in helping me develop a suitable profile as a preferred PhD candidate at Virginia Tech. First and foremost, I would like to thank Prof. Sanjeev Kumar Gupta, Indian Institute of Science, Bangalore ,my master's thesis advisor. He introduced me to research arena and also gave a recommendation for pursuing doctoral studies. I want to thank Prof. Ashwini Sood, HBTI Kanpur, for his recommendation and guidance. I am indebted to my colleagues and managers at SABIC for their guidance, especially, Mr. Samir Anapat, Chief Scientist SABIC, for sharing his expertise in process modeling. I would like to thank all my teammates at SABIC especially Dr. Tukaram Gunale and Dr. Prashant Kumar for their recommendations.

My PhD journey would not have been successful without the support from these members at Virginia Tech. I would like to thank Mr. David Tremblay Senior Director, Aspen Tech for sharing his knowledge and expertise on polymer simulation. Our lab is grateful for support and collaboration with Aspen Technology, Inc, especially, Mr. Antonio Pietri, CEO of AspenTech and Mr. Willie K. Chan, Chief Technology Officer. I would like to thank Mr. Brendan Mcsheehy, VP Innovation at Universal Fibers, for providing me an opportunity to learn about fiber processing industry. I thank Dr. Jay Yun, CEO of Simacro, for the collaboration on polymer process modeling. I thank Dr. Chris McDowell, Head of Operations Novozymes, for the collaboration. I thank Dr. Kevin Seavey, Automation leader Dow, for sharing his process control expertise and recommendation. I want to thank all Professors at Department of Chemical Engineering and Computer Science at Virginia Tech for all their guidance and the knowledge they have shared through the courses taught and otherwise. I want to thank all the administrative staff at Virginia Tech especially Ms. Dianne Cannady for her administrative support all these years. I thank all my lab-mates over the years, especially Youngju Lee and Adam McNeeley for their collaboration and technical discussions.

I dedicate my dissertation to my parents. I also want to thank rest of my family members, especially my sister, Dr. Nivedita Sharma, who has guided me personally and professionally and has advised me in all major decisions of my life. I want to thank my brother-in-law Dr. Rahul Sheel for his insights and support. I thank all my friends and colleagues at the Department of Chemical Engineering Virginia Tech namely Vikas Parakh, Hemanth Pillai, Dr. Mimosa Sarma and many others for their support. I also want to acknowledge rest of my friends and colleagues from my previous school, college, work for their encouragement.

In the end I would like to thank all my well-wishers whom I have missed here, who has played a role in my life to help me achieve this feat of completing my doctorate.

Original Contribution

1. First-Principle Steady-State and Dynamic Model of Polyolefin Processes

- We demonstrate a general and effective methodology for estimating kinetic parameters for Ziegler-Natta polymerization for commercial processes producing polyolefins, such as HDPE, PP and LLPDE.
- Use all commercially important production targets for prediction to simultaneously estimate multiple reaction rate constants for Ziegler-Natta kinetics to match several data sets of production targets which differentiates from the previous sequential estimation approach in the literature.
- Our methodology also greatly simplifies the kinetic parameter estimation for the multisite model, in that we only need to regress selected kinetic parameters for the multisite model.
- Showcase the application of dynamic polyolefin models in simulating plant data and illustrate the advantages and limitations of first-principle polyolefin process models.

2. Application of Machine Learning and Multivariate Statistics for Polymer/Polyolefin Process Data Analytics

- Improve Melt Index prediction of the industrial HDPE process than in the literature.
- Comparison of casual multivariate statistical models and predictive machine learning models for quality prediction in industrial polyolefin processes.
- Showcase the application of semi-supervised learning machine learning methods like self-training and generating models to improve prediction for industrial polyolefin processes.
- Application of data analytics and anomaly detection for extrusion process monitoring in industrial textile manufacturing process.
- Showcase the advantages and limitations of application of machine learning in polymer/polyolefin process data analytics by pointing out the scientific inconsistency of predictions beyond operating range.

3. Hybrid Science-Guided Machine Learning Approach for Modeling and Optimizing Chemical and Polymer Processes

- Presentation of a broader hybrid SGML methodology of integrating science-guided and data-based models, and not just the direct combinations of first-principle and ML models.
- Classification of the hybrid model applications according to their methodology and objectives, instead of their areas of applications.

- Identification of the themes and methodologies which have not been explored much in chemical engineering applications, like the use of scientific knowledge to help improve the ML model architecture and learning process for more scientifically consistent solutions.
- Illustrations of the use of these hybrid SGML methodologies applied to industrial polymer processes, such as inverse modeling, and science-guided loss which have not been applied previously in such applications.

Outline of the thesis

The contents of this dissertation are as follows. Chapter 1, covers the introduction and motivation for the research. Chapter 2 deals with first-principle steady-state modeling of polyolefin processes mainly using Ziegler Natta as catalyst. In this chapter, we present an effective methodology for estimating the kinetic parameters based on plant data in the development of simulation and optimization models for commercial polyolefin processes using efficient software tools.

Chapter 3 is about first-principle of dynamic modeling of polyolefin processes. In this chapter, we have showcased the use of dynamic models and efficient grade transition strategies for polyolefin processes. We also showcase the use of first principle dynamic models to produce steady state results for predicting polymer quality and state their advantages and disadvantages for polymer quality predictions.

Chapter 4 deals with the application of machine learning and multivariate statistics for polymer process data analytics. In this chapter, we showcase the use of predictive Machine Learning models like Neural Networks, ensemble based regressors for predicting polymer quality indicators. We also demonstrate the utility of causal models like partial least squares to study the causal effect of the process parameters on the polymer quality variables. We make use of anomaly detection methods as well to identify the process outliers and also the reasons for their outlier behavior.

Chapter 5 reviews the hybrid science-guided machine learning approach for modeling and optimizing chemical processes. The objective of this paper is to present a comprehensive review and exposition of scientific and engineering literature relating to the hybrid SGML approach, and propose a systematic classification of hybrid SGML models focusing on both sciences complementing ML models, and ML complementing science-based models. Chapter 6 deals with the applications of the Hybrid SGML techniques for polymer process improvement by showcasing case studies of industrial polyolefin processes. Chapter 7 summarizes the conclusion of the research and future research directions. Appendix A consists of the steady state model details covered in Chapter 2. Appendix B have more details of dynamic process control details covered in Chapter 3.

Table of Contents

Abstract.....	ii
General Audience Abstract.....	iii
Dedication.....	iv
Acknowledgement.....	v
Original Contribution.....	vii
Outline of Thesis.....	ix
Table of Contents.....	x
List of Figures.....	xiv
List of Tables.....	xix

Chapter 1: Introduction and Motivation.....	1
References.....	4

Chapter 2: First Principle Steady-State Modeling of Polyolefin Process: Ziegler-Natta Polymerization	6
2.1. Introduction.....	6
2.2. Polyolefin Ziegler-Natta Polymerization Kinetics.....	7
2.2.1. Ziegler-Natta Catalysts	8
2.2.2. Ziegler-Natta Polymerization Kinetics	9
2.3. Commercial Polyolefin Production Targets.....	12
2.3.1 General Production Targets	12
2.3.1.1. Production Rate.....	12
2.3.1.2. MWN	13
2.3.1.3. MI.....	13
2.3.1.4. Conversion	13
2.3.1.5. PDI.....	13
2.3.1.6. SMWN and SPFRAC	13
2.3.1.7. SFRAC and SCB.....	13
2.3.1.8. Rho.....	13
2.3.1.9. Residence Time.....	14
2.3.2. Polymer-Specific Targets.....	14
2.3.2.1. CISFRAC.....	14
2.3.2.2. ATFRAC.....	14
2.4. Modeling Considerations.....	15
2.4.1. Reactor Types	15
2.4.2. Polymer Types	17
2.4.3. Molecular Weight Distribution	17
2.4.4. Process Flowsheets	18
2.4.5. Thermodynamics.....	20
2.4.6. Global Kinetics versus Local Kinetics.....	21

2.5. Methodology for Polyolefin Kinetic Estimation.....	21
2.5.1. Efficient Use of Software Tool: Data Fit.....	22
2.5.2. Flowchart of the Methodology for Kinetic Parameter Est.....	23
2.5.2.1. Multiple Product Grades and Single Active Catalyst Sites	24
2.5.2.2. Multisite Model and Deconvolution Analysis	28
2.5.3. Efficient Use of Software Tool: Sensitivity Analysis.....	32
2.5.4. Efficient Use of Software Tool: Design Specification	36
2.5.5. Model Applications.....	37
2.6. Key Points in Modeling Some Industrial Polyolefin Process	38
2.6.1. Modeling Polymer Phase Equilibrium in Slurry HDPE Process	38
2.6.2. Modeling of Horizontal Stirred-Bed Gas-Phase Reactor for PP	39
2.6.3. Condensed Mode Modeling of UNIPOL LLDPE process	40
2.7. Metallocene Polymerization Modeling.....	42
2.8. Conclusion	43
References.....	45
Chapter 3: First-Principle Dynamic Modeling of Polyolefin Processes.....	48
3.1. Introduction.....	48
3.2. Polyolefin Grade Transition.....	48
3.3. Grade Change for Series Flow Slurry HDPE Process	49
3.4. Dynamic Simulation and Control of a Commercial Slurry HDPE Process Using H ₂ /C ₂ Ratio	53
3.5. Dynamic Simulation and Control of a Gas-Phase Fluidized-Bed Process for Producing LLPDE in Condensed Mode Operation	55
3.6. Dynamic Simulation and Control of a Slurry HDPE Process Using an Inferential Controller	58
3.6.1 Objective	58
3.6.2 Inferential Control Theory and Recent Applications.....	58
3.6.3. HDPE Process Description and Steady-State Model Empirical	59
3.6.4. Grade Change Transition Using Basic H ₂ -Based Controller	61
3.6.5. Open-loop Inferential Controller Using Dynamic Model.....	61
3.6.6. Closed-Loop Inferential Controller.....	63
3.7. Using First Principle Dynamic models as polymer quality sensors	65
3.8. Conclusion	66
References.....	67
Chapter 4: Application of Machine Learning and Multivariate Statistics for Polymer Process Data Analytics	69
4.1. Introduction.....	69
4.2 An Overview of Relevant Machine Learning Concepts and Models	70

4.3. Literature on application of Data Analytics in Chemical and Polymer processes.	73
4.3.1 Literature on Application of Multivariate Statistics in Chemical Process Monitoring and Fault Diagnosis	73
4.3.2. Literature on Application of Machine Learning Models in Chemical.....	74
4.3.3. Literature on Application of Data Analytics/Machine Learning in Polymer ..	74
4.4 Illustrative Example of Machine Learning Applications in an Industrial Polyolefin Manufacturing Process	75
4.4.1. Multivariate Statistical Causal Model.....	78
4.4.2. Predictive Machine Learning Models.....	84
4.5. Disadvantages of Stand-alone Data-Based Models	88
4.6. Semi-supervised Learning for Polymer Process Data Analysis	89
4.6.1. Self-Training.....	89
4.6.2. Generative Model GAN.....	90
4.7. Batch Data Analysis.....	93
4.8. Industrial Case study of Extrusion Process Monitoring	96
4.9. Conclusion	98
References.....	98

Chapter 5: A Hybrid Science-Guided Machine Learning Approach for Modeling and Optimizing Chemical Processes: A Review.....	104
5.1. Introduction.....	104
5.2. Applications of Hybrid SGML Approach in Bioprocessing and Chemical Eng.	106
5.3. A Classification and Exposition of Hybrid SGML Models.....	108
5.4. ML Complements Science.....	109
5.4.1. Direct Hybrid Modeling.....	109
5.4.1.1. Parallel Direct Hybrid Model.....	109
5.4.1.2. Series Direct Hybrid Model.....	112
5.4.1.3. Serial-Parallel or Combined Direct Hybrid Model.....	113
5.4.2. Inverse Modeling	114
5.4.3. Reduced-Order Models.....	116
5.4.4. Hybrid SGML Modeling for Uncertainty Quantification.....	117
5.4.5. Hybrid HGML Modeling to Aid in Discovering Scientific Laws using ML ..	118
5.5. Science Compliments ML.....	119
5.5.1. Science-Guided Design.....	119
5.5.2. Science-Guided Learning.....	120
5.5.3. Science-Guided Refinement	121
5.6. Conclusion	122
References.....	125

Chapter 6: Application of Hybrid Science-Guided Machine Learning for Polymer Processes Improvement.....	135
6.1. Introduction.....	135
6.2. Polyolefin Process and Data Description.....	136
6.2.1. Industrial parallel/single reactor HDPE process	136
6.2.2. Industrial series reactors slurry HDPE process.....	137
6.2.3. Industrial Hypol PP process.....	138
6.2.4. Industrial LDPE process	139
6.3. An Application of Combined Direct Hybrid Modeling to Polyolefin Manufacturing.....	141
6.4. An Application of Inverse Modeling to Polymer Manufacturing.....	142
6.4.1. Predicting Operating Conditions of Different Polymer Grade	142
6.4.2. Kinetic Estimation Using Inverse Modeling.....	146
6.5. An Application of Reduced-Order Modeling to Polymer Manufacturing.....	147
6.5.1. Reduced-Order Modeling of Hypol PP process.....	147
6.5.2. Reduced-Order Modeling of Industrial LDPE process.....	149
6.6. An Application of HGML Modeling to Uncertainty Quantification in Polymer Manufacturing	149
6.7. An illustrative Example of Science-Guided Learning	151
6.8. Conclusion	152
References.....	152
Chapter 7: Conclusion and Future Work.....	154
7.1. Conclusion	154
7.2. Future Work.....	155
Appendix A (Chapter 2)	156
A.1 Hypol PP Process	156
A.2. Mitsui Slurry HDPE process.....	162
A.3. Innovene and Horizone PP process.....	167
A.4. Spheripol PP process.....	172
A.5. Unipol LLDPE process	175
Appendix B (Chapter 3)	180
B.1. Configuring a PID Controller.....	180
B.2. Controller tuning for HDPE slurry process dynamics and control	182

List of Figures

Figure 2.1a. Mitsui slurry HDPE process: serial reactor configuration.....	18
Figure 2.1b. Borstar bimodal HDPE process with a pre-polymerization reactor	18
Figure 2.1c. Polymerization section of the Mitsui HYPOL PP process	19
Figure 2.1d. Basell Spheripol PP process using two slurry loop reactors	19
Figure 2.1e. Innovene gas-phase PP process using a horizontal stirred-bed reactor	20
Figure 2.1f. Univation UNIPOL LLDPE process using a fluidized-bed reactor.....	20
Figure 2.2a Methodology for kinetic parameter estimation for polyolefin process models from plant data using simulation software tools(Summary).	23
Figure 2.2b Methodology for kinetic parameter estimation for polyolefin process models from plant data using simulation software tools (Detailed)	24
Figure 2.3. An Aspen Polymers simulation flowsheet of the Mitsui HYPOL PP process	26
Figure 2.4. GPC deconvolution of a homopolymer sample from a UNIPOL LLDPE Process	29
Figure 2.5a. Sensitivity of the PDI, MWN and SMWN for the Unipol LLDPE process on the pre-exponential factor of the reaction rate constant for chain transfer to hydrogen	33
Figure 2.5b. Sensitivity of the PDI, MWN and SMWN for the Unipol LLDPE process on the pre-exponential factor of the reaction rate constant for chain transfer to monomer	33
Figure 2.6a. The sensitivity of the Production rate and SPFRAC for the Unipol LLDPE process to changes in the propagation reaction rate constant.....	34
Figure 2.6b. The sensitivity of the atactic fraction ATFRAC to changes in the atactic propagation reaction rate constant for the Spheripol PP process.	34
Figure 2.7a. The sensitivity of the production rate for the slurry HDPE process to changes in the reaction rate constant for catalyst activation by cocatalyst.....	35
Figure 2.7b. The sensitivity of the production rate for the slurry HDPE process to changes in the reaction rate constant for spontaneous catalyst deactivation.	35
Figure 2.8. Sensitivity of the MWD from a Mitsui slurry HDPE process to changes in the reaction rate constant for catalyst inhibition	36
Figure 2.9. The sensitivity of the production rate from an Innovene gas-phase PP process to changes in the propagation reaction rate constant.	36
Figure 2.10. Spheripol PP process flowsheet indicating the design specification.....	37
Figure 2.11. Sensitivity Analysis of the MWN and production rate on changes in hydrogen flow rates on the Unipol LLDPE process	38
Figure 2.12. The front end of a two-reactor system for producing gas-phase PP polymer using stirred-bed reactors (closed-loop)	40

Figure 3.1. The dynamic simulation flowsheet of HDPE series process	49
Figure 3.2. Specification of task G1-G4	51
Figure 3.3. Specification of the flowsheet constraints, MI and copolymer density correlations.	52
Figure 3.4. Evolution of R1 feed mass flow rates for producing grades G1 to G4 beginning at 24, 120, 240 and 360 hr, respectively	52
Figure 3.5. Evolution of the computed melt index and copolymer density	53
Figure 3.6. The starting dynamic simulation flowsheet.....	54
Figure 3.7. Adding a hydrogen/ethylene ratio controller to the recycle gas.....	54
Figure 3.8. Performance of controllers after increasing ethylene mass flow rate to 9000 kg/hr, catalyst mass flow rate to 60 kg/hr and C3 mass flow rate to 100 kg/hr...55	55
Figure 3.9. Dynamic simulation flowsheet with default controllers.....	56
Figure 3.10. An illustration of a split-range (SR) controller.....	56
Figure 3.11. A modified dynamic process simulation flowsheet with a split-range Controller	57
Figure 3.12. The configuration specifications of the split-range controller	57
Figure 3.13. Keeping the reactor pressure at 21.6975 bar by increasing the mass flow rate of N2 from 25 to 46.4267 kg/hr as determined through a split-range controller...58	58
Figure 3.14. A simplified steady-state flowsheet for a slurry HDPE process	60
Figure 3.15. Dynamic HDPE process flowsheet	60
Figure 3.16. Grade change using H2-setpoint-based controller	61
Figure 3.17. Comparison of MI values from the open-loop inferential control MI with the actual correlation-based MI	63
Figure 3.18. Snapshot of the overall constraints and the local variable specification ..	64
Figure 3.19. MI grade change from 10 to 20 using Inferential Control.....	64
Figure 3.20 Comparison of grade change process using the inferential control with the basic H2-based control.....	65
Figure 3.21. Methodology of simulating plant data from dynamic model	66
Figure 3.22. Comparison of MI predictions of the first-principle model and plant data	66
Figure 4.1. Classification of Machine Learning models.....	72
Figure 4.2. Process flowsheet of industrial parallel HDPE process	76
Figure 4.3. Visualization of the HDPE process data	77
Figure 4.4. Correlation plot of the HDPE process data	78
Figure 4.5. Hotelling's T2 plot deviation plot	78
Figure 4.6. Contribution plot of process outlier compared to the average score to identify the cause of process abnormality.....	79
Figure 4.7. Principal Component R2 score for PLS model without lag	79
Figure 4.8. T2 plot of the data after removing the process outliers	80

Figure 4.9. Prediction plot for PLS model without lag.....	80
Figure 4.10. Variable Importance plot for PLS model without lag	81
Figure 4.11. Loading plot for PLS model without lag.....	81
Figure 4.12. Principal Component of dynamic PLS model with lag	82
Figure 4.13. Prediction plot of dynamic PLS model with lag	83
Figure 4.14. Variable Importance Plot for Dynamic PLS model including lag	83
Figure 4.15. Development of a soft sensor of MI based on Causal PLS model	84
Figure 4.16. Deep Neural Network Architecture with three hidden layers	85
Figure 4.17. Loss curve of Deep Learning model for MI prediction.....	85
Figure 4.18. The variation of hyperparameter in a Random Forest Model	86
Figure 4.19. Visualization of a tree from the Random Forest Model	87
Figure 4.20. Development of a soft sensor of ML based on Predictive random forest model.....	87
Figure 4.21. Comparison of different ML models for MI prediction	88
Figure 4.22. Accuracy v/s the sampling rate for Semi-Supervised Learning MI prediction	90
Figure 4.23. The comparison of the real and fake(generated data) in terms of means.	91
Figure 4.24. Comparison of each of the real and generated data for each of the features using the GAN model.....	92
Figure 4.25. Comparison of each feature b/w real and fake data with Probability Density Distribution of each feature comparison	93
Figure 4.26. Batch wise unfolding methodology.....	94
Figure 4.27. Score plot of PCA polymer batches	95
Figure 4.28. Contribution to scores of bad batches	95
Figure 4.29. Observation wise Analysis of Batch data.....	96
Figure 4.30. Score plot of the extruder process data.....	97
Figure 4.31. Contribution to score plot of process anomaly in an industrial extrusion process.....	97
Figure 4.32. Loading Plot for the PLS analysis of the extruder data.....	98
Figure 5.1. Classification of hybrid SGML models.....	109
Figure 5.2. Parallel direct hybrid model	110
Figure 5.3. Parallel direct hybrid residual model.....	111
Figure 5.4. Serial direct hybrid model	112
Figure 5.5. Combined direct hybrid model.....	113
Figure 5.6. Inverse modeling framework.....	115
Figure 5.7. Reduced order process modeling framework	116
Figure 5.8. Uncertainty quantification modeling framework	118
Figure 5.9. Discovering scientific laws.....	119
Figure 5.10. Science-guided design framework of neural network architecture	120

Figure 5.11. Science-guided loss function representation	121
Figure 5.12. Science-guided refinement framework.....	122
Figure 6.1. Process flowsheet of industrial parallel HDPE process	137
Figure 6.2. Process flowsheet for industrial series HDPE process	137
Figure 6.3. The variation of the quality data (MI and Rho) with time for different HDPE grades.....	138
Figure 6.4. Process flowsheet for industrial Hypol process.....	139
Figure 6.5. Process flowsheet of the industrial LDPE process	140
Figure 6.6. Melt index prediction of a combined direct hybrid model compared to the first-principle model and plant data	142
Figure 6.7. Hydrogen feed predictions for single reactor HDPE process using inverse modeling including the uncertainty of predictions.....	143
Figure 6.8. Stacked Regression Algorithm	144
Figure 6.9a. Inverse ML model prediction v/s the observed data for hydrogen flow(H21).....	145
Figure 6.9b. Inverse ML model prediction v/s the observed data for ethylene monomer flow (C21).....	145
Figure 6.9c. Inverse ML model prediction v/s the observed data for catalyst flow (CAT1).....	146
Figure 6.9d. Inverse ML model prediction v/s the observed data for butlene comonomer flow(C42).....	146
Figure 6.10. Inverse Modeling modelling framework for kinetic parameter estimation	147
Figure 6.11. Loss curve for prediction of inverse modeling kinetic parameter estimation.....	147
Figure 6.12a. Melt Index comparison of observed v/s prediction	148
Figure 6.12b. Feature importance for melt index prediction	148
Figure 6.13a. Prediction v/s Observed values of branching SCB.....	149
Figure 6.13b. Prediction v/s Observed values of branching LCB	149
Figure 6.14. Uncertainty prediction of Melt Index using Bayesian Neural Networks	150
Figure 6.15. Uncertainty quantification of melt Index prediction of a slurry HDPE process.....	151
Figure 6.16. Melt index and polymer density prediction with a ML model with a science-guided loss function	152
Figure A1. Flowsheet for Hypol simulation	157
Figure A2. Deconvolution Curve for PP made from catalyst with 4 active sites	158
Figure A3. Sensitivity of the PDI, MWN and SMWN for the HYPOL PP process on the pre-exponential factor of the reaction rate constant for chain transfer to	

monomer	161
Figure A4. Comparison of model molecular weight with actual molecular weight ...	162
Figure A5. Comparison of model PDI with actual PDI.....	162
Figure A6. Flowsheet for the slurry HDPE process with reactor in series	162
Figure A7. MWD of the product in the outlet of the first reactor.....	166
Figure A8. The effect of the sensitivity of the activation reactions on production rate for Mitsui HDPE process	166
Figure A9. The effect on the MWD by varying the catalyst inhibition reaction rate for the Mitsui HDPE process	167
Figure A10. Flow-sheet of Innovene process	167
Figure A11. The sensitivity of the production rate from an Innovene gas-phase PP process to changes in the propagation reaction rate constant	172
Figure A12. Flowsheet of Spheripol PP process	172
Figure A13. The sensitivity of the atactic fraction ATFRAC to changes in the atactic propagation reaction rate constant for the Spheripol PP process	175
Figure A14. Flowsheet of the Unipol process	176
Figure A15. Sensitivity of the PDI, MWN and SMWN for the UNIPOL LLDPE process on the pre-exponential factor of the reaction rate constant for chain transfer to hydrogen	179
Figure B1. Gain and integral time for the H2C2 controller	183
Figure B2. Controller Tune interface.....	183
Figure B3. Choosing tuning rule.....	184
Figure B4. Updated tuning parameters.	184
Figure B5. Continually decaying response resulting from the updated tuning parameters	185

List of Tables

Table 2.1. Examples of production targets for kinetic parameter estimation for modeling commercial processes from plant data.....	14
Table 2.2. Examples of Common Reactors for Producing Polyolefins	16
Table 2.3. Production targets for single-site and multisite models.....	22
Table 2.4. Major kinetic parameters affecting the single-site production target	25
Table 2.5. Plant data for kinetic modeling a commercial Mitsui HYPOL PP process ..	26
Table 2.6. Comparison of single-site model predictions with production targets obtained by data fit.....	28
Table 2.7. Deconvolution results for a representative LLDPE homo-polymer sample....	29
Table 2.8. Comparison of multi-site model predictions with production targets obtained by data fit.....	31
Table 2.9. Major kinetic parameters affecting the multi-site simulation targets	32
Table 2.10: Design specification for the Spheripol PP process	37
Table 2.11. Design specification for the UNIPOL LLDPE process	38
Table 3.1 Process and quality variables for slurry HDPE process	50
Table 3.2 Values of process variables for grades 1 to 4 for slurry HDPE process	50
Table 4.1. Process Variables for industrial HDPE Process	76
Table 4.2. Comparison of different ML models for MI prediction	88
Table 4.3. Model comparison based on MI values at varying hydrogen flow.....	89
Table 5.1. Summary of hybrid SGML approach	123
Table 6.1. Process variables and quality targets for the parallel HDPE process	136
Table 6.2. Process variables for the series reactor HDPE process.....	138
Table 6.3: Process and quality variables of Hypol process	139
Table 6.4. Process variables and Quality for LDPE process	140
Table 6.5. Model comparison based on MI values at varying hydrogen flow.....	142
Table 6.6. Process variable prediction for parallel HDPE process using inverse Modeling	144

Table 6.7. Prediction of operating conditions for series HDPE process.....	145
Table B1. Typical PID controller algorithms	180
Table B2. Initial PID controller tuning parameters	181
Table B3. PID controller actions	181
Table B4. Guidelines for AD default controllers.....	182

Chapter 1: Introduction and Motivation

This dissertation covers the ‘Integrated Process Modeling and Data Analytics for Polyolefin Process Optimization’. We introduce the scope of this work and our motivation below.

Polyolefins are one of the most widely used commodity polymers with applications in films, packaging and automotive industry. The modeling of polymerization processes producing polyolefins, including high-density polyethylene (HDPE), polypropylene (PP), and linear low-density polyethylene (LLDPE) using Ziegler-Natta catalysts is a complex and challenging task. Ziegler-Natta (ZN) catalyst is one of the most widely used catalysts for manufacturing commercial polyolefins. Polyethylene and polypropylene are two commodity polymers of the highest demands. Polyolefins have a wide application requiring different properties with different molecular weight distribution and branching distribution. The ZN polymerization follows the coordination mechanism and produces polymers with different structure/branching than the polymers formed from free radical polymerization mechanism used for producing high-pressure LDPE. Thus, catalyst design plays an important role in polyolefin processes. Different process types with different reactors and phases is another variable to modify polyolefin properties. The process for producing polyolefins can be in three phases, including solution, slurry and gas phase. Autoclaves/CSTR, loop reactors, fluidized bed reactors (FBR) are some of the main reactors used for polyolefin processes for different phases. For example, the loop reactors are used for slurry-phase process and FBR are used for gas-phase process. The book by Soares and Mckenna ¹ covers different polyolefin processes in detail.

The modeling of the ZN kinetics is complex because of the multiple active catalyst sites in the ZN catalyst. The most common type of ZN catalyst is titanium tetrachloride TiCl_4 supported on MgCl_2 or SiO_2 which is heterogeneous in nature. ZN catalysts give high activity and productivity. Multiple active sites of the ZN catalyst enable the production of polymers with broad molecular weight distributions, and allow good polymer microstructural control. Khare et. al. ^{2,3} first showcased the steady-state and dynamic modeling and kinetic parameter estimation of polyolefin processes and since then there have been hundreds of articles after that on the topic. Each article has its merits, but most of them do not consider all of the commercially important production targets when quantifying the relevant polymerization reactions and their kinetic parameters based on measurable plant data. Most of the published articles also do not make efficient use of simulation tools, particularly sensitivity analysis, design specifications, and data fit, that are available in commercial modeling software for polymerization processes, such as Aspen Polymers. Thus, there is a need to develop a general methodology to model complex polyolefin models by estimating their kinetic parameters from limited plant data.

Dynamic models of polyolefin processes are useful in maximizing the safety, operability and productivity of plants. Most polyolefin processes have a wide range of polymer grades

with many applications. Thus, efficient grade transition is an important consideration for optimization of polymer processes to improve process economics. Polyolefin processes can be used for different applications by changing their physical properties like melt index and density. These physical properties are varied by changing the process operating conditions hence grade transition is critical as we change process conditions to make a new polymer grade. In one of the early applications of dynamic modeling of polyolefin processes. In one of the first applications Debling et. al. ⁴ presented grade transition strategies for polyolefin processes and compared that for different polyolefin processes in terms of the off-spec products produced during grade transition.

Dynamic process models are useful for simulating digital twins to simulate the whole polymer process. In polymer processes, it is difficult to measure certain product quality targets. In such cases, we measure some secondary process outputs in order to correlate the product quality with primary outputs for quality control, this approach is known as inferential control, which is yet another application of dynamic modeling. Ogawa et. al. ⁵ use inferential control for quality control of a HDPE process in one of the earliest applications to polymer processes. Dynamic can also be useful in generating simulation data for further data analysis. Thus, there is a need to build first-principle dynamic models of complex polymer/polyolefin processes in addition to the steady-state models. First-principle models are scientifically consistent, but tend to be less accurate due to many modeling assumptions in a complex system, thus for applications requiring higher accuracy process data analytics becomes more useful.

With the advancements in machine learning over the years, its application for chemical process data analytics have been known to be particularly useful and profitable for the industry. Data analytics is also instrumental in detection of process anomalies. Beginning in late 1980 to early 1990, chemical engineers have been paying greater attention to artificial intelligence, neural computing, machine learning and big data analytics, and their applications to bioprocessing and chemical industries ^{6,7,8}. In particular, McGregor and others have demonstrated the significant applications of multivariate statistical analysis and big data analytics to optimizing the manufacturing of chemical and polymer processes ^{9,10}. Some of the main applications of process data analytics have been in dimensionality reduction, outlier detection, process monitoring and data visualization ¹¹.

Generally, process data consists of the independent variable which are the process input variables and operating conditions like feed flows, temperature, pressure etc. and the dependent variable are the process outputs and product quality measurements like concentrations, molecular weights, density etc. For most common machine learning applications like process monitoring control, soft sensors, we use regression models to fit an empirical model for any of process outputs/product quality as a function of the process inputs. We can also just use the process data to find patterns for fault diagnosis and anomaly detection. Specifically, polymer process data analytics is critical since the polymer quality measurements like polymer melt index, molecular weight etc. are usually less frequent

compared to the continuous process variable measurements, hence, the use of data-based sensors become useful.

Modeling of many physiochemical systems requires detailed scientific knowledge of the system which is not always feasible for complex processes. We make some assumptions when modeling the system with first principles that ultimately leads to some knowledge gaps in describing the original system. Even for the systems where the scientific knowledge is sufficient to model the system, there are too many model parameters to estimate. We often apply data-based models to study the systems where scientific data are available since they are more accurate in prediction. However, data-based/machine learning models are black-box models which can over-fit the data and also produce scientifically inconsistent results. For better accuracy, ML models also require more data which is not always feasible for many problems. Therefore, it is important to integrate science-based knowledge and data-based knowledge for an accurate and scientifically consistent prediction in the form of hybrid models.

Among the earliest applications of hybrid modeling in chemical/bio processes Psychogios and Unger¹¹ combine a partial first-principle model based on prior process knowledge with a neural network to a fed-batch bioreactor for more accurate extrapolations and scientifically consistent predictions. Hybrid modeling has been applied in bioprocesses, chemical and oil and gas process industries and polymer processes industry for more accurate and scientifically consistent predictions over the years^{12,13,14}. The main applications of hybrid modeling in chemical processes includes process control, design of experiments, process development and scale-up, process design and optimization¹⁵. Most of the literature in chemical engineering application in hybrid modeling deals with a direct combination of first-principle and ML models.

In a recent article Karpatne et. al.¹⁶ suggest the theory-guided data science as a new paradigm for scientific discovery from data where they give a broader perspective of a hybrid science- guided machine learning (SGML) methodology where they showcase different applications showcases complementing ML models, and ML complementing science-based models complements. This SGML approach has been applied in physics¹⁷ and other scientific fields but not in chemical process data analysis. Thus, there is a need for a broader application of scientific principles in machine learning and industrial chemical processes. In particular, polymer processes requiring accurate and scientifically consistent data-based sensors for quality target predictions, but there are not many studies showcasing a hybrid modeling approach. Hence, there is utility in applying this hybrid SGML approach by integrating the polyolefin process models and Data Analytics for polyolefin process improvement and optimization.

References

1. Soares, J. B. P.; McKenna, T. F. L. *Polyolefin Reaction Engineering*, Wiley-VCH, Weinheim, Germany, **2012**.
2. Khare, N. P.; Seavey, K. C.; Liu, Y. A.; Ramanathan, S.; Lingard, S.; Chen, C. C. Steady-State and Dynamic Modeling of Commercial Slurry High-Density Polyethylene (HDPE) Processes. *Ind. Eng. Chem. Research*, **2002**, *41*, 5601.
3. Khare, N. P.; Lucas, B.; Seavey, K.C.; Liu, Y. A.; Sirohi, A.; Ramanathan, S.; Lingard, S.; Song, Y.; Chen, C.C. Steady-State and Dynamic Modeling of Commercial Gas-Phase Polypropylene Processes Using Stirred-Bed Reactors. *Ind. Eng. Chem. Research*, **2004**, *43*, 884.
4. Debling, J.A., Han, G.C., Kuijpers, F., VerBurg, J., Zacca, J. and Ray, W.H., Dynamic modeling of product grade transitions for olefin polymerization processes. *AIChE journal* **1994**, *40*, 506
5. Ogawa, M.; M. Ohshima; K. Morinaga; Watanabe, F. , Quality Inferential Control of an Industrial High Density Polyethylene Process. *Journal of Process Control* **1999**, *9*, 51
6. Baughman, D. R.; Liu, Y. A., *Neural networks in bioprocessing and chemical engineering*. Academic press: **2014**
7. Qin, S. J., Process data analytics in the era of big data. *AIChE Journal* **2014**, *60*, 3092
8. Chiang, L.; Lu, B.; Castillo, I., Big data analytics in chemical engineering. *Annual review of chemical and biomolecular engineering* **2017**, *8*, 63.
9. Skagerberg, B.; MacGregor, J. F.; Kiparissides, C., Multivariate data analysis applied to low-density polyethylene reactors. *Chemometrics and intelligent laboratory systems* **1992**, *14* (1-3), 341-356
10. MacGregor, J. F., Using on-line process data to improve quality: challenges for statisticians. *International Statistical Review* **1997**, *65* (3), 309-323
11. Ge, Z.; Song, Z.; Ding, S. X.; Huang, B., Data mining and analytics in the process industry: The role of machine learning. *Ieee Access* **2017**, *5*, 20590-20616
12. Psychogios, D. C.; Ungar, L. H., A Hybrid Neural Network-First Principles Approach to Process Modeling. *AIChE Journal*. **1992**, *38*, 1499
13. Yang, S.; Navarathna, P.; Ghosh, S.; Bequette, B. W., Hybrid Modeling in the Era of Smart Manufacturing. *Computers and Chemical Engineering*. **2020**, *140*, 106874.
14. Sansana, J.; Joswiak, M. N.; Castillo, I.; Wang, Z.; Rendall, R.; Chiang, L. H.; Reis, M. S., Recent Trends on Hybrid Modeling for Industry 4.0. *Computers and Chemical Engineering* **2021**, *151*,107365
15. Von Stosch, M.; Oliveira, R.; Peres, J.; de Azevedo, S. F., Hybrid Semi-Parametric Modeling in Process Systems Engineering: Past, Present and Future. *Computers and Chemical Engineering*. **2014**, *60*, 86

16. Karpatne, A.; Atluri, G.; Faghmous, J. H.; Steinbach, M.; Banerjee, A.; Ganguly, A.; Shekhar, S.; Samatova, N.; Kumar, V., Theory-Guided Data Science: A New Paradigm for Scientific Discovery from Data. *IEEE Transactions on Knowledge and Data Engineering*. **2017**, *29*, 2318.
17. Willard, J.; Jia, X.; Xu, S.; Steinbach, M.; Kumar, V., Integrating Physics-Based Modeling with Machine Learning: A Survey. **2020**, *arXiv preprint arXiv:2003.04919v4 [physics.comp-ph]*.

Chapter 2: First Principle Steady State Modeling of Polyolefin Process: Ziegler-Natta Polymerization

"Reprinted with permission from [110th Anniversary: An Effective Methodology for Kinetic Parameter Estimation for Modeling Commercial Polyolefin Processes from Plant Data Using Efficient Simulation Software Tools, Niket Sharma and Y. A. Liu, *Industrial & Engineering Chemistry Research* **2019** 58 (31), 14209-14226, DOI: 10.1021/acs.iecr.9b02277] . Copyright [2019] American Chemical Society."

Niket Sharma and Y. A. Liu
AspenTech-PetroChina Center of Excellence in Process System Engineering
Department of Chemical Engineering
Virginia Polytechnic Institute and State University
Blacksburg, VA 24061

2.1. Introduction

Polyolefins are one of the most widely used commodity polymers with applications in films, packaging and automotive industry. The modeling of polymerization processes producing polyolefins, including high-density polyethylene (HDPE), polypropylene (PP), and linear low-density polyethylene (LLDPE) using Ziegler-Natta catalysts with multiple active sites, is a complex and challenging task. This chapter presents an effective methodology to estimate kinetic parameters that have the most significant impacts on specific production targets, and to develop the kinetics using all commercially important production targets validated over polyolefin processes producing HDPE, PP and LLDPE using Ziegler-Natta catalysts. This chapter is modified from our publication - (Sharma and Liu) ¹. Since the publication of our 2002 and 2004 articles ^{2,3}, there have been at least 100 articles about estimating kinetic parameters and modeling of commercial polyolefin processes producing high-density polyethylene (HDPE), polypropylene (PP), and linear low-density polyethylene (LLDPE) involving Ziegler-Natta (Z-N) polymerization. Each article has its merits, but most of them do not consider all of the commercially important production targets when quantifying the relevant polymerization reactions and their kinetic parameters based on measurable plant data. Most of the published articles also do not make efficient use of simulation tools, particularly sensitivity analysis, design specifications, and data fit, that are available in commercial modeling software for polymerization processes, such as Aspen Polymers which is an extension of Aspen Plus® simulation software. In particular, *sensitivity analysis* quantifies the effect of varying kinetic parameters on the production targets. *Design specification* finds the desired kinetic parameters to match the specified production targets. *Data fit* is an efficient nonlinear regression tool that determines statistically acceptable, kinetic parameters from constant, time-varying, or

temperature-dependent laboratory measurements, or from matching the process simulation to production targets.

The objective of this study is to present an effective methodology for estimating the kinetic parameters based on plant data in the development of simulation and optimization models for commercial polyolefin processes using efficient software tools. We first describe the Ziegler-Natta polymerization kinetics for polyolefin processes, and present commercially important production targets involving slurry, solution and gas-phase reactors. We identify the kinetic parameters that have the most significant impacts on the specific production targets, and demonstrate an effective methodology for estimating the kinetic parameters to fit production targets in a computer-aided step-by-step procedure. We report our insights and experiences from training practicing engineers to successfully apply our methodology to several dozen commercial HDPE, PP and LLPDE processes to achieve sustainable operation goals and generate significant economic payback at two of the world's largest petrochemical companies in the Asia-Pacific over the past two decades. To help our reader in applying our methodology, we present supplements of detailed modeling examples and Excel modeling spreadsheet for commercial polyolefin processes. This study is motivated in part by the minimum coverage of developing models for industrial polyolefin reactors from plant data in two premier textbooks^{5,6}.

This chapter deals with first-principle based modeling of HDPE, PP, LLDPE and manufacturing processes using Ziegler-Natta (ZN) catalyst. We will also briefly cover Metallocene based catalyst modeling for producing EPDM. We use simulation software Aspen Polymers for this study. We deal with the methodology and procedure to model the ZN polymerization kinetics. In particular, we present an effective methodology for estimating the kinetic parameters based on plant data in the development of simulation and optimization models for commercial polyolefin processes using efficient software tools. We showcase the methodology of making first principle models for polyolefins processes.

2.2. Polyolefin Ziegler-Natta Polymerization Kinetics

Ziegler-Natta (ZN) catalyst is one of the most widely used catalysts for manufacturing commercial HDPE, PP, LLDPE and EPDM. Polyethylene and polypropylene are two commodity polymers of the highest demands. Polyolefins have a wide application requiring different properties with different molecular weight distribution and branching distribution. The polymerization follows the coordination mechanism which is different from the free radical polymerization mechanism used for producing high-pressure LDPE. The microstructure of polyolefins made with coordination catalysts is different from that made with free radical kinetics. The LDPE made using the free radical mechanism consists of both short chain branching (SCB) and long chain branching (LCB), while that made by coordination mechanism consists of only SCB. Thus, catalyst design plays an important role in polyolefin processes. Different process types with different reactors and phases is another variable to modify polyolefin properties. The process for producing polyolefins

can be in three phases, including solution, slurry and gas phase. Autoclaves/CSTR, loop reactors, fixed bed reactors (FBR) are some of the main reactors used for polyolefin processes for different phases. For example, the loop reactors are used for slurry-phase process and FBR are used for gas-phase process. The book by Soares and McKenna² covers different polyolefin processes in detail.

The modeling of the ZN kinetics is complex because of the multiple active catalyst sites in the ZN catalyst. The most common type of ZN catalyst is titanium tetrachloride TiCl_4 supported on MgCl_2 or SiO_2 which is heterogeneous in nature. ZN catalysts give high activity and productivity. Multiple active sites of the ZN catalyst enable the production of polymers with broad molecular weight distributions, and allow good polymer microstructural control.

This chapter focuses on ZN catalysts, not other catalyst types, such as Phillips, metallocene and late transition metal catalysts discussed in Chapters 3 and 5 of Soares and McKenna⁶. Phillips catalyst is similar to the ZN catalyst with multiple active sites, and is used for producing HDPE consisting of chromium compounds like CrO_3 supported on SiO_2 . Metallocene catalyst and late transition metal catalysts are used to produce HDPE/LLDPE with uniform properties and narrow MWD. The metallocene catalysts are considered to be single site and homogeneous, i.e., soluble in the reaction medium. This chapter also does not deal with any processes that may use more than one catalyst type. Our limitation results from the lack of sufficient published plant data that would enable us to develop an effective methodology for kinetic parameter estimation for other catalyst types.

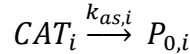
2.2.1. Ziegler-Natta Catalysts

The ZN catalyst requires a co-catalyst AlR_3 such as triethyl aluminum (TEAL), $\text{Al}(\text{C}_2\text{H}_5)_3$, for activation. The co-catalyst is used to alkylate the Ti salt to yield an active site. The catalyst and co-catalyst react in a series of reactions to form a complex. The co-catalyst extracts the chlorine atoms and transfer the alkyl group to the catalyst. Thus, the co-catalyst acts as a reducing agent and the electron-deficient site acts as the active site initiating the polymerization. The ZN catalyst is usually heterogeneous and has multiple active sites and produces polymer with broad molecular weight distribution. The catalyst structure of ZN catalyst can be designed based on the required stereoregularity of the polymer. The homogeneous form of the ZN catalyst usually contains different cocatalyst like methylalumoxane along with the titanium complex. We will focus mostly on the heterogeneous catalyst in this chapter.

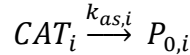
2.2.2. Ziegler-Natta Polymerization Kinetics

The most important reactions in the ZN kinetics are the same as in any polymerization kinetics, namely, the chain initiation, propagation and chain transfer reactions which can be with monomer, hydrogen, and solvent. The ZN catalyst consists of different catalyst site types with each having its own relative reactivity, because of variations in the local chemical composition of each site type. The catalyst activation, deactivation and inhibition reactions are also specific to ZN catalyst. Site activation reactions convert potential sites to active sites, while site deactivation reactions convert active sites to dead sites. As discussed previously, Aspen Polymers builds the kinetic model in terms of repeating units or segments. All the main reactions in ZN kinetics are as follows. The Ziegler Natta kinetics have also been explained previously by Khare ⁴ in his thesis . We summarize below our kinetic model reactions. For detailed description of each reaction, references to 2-4.

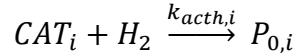
(1a) ACT-SPON: Spontaneous catalyst activation ($P_{0,i}$ is vacant site of type i):



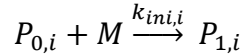
(1b) ACT-COCAT: Catalyst site activation by cocatalyst:



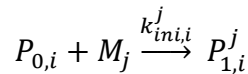
(1c) ACT-H2: Catalyst site activation by hydrogen:



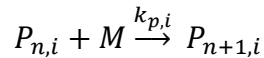
(2) CHAIN-INI: Chain initiation by monomer (M) ($P_{1,i}$ is a propagation site of type i with an attached polymer chain containing one segment):



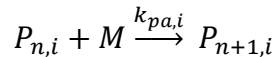
(2') CHAIN-INI: Chain initiation by monomer j (M_j) for copolymerization:



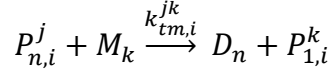
(3a) PROPAGATION: Chain propagation ($P_{n,i}$ and $P_{n+1,i}$ are polymer chains of length n and $n + 1$ segments):



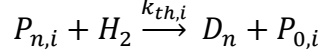
(3b) ATRACT-PROP: Atactic chain propagation ($k_{pa,i}$ is the rate constant for atactic chain propagation at site type i):



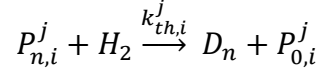
(4a) CHAT-MON: Chain transfer to monomer ($k_{tm,i}^{jk}$ is the rate constant for chain transfer to a monomer of type k reacting with a growing chain transfer ending with a monomer unit of type j at site type i):



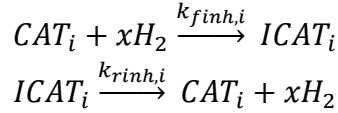
(4b) CHAT-H2: Chain transfer to hydrogen (Chain transfer to hydrogen and other transfer reactions generate a vacant site of type i , $P_{0,i}$. D_n is a dead polymer chain of length n).



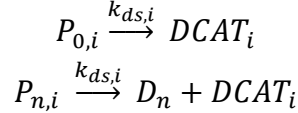
(4b') CHAT-H2: Chain transfer to hydrogen for copolymerization (Chain transfer to hydrogen and other transfer reactions generate a vacant site of type i , $P_{0,i}$. D_n is a dead polymer chain of length n).



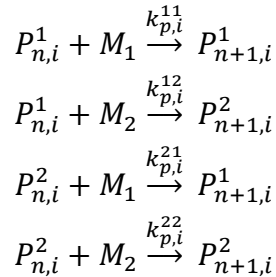
(5) FSINH-H2 and RFINH-H2: “Forward and reverse catalyst Inhibitions by hydrogen ($ICAT_i$ is the inhibited”^{2,4} catalyst of site type i):



(6) DEACT-SPON: Spontaneous catalyst deactivation ($DCAT_i$ is deactivated catalyst site of type i . D_n is a dead polymer chain of n segments):



(7) Copolymerization Kinetic Scheme (“ $k_{p,i}^{jk}$ is the rate constant for propagation, associated with site type i , for a monomer of type k adding to a chain with an active segment of type j ”^{2,4}):



We note that the reaction rate constants listed in the chemical reactions (1) to (7) above have the following standard Arrhenius form:

$$k = k_0 * e^{-\frac{E}{R}(\frac{1}{T} - \frac{1}{T_r})} \quad (2.1)$$

where k_0 is the pre-exponential factor, E is the activation energy, R is the ideal gas constant, and T is the temperature of the reaction system and T_r is the reference temperature.

We discuss below our reasoning for including certain model reactions, and our simplification in ignoring other model reactions.

- (1) Touloupidis ⁷ and Zacca and Ray ⁸ include the catalyst site activation by monomer (ACT-MON) and by electron donor (ACT-EDONOR) in their modeling studies. These reactions are available within the Ziegler-Natta kinetic model in Aspen Polymers when needed.
- (2) To quantify the catalyst activation, the Aspen Polymers model for Ziegler-Natta kinetics includes a parameter (called *max sites*) for the concentration of catalyst sites per unit mass of catalyst, in addition to the catalyst activation reaction rate constants. Typical values of the max sites parameter range from 1.0E-5 to 1.0 E-3 mol of sites per g of catalyst. When employing titanium tetrachloride as the catalyst, we typically use a value of 2E-4 mol of sites per g of catalyst ^{2,9}. We can vary this parameter to change the polymer production rate, *without* affecting the polymer molecular weight or copolymer composition.
- (3) Chain transfer to transfer agent (CHAT-AGENT), to solvent (CHAT-SOL), to cocatalyst (CHAT-COCAT), and to electron donor (CHAT-EDONOR) follows reaction (4b), for chain transfer to hydrogen (CHAT-H2). These reactions are available within the Ziegler-Natta kinetic model in Aspen Polymers. We ignore them as in references 2, 3 .
- (4) Zhang et al. ¹⁰ include the beta-hydride elimination in their slurry HDPE modeling study. Soares and McKenna ⁴, p.162 state that this reaction produces metal hydride sites that are indistinguishable from those made by chain transfer to hydrogen. Therefore, it would be appropriate to consider only the reaction of chain transfer to hydrogen, without the reaction of beta-hydride elimination, as in references 2,3.
- (5) After considering chain-transfer reactions, Touloupidis ⁷ includes site-transformation reactions that convert one vacant catalyst site type to another by means of specific reactions, such as transformation to hydrogen, to cocatalyst, to solvent and to poison, as well as spontaneous site transformation. Touloupidis further states that “site transformation reactions do not seem to play an important role, as they are rarely employed. Moreover, they pose difficulties on the way site transformation can be experimentally measured and validated” ⁷, p. 518 . Therefore, we ignore site-transformation reactions.
- (6) As explained in reference 2 , by adding hydrogen to polyolefin processes with ethylene as a monomer, the rate of polymerization decreases. We can model this effect by including the forward and backward catalyst site inhibition reactions due to hydrogen (FSINH-H2 and RFINH-H2). The rate constants of these inhibition reactions affect the polymer production rate. The Aspen Polymers model also calculates the equilibrium mole of inhibited catalyst sites (CISFRAC).
- (7) In certain polyolefin systems such as HDPE ², we may get a bimodal homopolymer from a single reactor. This is different from the bimodal copolymer produced in a reactor series for HDPE ^{10,11,12}, PP ^{3,13,14} or LLDPE ¹⁵ due to the difference in the hydrogen concentrations in the two reactors in series. We can model this bimodal

copolymer by the forward and reverse catalyst inhibition reactions due to hydrogen (FSINH-H2 and RFINH-H2) ². The Aspen Polymers model also calculates the equilibrium mole of inhibited catalyst sites (CISFRAC).

- (8) Many HDPE ^{2, 9, 10, 11, 12}, PP ^{3, 13, 14} and LLPDE ¹⁵ models include the reaction of spontaneous catalyst deactivation (DEACT-SPON). For PP, the tacticity control agent deactivates a portion of the catalyst sites that produces atactic polymer. We account for this by the reaction of catalyst deactivation by tacticity control agent (DEACT-TCA) ². The Aspen Polymers model includes also catalyst deactivation reactions by hydrogen (DEACT-H2), by cocatalyst (DEACT-COCAT), by monomer (DEACT-MON), by poison (DEACT-POISON), and by electron donor (DEACT-EDONOR), as listed in 5. In **Appendix A.3 and A.5**, we include DEACT-POISON and DEACT-H2 reactions.
- (9) Certain polyolefin processes, such as slurry HDPE, produce an oligomer, which is a low-molecular-weight polymer species that dissolves in the hexane diluent. Using plant data for the molecular weight of the oligomer, we model the oligomer production by reacting stoichiometric amounts of ethylene and hydrogen according to the equation ²: $x \text{ C}_2\text{H}_4 + \text{H}_2 \rightarrow \text{oligomer}$, where x is a stoichiometric coefficient determined from plant data.
- (10) As our section title, “Polyolefin Ziegler-Natta Polymerization Kinetics”, implies, we focus only on the kinetic reactions that are applicable to commercial processes using Z-N catalysts, not other catalyst types, such as Phillips, metallocene and late transition metal catalysts discussed in Chapters 3 and 5 of Soares and McKenna ⁶. We do not deal with any processes that may use more than one catalyst type. Our limitation results from the lack of sufficient published plant data that would enable us to develop an effective methodology for kinetic parameter estimation for other catalyst types.

2.3. Commercial Polyolefin Production Targets

The important commercial production targets for kinetic parameter estimation of polyolefin processes are as follows.

2.3.1 General Production Targets

2.3.1.1. Production Rate: We use the mass flow rate of polymer within the outlet stream from each reactor for a process with reactors in series for kinetic parameter estimation. It is an important production target for process modeling, since the production rates are increased for production expansion and the kinetics should be dependent on it. The propagation reaction determines the polymerization rate hence directly affects the production rate.

2.3.1.2. MWN: The number-average molecular weight (MWN) of the polymer is an important target. MWN varies for different polymer grades. The reaction rate constants for chain transfer to H₂ (CHAT-H2) and to monomer (CHAT-MON) significantly affect the molecular weight of the polymer since the reactions lead to breaking the growing polymer chain and forming the dead polymer chain.

2.3.1.3. MI: In the literature, most empirical correlations for MI for polyolefins with broad MWD or large PDI are based on the weight-average molecular weight (MWW). For example, a general MI correlation with MWW is in the form of ^{16,17}:

$$MI = a (MWW)^{-b} \quad (2.2)$$

where a and b are correlating parameters. For PP, the MI may depend on the MWW as well as the atactic fraction (ATFRAC), calculated by the atactic chain propagation reaction (ATACT-PROP) ².

2.3.1.4. Conversion: The conversion percentages of the monomer and the co-monomer are required to determine the yield of the process.

2.3.1.5. PDI: The polydispersity index is the ratio of the weight-average molecular weight to the number-average molecular weight, MWW/MWN. It is an important polyolefin property. It is measured by performing gel permeation chromatography (GPC) of the polyolefin sample obtained at the product outlet or at each reactor outlet in a process with reactors in series.

2.3.1.6. SMWN and SPFRAC: SMWN represents the number-average molecular weight produced at each active catalyst site. SPFRAC is the weight fraction of polymer produced at each active site. They are determined by deconvolution of the polymer GPC curve, and are required for estimating individual site-specific kinetic parameters.

2.3.1.7. SFRAC and SCB: SFRAC is the mole fraction of segments of the comonomer and is usually determined by the short chain branching distribution (SCBD). The use of online Fourier transform infrared spectroscopy (FTIR) with gel permeation chromatography (GPC) permits the detection of the SCB as a function of the weight-average molecular weight ¹⁸. We use this simulation target to predict the co-monomer content in the copolymer. SFRAC depends on the co-monomer kinetics.

2.3.1.8. Rho: The polymer density is usually measured for the pellets, and correlated as a function of the MWW. For copolymerization, we often correlate the polymer density as a function of mole fraction of the comonomer and the MWW ^{11,18}. In reference 9, the HDPE density obtained from ethylene copolymerization with comonomer 1-butene follows the following correlation:

$$\rho = (1 - 0.009165 xB^{0.148895}) \times 1.137247 - 0.014314 \ln (MWW) \quad (2.3)$$

where xB is the mole fraction of 1-butene. In reference 18, we see an example of correlating the polymer density to MWW and SCB content for a bimodal HDPE copolymer process:

$$\rho = 1.0748 - 0.0241 \log MWW - 0.01145 \left(\frac{\sum_{j=1}^N m(j) SCB(j) w_{\log MWW}(j)}{\sum_{j=1}^N m(j) w_{\log MWW}(j)} \right)^{0.47332} \quad (2.4)$$

where m(j) is mass fraction of polymer formed at active site j, SCB(j) is the average short chain branching in copolymer formed at active site j, and $w_{\log MWW}(j)$ is the weight chain length distribution of the polymer formed at active site j.

2.3.1.9. Residence Time: This refers to the reactor residence time. It can be the residence time of each reactor in a process with a series of reactors. It is an important target affecting the polymer properties. The residence time is dependent on the polymer solution density which depends on the thermodynamic property parameters.

2.3.2. Polymer-Specific Targets:

2.3.2.1. CISFRAC: It is the ratio of the moles of the inhibited catalyst sites to the total number of moles of the catalyst sites. It may be considered as a target for HDPE process when catalyst inhibition reactions are considered.

2.3.2.2. ATFRAC: It is the ratio of the atactic propagation to the total propagation. It is a commercial target for atactic PP production.

Table 2.1 give examples of production targets for kinetic parameter estimation for modeling commercial polyolefin processes from plant data.

Table 2.1. Examples of production targets for kinetic parameter estimation for modeling commercial polyolefin processes from plant data

Polymer reference	Pr od. rat e	MWN and MI	Conv	SFRAC	PD I	Rho	SMWN and SPFRAC	Res. tim e	Polymer specific
HDPE, Khare et al. ²	✓	✓	✓	✓	✓	✓	✓	✓	✓
HDPE, Chen et al. ⁹	✓	✓		✓	✓	✓	✓	✓	
HDPE, Zhang et al. ¹⁰	✓	✓		✓	✓		✓		
HDPE, Meng et al. ¹¹	✓	✓		✓	✓	✓	✓	✓	
HDPE, Zhao, et al. ¹²	✓	✓	✓		✓	✓	✓	✓	✓
PP, Khare, et al. ³	✓	✓	✓	✓	✓		✓	✓	✓
PP, Zheng et al. ¹³	✓	✓		✓	✓	✓	✓		
PP, Luo et al. ¹⁹	✓	✓	✓		✓	✓	✓	✓	
PP, You and Li ²⁰	✓	✓	✓	✓	✓		✓	✓	

PP, Luo et al. ²¹	✓	✓		✓	✓		✓	✓	
PE, Kou et al. ^{22,23}	✓	✓			✓				
LLPDE, Touloupidis et al. ¹⁵	✓	✓			✓		✓		
LLPDE, Kashani et al. ²⁴	✓	✓			✓		✓		

We conclude this section by noting two points.

(1) Not all of these production targets are fully independent of each other. As an example, MI typically depends on MWW for most polyolefins, and also depends on atactic fraction (ATFRAC) for PP. In our simulation, we use a FORTRAN block to calculate the MI based on a correlation developed from past plant data for MWW, and compare the calculated MI value with the current plant data. If the resulting deviation between the calculated and measured MI values is not acceptable, we would fine-tune the simulation parameters for better MWW predictions, and possibly update the MI-MWW correlation with new plant data.

(2) Not all of the suggested production targets in reported modeling studies have the relevant plant data for model validation. Depending the intended purposes for using the resulting simulation model and the accuracy requirements of model predictions, the model developers must decide if they wish to make a serious effort to collect plant data of certain production targets for validating the simulation model. Alternatively, they could use available data of relevant process variables or the values of simulation output variables as independent variables to develop soft sensors or inferential models (such as those based on neural networks ²⁵) for production targets (e.g., MI and ATFRAC) that are not routinely measured.

2.4. Modeling Considerations

2.4.1 Reactor Types

Chapter 4 of Soares and McKenna ⁶ describes the various types of reactors used for polyolefin processes, depending on the type of polyolefin, process technology and reactant phase. The most common reactors used in polyolefin processes are *stirred autoclave or continuous stirred tank reactor (CSTR), loop reactor, fluidized-bed reactor (FBR), and horizontal stirred-bed reactor (HSBR)*. The modeling of the reactors requires certain assumptions.

Table 2.2 gives examples of common reactor types in commercial polyolefin processes. We can model the stirred autoclave reactors in the Mitsui slurry HDPE process ^{2,10,11} and in the DOWLEX solution LLPDE process ²⁶ as continuous stirred tank reactors (CSTRs). Loop reactors are used in the Borstar slurry HDPE process ^{6, p. 120; 9, 11} as well as the Basell

Spheripol^{13,14}; 6, p. 106 and Mitsui HYPOL^{20,21} PP processes. In the modeling of a loop reactor when the recycle ratio is 30 or higher as calculated by Zacca and Ray⁸, we can simulate the loop reactor as a CSTR. High recycle ratios give very low axial concentration of the reactant and uniform temperature and residence time distribution (RTD) so that we can model a loop reactor as a CSTR. The loop reactors have a higher space-time yield and a high ratio of heat transfer per unit volume. Luo et. al.¹⁹, Zheng²⁷, among others, have modeled the loop reactor series as CSTRs for PP production.

Table 2.2. Examples of Common Reactors for Producing Polyolefins

Polymer	Stirred autoclave, or continuous stirred tank reactor (CSTR)	Slurry Loop Reactors (SLRs)	Fluidized-Bed Reactors (FBRs)	SLRs + FBRs	Stirred-Bed Reactors (SBRs)
HDPE	Mitsui slurry process 2, 10, 11			Borstar bimodal process 9, 12	
PP		Loop reactor series 19,27	Univation UNIPOL ²⁸	Basell Spheripol process 6, p.26; 13, 14 , HYPOL process 20,21	Innovene ³
LLPDE	DOWLEX solution process 6, p. 120; 26	Loop reactor series 15	Basell Spherilene 26 , Univation UNIPOL ²⁴		

Fluidized-bed reactors are mainly used for gas-phase and mixed-phase processes, such as the Borstar bimodal HDPE^{11,12}, Basell Spheripol PP^{13,14}, Mitsui HYPOL PP^{20,21}, Basell Spherilene²⁶ and Univation UNIPOL²⁴ LLPDE processes. FBRs have a high overall conversion as well as high heat removal capacity. FBRs are mostly used as a finishing reactor for making copolymers in a series polyolefin process, as varying levels of co-monomers can be added without any solubility issues. The high recycle ratios of the recycle gas lead to uniform temperature and low concentration gradient in the FBRs, making it reasonable to model the FBR as a CSTR. Chen et al.¹¹ and Zhao et al.¹⁴ have modeled the FBR as a CSTR in the finishing reactor for making bimodal HDPE.

The HSBR (horizontal stirred-bed reactor) has been used for gas-phase polymerization processes, such as the Innovene (formerly BP Amoco) PP process³. It has a plug-flow characteristic and can be used for fast grade change and making wide variety of products. We can simulate the HSBR as a series of CSTRs to approximate the RTD of the plug flow³.

2.4.2 Polymer Types:

HDPE, PP and LLDPE are mostly made using Ziegler-Natta catalysts. The strategy for process modeling and kinetic parameter estimation does not change when considering different polymers. We only need to include certain reactions specific to the polymers. For HDPE processes, it is appropriate to consider the forward and reverse catalyst inhibition reactions by hydrogen (FSINH-H₂ and RFINH-H₂), since the rate of polymerization for ethylene polymer decreases with the addition of hydrogen. For PP processes, we need to consider the atactic propagation reaction (ATACT-PROP), depending on the atactic content of the polymer. The atactic polymer is amorphous and has low commercial value; it is desirable to have high isotactic PP.

2.4.3 Molecular Weight Distribution (MWD) and Multi-Modal Distributions:

The MWD of the polymer can be unimodal or multi-modal, depending on the operating conditions. The kinetic estimation and modeling strategy remain the same whether the MWD distribution is unimodal or bimodal. The homopolymer MWD is usually unimodal.

For obtaining bimodal MWD in many polyolefin processes, the catalyst is exposed to two different operating conditions in a cascade of reactors. We can use two reactors in series to produce bimodal HDPE. The first reactor makes low MWN HDPE with the help of a higher hydrogen concentration, while the second reactor has a lower hydrogen concentration producing a higher molecular weight polymer. A comonomer alpha olefin is often added to make a copolymer. Chen et. al.⁹ and Meng, et al.¹¹ have modeled the Borstar HDPE process to predict the bimodal MWD. In the Borstar process, the low-molecular-weight homopolymer is made in the slurry loop reactor (SLR) and the high-molecular-weight copolymer is made in the FBR. There can be other reasons for obtaining a bimodal MWD apart from operating conditions if we obtain a bimodal MWD in a single reactor. The other reasons for bimodal MWD can be different types of reacting sites in the catalyst, inhibition of catalyst sites due to hydrogen or other poisoning and non-ideal mixing in the reactor²⁹.

2.4.4 Process Flowsheets

Figures 2.1a to 2.1f illustrate the simplified flowsheets of several commercial polyolefin production processes that we use below to demonstrate our methodology for kinetic parameter estimation from plant data using simulation software tools.

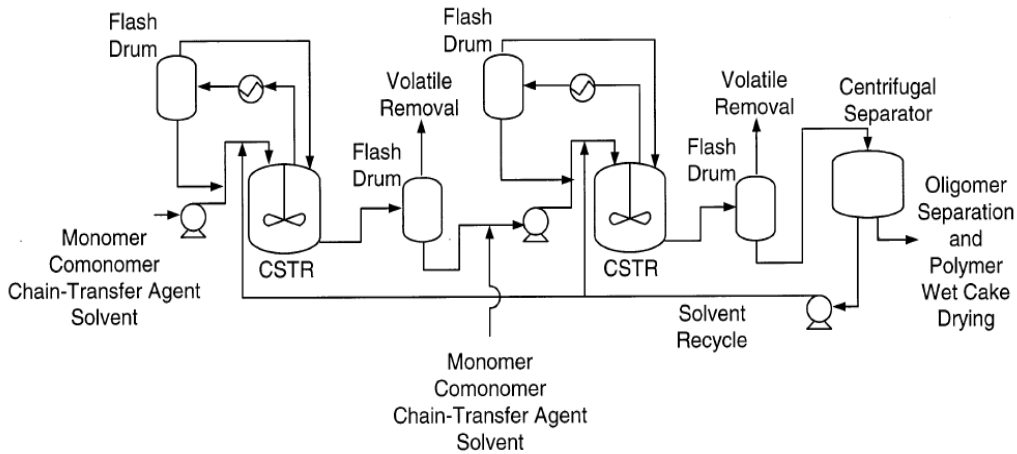


Figure 2.1a. Mitsui slurry HDPE process: serial reactor configuration ²

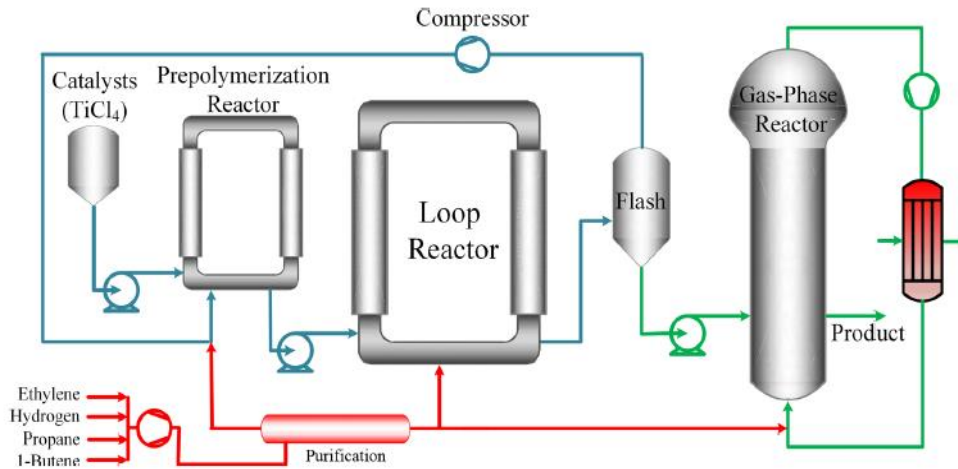


Figure 2.1b. Borstar bimodal HDPE process with a prepolymerization reactor, a slurry loop reactor (SLR), a flash unit, and a finishing fluidized-bed reactor (FBR) ¹².

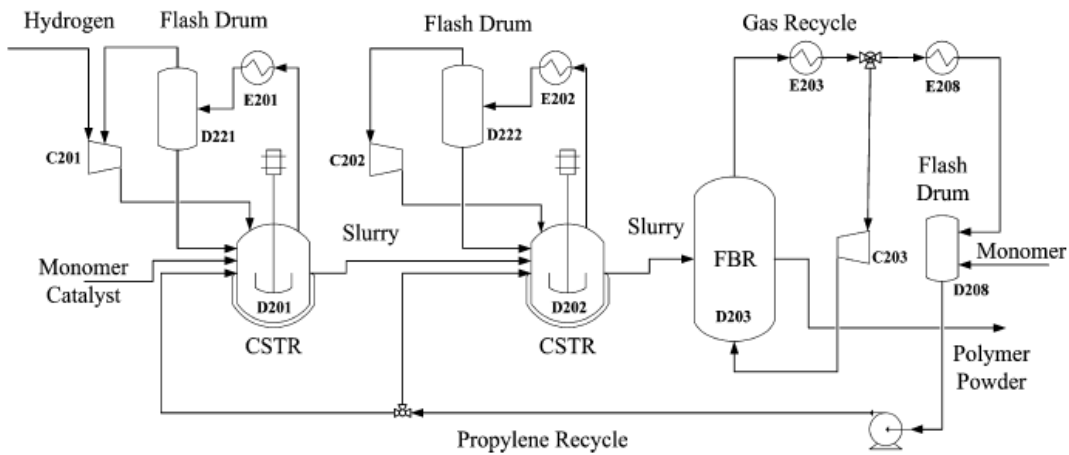


Figure 2.1c. Polymerization section of the Mitsui HYPOL PP process: C201, C202 and C203- compressor; D201 and D202- slurry polymerization reactor (SLR); D203- fluidized-

bed reactor (FBR); D221, D222, and D228- flash drum; E201, E202, E203 and E208- heat exchanger ²¹. In our example and in Supplement 1a, we have another FBR, D204.

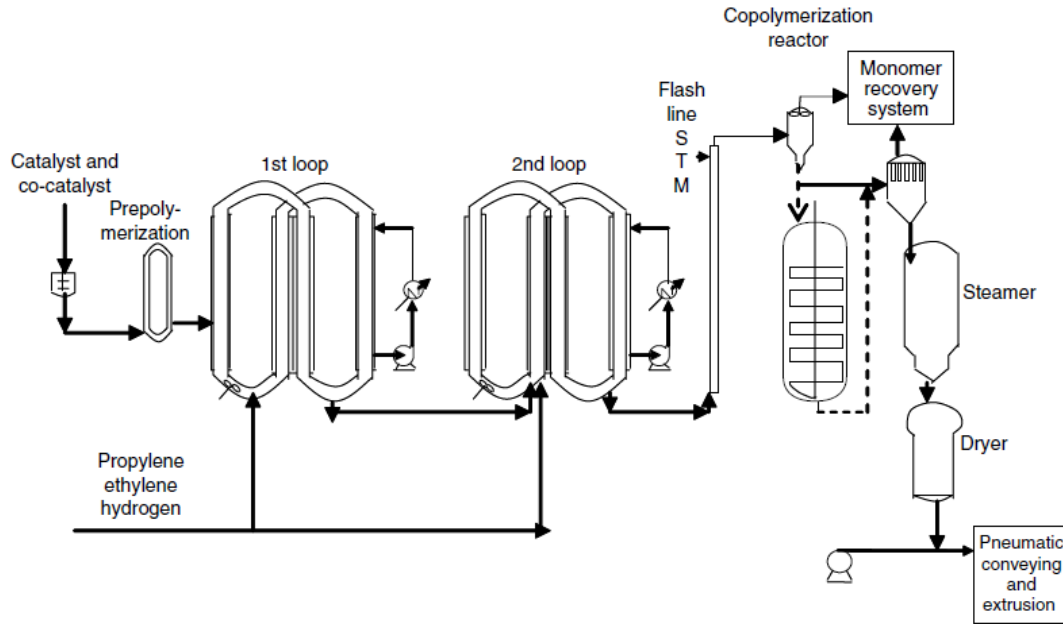


Figure 2.1d. Basell Spheripol PP process using two slurry loop reactors (SLRs), followed by a flash unit and a fluidized-bed reactor (FBR) for copolymerization (Soares, J. B. P.; McKenna, T. F. L. *Polyolefin Reaction Engineering*, p. 126, **2012**. Copyright Wiley-VCH Verlag GmbH & Co. KGaA. Reproduced with permission).

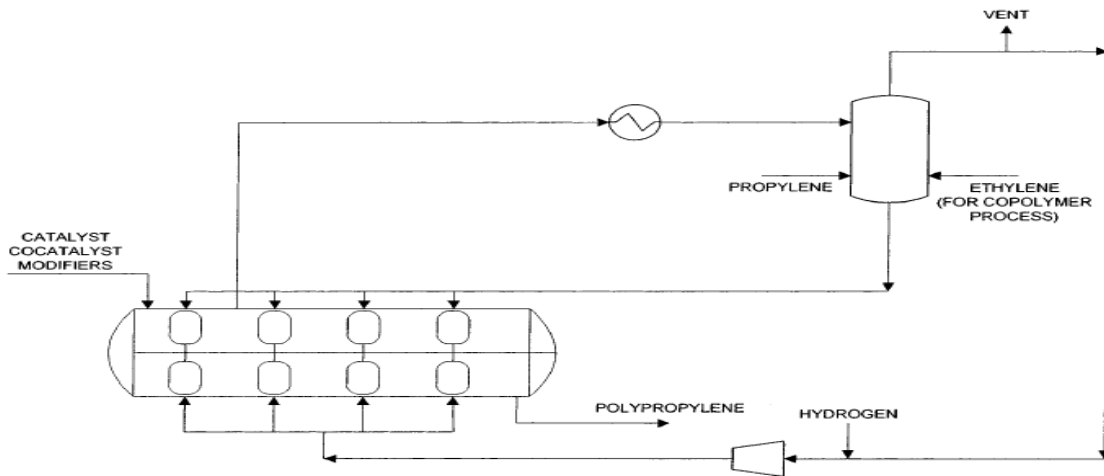


Figure 2.1e. Innovene gas-phase PP process using a horizontal stirred-bed reactor ³.

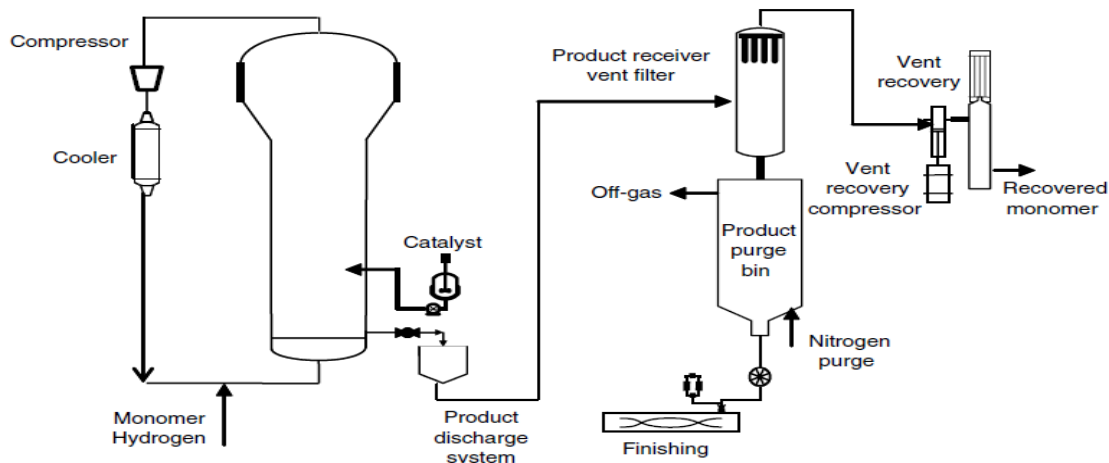


Figure 2.1f. Univation UNIPOL LLPDE process using a fluidized-bed reactor (Soares, J. B. P.; McKenna, T. F. L. *Polyolefin Reaction Engineering*, p. 116, **2012**. Copyright Wiley-VCH Verlag GmbH & Co. KGaA. Reproduced with permission).

2.4.5 Thermodynamics:

Thermodynamics is an essential component of the model. The perturbed chain statistical fluid theory (PC-SAFT) is one of the most useful thermodynamic models for simulating polyolefin processes^{3,29}. The PC-SAFT model is based on the perturbation theory. The underlying idea is to divide the total intermolecular forces into repulsive and attractive contributions. The model uses a hard-chain reference system to account for the repulsive interactions. The attractive forces are further divided into different contributions, including dispersion, polar, and association. A correct thermodynamic model is very important in predicting certain commercial targets like the polymer solution density (not the polymer pellet density which depends on MWW and SCB content^{11,18}). We use the polymer solution density to match the reactor residence time before estimating the kinetic parameters.

2.4.6 Global Kinetics versus Local Kinetics³⁰

Reaction kinetics, like thermodynamics, are expected to be a global phenomenon. As long as the same catalyst is used in all the reactors, a good model should be capable of covering the full range. Using different kinetics in different reactors significantly raises the degree of freedom of the problem, which is already enormously complex. Instead, we should treat the data from the different stages of the process as a sort of ‘natural experiment’ to further confirm a single set of rate parameters.

If we had samples after each stage, we could use the molecular weight distribution to further enrich our understanding of what is happening within the process. We have seen projects where engineers have used different kinetics in different reactors, or different kinetics for different product grades. We have also seen in some cases of force-fitting the kinetics where the maximum sites concentration (*max sites*) is not realistic, or the inhibition reaction and catalyst poisoning reaction rate constants may not be correct, resulting in the

incorrect catalyst activity predicted by the model. We always consider these symptoms of an imperfect model. Using local kinetic models may be ‘over-fitting’ the limited available data, which can lead to bad extrapolations away from the base-case conditions. Since the goal of modeling is usually to optimize the process to increase throughput, improve quality, or reduce energy consumption, it is important to be able to predict behavior outside the current operating envelope.

Additionally, when fitting a kinetic model, we should always use the reference temperature form of the kinetic expression, Eq. (1). This form makes the pre-exponential factor k_0 and the activation energy E independent of each other at T_r . Otherwise, small changes to E overwhelm the data fitting of the k values and the fitting algorithm usually fails. We also find it easier to compare rate constants when they are on a consistent reference temperature basis.

2.5. Methodology for Polyolefin Kinetic Estimation

Table 2.3 summarizes the important commercial production targets that we have considered for kinetic parameter estimation. The number of targets that can be used for estimation depends on the data availability. In our strategy to estimating kinetic parameters, we first try to match some production targets in a single catalyst site model and we fit the remaining targets after converting the single-site model into a multisite model. In this procedure, we consider the rate constants for all the reactions involved in the Ziegler Natta polyolefin kinetics, including the catalyst activation, initiation, propagation, chain transfer, deactivation and other polymer-specific reactions. The kinetic rate constants follow the Arrhenius form given in Eq. (1). For polyolefin reactors operating in a small temperature range, we only estimate the pre-exponential factor k_0 and keep the activation energy E constant with values from the literature. Our methodology for kinetic parameter estimation does allow us to estimate the activation energy if necessary.

Table 2.3 Production targets for single-site and multisite models

Single-Site Targets	Multisite Targets
Production Rate	PDI of polymer
MWN overall	MWN produced at catalyst site
Monomer Conversion	Mass fraction for polymer produced at each site
Co-monomer Conversion or SFRAC	Atactic fraction ATFRAC for each site for PP
Polymer solution density	Catalyst site inhibition fraction CISFRAC for each site for HDPE
Residence time	Rho /Polymer pellet density
Atactic fraction ATFRAC for PP	

2.5.1. Efficient Use of Software Tool: Data Fit

We develop models using Aspen Polymers and fit the kinetic parameters to plant data using the data fit tool. Data fit is an efficient nonlinear regression tool that allows the user to determine statistically acceptable, kinetic parameters from constant, or time-varying, or temperature-dependent laboratory measurements, or from matching the process simulation to plant targets. We can use both point data or time-profile data for regression. We need to define the data with reconciled input variables and a standard deviation. We estimate the model parameters using the data within the specified range.

The least-square regression objective function that the data fit minimizes is as follows:

$$f = \min_{X_p, X_{ri}} \frac{1}{2} \sum_{i=1}^{N_{set}} (W_i \times (\sum_{j=1}^{N_{exp}} (\sum_{i=1}^{N_{ri}} \left(\frac{X_{mri} - X_{ri}}{\sigma_{X_{mri}}} \right)^2 + \sum_{m=1}^{N_{rr}} \left(\frac{X_{mrr} - X_{rr}}{\sigma_{X_{mrr}}} \right)^2))) \quad (2.5)$$

$$\text{subject to} \quad X_{plb} \leq X_p \leq X_{pub}, \quad X_{rilb} \leq X_{ri} \leq X_{riub}$$

where:

N_{sets}	=	Number of data sets specified for regression
N_{expi}	=	Number of experiments in data set i
N_{ri}	=	Number of reconciled input variables
N_{rr}	=	Number of measure output variables
W_i	=	Weight for each data set i for regression
X_p	=	Vector of varied parameters
X_{mri}	=	Measured values of the reconciled independent variables
X_{ri}	=	Calculated values of the reconciled input variables
X_{mrr}	=	Measured values of the output variables
X_{rr}	=	Calculated values of the output variables
σ	=	Standard deviation specified for the measured variables

Since kinetic parameter estimation is a complex regression problem, we can vary some numerical parameters within the data fit to speed up the convergence calculations. We vary the maximum algorithm iterations and the maximum number of passes through the process flowsheet which are required to compute the residuals. We specify a bound factor which gives the upper and lower bounds for variables by multiplying by the standard deviation. We also specify the absolute sum-of-squares objective function tolerance, so that the problem converges whenever the objective function value is less than the tolerance value.

The tool performs the least-square regression using a trust region algorithm for parameter estimation. Specifically, the algorithm maintains an estimate of the diameter of a region, called the trust region, about the current estimate of the vector of varied values in which it can predict the behavior of the least-squares objective function. If an adequate model is found within the trust region, the region is expanded; if the model is a poor approximation, then the trust region is contracted. The tool also provides certain handles to implement the regression with the trust region optimization algorithm.

2.5.2 Flowchart of the Methodology for Kinetic Parameter Estimation

Figure 2.2 a and b shows our methodology for estimating kinetic parameters for polyolefin process models from plant data using simulation software tools. In the following, we discuss the details of the algorithm and present illustrative applications to commercial polyolefin processes. We also give some useful suggestions based on our experiences in guiding practicing engineers to apply the methodology to several dozen commercial HDPE, PP and LLPDE processes in the Asia-Pacific.

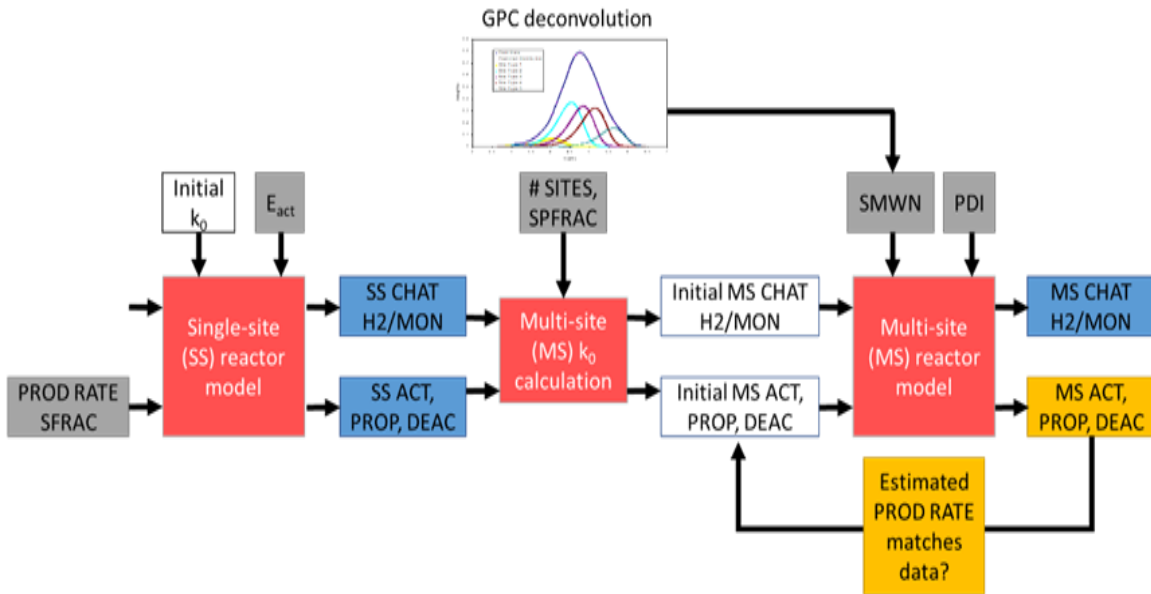


Figure 2.2a. The methodology for kinetic parameter estimation for polyolefin process models from plant data using simulation software tools (Summary)

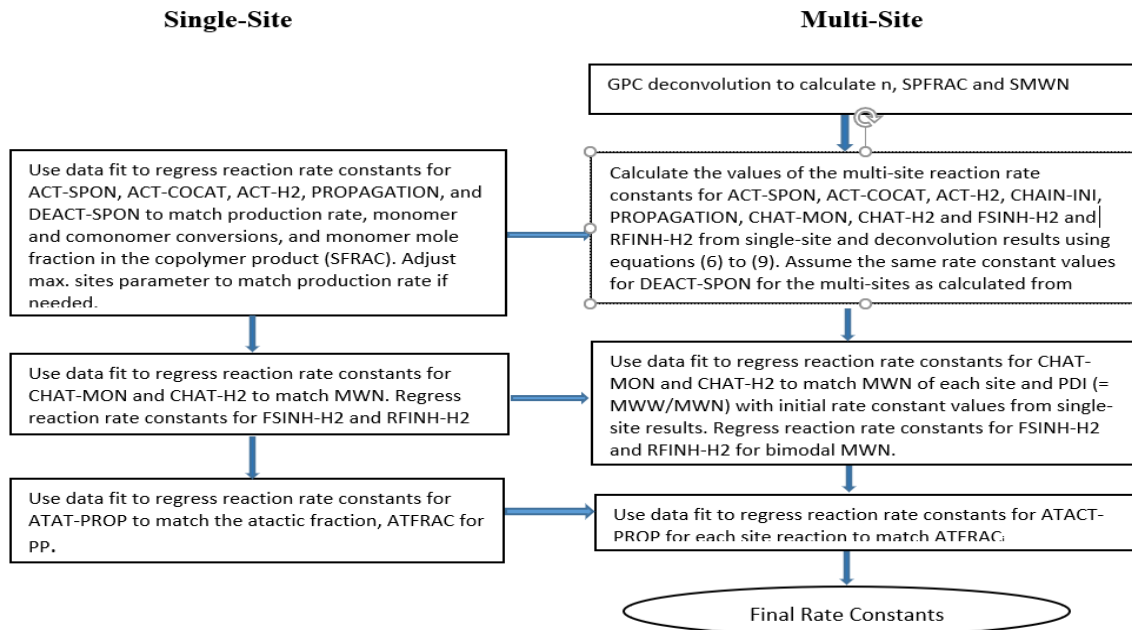


Figure 2.2b. The methodology for kinetic parameter estimation for polyolefin process models from plant data using simulation software tools (Detailed)

2.5.2.1 Multiple Product Grades and Single Active Catalyst Sites

We first make a single-site model and try to estimate the kinetic parameters based on single-site production targets for multiple product grades. Using the production rate data for multiple grades, the data fit tool enables us to *simultaneously* regress the reaction rate constants for catalyst activation (ACT-SPON, ACT-COCAT, and ACT-H2), propagation (PROPAGATION) reactions for monomer, and deactivation (DEAC-SPON) reactions, and any inhibition (FSINH-H2 and RSINH-H2) reactions if considered. This is different from most of the previous studies, including our previous work^{2,3}, which *sequentially* estimate these reaction rate constants.

Before matching the production rates, we must ensure that the residence time matches plant data. We can adjust the PC-SAFT thermodynamic parameters and change the mixing model equation to adjust the polymer solution density. The residence time of the reactor depends on the solution density. We estimate the rate constants for propagation (PROPAGATION) reactions for the monomer using the production rate for the homopolymer and monomer conversion. We use the production rate for the copolymer and the ratio of the reaction rates of comonomer to monomer (SFRAC) or conversion of comonomer to estimate the rate constants of the propagation reactions for the comonomer.

For PP, we need to ensure that the isotacticity of the homopolymer matches the plant data. We do so by including the atactic propagation (ATACT-PROP) reaction and estimate the rate constant using the atactic fraction (ATFRAC), which is the ratio of the atactic polymer formed over the total polymer. We want the calculated ATFRAC to be close to $1 - \text{isotacticity}/100$.

For HDPE, we also consider the inhibition of the catalyst due to the polymers since the rate of polymerization decreases with hydrogen concentration for ethylene-based polymer reactions. We usually estimate the forward inhibition and backward inhibition (FSINH-H2 and RSINH-H2) reactions using the MWN. In the single-site model, we can also match the weight-average molecular weights and use them to estimate the rate constants of chain transfer to hydrogen and monomer/comonomer.

Depending on data available, the melt index of polymer is also useful in matching the molecular weight of polymer. Melt index is usually a function of weight-average molecular weight (MWW), but for the case of polypropylene homopolymer, it is also a function of atactic fraction (ATFRAC).

In case SFRAC and comonomer content data are not available, we may use the final polymer pellet density to estimate the comonomer propagation rate constants, as the polymer density depends on the SCB and comonomer content.

Table 2.4 shows the major kinetic parameters that significantly affect the single-site production targets.

Table 2.4 Major kinetic parameters affecting the single-site production target

Single-Site Target	Major Kinetic Parameters Affecting the Target
Production Rate	Max sites parameter, propagation rate constant, catalyst activation, inhibition reaction
MWN overall	Chain transfer reactions –monomer and H2
Monomer conversion	Monomer propagation rate constant
Co-monomer conversion or SFRAC	Co-monomer propagation rate constant
Reactor residence time	Polymer solution density and thermodynamic property parameters
ATFRAC	Atactic propagation rate constant
Melt Index	Chain transfer reactions and ATFRAC
Polymer pellet density	Comonomer content/comonomer propagation rate constants

We illustrate the application of the methodology to estimating the kinetic parameters for modeling a commercial Mitsui HYPOL PP process. **Appendix A.1** gives details of our kinetic model and kinetic parameter estimation, including the reaction rate constants chosen and their initial values. We demonstrate below the efficient use of data fit tool for the simultaneous estimation of kinetic parameters.

Table 2.5 lists the plant data for single-site modeling for a commercial Mitsui HYPOL PP process of Figure 1c, and Figure 3 shows an Aspen Polymers simulation flowsheet of the process with the addition of one more fluidized-bed reactor, D204.

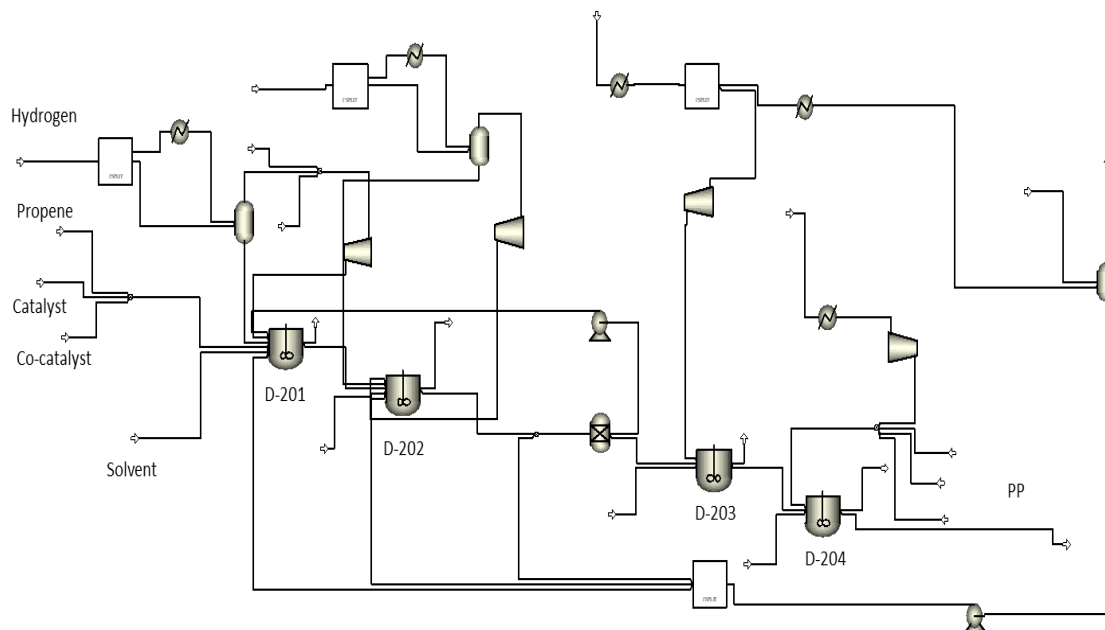


Figure 2.3. An Aspen Polymers simulation flowsheet of the Mitsui HYPOL PP process.

Table 2.5. Plant data for kinetic modeling a commercial Mitsui HYPOL PP process²⁹

			Grade 1	Grade 2
Data set	Process parameters	Reactor	Production target	Production target
PROD123	Polymer production rate (kg/hr)	D-201	1560	1560
		D-202	3120	3120
		D-203	6240	6240
		D-204	8600	8600
MWN123	Number-average molecular weight (MWN)	D-201	60000	76000
		D-202	63000	83000
		D-203	77000	88000
		D-204	80000	96000
SFRAC4	Ethylene content in copolymer, mole fraction	D-204	0.145	0.15
PDI	Polydispersity index	D-201	5.50	5.60

		D-202	5.52	5.70
		D-203	5.54	5.80
		D-204	6.00	6.20
H2/C3H6 mole ratio x 10E3	H2/monomer mole ratio in reactor overhead	D-201	188	17
		D-202	209	9.3
		D-203	15	1.7
		D-204	38	1.15

To simplify the kinetic parameter estimation, we begin by setting some kinetic parameters to be equal to each other. For example, we make the pre-exponential factors for propagation (PRPRE-EXP) from ethylene segment (C2-SEG) and from propylene segment (C3-SEG) to ethylene comonomer (C2H4) equal. Therefore, we use a Calculator (FORTRAN block) to make PRPRE-EXP PROPAGATION (C2-SEG/C2H4) equal to PRPRE-EXP PROPAGATION (C3-SEG/C2H4). Appendix A.1 gives additional details about this simplification.

Our data fit application includes the *simultaneous* execution of two regression runs for the first three reactors D201 to D203, and a regression run for the fourth reactor, D204 that focuses on copolymer production. First, *regression run RPROD123* varies the pre-exponential factors for spontaneous site activation (ACT-SPON), catalyst activation by cocatalyst (ACT-COCAT), propagation (PROPAGATION) reactions for monomer, and deactivation (DEAC-SPON) reactions, to match data set *PROD123* listed in Table 2.6 Next, *regression RMWN123* varies the pre-exponential factors for chain transfer of propylene segment and of ethylene segment to H2 and to propylene monomer to match data set *MWN123*. Lastly, *regression RD204* varies the pre-exponential factors for chain propagation of propylene segment and from ethylene segment to comonomer C2H4, and chain transfer from propylene segment and from ethylene segment to comonomer C2H4, to match the data sets *PROD4*, *MWN4* and *SFRAC4*.

Table 2.6 demonstrates that the data fit tool enables us to accurately estimate the kinetic parameters for the single-site model that have the most impacts on specific production targets (see Table 2.4) for the Mitsui HYPOL PP process. The comparison between model predictions and production targets shows minimum errors of 0.37% to 3.22%.

Table 2.6. Comparison of single-site model predictions with production targets obtained by data fit

	Grade one			Grade two		
Polymer production, kg/hr	D201	D202	D203	D201	D202	D203
Plant data	1560	3120	6240	1560	3120	6240
Prediction	1541	3153	6151	1538	3211	6236
% Error	1.18%	0.76%	0.83%	2.17%	2.39%	0.37%
MWN	D201	D202	D203	D201	D202	D203
Plant data	60000	63000	70000	80000	83000	88000
Prediction	61797	61511	68598	80547	82693	85167
% Error	3.06%	2.36%	2.00%	0.68%	0.37%	3.22%
	D204 Production, kg/hr	D204 MWN	D204 SFRAC, mole fraction	D204 Production, kg/hr	D204 MWN	D204 SFRAC, mole fraction
Plant data	8600	80000	0.145	8600	96000	0.150
Prediction	8812	78004	0.142	8730	95099	0.152
% Error	2.45%	2.49%	1.80%	1.52%	0.94%	1.60%

2.5.2.2 Multisite Model and Deconvolution Analysis

We now convert our single-site model into a multisite model by changing the specified number of sites in the model. We then make use of the gel permeation chromatography (GPC) analysis of the polymer samples.

Using the GPC characterization data, we apply the deconvolution procedure first presented by Soares and Hamielec³². We deconvolute the MWD to determine the most probable chain length distribution (CLD) for each active catalyst site. We assume that the CLD of the polyolefins produced by each active site of Ziegler-Natta catalyst follows the Flory distribution.

We represent the instantaneous weight chain length distribution (WCLD) by averaging the distribution of each catalyst site in equation (2.6)

$$W \log M = \sum_{i=1}^n w_i (2.30268 \times M^2 \tau_i^2 e^{-M \tau_i}) \quad (2.6)$$

where $W \log M$ is the mass fraction of the chains of polymer having molecular weight M in logarithmic scale; n is the total number of active sites; w_i is the mass fraction of polymer formed at each site i ; τ_i is the fitting parameter for each site i , which is equal to the inverse of the number-average molecular weight of polymer formed at each site, that is, $\tau_i =$

$1/MWN_i$. Here, w_i and MWN_i are equivalent to the production targets SPFRAC and SMWN defined previously.

We fit the model in equation (6) to the experimental GPC data and estimate the parameters by minimizing the difference between the model and experimental values. We estimate the minimum number of Flory distributions, n , required to describe the experimental MWD, which in turn gives the minimum number of active catalyst sites. We also estimate the MWN of polymer produced at each active catalyst site, MWN_i and the mass fraction of polymer produced at each active site, w_i . Appendix A.2 presents details of our kinetic model and kinetic parameter estimation, including the reaction rate constants chosen and their initial values for this slurry HDPE process.

Table 2.7. Deconvolution results for a representative LLDPE homo-polymer sample

Active catalyst site type, i	Polymer weight fraction, w_i	τ_i (or $1/MWN_i$)	MWN_i
1	0.562	3.156e-5	31685
2	0.299	9.17e-6	109012
3	0.139	1.28e-4	7763

Figure 2.4 plots the weight chain length distribution as given in equation 6 for the example of Table 2.7. The figure shows the weight chain length distribution for each catalyst active site and distribution of the plant data. The sum of the three individual distributions of the catalyst site weighted with the mass fraction of polymer formed for each site predicts the chain length distribution of the polymer.

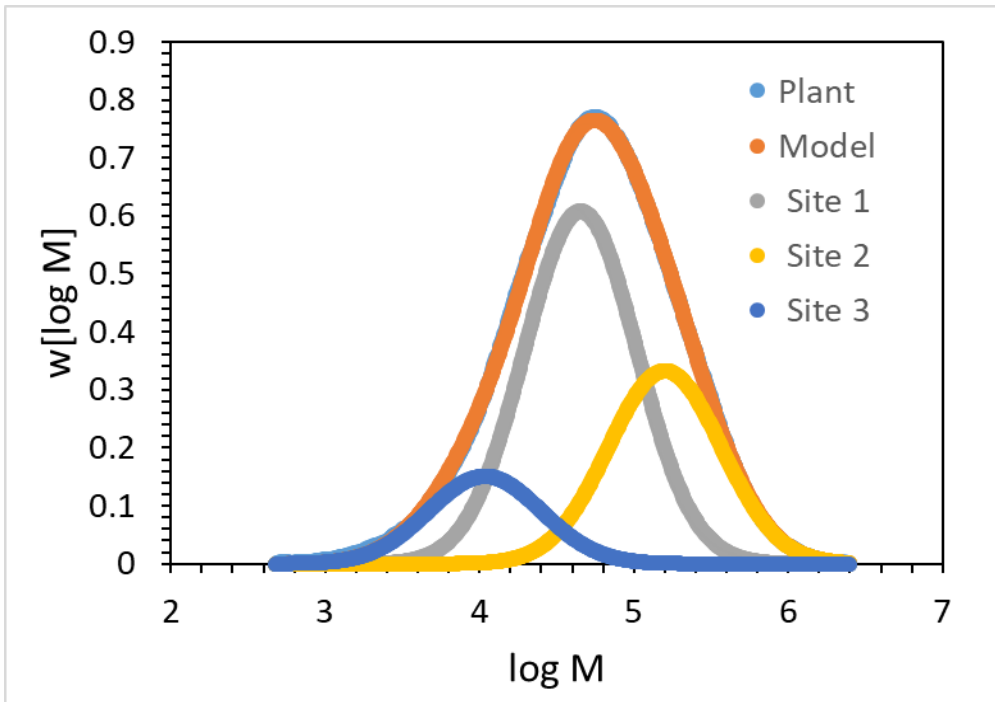


Figure 2.4. GPC deconvolution of a homopolymer sample from a UNIPOL LLDPE process

We use the rate constants from single-site modeling and the deconvolution results of Table 2.8 to further calculate the rate constants for the multi-site kinetics. “We calculate the pre-exponential factors for catalyst activation reactions (ACT-SPON, ACT-COCAT and ACT-H2) at each site k_{ai} from the single-site value k_a ,

$$k_{ai} = \frac{k_a}{n} \quad (2.7)$$

Eq. (2.7) results from the fact that the concentration of potential catalyst sites is identical for both single-site and multisite models, but the concentration of vacant catalyst sites must be divided by the number of site types, n . We resolve this issue by dividing the pre-exponential factors for catalyst activation reactions by the number of catalyst site types, n .

We estimate the pre-exponential factor for the chain initiation reaction (CHAIN-INI) at each site by

$$k_{ii} = k_i * w_i * n \quad (2.8)$$

We calculate the pre-exponential factor for the propagation reaction (PROPAGATION) at each site by

$$k_{pi} = k_p * w_i * n \quad (2.9)$$

Equations (2.7) to (2.9) give the actual values of the activation, chain initiation and propagation rate constants for the multisite model directly. Based on our modeling experience with polyolefin processes, further data fit runs that vary these reaction constants, obtained from applying equations (2.7) to (2.9), to match the relevant data sets for production rate, MWN, SFRAC, etc. within the multisite model would produce only minimum or no changes to the reaction rate constant values.

We calculate the initial value for pre-exponential factor for the chain transfer reaction (CHAT-MON and CHAT-H2) at each site by

$$k_{ci} = k_c * w_i * n \quad (2.10)$$

It is important to maintain the same relative contributions of chain transfer to hydrogen (CHAT-H2) and to monomer (CHAT-MON) from the same single-site model in the multisite model, in order to preserve the sensitivity of these reactions to the concentrations of hydrogen and monomer”²⁻⁴. We do this by using a Calculator (FORTRAN block) in Aspen Polymers.

To estimate the rate constants for chain transfer to H2 and to monomer for each site, we regress the PDI and MWN data for the polymer stream exiting each reactor, along with the SMWN results from GPC analysis. For more accurate estimates of these kinetic parameters, it is helpful to have these data obtained with varying H2 and monomer flow rates. In the example presented in Tables 5 and 8, we use the measured PDI and MWN data for the polymer stream exiting each reactor to estimates the chain transfer rate constants. We should also make sure that measured MWD matches the model MWD by matching the SMWN and SFRAC values obtained from GPC analysis.

The other rate constants, such as the deactivation rate constants (DEACT-ACT and DEACT-TCA), and inhibition reactions (FSINH-H2 and RSING-H2), are all identical to

those of the single-site model. If we consider the catalyst inhibition reactions (FSINH-H2 and RSING-H2), we must ensure that the total CISFRAC for the multisite model is the sum of CISFRAC_i for all single sites. Also for the PP model, the ATFRAC considered should be the same for each site and matching the plant data. After updating all the rate constants, the multisite model matches all the targets.

To simplify the kinetic parameter estimation, we begin by setting some kinetic parameters to be equal to each other. We make the pre-exponential factors for chain transfer (CTPRE-EXP) from ethylene segment (C2-SEG) and from propylene segment (C3-SEG) to propylene monomer (C3H6) and to ethylene co-monomer (C2H4) equal. Therefore, we use a Calculator (FORTRAN block) to make PRPRE-EXP CHAT-MON (C2-SEG/C3H6) equal to PRPRE-EXP CHAT-MON (C3-SEG/C3H6), and make PRPRE-EXP CHAT-MON (C2-SEG/C2H4) equal to PRPRE-EXP CHAT-MON (C3-SEG/C2H4). We can see the pre-exponential factor and activation energy values for these reaction rate constants in Appendix A.3.

We apply data fit to execute a *regression run RPDI* that varies the reaction rate constants for chain transfer to hydrogen (CHAT-H2) and to monomer C3H6 and comonomer C2H4 (CHAT-MON) in order to match the data set *PDI* (and hence the MWW data) given in Table 2.5 from reactors D201 to D204 for two grades with different H2/C3H6 ratios in the reactor overheads. Section A.1.6 shows the resulting reaction rate constants for the multisite model, and we note that the resulting pre-exponential factors for chain transfer to hydrogen and to monomer are indeed different. Table 2.8 compares minimum errors between the model predictions and plant data for PDIs. We note the percent errors between our model predictions and plant data in Table 6 (0.37% to 3.06%) and Table 2.8 (0.25% to 1.84%) are equivalent to or smaller than those in reported modeling studies for polyolefin processes (approximately 5% in our previous work for HDPE ² and for PP ³).

Table 2.8. Comparison of multi-site model predictions with production targets obtained by data fit

	Grade one				Grade two			
PDI	D-201	D-202	D-203	D-204	D-201	D-202	D-203	D-204
Plant data	5.50	5.52	5.54	6.00	5.60	5.70	5.80	6.20
Model Prediction	5.48	5.50	5.64	5.95	5.62	5.67	5.76	6.26
Error %	0.25%	0.37%	1.84%	0.67%	0.33%	1.42%	0.68%	1.03%

Table 2.9 shows the different reaction constants that have the major effect on the production targets in a multisite model. We can use sensitivity analysis as described in Section 5.3 to quantify the effect of varying kinetic parameters on the simulation targets.

Table 2.9. Major kinetic parameters affecting the multi-site simulation targets

Multisite Targets	Major Affecting Kinetic Parameters
1. PDI of polymer	Chain transfer reaction rate constant
2. MWN produced at catalyst site and overall MWN	Chain transfer reaction rate constant for each site
3. Mass fraction for polymer produced at each site and overall production rate	Propagation reactions for each site
4. ATFRAC for each site	Atactic propagation reaction rate constant
5. Polymer solution density	Comonomer rate constants

2.5.3 Efficient Use of Software Tool: Sensitivity Analysis

Sensitivity analysis enables us to quantify the dependence of the production targets on the reaction kinetic parameters. The analysis helps us in deciding which directions to vary the operating conditions in order to match the production targets. Sensitivity analysis also helps in validating the kinetic estimation procedure for polyolefins. We illustrate below some examples of sensitivity analysis of the different polyolefin processes that we have modeled and estimated kinetics using our procedure.

Appendix A.3 gives details of our kinetic model and kinetic parameter estimation, including the reaction rate constants chosen and their initial values for the Unipol LLPDE process. Applying the sensitivity analysis, we illustrate in Figure 2.8a how varying the reaction rate constant for chain transfer to hydrogen, $k_{th,i}$ of just one of the three active site affects the final LLPDE polymer properties, including the polydispersity index PDI, the number-average molecular weight at the chosen catalyst site SMWN, and the overall MWN. As we increase the reaction rate constant for chain transfer to hydrogen, both the SMWN and MWN decreases, while the PDI increases gradually. In other words, we can vary the hydrogen flow rate to change the rate of chain transfer reaction in order to achieve the desired MWN and PDI.

As another example, for the Mitsui Hypol PP (Appendix A.1) illustrates that varying the reaction rate constant for chain transfer to monomer, $k_{tm,i}$ results in similar trends of changes in PDI, SMWN and MWN, as with the chain transfer to hydrogen. The similar trends observed in Figures 2.5a-b below, support our approach of applying the same methodology for kinetic parameter estimation for modeling different commercial polyolefin processes from plant data.

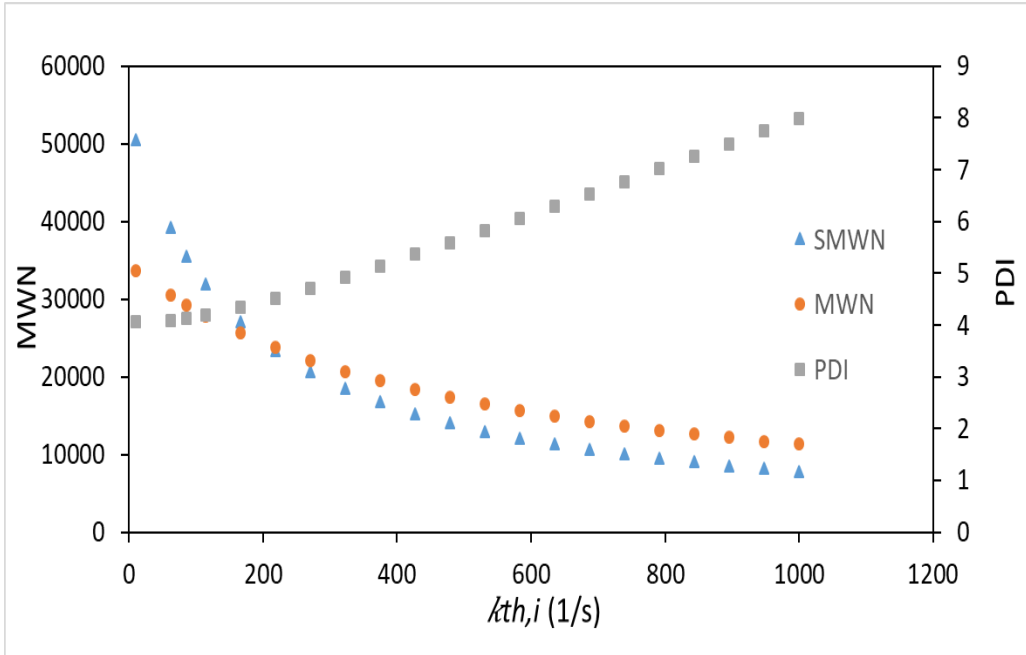


Figure 2.5a. Sensitivity of the PDI, MWN and SMWN for the Unipol LLDPE process on the pre-exponential factor of the reaction rate constant for chain transfer to hydrogen

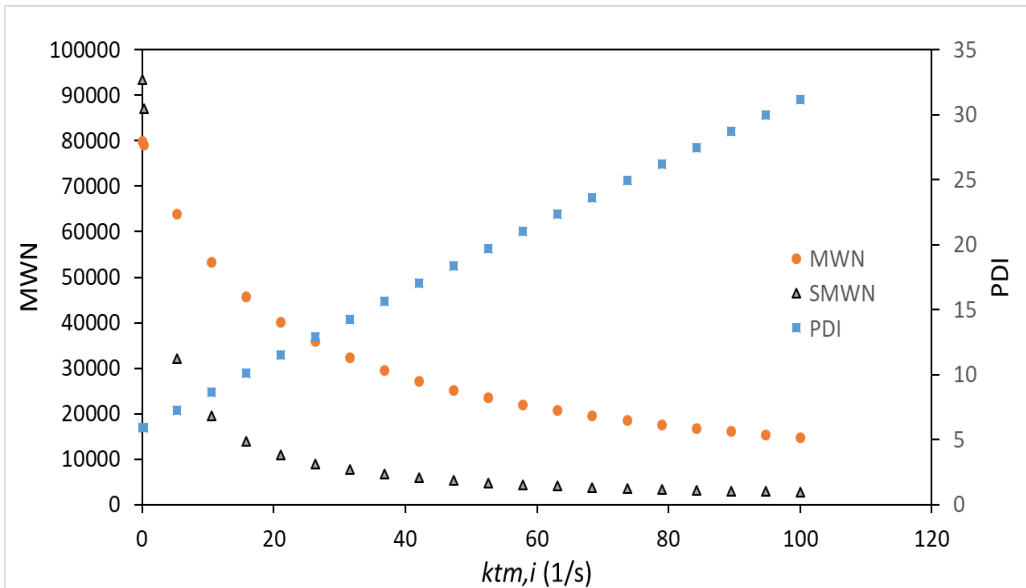


Figure 2.5b. Sensitivity of the PDI, MWN and SMWN for the Unipol LLDPE process on the pre-exponential factor of the reaction rate constant for chain transfer to monomer

We demonstrate the further use of sensitivity analysis for the Unipol LLDPE process. Figure 2.6 a shows how increasing the pre-exponential factor of the propagation rate constant, $k_{p,i}$ for one of the three active sites increases the production rate and mass fraction of polymer produced at that site (SPFRAC).

Appendix A.4 gives details of our kinetic model and kinetic parameter estimation, including the reaction rate constants chosen and their initial values for the Basell Spheripol PP process . In Figure 2.6b, we show how increasing the atactic propagation rate constant increases the atactic fraction, ATFRAC, for the Spheripol PP process.

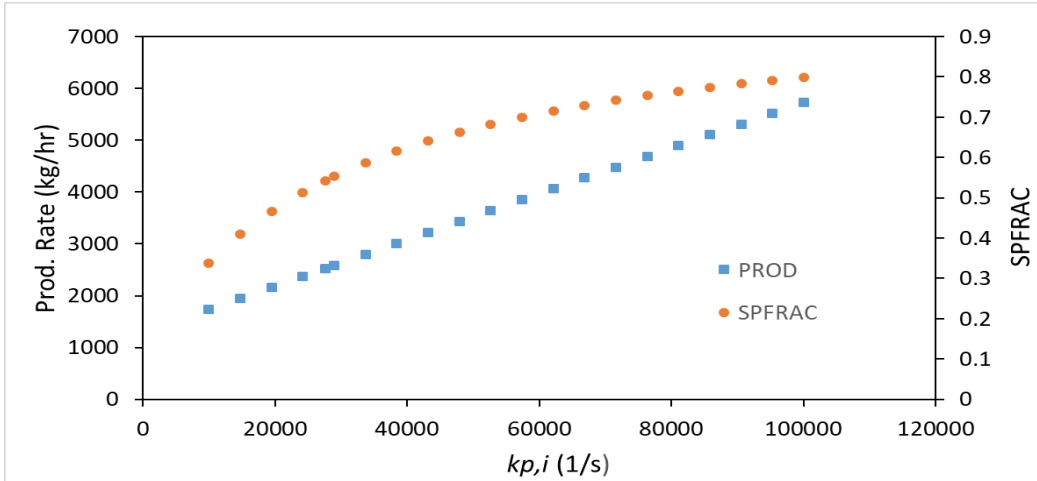


Figure 2.6a. The sensitivity of the a)Production rate and SPFRAC for the Unipol LLPDE process to changes in the propagation reaction rate constant

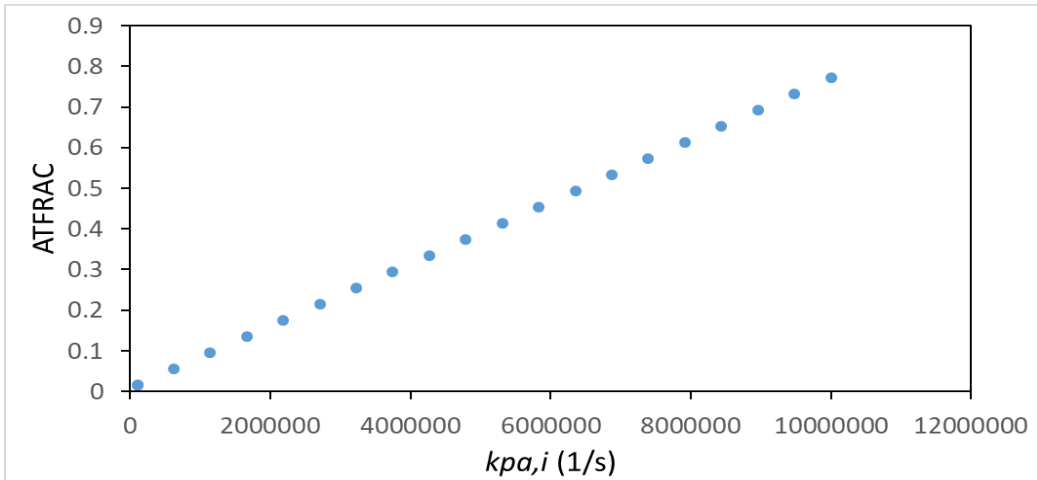


Figure 2.6b. The sensitivity of the atactic fraction ATFRAC to changes in the atactic propagation reaction rate constant for the Spheripol PP process.

For the Mitsui slurry HDPE process with serial reactor configuration we show in Figure 2.7- a-b showcase the sensitivity of the polymer production rate to changes in the reaction rate constants for catalysts activation by cocatalyst, $k_{act,i}$ and for spontaneous catalyst deactivation $k_{ds,i}$ for one of the five active catalyst sites.

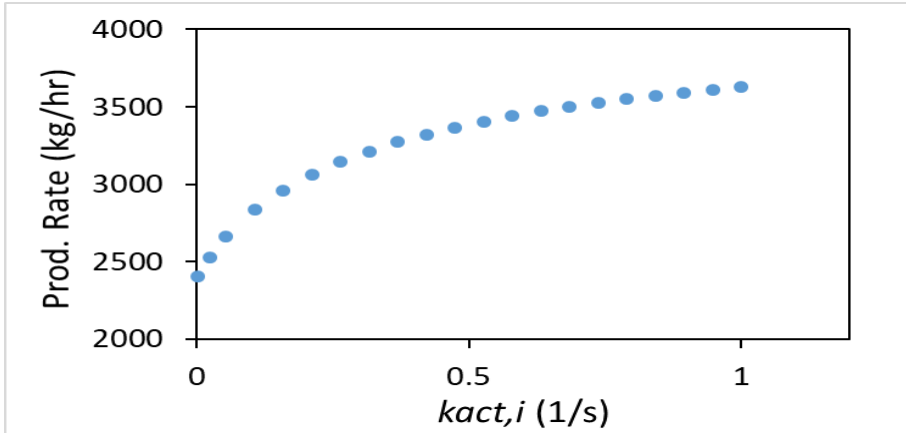


Figure 2.7a. The sensitivity of the production rate for the slurry HDPE process to changes in the reaction rate constant for catalyst activation by cocatalyst

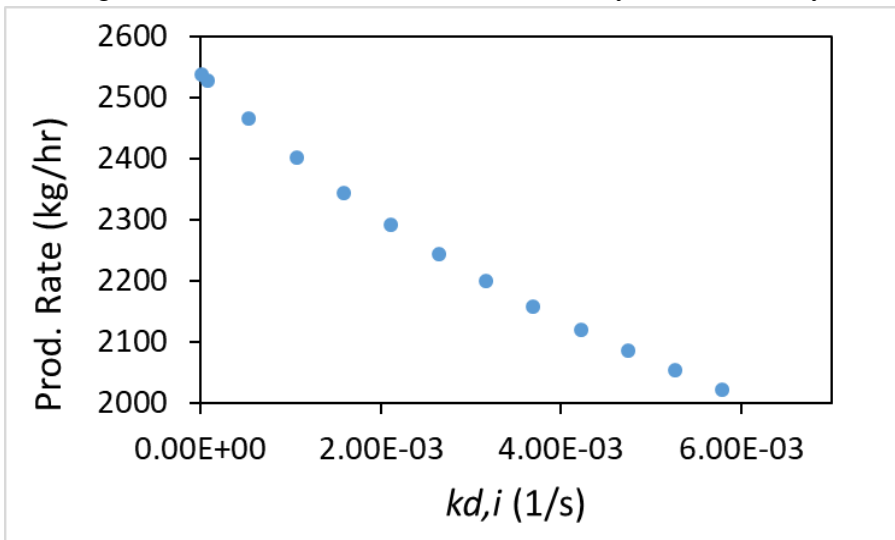


Figure 2.7b. The sensitivity of the production rate for the slurry HDPE process to changes in the reaction rate constant for spontaneous catalyst deactivation

Figure 2.8 illustrates the sensitivity of the MWD from a Mitsui slurry HDPE process changes in the reaction rate constant for forward catalyst inhibition by hydrogen, $k_{finh,i}$, for two different of the five active catalyst sites. The MWD of the HDPE produced from a single reactor can change from unimodal to bimodal. This happens since the difference in the rate of inhibition for different catalyst sites.

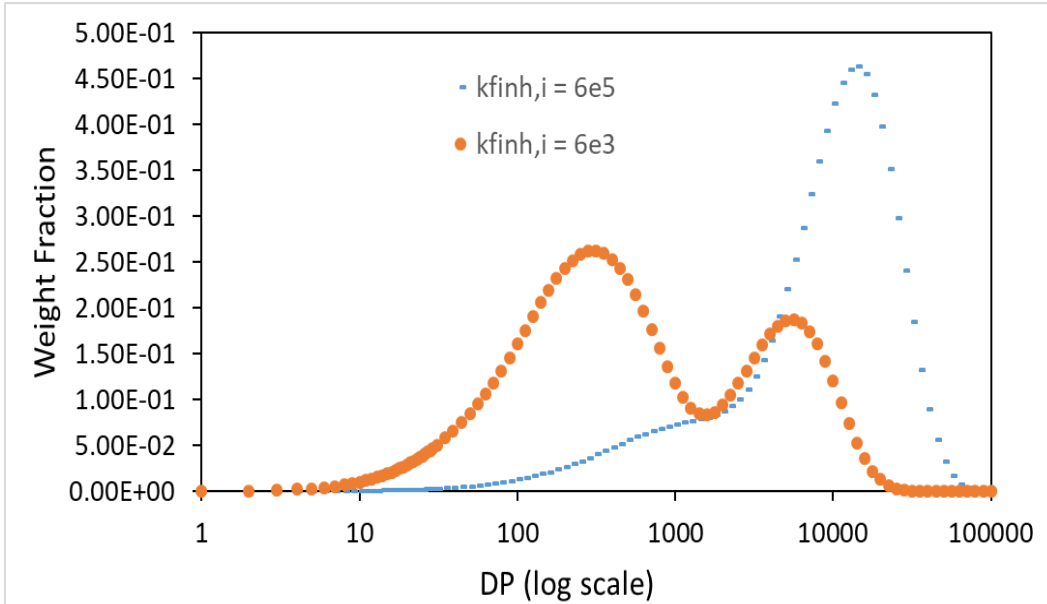


Figure 2.8. Sensitivity of the MWD from a Mitsui slurry HDPE process to changes in the reaction rate constant for catalyst inhibition for two different of the five active catalyst sites.

Figure 2.9 shows the effect on the production rates for the two horizontal bed reactors (represented as P1, P2 in the figure 2.10) in the Innovene gas-phase PP process by varying the pre-exponential rate constant of propagation reaction for a particular active site.

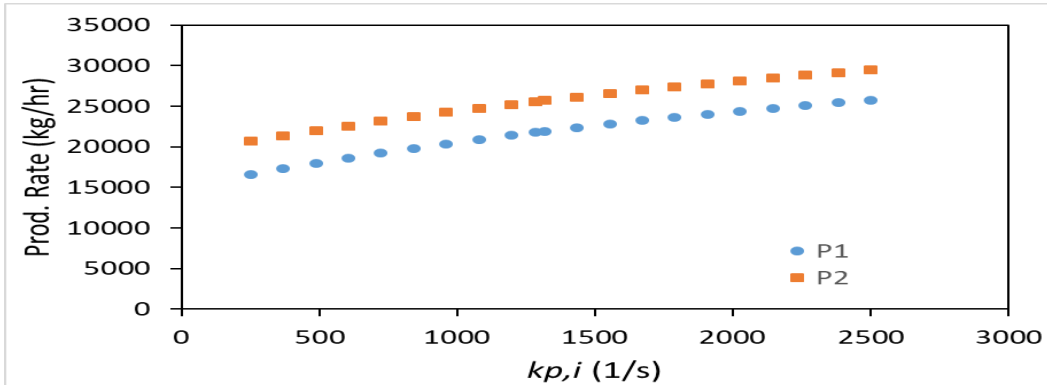


Figure 2.9. The sensitivity of the production rate from an Innovene gas-phase PP process to changes in the propagation reaction rate constant.

2.5.4 Efficient Use of Software Tool: Design Specification

Design specification (design spec) is an important tool that supports process modeling and kinetic estimation. While sensitivity analysis quantifies an increasing or a decreasing trend of a production target when varying a reaction rate constant within a chosen range of values, applying the design spec enables us to identify the reaction rate constant value within the chosen range to reach a specific production target.

Design spec is particularly useful in converging models of polyolefin processes having recycle loops. We can fix a particular ratio of components in a recycle stream and the model can vary input flow rates to maintain the ratio. As an illustration, in the Spheripol PP

process (Appendix A.4), we can use a design spec to maintain the ratio of ethylene to propylene in a recycle stream into the fluidized-bed reactor where the stream is a combination of the overall recycle stream and a feed of ethylene and hydrogen. Design spec varies the flow rates of ethylene (comonomer) and the hydrogen to maintain the desired ratio of ethylene and propylene in the recycle stream. Similarly, we can use another design spec for the recycle flow into the loop reactor by varying the flow of the propylene and hydrogen in the feed stream. Figure 2.10 show a flowsheet of the Spheripol PP process with the design specs ³¹.

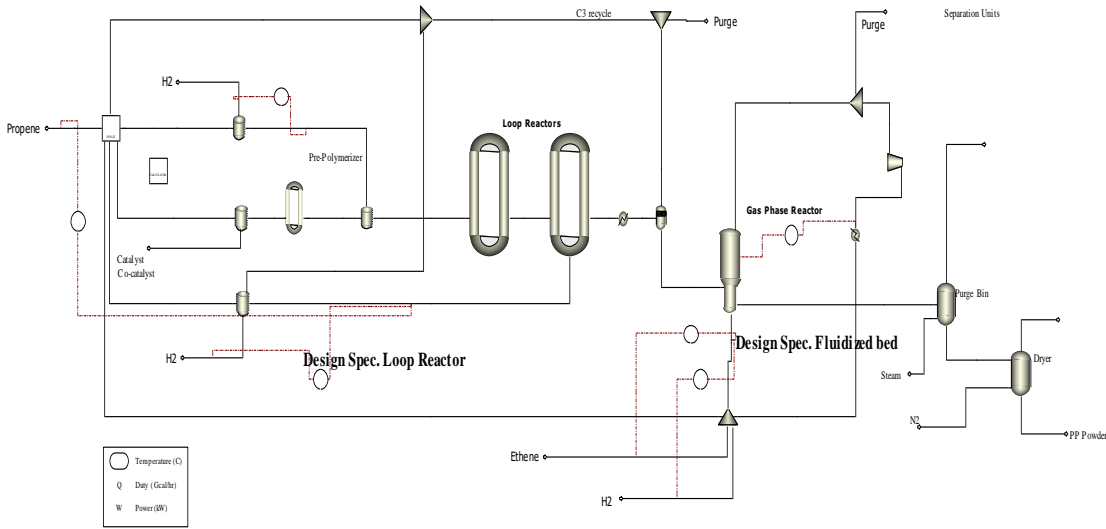


Figure 2.10. Spheripol PP process flowsheet indicating the design specification. Specifically, for the Spheripol PP model, we define the design specs as follows:

- 1) Design specification for the hydrogen mass fraction in the recycle stream entering the loop reactor, while the manipulated variable is the make-up hydrogen flow rate
- 2) Design specification for ratio of propene to ethylene in the recycle stream entering the fluidized-bed reactor, while the manipulated variable is the flow rate of ethane.

Table 2.10 shows the design spec results.

Table 2.10: Design specification for the Spheripol PP process

Design spec	Target Value	Model Result	Initial Vary (kg/hr)	Final Vary (kg/hr)	Range set (kg/hr)
1	4 e-5	3.9e-5	0.1	0.16	0.01 -10
2	0.5	0.48	1000	3250	5- 1000

2.5.5 Model Applications

A polyolefin process model validated by plant data can have many useful applications. The model will be helpful for the capacity expansion of the current plant. The model will also be useful in the process development stage for a new plant. We can use the validated model to study the effect of changes in process variables on production targets.

We can use the model to change certain production target, while maintaining the same value for other targets. As an example, we can vary certain process conditions to make polymer grades of different MWNs for the same throughput as shown in Figure 2.11. It shows a sensitivity analysis for the effect of changes in hydrogen flow rates on MWN, while the production rate remains same for the UNIPOL LLDPE process.

In another application of model, we can increase the throughput, while keeping the same MWN using design specification and we demonstrate this on the UNIPOL LLDPE process as well. We use design specification to vary the hydrogen flow rate to keep the same MWN at 29000 approximately, while increasing the production rate of LLDPE from 2400 to 3200 kg/hr. Table 11 summarizes the results of the UNIPOL process design specification. Lastly, when combined with process control and optimization techniques, a validated model can be useful for polymer quality control and effective polymer grade changes.

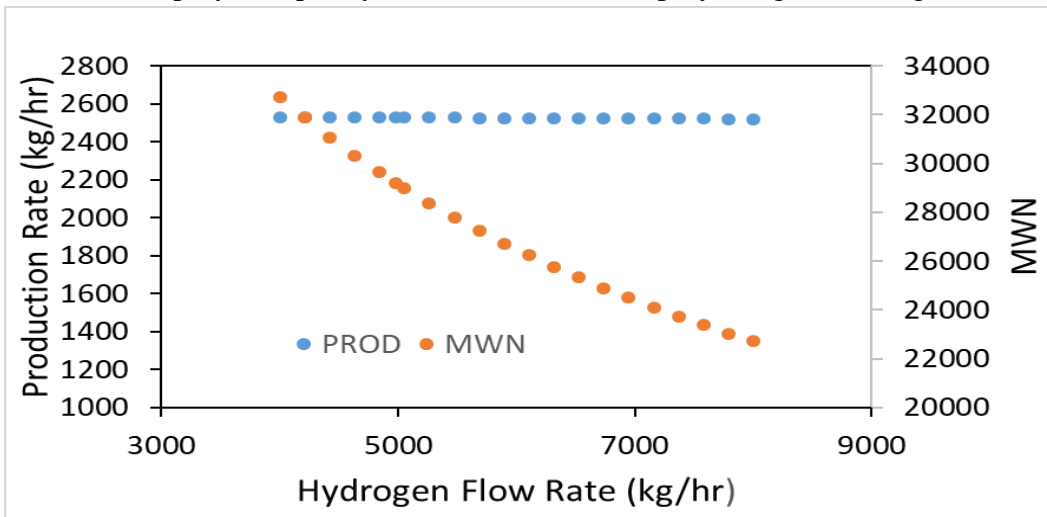


Figure 2.11. Sensitivity Analysis of the MWN and production rate on changes in hydrogen flow rates on the Unipol LLDPE process

Table 2.11. Design specification for the UNIPOL LLDPE process

Target MWN	Model MWN	Initial H2 flow (kg/hr)	Final H2 flow (kg/hr)	Range set (kg/hr)
29194	29217	4938	7515	3000-9000

2.6. Key Points in Modeling Some Industrial Polyolefin Process

2.6.1. Modeling Polymer Phase Equilibrium in Slurry HDPE Process

In the reactor, ethylene molecules react to form long polymer chains. In the slurry process, the reactor temperature (70 to 85 °C) is below the melting point of the polymer (140 °C). The polymer molecules solidify upon formation, creating a slurry system. “In the actual process, the solid polymer does not interact thermodynamically with the other components in the reactor. Our primary assumption in phase calculations is that *the polymer is dissolved in the liquid phase with the solvent*, as would be the case in solution

polymerization of ethylene, where the reactor temperature would be above the melting point of the polymer. Although this modeling simplification does not represent the physical picture of what is happening in the slurry polymerization of ethylene, the effect of it on thermodynamic modeling is relatively small. In reference 2 Khare et. al. have presented quantitative evidence to demonstrate that we can make this assumption without undermining the robustness of the reactor model. The details of slurry HDPE model are shown in Appendix A.2.

2.6.2. Modeling of Horizontal Stirred-Bed Gas- Phase Reactor for PP manufacturing

During steady-state operation of the gas phase PP process, the polymer level remains constant along the reactor length of the horizontal stirred bed reactor. The paddles along the reactor agitate the polymer only mildly, and the solids are not fluidized³⁴. The polymer phase essentially experiences plug flow conditions along the reactor length. We can simulate the plug flow situation by using several continuous stirred-tank reactors (CSTRs) configured in series. Experimental studies on the residence-time distribution (RTD) of polymers produced in horizontal stirred-bed reactors suggest that the polymer RTD is equivalent to that produced by three to five CSTRs³⁴. Each CSTR receives liquid and vapor recycled from the overhead condenser, which includes fresh monomer and hydrogen. Only the first CSTR receives fresh catalyst and co-catalyst. The temperature and pressure are the same for all zones.

The concept of residence time is significantly different between this situation and that for multiple CSTRs in series. Furthermore, a residence-time calculation requires knowledge of the volumetric holdup in the reactor. We cannot measure the volume holdup very accurately because the paddles are always agitating the polymer and there is a void fraction associated with the solid phase. Therefore, we do not use residence time as a simulation target in the model and instead use reactor mass holdup. In the simulation, we constrain the CSTRs to the same polymer mass to maintain the same level along the bed length. This results in monotonically decreasing residence times for the four CSTRs corresponding to a given stirred-bed reactor, which conforms to reported experimental results³⁴.

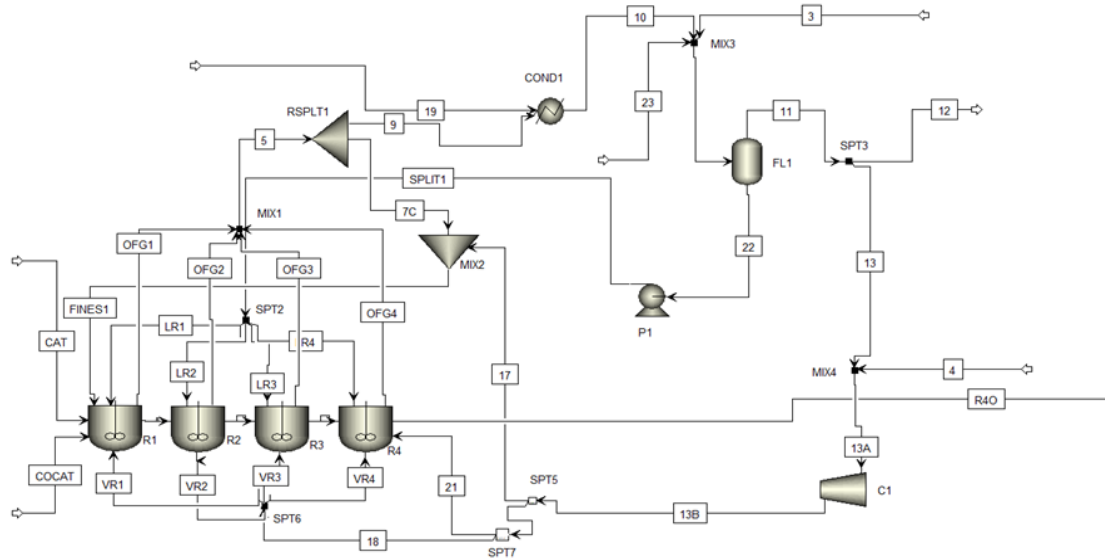


Figure 2.12. The front end of a two-reactor system for producing gas-phase PP polymer using stirred-bed reactors (closed-loop).

Figure 2.12. showcases a part of the process flowsheet for the Horizontal Stirred bed Gas phase PP process

2.6.3. Condensed Mode Modeling of UNIPOL LLDPE process

U. S. patents 454399A and 4588790 by Jenkins et. al. ³⁵⁻³⁷ present the concept of condensed mode cooling in ethylene polymerization in a fluidized-bed reactor (FBR). According to Jenkins et. al. ³⁶, condensed mode cooling in a FBR for an exothermic polymerization reaction cools the recycle stream to below its dew point and returns the resulting two-phase fluid stream to the reactor in order to maintain the fluidized bed at a desired temperature above the dew point of the recycle stream. This can increase the yield of polymer production, among other significant benefits. McKenna ³⁸ presents a comprehensive review and detailed analysis of condensed model cooling in ethylene polymerization. He illustrates the concept of condensed mode cooling with a. We summarize his basic analysis below.

Figure 2.15. An illustration of a fluidized-bed reactor (FBR) system for ethylene polymerization under condensing mode operation ³⁸. In the figure, ICA represents an induced condensing agent.

First of all, we note that heat removal is the number one factor limiting the production rate of polyethylene on an industrial scale. For a fluidized-bed polymerization reactor system producing LLPDE and PP, such as the UNIPOL process of Figure 2.15 with modeling details, McKenna ³⁸ notes that the melting point of a typical LLPDE is on the order of 110°C, and a typical reactor operating temperature is 85°C to 95°C. Therefore, we have a very little margin for error in terms of heat removal. In order to understand the tools

available for maximizing the heat removal, we present a simple enthalpy balance around a gas-phase FBR by McKenna which after simplifying looks the same as below.

$$R_p V_R = \frac{F_{g,in} C_{pg,in} (T_R - T_{g,in}) + UA(T_R - T_W) + Q_{vap}}{-\Delta H_p}$$

(2.11)

$F_{g,in}$ and $F_{g,out}$ = the inlet and outlet mass flow rates of process gas stream

$F_{s,out}$ = the outlet mass flow rate of the solid polymer stream

$C_{pg,in}$, $C_{pg,out}$ and $C_{ps,out}$

= the heat capacities of the inlet and outlet process gas stream, and of the solid polymer stream

$T_{g,in}$, $T_{g,out}$, $T_{s,out}$ and T_{ref} =

the temperatures of the inlet and outlet process gas stream, of the outlet solid polymer stream, and the reference temperature for the calculation of the enthalpy

U = the overall heat transfer coefficient

A = the surface area of contact between the reactor wall and the powder bed

T_R and T_W = the average temperatures of the reactor bed and the bed wall

Q_{vap} = the total enthalpy of change due to evaporation of any liquid in the reactor

R_p = the rate of reaction per unit volume of the reactor bed

V_R = the volume of the reactive bed

ΔH_p = the overall enthalpy of polymerization

What can we learn from this defining relationship for maximizing our polymer production rate, $R_p V_R$?

(1) The reactor temperature T_R (85° to 95°C) has a very narrow operating range for producing LLPDE, as the melting temperature of LLPDE is about 110°C and higher bed temperature tends to promote softening and sticking of the polymer particles.

(2) It is difficult to increase the overall heat transfer coefficient between the reactor wall and the powder bed. Increasing the gas velocity through the reactor may cause changes to the fluidizing medium.

(3) This basically leaves changes to the heat capacity $C_{pg,in}$ of the inlet process gas stream and to the total enthalpy due to evaporation of any liquid in the reactor Q_{vap} as our manipulative variables for maximizing the polymer production.

The conclusion is that we can use the composition and phase conditions of the feed stream (only the inert components obviously) to increase the amount of heat that can be removed, thus increasing the polymer production rate. As illustrated in Figure 2.15, the feed to the bottom of the reactor below this distributor plate is composed of ethylene (monomer), nitrogen (inert), comonomer, hydrogen (chain transfer agent) and at least one *induced condensing agent (ICA)* that is a partially liquefied, chemically inert species. An ICA is typically an alkane. Isomers of butane, pentane and hexane appear to be most common, as referred to in the original patents^{36,37}.

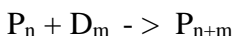
2.7. Metallocene Polymerization Modeling

Till now we have only talked about Ziegler Natta catalyst we will briefly touch upon the modeling using Metallocene catalysts. Polymerization kinetics using a metallocene catalyst system include most of the reactions for Ziegler-Natta catalysts described in Section 2.2, except for two differences. First, a metallocene catalyst system mostly exhibits only a single active catalyst site, and results in a narrow molecular weight distribution. Second, a metallocene catalyst system includes additional reactions involving terminal double bond (TDB) end groups that are absent in the traditional Ziegler-Natta polymerization kinetics.

Hagg, et al.³⁹ have presented a generic reaction mechanism, reaction rate equations and experimental reaction rate constants for an EPDM (ethylene propylene diene) terpolymerization using a metallocene Et(Ind)₂ZrCl₂/MAO catalyst system. Since we do not have ENB (ethylidene norbornene) in Aspen plus database we showcase a methodology to produce EPM (ethylene-propylene copolymer) instead of EPDM with the same kinetics.

Polymerization with a metallocene catalyst system typically leads to the formation of long chain branching (LCB), but the LCB frequency is usually small. The long chain branches likely result from chain propagation reactions involving a growing polymer chain and a terminal double bond on a dead polymer chain. Polymer chains with terminal double bonds are formed by some of the chain transfer reactions. To form long chain branches, the metal catalytic center must be open to provide a favorable reactivity ratio for the macromonomer.

Aspen Polymers tracks the concentration of TDB end groups on the dead polymer chains through a segment called TDB Segment, which typically has one less hydrogen atom than the related repeated segment. We specify a C₃H₅-TDB end segment (C₃H₅-E) corresponding to a C₃H₆ SEG repeated segment (C₃H₆-R). TDB segments are generated through chain transfer reactions and are consumed through the TDB polymerization reaction as shown in equation below.



P_n, P_{n+m} are the active segment (C₃H₆-R/C₂H₄-R) and D_m is the TDB end segment (C₃H₅-TDB).

We set the TBD-frac greater than 0 for the chain transfer reactions so that TDB segment could be formed. We can assume the rate constants for TDB reaction same as propagation reactions and use the TBD-frac as the estimation parameter. The TDB polymerization reaction increases the Molecular Weight of the polymer.

2.8 Conclusions

In this chapter, we have demonstrated an effective methodology for estimating kinetic parameters for Ziegler-Natta polymerization for commercial processes producing polyolefins, such as HDPE, PP and LLPDE. We consider the catalyst activation, initiation, propagation, chain transfer, deactivation and other polymer-specific reactions. We have

identified the reaction rate constants in Ziegler-Natta polymerization kinetics that have most significant impacts on common production targets, which greatly simplifies the kinetic parameter estimation for simulation and optimization models for polyolefin processes from plant data.

Our methodology begins with a kinetic model considering a single active catalyst site, followed by converting the single-site model into a model involving multiple active catalyst sites. We apply deconvolution analysis to characterize the GPC MWD data in order to determine the most probable chain length distribution for each catalyst site assuming a Flory distribution. The deconvolution analysis identifies the expected number of active catalyst sites together with the weight fraction and number-average molecular weight for each active catalyst site.

We demonstrate an effective methodology to use efficient software tools, such as data fit, sensitivity analysis and design specification in Aspen Polymers, to *simultaneously* estimate multiple reaction rate constants for Ziegler-Natta kinetics to match several data sets of production targets, such as production rates, MWN, SFRAC, etc. in a computer-aided step-by-step procedure. This differentiates our study from most of the previous studies which *sequentially* estimate these reaction rate constants. Our methodology also greatly simplifies the kinetic parameter estimation for the multisite model, in that we only need to regress *selected* kinetic parameters for the multisite model in order to match the plant data for PDI and related production targets, such as atactic fraction for PP production.

Our methodology results in part from our insights and experiences from applying our methodology to several dozen commercial polyolefin processes at two of the world's largest petrochemical companies in the Asia-Pacific over the past two decades. Applying our methodology using efficient software tools results in validated simulation and optimization models that we can use to quantify changes in process operations, process capacity scale-up, polymer quality control, and product grade change, etc.

Our detailed supplements of modeling examples will be useful to practicing engineers interested in applying process modeling and optimization to commercial polyolefin production. Thus, overall we present here a methodology to make first principle polyolefins models and if kinetic parameters are unknown we showcase a strategy to estimate parameters which can also be considered as a basic hybrid model which we will discuss further in Chapter 5.

Symbols

CAT_i = inactive catalyst

COCAT = cocatalyst

D_n = inactive polymer chain containing n segments

$ICAT_i$ = inhibited catalyst of site type i

$k_{act,i}$ = rate constant for activation of catalyst site type i

$k_{f_{inh},i}$ = rate constant for forward hydrogen inhibition of catalyst site type i

$k_{ini,i}$ = rate constant for chain initiation for catalyst site type i
 $k_{p,i}$ = rate constant for chain propagation for catalyst site type i
 $k_{rinh,i}$ = rate constant for reverse hydrogen inhibition of catalyst site type i
 $k_{th,i}$ = rate constant for chain transfer to hydrogen for catalyst site type i
 $k_{tm,i}$ = rate constant for chain transfer to monomer for catalyst site type i
 $k_{p,i}^{jk}$ = rate constant for total chain propagation for monomer type j adding to segment
 $k_{pa,i}$ = rate constant for atactic chain propagation for catalyst site type i
M = monomer species
 M_i = monomer of type i
 $P_{0,i}$ = activated catalyst site of type i
 $P_{1,i}$ = initiated catalyst site of type i
 $P_{n,i}$ = live polymer chain containing n segments attached to catalyst site type i

References

1. Sharma, N.; Liu, Y. A. , 110th Anniversary: An Effective Methodology for Kinetic Parameter Estimation for Modeling Commercial Polyolefin Processes from Plant Data Using Efficient Software Tools, *Ind. Eng. Chem. Res.* **2019**, *58*, 14209.
2. Khare, N. P.; Seavey, K. C.; Liu, Y. A.; Ramanathan, S.; Lingard, S.; Chen, C. C. Steady-State and Dynamic Modeling of Commercial Slurry High-Density Polyethylene (HDPE) Processes. *Ind. Eng. Chem. Research*, **2002**, *41*, 5601.
3. Khare, N. P.; Lucas, B.; Seavey, K.C.; Liu, Y. A.; Sirohi, A.; Ramanathan, S.; Lingard, S.; Song, Y.; Chen, C.C. Steady-State and Dynamic Modeling of Commercial Gas-Phase Polypropylene Processes Using Stirred-Bed Reactors. *Ind. Eng. Chem. Research*, **2004**, *43*, 884.
4. Khare, N.P., *Predictive modeling of metal-catalyzed polyolefin processes*. Virginia Polytechnic Institute and State University **2003**.
5. Dotson, N. A.; Galvan, R.; Laurence, R. L.; Tirrell, M. *Polymerization Process Modeling*, VCH Publishers, Inc., New York, New York, **1996**.
6. Soares, J. B. P.; McKenna, T. F. L. *Polyolefin Reaction Engineering*, Wiley-VCH, Weinheim, Germany, **2012**.
7. Touloupidis, V. Catalytic Olefin Polymerization Process Modeling: Multi-Scale Approach and Modeling Guidelines for Micro-Scale/Kinetic Modeling. *Macromol. React. Eng.*, **2014**, *8*, 508.

8. Zacca, J. J.; Ray, W. H. Modeling of Liquid Phase Polymerization of Olefins in Loop Reactors. *Chem. Eng. Sci.*, **1993**, *48*, 3743.
9. Chen, K.; Tian, Z.; Luo, N.; Liu, B. Modeling and Simulation of Borstar Bimodal Polyethylene Process Based on a Rigorous PC-SAFT Equation of State Model. *Ind. Eng. Chem. Research*, **2014**, *53*, 19905.
10. Zhang, C.; Shao, Z.; Chen, X.; Yao, Z.; Gu, X. and Biegler, L. T. Kinetic Parameter Estimation of HDPE Slurry Process from Molecular Weight Distribution: Estimability Analysis and Multistep Methodology. *AIChE J.*, **2014**, *60*, 3442.
11. Meng, W.; Li, J.; Chen, B.; Li, H. Modeling and Simulation of Ethylene Polymerization in Industrial Slurry Reactor Series, *Chin. J. Chem Eng.*, **2013**, *21*, 850.
12. Zhao, X.; Guo, X.; Chen, P.; Niu, L.; Yang, J.; Xu, X. Simulation and Analysis of an Ethylene Slurry Polymerization System Using Supercritical Propane. *Ind. Eng. Chem. Research*, **2012**, *51*, 682.
13. Zheng, Z. W.; Shi, D. P.; Su, P. L.; Luo, Z. H.; Li, X. J. Steady-State and Dynamic Modeling of the Basell Multireactor Olefin Polymerization Process. *Ind. Eng. Chem. Research*, **2011**, *50*, 322.
14. Lu, C.; Zhang, M.; Jiang, S.; Song, D. Application of ASPEN PLUS in Large-Scale Polypropylene Plant. *Qilu Petrochemical Technology*, **2006**, *34*, 404.
15. Touloupidis, V.; Kanellopoulod, V.; Pladis, P.; Kiparissides, C.; Mignon, D.; Van-Grambezen, P., Modeling and Simulation of an Industrial Slurry-Phase Catalytic Olefin Polymerization Reactor Series. *Chem. Eng. Sci.*, **2010**, *65*, 3208.
16. Seavey, K. C.; Khare, N. P.; Liu, Y. A.; Bremner T.; Chen, C. C. Quantifying Relationships among the Molecular Weight Distribution, Non-Newtonian Shear Viscosity and Melt Index for Linear Polymers". *Ind. Eng. Chem. Research*, **2003**, *42*, 5354.
17. Mattos Neto, A. G.; Freitas, M. F.; Nele, M.; Pinto, J. C. Modeling Ethylene/1-Butene Copolymerizations in Industrial Slurry Reactors. *Ind. Eng. Chem. Res.*, **2005**, *44*, 2697.
18. Tian, Z.; Chen, K. R.; Liu, B. P.; Luo, N.; Du, W. L.; Qian, F. Short-chain Branching Distribution Oriented Model Development for Borstar Bimodal Polyethylene Process and Its Correlation with Product Performance of Slow Crack Growth. *Chem Eng. Sci.*, **2015**, *130*, 41.
19. Luo, Z. W.; Zheng, Y.; Cao, Z. K.; Wen, S. H. Mathematical Modeling of the Molecular Weight Distribution of Polypropylene Produced in a Loop Reactor. *Poly. Eng. Sci.*, **2007**, *47*, 1643.
20. You, C.; Li, S. Analysis and Application of Model Building Procedure in Polypropylene Plant. *Petrochemical Industry Technology* **2007**, *14*(2), 56.

21. Luo, Z. H., Su, P. L.; Shi, D. P.; Zhang, Z. W. Steady-State and Dynamic Modeling of Commercial Bulk Polypropylene Process of Hypol Technology. *Chem. Eng. J.*, **2009**, *149*, 370.
22. Kou, B.; McAuley, K. B.; Hsu, C. C.; Bacon, D. W.; Yao, K. Z. Mathematical Model and Parameter Estimation for Gas-Phase Ethylene Homopolymerization with Supported Metallocene Catalyst. *Ind. Eng. Chem. Res.*, **2005**, *44*, 2428.
23. Kou, B.; McAuley, K. B.; Hsu, C. C.; Bacon, D. W. Mathematical Model and Parameter Estimation for Gas-Phase Ethylene-Hexene Copolymerization with Metallocene Catalyst. *Macromol. Mater. Eng.*, **2005**, *290*, 537.
24. Kashani, A. F.; Abedini, H.; Kalace, M. R. Simulation of an Industrial Linear Low Density Polyethylene Plant. *Chem. Prod. and Proc. Modeling*, **2011**, *6*, Art.34.
25. Baughman, D. R.; Liu, Y. A. *Neural Networks in Bioprocessing and Chemical Engineering*, **1995**, Elsevier, Atlanta, GA.
26. Knuutila, H.; Lehtinen, A.; Nummila-Pakarinen, A. Advanced Polyethylene Technologies- Controlled Material Properties. *Adv. Polym. Sci.* , **2004**, *169*, 13.
27. Zheng, X. G., Operation Optimization of Dual-Loop Polypropylene Process by Polymers Plus Software. *Petrochemical Technology*, **2015**, *44*, 612.
28. Shamiri, A.; Hussain, M. A.; Mjalli, F. S.; Mostoufi. Kinetic Modeling of Propylene Homopolymerization in a Gas-Phase Fluidized-Bed Reactor. *Chem. Eng. J.*, **2010**, *161*, 240.
29. Gross, J.; Sadowski, G.; Perturbed-Chain SAFT: An Equation of State Based on a Perturbation Theory for Chain Molecules. *Ind. Eng. Chem. Res.* **2001**, *51*, 1244.
30. Tremblay, D. Modeling Polymerization Processes. Presented at Aspen Optimize Training, OPTIMIZE 2017, Houston, TX, April, **2017**.
31. You, C. Modeling and Analysis of Polypropylene Process in Steady and Dynamic States, M. S. thesis, College of Chemical Engineering, Tianjin University, June, **2006**.
32. Soares, J. B. P.; Hamielec, A. E. Deconvolution of Chain-Length Distribution of Linear Polymers Made by Multiple-Site-Type Catalysts. *Polymer*, **1995**, *36*, 2257.
33. Aspen Technology, Inc., Bessel Spheripol polypropylene process simulation example, Aspen Polymers V10.0->Examples ->Polymers ->Polypropylene -> High Impact Spheripol Polypropylene Copolymer Process, **2019**.
34. Caracotsios, M.. Theoretical Modelling of Amoco's Gas Phase Horizontal Stirred Bed Reactor for the Manufacturing of Polypropylene Resins. *Chem. Eng. Sci.* **1992**, *47*, 2591.
35. Zecca, J. J.; Dehling, J. A.; Ray, W. H.. Reactor Residence Time Distribution Effects on the Multistage Polymerization of Olefins. I. Basic Principles and Illustrative Examples. Polypropylene. *Chem. Eng. Sci.* **1996**, *51*, 4859.
36. Jenkins, III, J. M.; Jones, R. L.; Jones, T. L. (1985). Fluidized Bed Reaction Systems. U. S. patent 4588790.

37. Jenkins, III, J. M.; Jones, R. L.; Jones, T. L.; Beret, S. (1986). Method for Fluidized Bed Polymerization. U. S. patent 4543399A.
38. McKenna, T. F. L. (2019). Condensed Mode Cooling of Ethylene Polymerization in Fluidized Bed Reactors. *Macromolecular Reaction Engineering*, 13, 1800026.
39. Hagg, M. C.; Henrique, J.; Dantos, J. H. Z. D.; Dupont, J.; Secchi, A. R. (2000). Dynamic Simulation and Experimental Evaluation of EPDM Terpolymerization with Et(Ind)₂ZrCl₂/MAO Catalyst System., *J. Applied Polymer Sci.*, **76**, 425

Chapter 3: First-Principle Dynamic Modeling of Polyolefin Processes

3.1. Introduction

We can convert a steady-state polyolefin model to a dynamic model using Aspen Dynamics. Dynamic models are useful in maximizing the safety, operability and productivity of plants. During a dynamic simulation, we can manipulate operating variables to change the feed conditions, introduce feed disturbances to test operability, and to simulate feedstock changes or grade transitions. Thus, we can use the dynamic model to vary process operating conditions with time for polymer grade transitions. The Aspen Dynamics model has its own declarative language which allows us to write scripts to perform tasks like changing process operating conditions. We use these tasks to schedule polymer grade transitions at different time intervals. Thus, we can even simulate plant data from the model.

In this chapter we demonstrate the use of dynamic models for efficient grade transition strategies for polyolefin processes. We also showcase the use of first-principle dynamic models to produce steady state results for predicting polymer quality and describe their advantages and disadvantages for polymer quality predictions.

3.2. Polyolefin Grade Transition

One of the most important applications of dynamic process modeling in polymer processes is for grade change. The main quality indicators of polyolefin grades are the melt index (MI) and density (ρ). The melt index is a function of the weight-average molecular weight (MWW), while the density is a function of MWW as well as SFRAC (mole fraction of co-monomer) as explained in chapter 2.

Most polyolefin processes have a wide range of polymer grades with many applications. Thus, efficient grade transition is an important consideration for optimization of polymer processes to improve process economics. Polyolefin processes can be used for different applications by changing their physical properties like melt index and density. We vary these physical properties by changing the process operating conditions hence grade transition is critical as we change process conditions to make a new polymer grade. The most important requirements of an efficient grade transition are (1) we need to conduct the grade transition process swiftly and (2) we need to minimize off-specification production. Thus, by reducing off-spec material there is significant reduction in production cost of polyolefins as well. The most important parameters that determine the grade transition performance of a process are reactor design, residence time, runtime per batch, and residence time distribution of the polymer, gas and/or solution phase.

Debling et. al. did a study on grade transition strategies for polyolefin processes and compared that for different polyolefin processes in terms of the off-spec products produced during grade transition.¹ The different grade transition strategies mainly includes a

combination of techniques like overshoot of hydrogen, monomer rates, quick venting to change composition of reactor gas quickly and bed-deinventorying etc. depending on the polyolefin process. They showed different combination of grade transition strategies being useful for different processes. Takeda et. al. ² applied optimal grade transition strategies for polyolefin reactors. Ben Amor et. al. ³ have showcased the application of real time optimization to non linear model control of a polymer grade transition. Similarly, Shi and Biegler ⁴ applied dynamic optimization to reduce off spec material and transition time. Prata et. al. ⁵ integrated scheduling and dynamic optimization of grade transition for a continuous polymer process.

3.3. Grade Change for Series Flow Slurry HDPE Process

We showcase how to implement grade-change operations applied to HDPE productions.

Step 1. Making the steady-state simulation model ready for conversion to a dynamic simulation model.

Step 2. Converting to a dynamic model (shown in figure 3.1)

Step 3. Our next step is to make initial adjustments to the Aspen Dynamics (AD) model, focusing on: (1) rigorous property option; (2) polymer attributes for streams and blocks; (3) heat duties and temperatures; (4) calculation of derived polymer attributes; and (5) revising the control scheme setup.

Step 5. We can fine tune the controller using heuristics and controller tuning (Appendix B.2)

Step 6. Simulating HDPE grade change.

We will focus on step 6, which highlights the grade change operations.

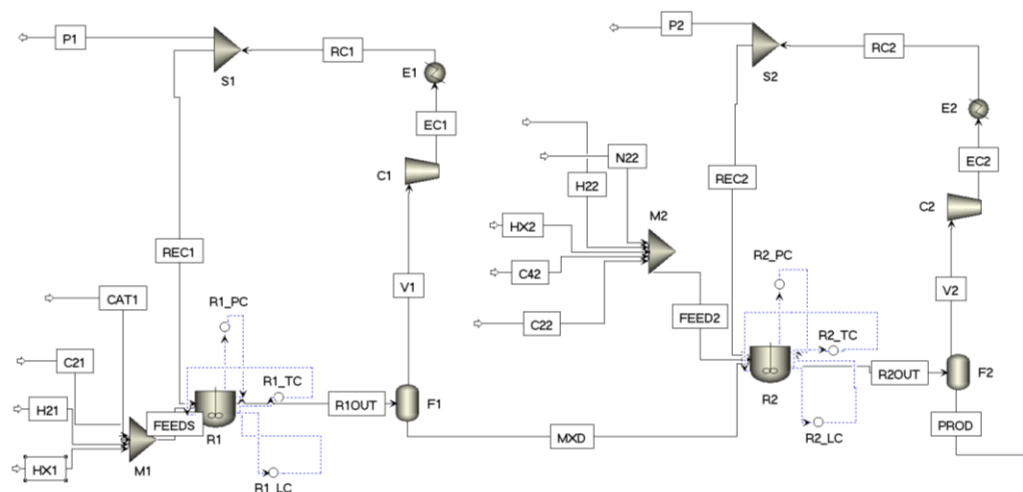


Figure 3.1. The dynamic simulation flowsheet of HDPE series process

Table 3.1 summarizes the key process and quality variable
 Table 3.1 Process and quality variables for slurry HDPE process

Process variable	Description
C21	Ethylene monomer flow in the feed to the first reactor (kg/hr)
H21	Hydrogen flow in the feed to the first reactor (kg/hr)
CAT	Catalyst flow to the first reactor (kg/hr)
HX1	Solvent (n-hexane) flow to the first reactor (kg/hr)
C42	1-Butene co-monomer flow to the second reactor (kg/hr)
C22	Ethylene monomer flow to the second reactor (kg/hr)
H22	Hydrogen flow to the second reactor (kg/hr)
HX2	Solvent (n-hexane) flow to the second reactor (kg/hr)
Quality variable	Description
MWW	Weight-average molecular weight of polymer in outlet stream
SFRAC	Co-monomer fraction in outlet polymer
Rate_pol	Polymer flow rate in outlet stream

For the purpose of demonstrating grade change for this case we only vary the hydrogen flow (H21, H22) and the comonomer flow(C42) here keeping rest of the variables same. The details of the grade change operations are shown in table 3.2. We can simulate tasks in AD as shown in figure 3.2.

Table 3.2 Values of process variables for grades 1 to 4 for slurry HDPE process

	Current	Grade 1	Grade 2	Grade 3	Grade 4
Tasks G1 to G4 run at	@0 hr	G1 @5 hr	G2 @40 hr	G3 @80 hr	G4 @120 hr
H21, kg/hr	8	4	4	10	10
H22, kg/hr	1	0.5	0.5	0.75	0.75
C42, kg/hr	1000	1000	750	750	900

Basically in task G1, the command SRAMP(Streams("H21"). FmR,4,4) changes the mass flow rate of stream H21 according to the shape of a sinusoidal curve to 4 kg/hr over an interval of 4 time units.

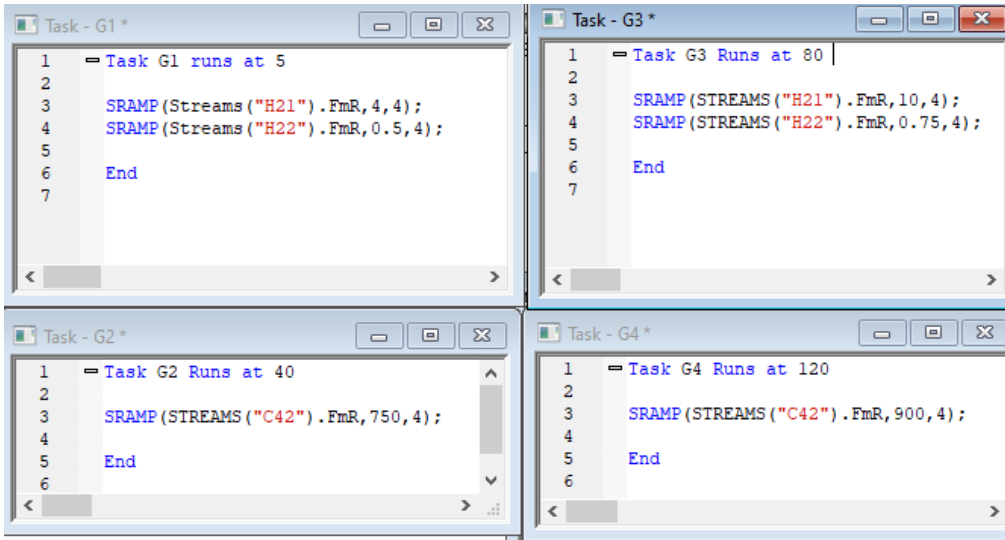


Figure 3.2. Specification of task G1-G4

Following Figure 3.2 and Table 3.2, we complete the specifications of tasks G2 to G4 in the same way. We create the plots for calculated process quality variables, such as melt index and copolymer density, based on empirical correlations suggested by Sinclair⁶. Specifically, we correlate plant data for melt index (MI) as a function of the weight-average molecular weight (MWW) of the HDPE product according to the equation:

$$MI = A_{MI} \left(\frac{MWW}{C_{MI}} \right)^{B_{MI}} \quad (3.1)$$

For illustrative purposes, we assume $A_{MI} = 901$, $B_{MI} = -5.14$ and $C_{MI} = 1e5$. When plant data for MI are available, the reader can regress new values of A_{MI} and B_{MI} . Additionally, we correlate the copolymer density (DENSITY) by the equation:

$$DENSITY = 0.996 - A_{DN} (SFRAC * 100)^{B_{DN}} \quad (3.2)$$

where $SFRAC_Comonomer$ is the mole fraction of segments of the comonomer, butene (C_4H_8), and the assumed correlation parameters $A_{DN} = 0.02386$ and $B_{DN} = 0.514$. We implement these correlations in Aspen Dynamic constraints as shown in figure 3.3.

```

1  CONSTRAINTS
2  // Flowsheet variables and equations...
3
4
5  A_MI as realparameter(901);
6  B_MI as realparameter(-5.14);
7  C_MI as realparameter(1e5);
8
9  Melt_Index as positive;
10
11
12  A_DN as realparameter(0.02386);
13  B_DN as realparameter(0.514);
14
15  Density as dens_mass (Description:"copolymer density");
16
17
18  Melt_Index = A_MI*(STREAMS("R2OUT").mw/C_MI)^B_MI;
19
20  Density = 0.966 - A_DN*((STREAMS("R2OUT").sfrac("R-C4H8")*100))^B_DN;
21
22  END
23

```

Figure 3.3. Specification of the flowsheet constraints, MI and copolymer density correlations.

We perform the grade changes with the process variables changes according to the tasks, specified in the figure 3.3. Figures 3.4 and 5.5 illustrate the changes in mass flow rates for producing grades G1 to G4 and the resulting polymer Melt Index and Density.

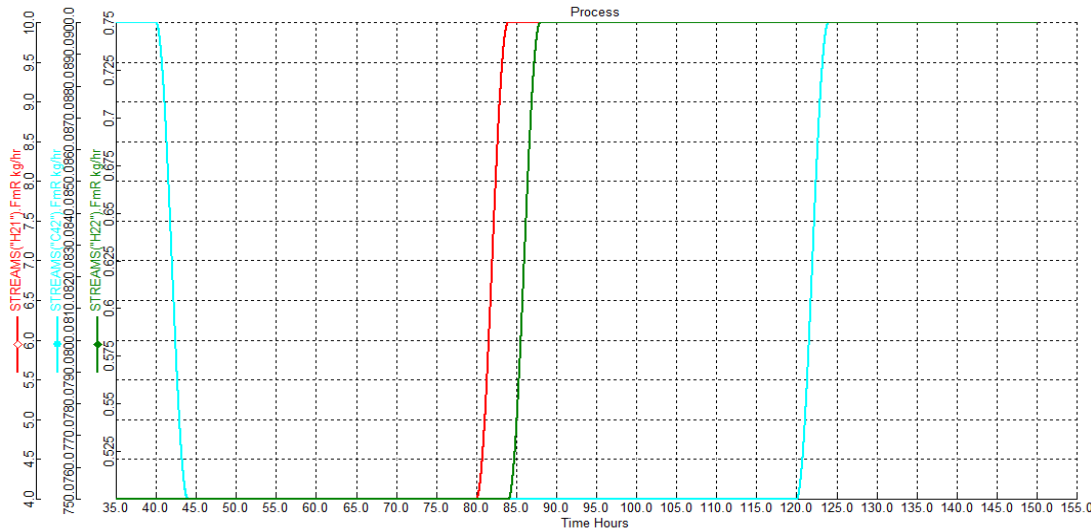


Figure 3.4. Evolution of R1 feed mass flow rates for producing grades G1 to G4 beginning at 24, 120, 240 and 360 hr, respectively.

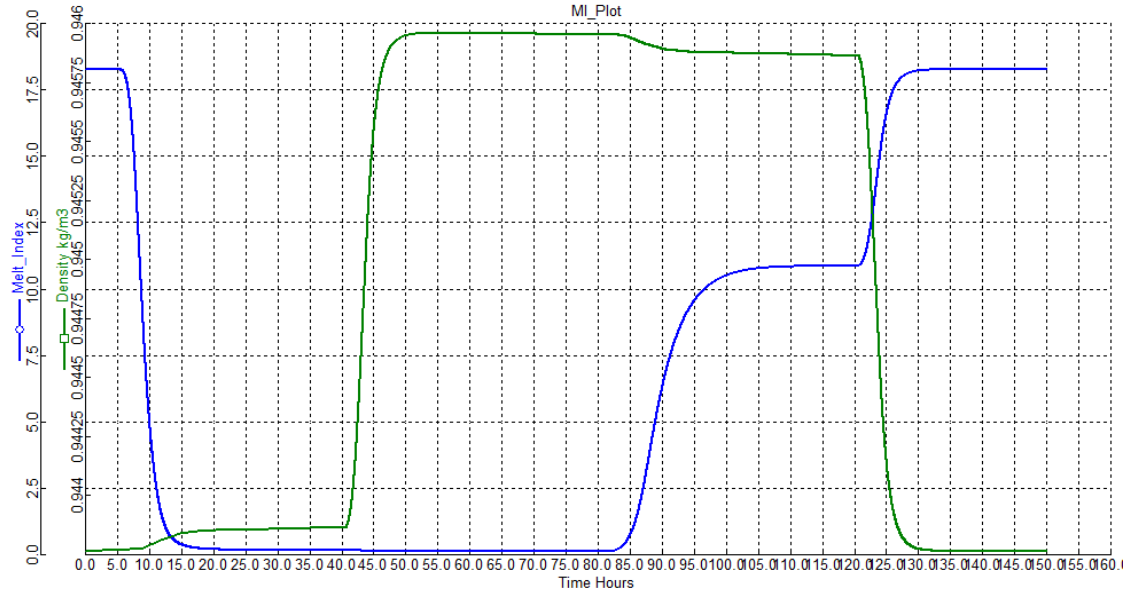


Figure 3.5. Evolution of the computed melt index and copolymer density.

3.4. Dynamic Simulation and Control of a Commercial Slurry HDPE Process Using H₂/C₂ Ratio

We demonstrate how to control the HDPE process using H₂/C₂ ratio in vapor flow. This ratio is also used in industry as a basis of polymer grade change. We simulate an industrial HDPE reactor process with a single reactor and recycle with heat exchangers and compressors. We list the steps below for making the model and explain the ratio controller in detail.

Step 1. Converting a steady-state simulation model to a dynamic simulation model with the process flowsheet without adding the ratio controllers is shown in figure 3.6.

Step 2. Initial adjustment of the model by using the Polymer attributes for streams and blocks. We also implement reactor level control using mechanical weir which we define using tasks.

Step 3. Improvement of reactor temperature controller by computing the pressure for the outlet of heat exchanger and also delete pressure controller.

Step 5. Add a Hydrogen/Ethylene ratio controller in the recycle using a ratio block which we will be explained in detail here.

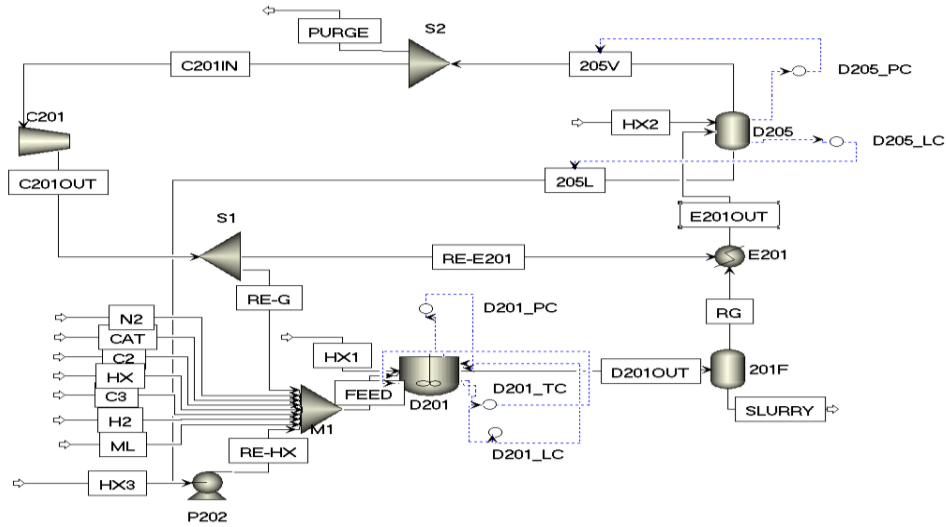


Figure 3.6. The starting dynamic simulation flowsheet

There is a controller that manipulates the feed rate of hydrogen and the purge rate from vessel D205 to maintain the hydrogen/ethylene ratio in the recycle gas. The process variable for this controller is the hydrogen-ethylene ratio in the recycle-gas stream. We introduce three blocks to the dynamic model when implementing this controller.

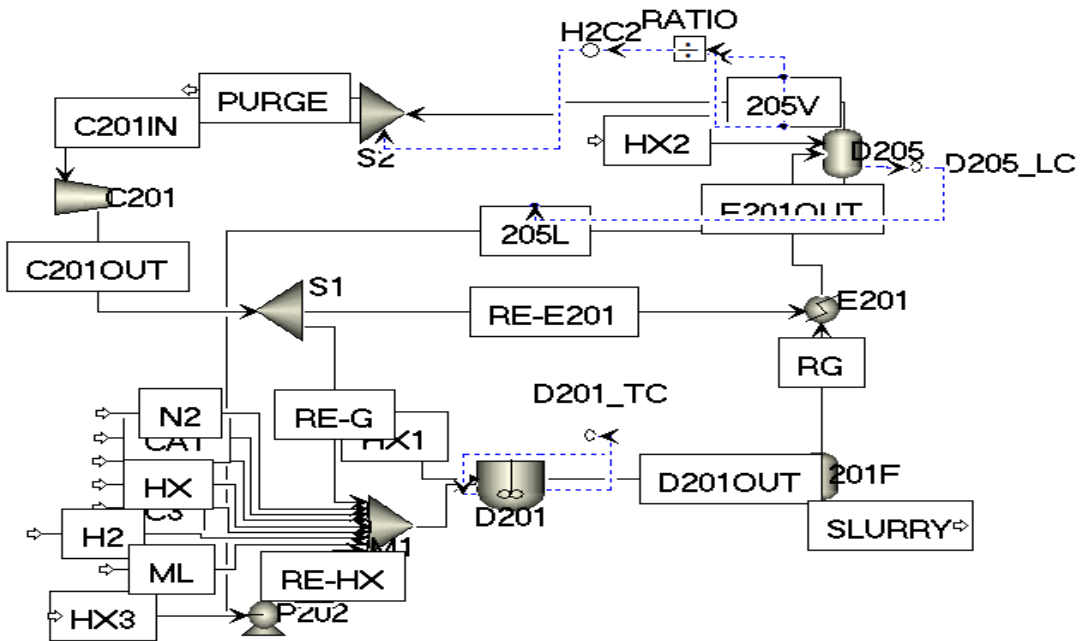


Figure 3.7. Adding a hydrogen/ethylene ratio controller to the recycle gas

The first block is a Ratio block, which computes the ratio of the mole flow of hydrogen, $\text{STREAMS}("205V").\text{Fcn}("H2")$ as input 1 to that of ethylene, $\text{TREAMS}("205V").\text{Fcn}("C2H4")$ as input 2 in the recycle gas, stream 205V. The controller

output is the computed mole ratio of hydrogen to ethylene. The second block is a PID controller that accepts the hydrogen/ethylene ratio from the ratio block. We name the controller as H2C2, and specify its controller action as reverse. We set the proportional gain and integral time according to those for composition controllers. The PID output signal specifies the mass split fraction of the purge stream exiting the flow splitter S2, BLOCKS("S2").sf("PURGE"). We open the faceplates and plots for controllers H2C2, D205_LC and D201_TC, make initialization and steady-state runs, and then make a dynamic run to pause at 10 hr. We tune the controller according to the procedure in appendix B.2 For the H2C2 controller, we find the current tuning parameters are: Gain= 30.97225 %/%, and integral time = 77.47908 min.

Now we specifically test the critical PID H2/C2 controller against a change in input ethylene flow rate (STREAMS("C2").FmR. We increase: (1) the flow rate of ethylene from 7500 kg/hr to 9000 kg/hr; (2) the specified catalyst total mass flow rate from 49.206 kg/hr to 60 kg/hr, and (3) the specified propylene total mass flow rate from 85 kg/hr to 100 kg/hr. We run the controllers to pause at 40 hr. Figure shows the performance plots. The process output curve matches the set point curve closely after the disturbance hence, the control strategy can be termed as stable.

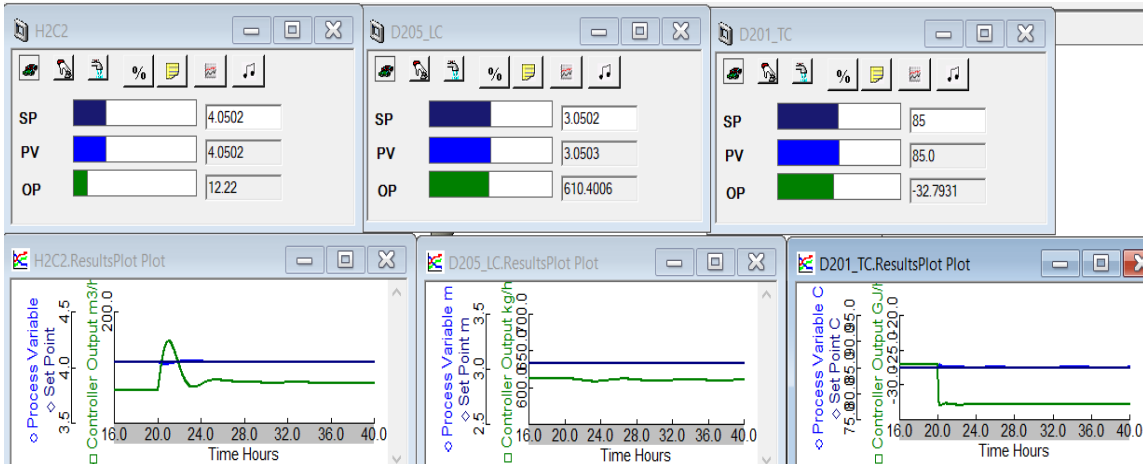


Figure 3.8. Performance of controllers after increasing ethylene mass flow rate to 9000 kg/hr, catalyst mass flow rate to 60 kg/hr and C3 mass flow rate to 100 kg/hr.

3.5. Dynamic Simulation and Control of a Gas-Phase Fluidized-Bed Process for Producing LLPDE in Condensed Mode Operation

We want to show how to implement various control schemes in a gas-phase fluidized-bed process for producing LLPDE in a condensed mode operation. We specifically demonstrate the reactor pressure control using a split-range controller. We follow the same

step for converting the steady state model to a dynamic model and figure 3.9 shows the resulting flowsheet with the added default controllers.

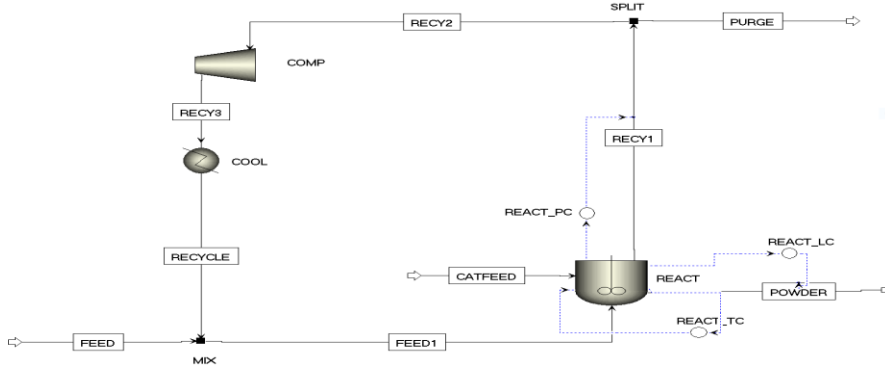


Figure 3.9. Dynamic simulation flowsheet with default controllers

As the RECY1 vapor recycle molar flow rate tends to increase, leading to an increase in the reactor pressure, we need a better control scheme for the reactor pressure. We want to introduce the use of a **split-range (SR) controller** for our reactor pressure control. Referring to Figure 3.10, we see that valve A opens when the controller output goes from 0 to 50%, and valve B opens when the controller output goes from 51 to 100%.

Figure 3.11 shows a modified flowsheet where we have added a split-range controller, where the PC controller output, BLOCKS("REACT_PC"), becomes the input to the SR controller. When this PC controller output is between 0 to 50%, the manipulated variable for the PC controller is the mass flow rate of N2 in the FEED stream, STREAMS("FEED").FmcR("N2"), whose value is bounded between 0 to 100 kg/hr. When this PC controller output is between 51 to 100%, the manipulated variable for the PC controller is the split fraction for the PURGE stream, BLOCKS("SPLIT").sf("PURGE"), whose value is bounded between 1E-6 to 0.1. We follow the path: Controller SplitRange -> Right-click "Forms" -> Configure: See Figure 3.12.

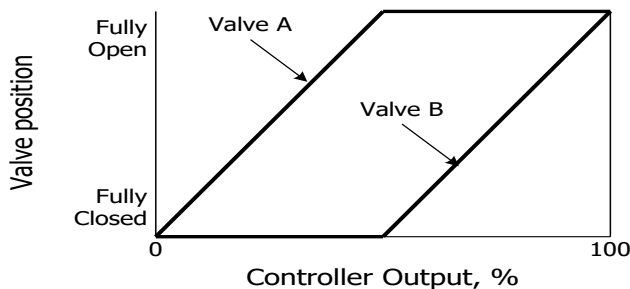


Figure 3.10. An illustration of a split-range (SR) controller

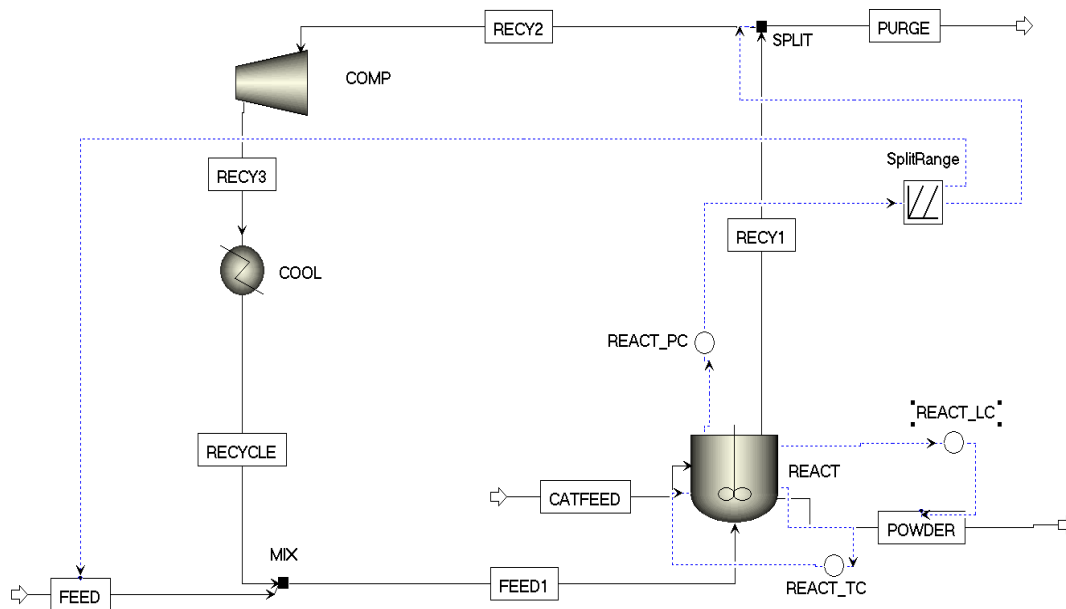


Figure 3.11. A modified dynamic process simulation flowsheet with a split-range controller

SplitRange.Configure Table			
	Description	Value	Units
Output1Action	Action for Output 1	Reverse	
Output1Min	Minimum value of Output 1	0.0	kg/hr
Output1Max	Maximum value of Output 1	100.0	kg/hr
Output1InMin	Value of input above which Output 1 starts to change	0.0	
Output1InMax	Value of input above which Output 1 stops changing	50.0	
Output2Action	Action for Output 2	Direct	
Output2Min	Minimum value of Output 2	1.e-006	
Output2Max	Maximum value of Output 2	0.1	
Output2InMin	Value of input above which Output 2 starts to change	50.0	
Output2InMax	Value of input above which Output 2 stops changing	100.0	

Figure 3.12. The configuration specifications of the split-range controller.

We run the dynamic simulation to pause at 5 hr. Figure 3.13 show that the controllers perform correctly. We change the FEED pressure from 30 bar to 25 bar. changes. We then run the dynamic simulation to pause at 15 hr. Figure displays that in response to the FEED pressure decrease from 30 to 25 bar, the pressure controller performs correctly. As the controller output is at 12.75%, the SR controller activates increase of the N2 mass flow rate from 25 to 46.4267 kg/hr, while keeping the PURGE split fraction unchanged and the reactor pressure at the set point of 21.6975 bar.

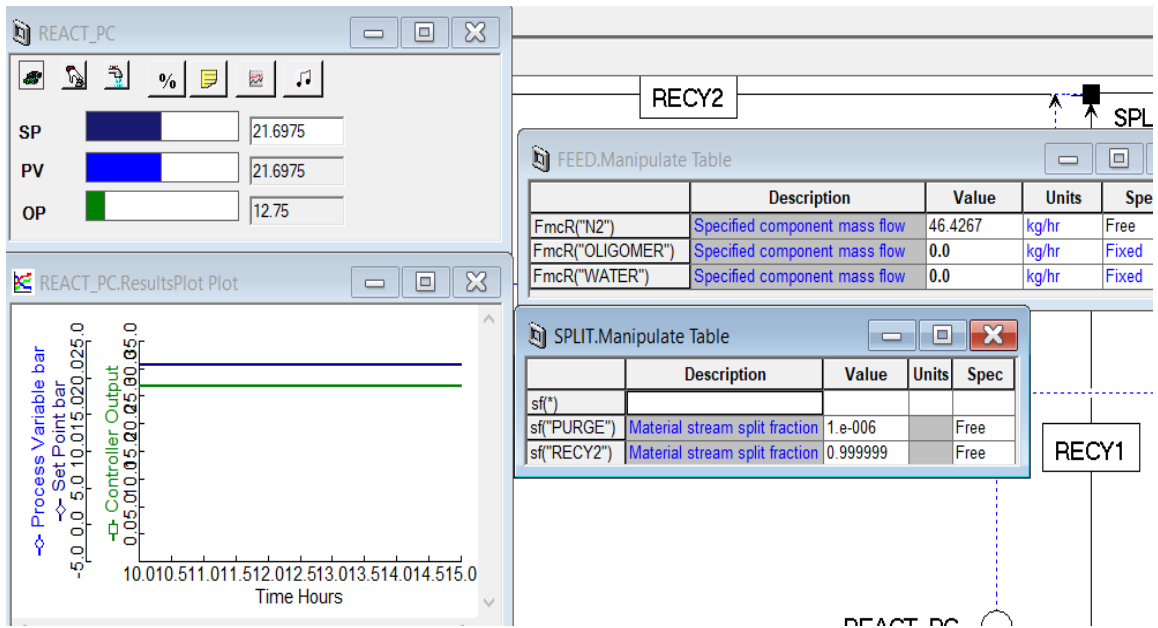


Figure 3.13. Keeping the reactor pressure at 21.6975 bar by increasing the mass flow rate of N2 from 25 to 46.4267 kg/hr as determined through a split-range controller.

3.6. Dynamic Simulation and Control of a Slurry HDPE Process Using an Inferential Controller

3.6.1 Objective:

The objective of this application is to develop an inferential control for melt index (MI) measurement in a HDPE production process. The controller controls the MI to target and minimize the difference between the target and measured MI values during grade transitions. We perform grade transition of the polymer for different MI values using the inferential controller, and we also try to improve the controller to minimize the off-spec product.

3.6.2 Inferential Control Theory and Recent Applications

In many industrial processes, it is difficult to measure certain product quality targets. In such cases, we measure some secondary process outputs in order to correlate the product quality with primary outputs for quality control. The additional measurement of the secondary output gives an inference on the key unmeasured variables, which is often called inferential control ⁷.

Inferential controllers use simple models to predict the controlled variables using plant measurements such as raw material feed rates and reactor temperature. Once a measurement is available for the controlled variable, we compare the measurement with

the model prediction to adjust the model. The model can then recommend a new control action.

In one of the first applications of inferential controllers, Joseph and Brosilow⁸ apply the inferential control to adjust the column temperature in a petroleum process. They build steady-state and dynamic inferential control systems⁹. Parrish and Brosilow¹⁰ showcase how inferential controller performs better than a cascade PID controller when applied to heat exchanger and industrial reactor control.

In a recent application, Wang et al.¹¹ use the inferential control for temperature and simultaneous composition control of a divided wall column. Behrooz¹² use the inferential control for controlling the product quality of crude oil distillation using stochastic optimization. Choi et. al.¹³ apply the inferential control for controlling the grade transition in pulping process. Durr et. al.¹⁴ use the inferential control for controlling the quality of produced granules in a fluidized-bed process. Nikhil et. al.¹⁵ apply the inferential control to control a fermentation process by maintaining product ethanol concentrations.

In polymer processes, the product quality measurements, such as melt index, are sparse and not very accurate. Therefore, control becomes important for reaching the quality target. MI is dependent on the hydrogen flow rate, which becomes an important manipulated variable. However, using a traditional feedback controller is inefficient, because the plant will only measure the MI of the product once every six hours, and there is a long time delay between where the hydrogen is fed to where the MI is measured. That is why we need an inferential controller for MI. Ogawa et. al.¹⁶ use the inferential control for quality control of a HDPE process in one of the earliest applications to polymer processes. Oshima and Tanigaki¹⁷ apply the inferential control for optimal grade change control.

3.6.3. HDPE Process Description and Steady-State Model Empirical Correlation

We consider a single CSTR for modeling the HDPE process. With a HDPE production rate of 5 metric ton (MT) per hour and with a product grades of 1 to 20, we wish to optimize the grade transition while minimizing the amount of off-spec product. The HDPE process also consists of a centrifuge and extruder, which we do not model. This follows because we can approximate the MI from the downstream equipment by the MI value at the reactor outlet by considering the time delay.

We first make a steady-state HDPE model with a single CSTR., Figure 3.14 shows a simplified HDPE process flowsheet with a single reactor and a flash drum. MI is dependent on the hydrogen feed flow, which represents an inferential variable. We use the model to determine an empirical correlation of MI with hydrogen feed flow rate by simulating data with different hydrogen flow rates, keeping other variables same and calculate the product MI value.

We approximate the steady-state MI data given by the following empirical equation:

$$\ln(MI_i) = 3.266\ln(H_2) - 3.215 \quad (3.3)$$

We refer to this steady-state MI_i as the instantaneous MI, which is a function of the hydrogen feed flow rate (H_2). Based on the steady-state model, we can calculate the hydrogen feed flow value for a particular MI grade.

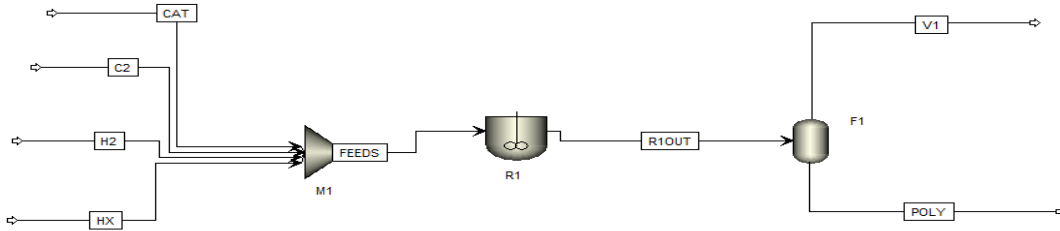


Figure 3.14. A simplified steady-state flowsheet for a slurry HDPE process.

We convert the steady-state model to a dynamic model as shown in Figure 3.15. We save the dynamic simulation file, and the property file as. We leave the default controller settings for the temperature (R1_TC) and level control (R1_LC), but delete the pressure controller since it is not critical for the liquid-phase reactor.

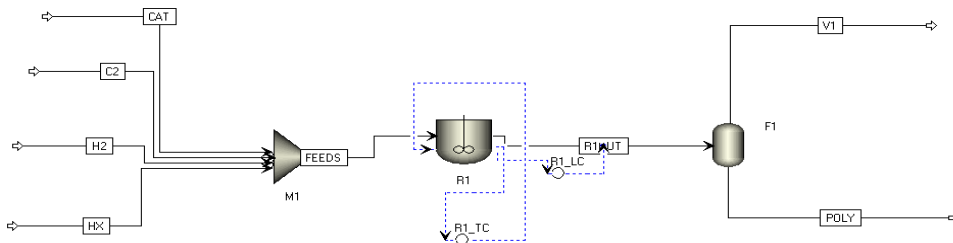


Figure 3.15. Dynamic HDPE process flowsheet

We consider the industrial correlation¹⁸ of the melt index (MI) as function of the Molecular Weight (MWW) to calculate the reactor outlet MI and assume that as the plant data.

$$Melt_Index = (11152.5/MWW)^{3.472} \quad (3.4)$$

We enter the MI correlation as a flowsheet constraint within AD as follows:

```
# Plant model (industrial MI correlation)
```

```
A_MI as realparameter(11152.5);
```

```
B_MI as realparameter(3.472);
```

```
Plant_MI as positive;
```

```
Melt_Index = (A_MI/(STREAMS("R1OUT").MWW))^B_MI;
```


where A_MI, B_MI are the parameters and STREAMS("R1OUT"), and MWW is the weight-average molecular weight of the polymer at the reactor outlet.

3.6.4. Grade Change Transition Using Basic H2-Based Controller

The basic traditional methodology of grade change is to change the grades by changing the hydrogen feed flow rate. From the steady-state model, we calculate the H2 feed flow value to produce a particular polymer MI. So in order to change the grade from MI of value 10 to 20, we increase the hydrogen flow rate from 5.41 kg/hr to 6.68 kg/hr, with the steady-state values obtained from the model to reach the respective MI value. we define the following task to increase H2 flow (STREAMS("H2").FmR) in minimum time (0.1 hr).

#Task for grade change using basic control using H2 feed flow rate

Task M1 runs at 5

SRamp (STREAMS("H2").FmR,6.68,0.1);

End

This basic control grade change process will lead to grade change, but with a constant H2-setpoint-based control, the transition will be slower leading to much larger amount of off-spec product. For the mentioned grade change, the amount off-spec material is approximately 75 metric tons (MT) in 15 hours as shown in Figure 3.16. Therefore, introducing an inferential control would become useful in reducing the off-spec material, as it constantly updates the hydrogen setpoint based on the controller error difference between the cumulative MI and the target MI.

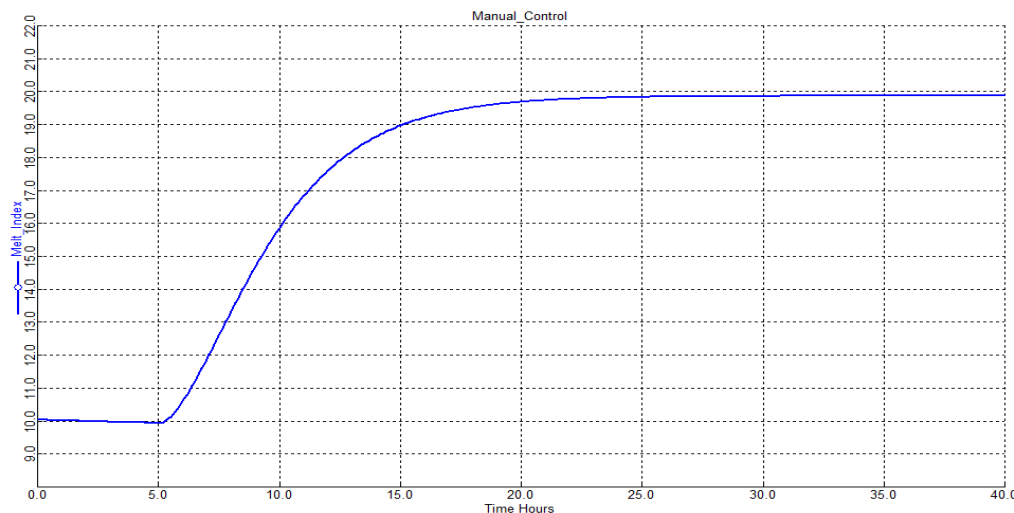


Figure 3.16. Grade change using H2-setpoint-based controller

3.6.5. Open-loop Inferential Controller Using Dynamic Model

To find a dynamic inferential control relation, we use the methodology showcased by Ogawa et. al.⁹ to calculate the cumulative MI exiting the reactor. They derive the ordinary

differential equation (ODE) using mass balance, quantifying the relation between the instantaneous MI and the cumulative MI formed at the exit of the reactor

$$\frac{d\ln(MI_c(t))}{dt} = \frac{1}{\tau_1} \log(MI_i(t)) - \frac{1}{\tau_1} \log(MI_c(t)) \quad (3.5)$$

where the MI_i is the instantaneous MI and MI_c is the cumulative MI at the exit of the reactor. We substitute Eq. (3.3) into Eq. (3.5) to calculate the cumulative MI and then use the dynamic model to tune the time constant (τ_1), and build an inferential controller.

We model the inferential controller by simulating the dynamic differential equation (3.5) and try to iterate for an appropriate value of time constant so that the inferential model matches the plant MI correlation (3.4) with error less than 5% described by the industrial correlation. We find a value of time constant of 4.077 hours gives a good match between plant and model values as shown in figure 3.14. By substituting Eq. (3.4) into Eq. (3.5) and considering value of time constant, we find the inferential model ODE as Eq. (3.6):

$$\frac{d(\ln(MI_c))}{dt} = \frac{1}{4.077} [3.266 \ln(H_2) - 3.215 - \ln(MI_c)] \quad (3.6)$$

MI_c gives the cumulative MI at the exit of the reactor and its logarithm is defined as `log_mi` in the AD tasks. The hydrogen feed flow rate (H_2) is represented by `STREAMS("H2").FmR` in the AD model. It is defined this way since AD does not allow the logarithm of a differential.

The flowsheet constraint commands for simulating the differential equation model are given below:

```
#Open Loop Inferential Model ODE
```

```
log_mi as realvariable;
```

```
$log_mi = (1/4.0775)*((3.266*LOGe(STREAMS("H2").FmR)) - 3.2157 - log_mi);
```

```
predicted_mi as realvariable;
```

```
predicted_mi = EXP(log_mi);
```

In order to compare the MI values and iterate value for the time constant for an open-loop controller, we perform grade transition by changing the values of H2 feed flow for grades of MI 1, 10, 20 by creating task as explained previously. We change the grades by using tasks to change H2 flow rate (`Streams("H2").FmR`) at 2 hrs to 5.46 kg/hr and at 25 hrs to 2.67 kg/hr, respectively, as explained previously. We set the H2 flow rate as a fixed variable prior to implementing the task.

Figure 3.17 compares MI values from the open-loop inferential control with the actual correlation-based MI values at a time constant of 4.07 hr, resulting in a lowest error of 3%.

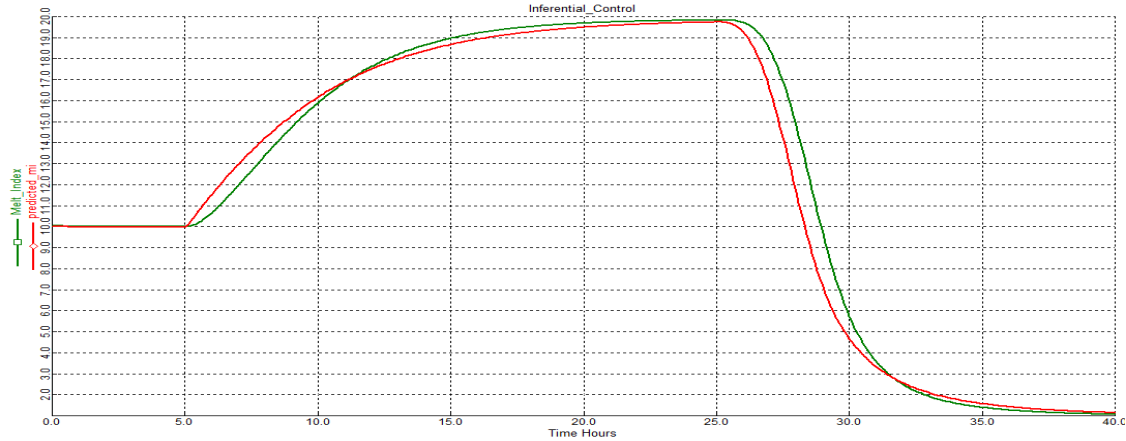


Figure 3.17. Comparison of MI values from the open-loop inferential control MI (predicted_MI) with the actual correlation-based MI (Melt_Index) (time constant = 4.07 hours)

3.6.6. Closed-Loop Inferential Controller

In order to automate the inferential controller, we need a closed-loop controller using the open-loop model ODE. This allows us to input a target MI, so that the inferential model can calculate the control action accordingly. In order to form the closed-loop inferential model, we need to discretize the inferential control ODE using the Euler method and simplify to get the following equation:

$$(\ln(MI_{target}) - \ln(MI_c))/\Delta t = (1/4.07) * (3.266 \ln(H2_{setpoint}) - 3.215 - \ln(MI_c)) \quad (3.7)$$

where MI_{target} is the fixed target MI that the controller need to achieve and MI_c is the cumulative MI at the exit of the reactor. We use the same open-loop time constant 4.07hr for the closed-loop discretized ODE. Thus, Eq. (3.7) closes the loop since by inputting a given target MI, it continuously back-calculates the hydrogen setpoint which can then be used to equate to the hydrogen flow rate resulting in the inferential control action. The time interval Δt is a fixed parameter that can be used to tune the controller and reduce overshoot. We enter the closed-loop inferential control as a flowsheet constraint within AD. #

Closed Loop Inferential Control

```
target_mi as realvariable(fixed,1);
delta_t as realvariable(fixed, 1);
h2_setpoint as realvariable(free);
(LOGe(target_mi)-log_mi)/delta_t = (1/4.0775)*((3.2667*LOGe(h2_setpoint)) - 3.2157 - log_mi);
h2_setpoint= STREAMS("H2").FmR;
```

The variable as defined in the constraint are MI_{target} as target_mi, $\text{Log}(MI_c)$ as log_mi, Δt as delta_t. We create a new variable called ‘target_mi’ and set it as a fixed variable and

use log_mi as the initial variable condition for the discretized ODE. Also make Streams("H2").FmR as a free variable since it is equal to the H2 setpoint.

Figure 3.18 shows all the three flowsheet constraints f.

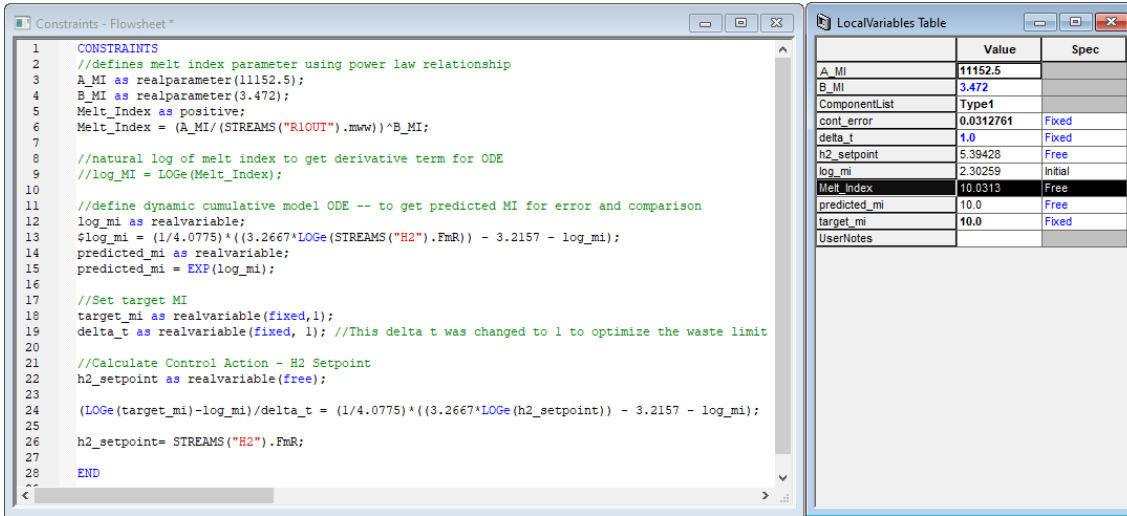


Figure 3.18. Snapshot of the overall constraints and the local variable specification

We simulate a grade change from 10 to 20 using AD tasks. The grade change for the MI happens in 5 hrs with only 25 metric ton (MT) of off-spec material. Figure 3.19 illustrates the inferential model prediction for grade change. The y-coordinate, predicted_mi, represents predicted MI value by the inferential controller.

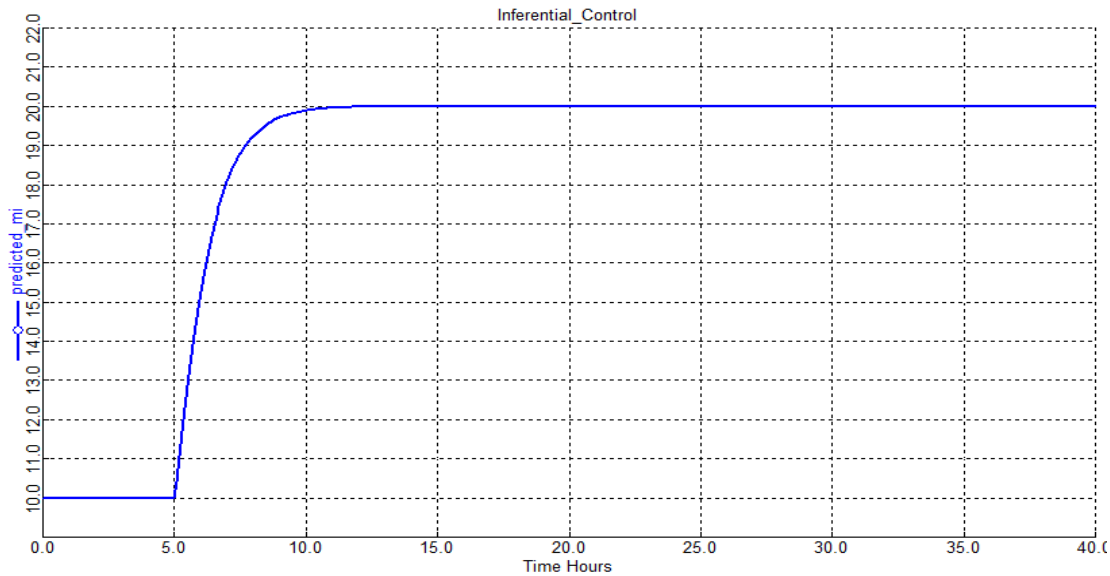


Figure 3.19. MI grade change from 10 to 20 using Inferential Control

Thus, we can compare the grade change due to the inferential control Melt Index with the basic constant hydrogen flow based control resulting in faster grade transition in inferential control (5hrs) compared to basic control (15 hrs). Figure 3.20 illustrates that the inferential control reduces off-spec material by 50 metric ton (MT) and by 10 hours to

reach the new MI target. Hence, we have showcased the utility of inferential control for polymer grade change.

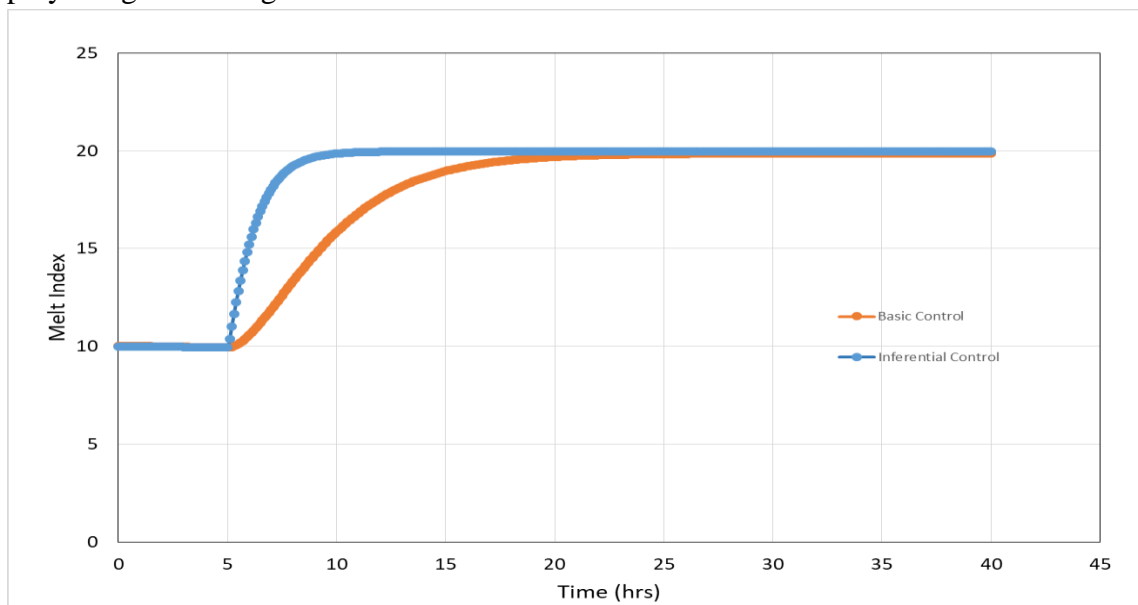


Figure 3.20 Comparison of grade change process using the inferential control with the basic H₂-based control

3.7. Using First Principle Dynamic models as polymer quality sensors

We can use the first-principle dynamic model to simulate polymer quality characteristics. Let us consider the prediction of MI from a slurry HDPE process with two reactors in parallel using actual plant data from LG Petrochemicals in South Korea by Park et. al.¹⁹ where they correlate the MI data by considering the following independent variables: (1) C₂: monomer ethylene feed flow rate; (2) C₄: comonomer 1-butene flow rate; (3) CAT: catalyst flow rate; (4) H₂: chain-transfer agent hydrogen flow rate; (5) HX: solvent n-hexane flow rate; (6) H₂/C₂: ratio of feed flow rates of H₂ and C₂; (7) T: reactor temperature; and (8) P: reactor pressure.

We convert a steady-state simulation model based on Aspen Plus to a dynamic (time-dependent) simulation model using Aspen Plus Dynamics. The resulting dynamic simulation model has similar independent variables as explained before. Both steady-state and dynamic simulation models are developed from first principles such as phase-equilibrium calculations and mass and energy balances. Therefore, they are scientifically consistent models. The methodology of simulation of plant data using dynamic process model is summarized in Figure 3.21.

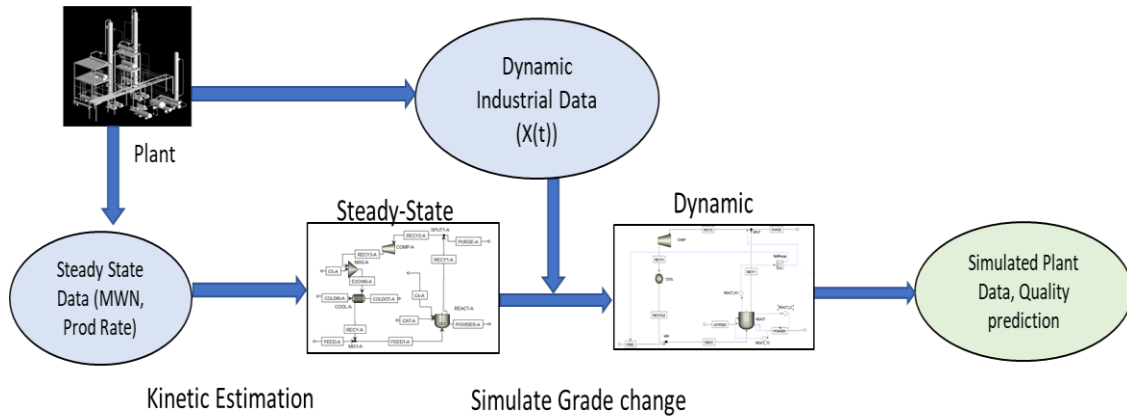


Figure 3.21. Methodology of simulating plant data from dynamic model

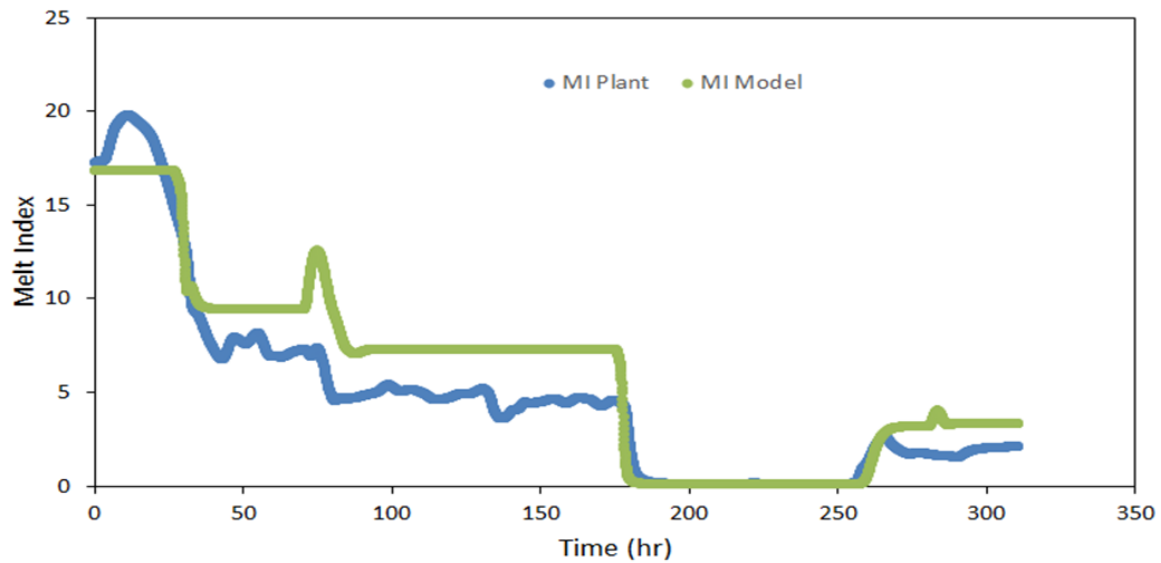


Figure 3.22. Comparison of MI predictions of the first-principle model and plant data

Figure 3.22. compares the predictions of the first-principle-based dynamic simulation model (in green) with the plant data with grade transitions (in blue). We see much deviation between the model predictions and the plant data. The accuracy of prediction decreases due to non-idealities and model assumptions. Also, for this particular case we also depend on the accuracy of the empirical correlation for MI since the dynamic model calculates MWW and we use that value to calculate MWW.

3.8. Conclusion

The first principle dynamic models are suitable for process development, optimization and control. The first principle model worked better for predicting steady state quality data seen in chapter 2 but not so accurate for predicting dynamic polymer quality as shown in figure. Hence, the data-based sensors based on Machine Learning techniques becomes more useful for such applications. Although first principle models are known to be much better at predicting beyond the operating range compared to data-based Machine Learning

models. In further chapters we will compare these results to a stand-alone data-based model and hybrid models and showcase their advantages and limitations.

References

1. Debling, J.A., Han, G.C., Kuijpers, F., VerBurg, J., Zacca, J. and Ray, W.H., Dynamic modeling of product grade transitions for olefin polymerization processes. *AIChE journal* **1994**, *40*, 506.
2. Takeda, M. and Ray, W.H., Optimal-grade transition strategies for multistage polyolefin reactors. *AIChE Journal* **1999**, *45*, 1776.
3. BenAmor, S., Doyle III, F.J. and McFarlane, R., Polymer grade transition control using advanced real-time optimization software. *Journal of Process Control* **2004**, *14*, 349-364.
4. Shi, J., Biegler, L.T., Hamdan, I. and Wassick, J., Optimization of grade transitions in polyethylene solution polymerization process under uncertainty. *Computers & Chemical Engineering* **2016**, *95*, 260.
5. Prata, A., Oldenburg, J., Kroll, A. and Marquardt, W., Integrated scheduling and dynamic optimization of grade transitions for a continuous polymerization reactor. *Computers & Chemical Engineering* **2008**, *32*, 463.
6. Sinclair, K. B., "Characteristics of Linear LPPE and Description of UCC Gas Phase Process," Process Economics Report, SRI International, Menlo Park, CA **1983**.
7. Marlin, T. A. Inferential Control. In *Process Control: Designing Processes and Control Systems for Dynamic Performance*; McGraw-Hill Inc. **2004**, 555.
8. Joseph, B.; Brosilow, C. B. ,Inferential Control of Processes: Part I. Steady State Analysis and Design., *AIChE Journal* **1978**, *24*, 85.
9. Joseph, B.; Brosilow, C., Inferential Control of Processes: Part III. Construction of Optimal and Suboptimal Dynamic Estimators. *AIChE Journal* **1978**, *24*, 500.
10. Parrish, J.; Brosilow, C., Inferential Control Applications. *Automatica* **1985**, *21*, 527.
11. Wang, J.; Yu, N.; Chen, M.; Cong, L.; Sun, L.. Composition Control and Temperature Inferential Control of Dividing Wall Column Based on Model Predictive Control and PI Strategies. *Chinese Journal of Chemical Engineering* **2018**, *26*, 1087.
12. Behrooz, H. A., Robust Set-Point Optimization of Inferential Control System of Crude Oil Distillation Units. *ISA Transactions* **2019**, *95*, 93.
13. Choi, H.-K.; Son, S. H.; Sang-II Kwon, J., Inferential Model Predictive Control of Continuous Pulping under Grade Transition. *Industrial and Engineering Chemistry Research* **2021**, *60*, 3699.

14. Dürr, R.; Neugebauer, C.; Palis, S.; Bück, A.; Kienle, A. , Inferential Control of Product Properties for Fluidized Bed Spray Granulation Layering. *IFAC-Papers OnLine* **2020**, 53, 11410.
15. Pachauri, N.; Singh, V.; Rani, A., Two Degree-of-Freedom PID-Based Inferential Control of Continuous Bioreactor for Ethanol Production. *ISA transactions* **2017**, 68, 235.
16. Ogawa, M.; M. Ohshima; K. Morinaga; Watanabe, F. , Quality Inferential Control of an Industrial High Density Polyethylene Process. *Journal of Process Control* **1999**, 9, 51.
17. Ohshima, M.; Tanigaki, M., Quality Control of Polymer Production Processes. *Journal of Process Control* **2000**, 10, 135.
18. Mattos Neto, A.G., Freitas, M.F., Nele, M. and Pinto, J.C., Modeling Ethylene/1-butene Copolymerizations in Industrial Slurry Reactors. *Industrial and Engineering Chemistry Research* **2005**, 44, 2697.
19. Park, T. C.; Kim, T. Y.; Yeo, Y. K., Prediction of the melt flow index using partial least squares and support vector regression in high-density polyethylene (HDPE) process. *Korean Journal of Chemical Engineering* **2010**, 27 (6), 1662-1668

Chapter 4: Application of Machine Learning and Multivariate Statistics for Polymer Process Data Analytics

4.1. Introduction

Data analytics have been known to be useful for chemical process industry. With the advancements in machine learning (ML) over the years its application for chemical process data analytics have been known to be particularly useful and profitable for the industry. Some of the major applications of process data analytics are in building data-based soft sensors for quality prediction, monitoring and control. Data Analytics is also instrumental in detection of process anomalies. Beginning in late 1980 to early 1990, chemical engineers have been paying greater attention to the emerging topics of artificial intelligence, neural computing, machine learning and big data analytics, and their applications to bioprocessing and chemical industries^{1, 2, 3, 4, 3, 5}. In particular, McGregor and others have demonstrated the significant applications of multivariate statistical analysis and big data analytics to optimizing the manufacturing of LDPE, HDPE, Nylon 6 and other polymers^{6, 7}. Multivariate statistical analysis^{8, 9, 10, 11} and its implementation using Python, R or softwares like Aspen ProMV, SAS, JMP etc. find many applications to polymer manufacturing, such as: (1) data quality deviation analysis; (2) unit yield analysis; (3) production capacity degradation analysis; (4) offline production optimization (discovery and optimization of key variables); (5) online process monitoring and troubleshooting; and (6) batch process variable analysis.

Qin discusses about the 4Vs of big data from the process data analytic point of view³.

Volume: There is massive process data available from process operation databases due to digital control systems.

Velocity: Most of the data is time sensitive and thus fault diagnosis using latent variable multivariate methods and time series analysis of data becomes useful for analysis.

Variety: Depending on the manufacturing process, there are different variety of process data available like equipment-based continuous sensor-based process measurements, lab-based quality data.

Veracity: Use of multivariate statistics and machine learning methods for accurate predictive and causal analysis of process data.

Qin and Chiang¹² have emphasized on the attributes required for process data analytics using ML methods. First is the importance of utilizing process knowledge or first principle models for accurate analysis. Second is the importance of considering the process uncertainties due to measurement errors and other non-idealities in the prediction. Lastly, the process data analysis should provide interpretable solutions to provide recommendations for manufacturing.

Ge et al. discuss the main steps of process data analytics in their study⁵. First step is the data preparation and collection of data from historical sources. Next comes the preprocessing of data for dealing with any missing data or inconsistency in data. Next we deal with appropriate machine learning model sections, its training and performance evaluation. Lastly comes the analysis of results based on its applications. They classify the machine learning models for process data analysis into four main applications including dimensionality reduction, outlier detection, process monitoring and data visualization. In their review Shang and You¹³ highlight the application of ML, especially reinforcement learning for optimal process control. ML have also been applied to predict property parameters by aiding molecular simulations which also indirectly helps in chemical process data analytics¹⁴. Similarly ML has been useful for catalyst design and discovery which aids process data analytics¹⁵. Ning and You¹⁶ highlight the use of machine learning for process optimization under process uncertainty.

Specifically, for polymer processes, data analytics is critical since the polymer quality measurements like polymer melt index (MI), molecular weight, etc. are usually less frequent compared to the continuous process variable measurements, hence the use of data-based sensors become useful¹⁷. In this chapter, we showcase the use of predictive ML models like neural networks and ensemble-based regressors for predicting polymer quality indicators. We also demonstrate the utility of causal models like partial least squares to study the causal effect of the process parameters on the polymer quality variables. We make use of anomaly detection methods as well to identify the process outliers and also the reasons for their outlier behavior.

4.2. An Overview of Relevant Machine Learning Concepts and Models

In the context of process data analytics majority of ML applications use *supervised learning* techniques, which basically means that your dependent variable and independent variables are available in the data. Usually for process data the independent variable (X) are the process input variables and operating conditions like feed flows, temperature, pressure etc., the dependent variable (Y) are the process outputs and product quality measurements like concentrations, molecular weights, density etc. For most supervised learning applications like process monitoring control, soft sensors, we use *regression* models to fit an empirical model for any of process outputs/product quality as a function of the process inputs. For some applications, we might also need to use *classification* models, for example, to classify some product batches given the product data labels.

Most supervised learning algorithms dealing with process data analysis can be classified into two major categories of *predictive* and *causal* models. Popular machine learning models are known for predictive modeling. *Neural Networks (NN)* are one of the most popular algorithms that are known to give highest prediction accuracy. They are made up of interconnected nodes that process information by its dynamic state to external inputs.² These are known to be kind of black box models which do not require much feature

engineering and can predict the output with high accuracy. The concept of neural network was first presented by Walter Mits in 1943 and since then the field has had many advancements. With the availability of computational resources, deep learning with many layers of NN have become popular which tend to give more accurate and generalized predictions. LeCun et. al. ¹⁸ have described how multiple layers of deep neural network models help to learn big data accurately and have led to breakthrough in various areas like speech recognition, image recognition, object detection, drug discovery. They identify the importance of the backpropagation algorithm in learning many parameters in deep learning. Similarly, there are many other conventional algorithms like Ridge/Lasso ¹⁹, Support Vector Machines ²⁰, Decision Tree ²¹ etc. which can be used for predictive modeling.

There are also other supervised learning predictive models available which can combine some of the individual models i.e. combining some of the weak learner/models to improve prediction which are known as *ensemble* models. Schapire ²² presented a theoretical proof that weak learners can be boosted to become strong learners. *Bagging* is the ensemble technique for combining the predictions of a model trained on random subsets of the data. The predictions are usually combined by averaging for regression and voting for classification. A popular bagging algorithm is *the random forest algorithm* ²³ using multiple decision trees. *Boosting* is a sequential technique where present model attempts to correct the errors of the previous model. *Gradient Boosting* is one of the popular boosting models based on decision trees ²⁴. Xgboost is an extreme form of Gradient boosting is a very efficient and scalable implementation of the gradient boosting algorithm²⁵. *Stacked regression* ²⁶ is an ensemble technique which combines base learner models, the output of which are input to a second level learner model.

Multivariate statistical methods which makes the use of latent variables are best suited for causal analysis to find the effect of multiple input/features on the output. Partial least squares ²⁷ (PLS) are one of the popular latent variable models for causal analysis that brings out the cause and effect relation in the independent (X) and the dependent Y variables. PLS provides a unique result unlike other data analytic models, since it simultaneously models the X and Y spaces. PLS is a latent variable (LV) model that provide causal models in low-dimensional LV space. These models can be used to actively alter the process to troubleshoot, optimize and control the process. They can give interpretable results, for any active changes in the manipulated variable, the model will reliably predict the output. Probabilistic models like Bayesian networks are also useful in identifying multiple causal relationships ²⁸.

Unsupervised Learning methods are useful when we have process data measurements (X) readily available, but do not have the quality measurements. Thus, we can use these methods to find patterns from the process data which can be useful for applications like fault diagnosis. A large data set with many variables termed as high dimensional data is expensive and difficult to analyze. Unsupervised learning methods can also be useful for

dimensional reduction. Principle Component Analysis (PCA) ²⁹ is one of the popular dimensional reduction algorithms which have the ability to reduce the dimensionality of the monitoring space by projecting the information in the data into low-dimensional spaces defined by a few latent variables and still retaining the maximum variance of the original dataset quality. As we will showcase later in the chapter PCA is also useful for anomaly detection.

Semi- Supervised learning methods can also be useful for process data analytics, especially for polymer processes where the output quality measurements (Y) are measured at lower frequency compared to the input process variables (X). Self-training methods like pseudo-labeling by entropy minimization can be used for semi-supervised learning ³⁰. There are also Generative ML models which can be used to generate more data. Generative Adversarial Networks ³¹ (GAN) is one of the popular generative models which consists of two main models the generator which generates fake data and the discriminator which classifies real or fake data. *Reinforcement learning* methods are emerging to be very popular in robotics/gaming , where an agent learns behavior through trial errors interactions in a dynamic environment ³². Reinforcement learning has also found application in process control and optimization as well ³³.

Figure 4.1 summarizes the classification of ML models.

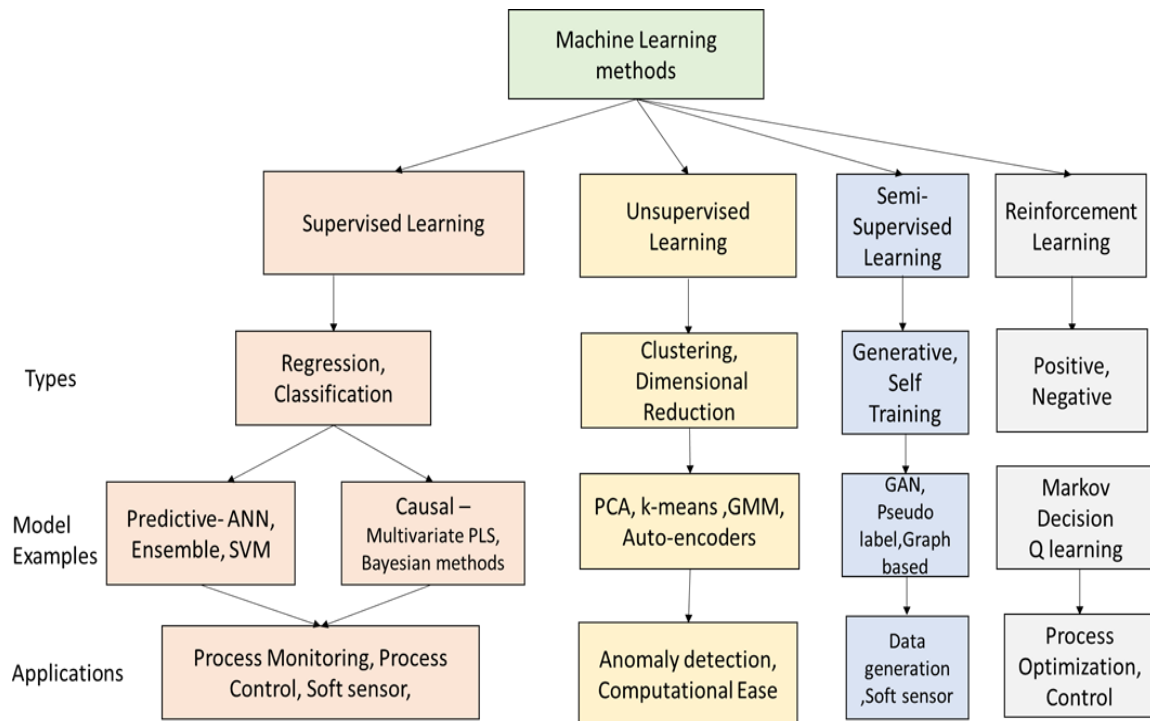


Figure 4.1. Classification of Machine Learning models

In this chapter, we will be mostly use supervised regression models .The regression models are evaluated based on the Root Mean Square Error (RMSE) value as well as the % Normalized RMSE (nRMSE):

$$MSE = \frac{1}{n} \sum_{i=1}^n (y_i - p_i)^2$$

$$RMSE = \sqrt{MSE}$$

$$nRMSE = \frac{RMSE}{y_m} 100$$

$$y_m = \frac{1}{n} \sum_{i=1}^n y_i$$

y_i = original observation ; p_i = model-predicted value; n = number of observation; MSE = mean square error; y_m = mean value of observations.

Most of these regression models are popular machine learning algorithms so we will not discuss them in too much detail. There are numerous textbooks and online resources that discuss the principle and implementation of gradient boosting algorithms, and their extensions for the interested readers. Scikit-learn machine learning ³⁴ is one of the most popular open source Python library which has most of the ML models available which we have used in our analysis. For deep learning models, we use the open source TensorFlow ³⁵ ML system.

4.3. Literature on application of Data Analytics in Chemical and Polymer processes

4.3.1 Literature on Application of Multivariate Statistics in Chemical Process Monitoring and Fault Diagnosis

Some of the major work in the applications of multivariate statistics have been done by MacGregor et. al ^{6, 11}. We highlight some recent applications of PCA and PLS below. Lou et. al. ³⁶ apply Sparse PCA for easier interpretation along with Particle Swarm Optimization for process monitoring. Ning and You ³⁷ apply PCA along with Kernel smoothing techniques to handle uncertainty data for process optimization and control. He et. al. ³⁸ used PCA on spectral data for analysis of crystallographic phases of explosives for quality control. Fezai et. al. ³⁹ apply the application of online kernel PCA for monitoring of non-linear processes. Harrou et. al. ⁴⁰ showcase a novel method of PCA-based anomaly detection to detect small abnormalities which are not possible in conventional methods. They use of control charts on uncorrelated PCA residuals helps to better detect anomalies.

Brestrich et. al. ⁴¹ use PLS for monitoring of protein chromatography methods using spectral data with PLS differentiating between different species. In a recent study,

Kocevska et. al. ⁴² use preprocess methods like blind source operations to identify independent components along with PLS for nuclear waste analysis using spectral data. Zhang et. al. ⁴³ showcase a novel locally weighted Kernel PLS methodology for bioprocess monitoring to accurately model non linearity and time varying dynamics of the process. Jiang et. al. ⁴⁴ use a novel optimized sparse PLS methodology for simultaneous bath-end quality prediction and variable selection for industrial process monitoring. In an application to biopharmaceutical process, Hattori and Otsuka ⁴⁵ use PLS for feed forward control of tablet compression process by integrating spectral data and granule physical property data.

4.3.2. Literature on Application of Machine Learning Models in Chemical processes

Artificial Neural Networks (ANN) have been widely used for process data analytics. In one of the early studies, Willis et. al. ⁴⁶ showcase the use of ANN for process control by inferential estimation. Iliyas et. al. ⁴⁷ have used ANN as inferential sensors for emission prediction of an industrial furnace. Sun et. al. ⁴⁸ use ANN along with weight shrinkage methods for soft sensor applications in industrial air separation processes. In a recent study, Hough et. al. ⁴⁹ use neural networks to reduce the computational expense of detailed kinetic models for biomass pyrolysis process. In more recent applications in chemical engineering, deep learning/deep neural networks have been quite popular. Shang et. al. ⁵⁰ use deep neural networks for estimation of distillation cut point in petroleum refining processes. Gao et. al. ⁵¹ use deep belief networks for classification of scheduling models for different types of crude oil feeds. Li et. al. ⁵² have applied deep belief networks in CO₂ capture process for prediction of CO₂ production rate and capture level. Zhang and Zhao ⁵³ showcase process fault diagnosis using deep belief networks on the Tennessee Eastman process.

Namdari et. al. ⁵⁴ have used support vector regression for fault diagnosis of incipient process faults which increase with time like reactor fouling and catalyst deactivation. Pani and Mohanta ⁵⁵ have used support vector regression for monitoring and control of particle size in cement grinding process. In another study, Gholami and Shahbazian ⁵⁶ used soft sensor to predict the hydrogen sulphide concentration of a stripper column using support vector regression along with fuzzy means clustering. Zio et. al. ⁵⁷ use Decision tree model for fault classification in a steam generation process in pressurized water reactor. Ge ⁵⁸ showcase the use of probabilistic Machine Learning models for process data analytics . Zhou et. al. ⁵⁹ use gaussian process regression model for adaptive quality monitoring in batch processes.

4.3.3. Literature on Application of Data Analytics/Machine Learning in Polymer process

There is a growing number of reported studies applying machine learning and multivariate statistical methods to polymer process monitoring, operation and control, and we mention a few examples here. Skagerberg et. al. ⁷ apply multivariate data analysis to

linear low-density polyethylene (LLPDE) reactors to build models for inferential control. MacGregor et. al. ⁶⁰ introduce the multiblock projection to latent structures or partial least squares (PLS) to the same process to diagnose process deviations. Gonzaga et. al. ⁶¹ used neural networks for using as soft sensor to predict polymer viscosity. In another application, Shi et. al. ⁶² predicted the melt index of polypropylene by combining independent component analysis and multi-scale analysis. Han et. al. ⁶³ use the support vector machines and neural networks to model melt index (MI) of industrial polymer processes. Sharmin et. al. ⁶⁴ develop an inferential PLS-based sensor to measure polymer quality parameters to provide physical insights in the process prediction in an application to batch polymerization.

Ao et. al. ⁶⁵ showcase a batch-to-batch iteration learning control using a data-based nonlinear model that improves prediction accuracy. Kaneko et. al. ⁶⁶ use a data-based soft sensor to detect the completion of transition of industrial polymer processes by predicting polymer quality parameters. Ge et. al. ⁶⁷ use gaussian process regression to handle nonlinear data for polypropylene melt index prediction. Liu and Chen ⁶⁸ apply the just-in-time support vector regression and probabilistic analysis for polymer quality. Liu and Xu ⁶⁹ have used dynamic fuzzy neural network to predict higher accuracy melt index prediction sensors for quality control of Poly Propylene process. Wang and Liu ⁷⁰ have used support vector least squares regression along with adaptive optimization algorithm for parameter estimation for melt index prediction.

Recently, Liu et. al. ⁷¹ use the ensemble deep kernel learning for quality prediction in industrial polymerization processes.

4.4. Illustrative Example of Machine Learning Applications in an Industrial Polyolefin Manufacturing Process

Objective: We illustrate a simple data-based sensor for predicting the MI from a slurry HDPE process with two reactors in parallel using actual plant data from LG Petrochemicals in South Korea ⁷².

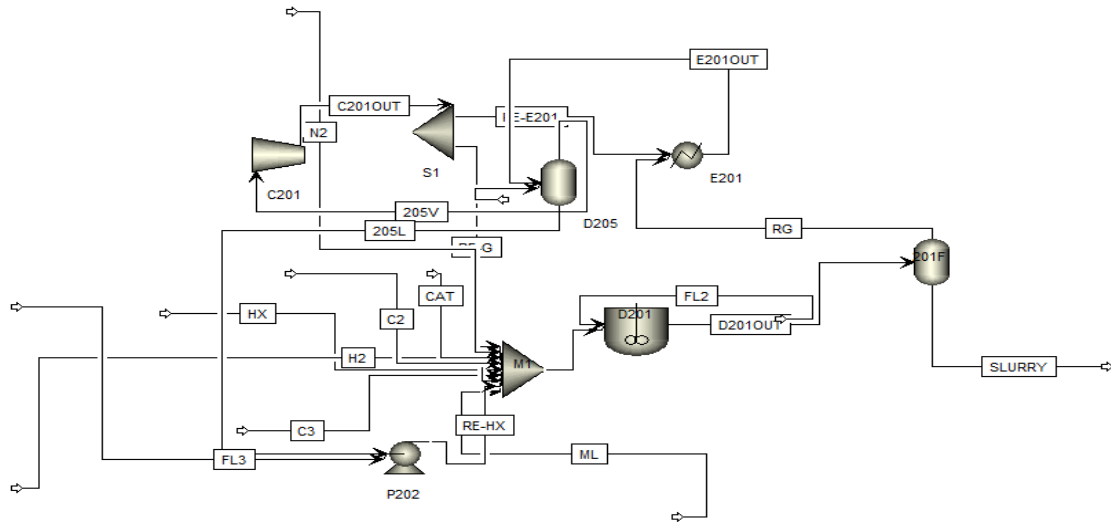


Figure 4.2. Process flowsheet of industrial parallel HDPE process

Figure 4.2 shows a schematic diagram of a general slurry HPDE process with parallel reactors

We consider the same process we used in Chapter 3 in comparison of dynamic first-principle model for comparing with plant data. Park et. al.⁷² correlate the MI data by considering the independent variables shown in table 4.1. The data set consists of 5000 observations and 9 main independent process variables and 1 MI as the quality target.

Table 4.1. Process Variables for industrial HDPE Process

Process variable	Description
C2	Ethylene feed flow rate
H2	Hydrogen feed flow rate
CAT	Catalyst feed flow rate
HX	Hexane solvent feed flow rate
C3	Comonomer feed flow rate
T	Temperature of the reactor
P	Pressure in the reactor
H2/C2	Feed concentration ratio in the reactor of ethylene to hydrogen
C3/C4	Feed concentration ratio of Propylene to Butylene monomer
MI	Melt Index of polymer

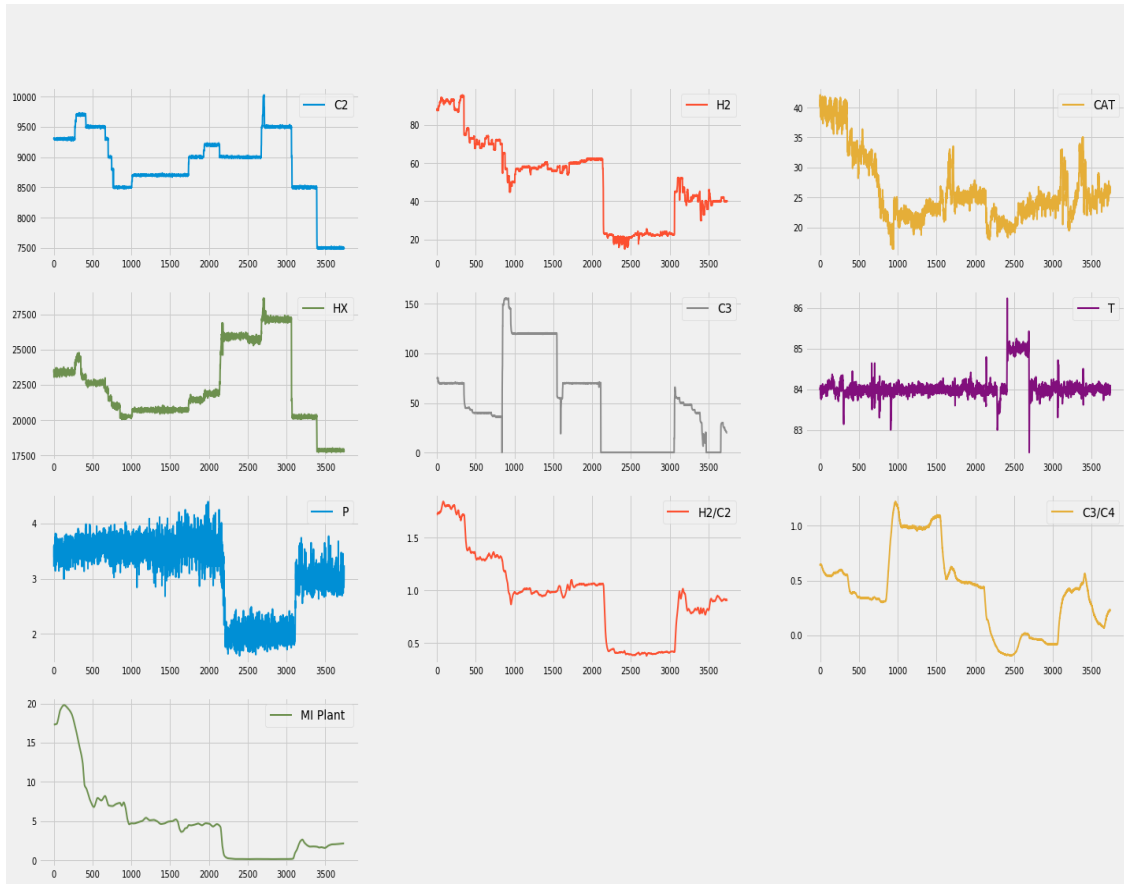


Figure 4.3. Visualization of the HDPE process data

Figure 4.3 shows the data visualization of all the variables with time of the process data.

Figure 4.4 shows the correlation mapping of the variables showcasing the correlation between all variables. From the data set, we can H2 is highly correlated with H2/C2. This correlation mapping is useful for understanding the data and also feature selection. In a larger data set we can drop highly correlated features to improve prediction, Although for this data analysis, we use all features to understand the process.

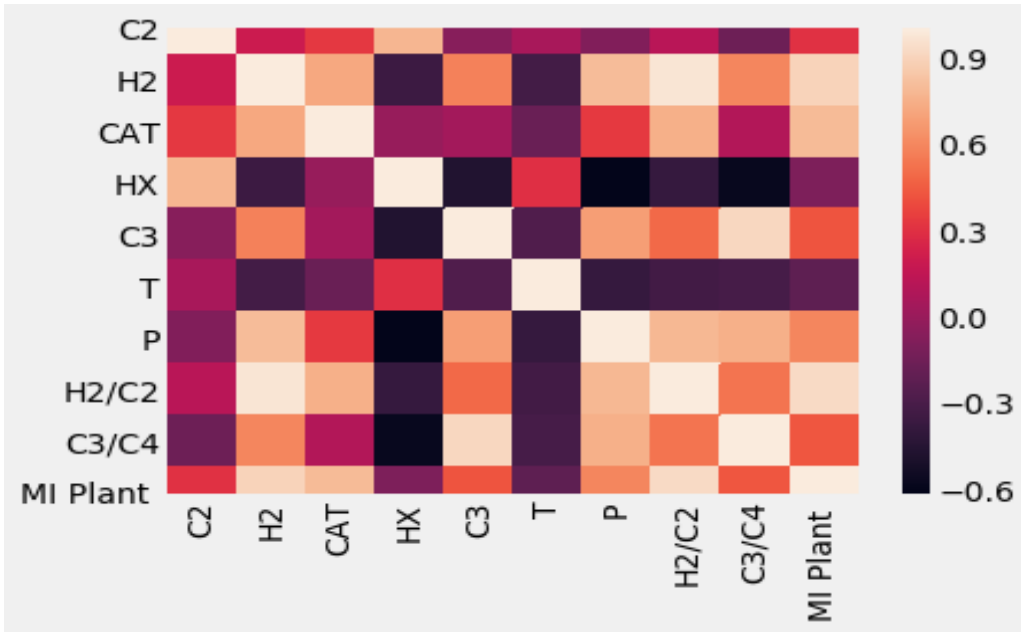


Figure 4.4. Correlation plot of the HDPE process data

4.4.1. Multivariate Statistical Causal Model

We use Aspen Pro MV for a latent variable causal analysis for the data analysis. We first fit the original data set PLS model which results in a R^2/Q^2 value of 0.95 which defines the %variance defined by the Principal Components with 4 principal components and RMSE 1.1. Then we use Hotelling's T2 methods to identify the process outlier as shown in Figure 4.5. Note the data points above the horizontal line labeled by the confidence limits of 0.99 and 0.96.

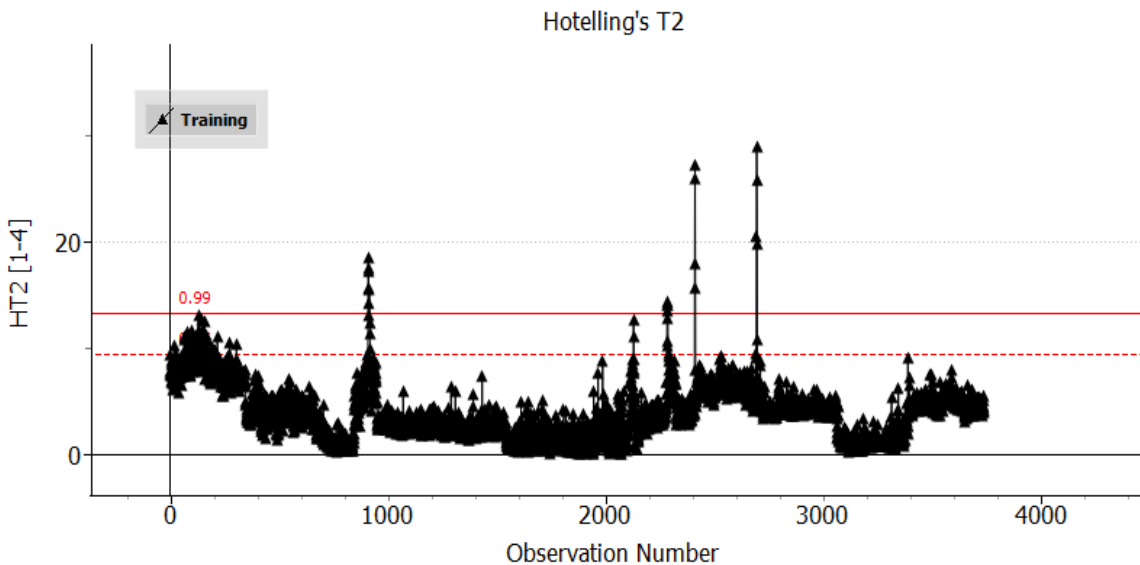


Figure 4.5. Hotelling's T2 plot deviation plot

The process outlier observations are 2412-15,2696-98 based on the confidence limits. (In the plot the close observation points are not clearly visible. We can even understand the

reasons for any of the observations to be an outlier based on their contribution scores. The 2413 observation (SPE score 200.196) being an outlier is due to temperature (T) being higher than the average as shown in contribution plot figure 4.6.

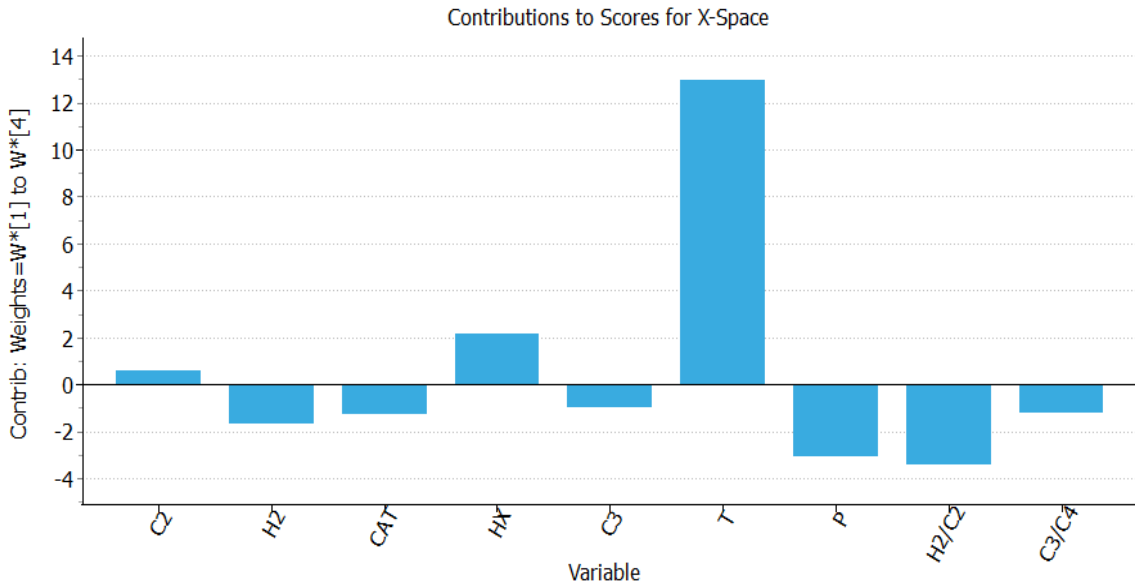


Figure 4.6. Contribution plot of process outlier compared to the average score to identify the cause of process abnormality

We remove the process outliers and fit the PLS model again. The R^2/Q^2 value of the PLS model with 4 principal components is 0.956 as shown in figure 4.7. Now we can again plot the Hotelling's plot and see none of the observations beyond 99 % confidence interval as shown in figure.

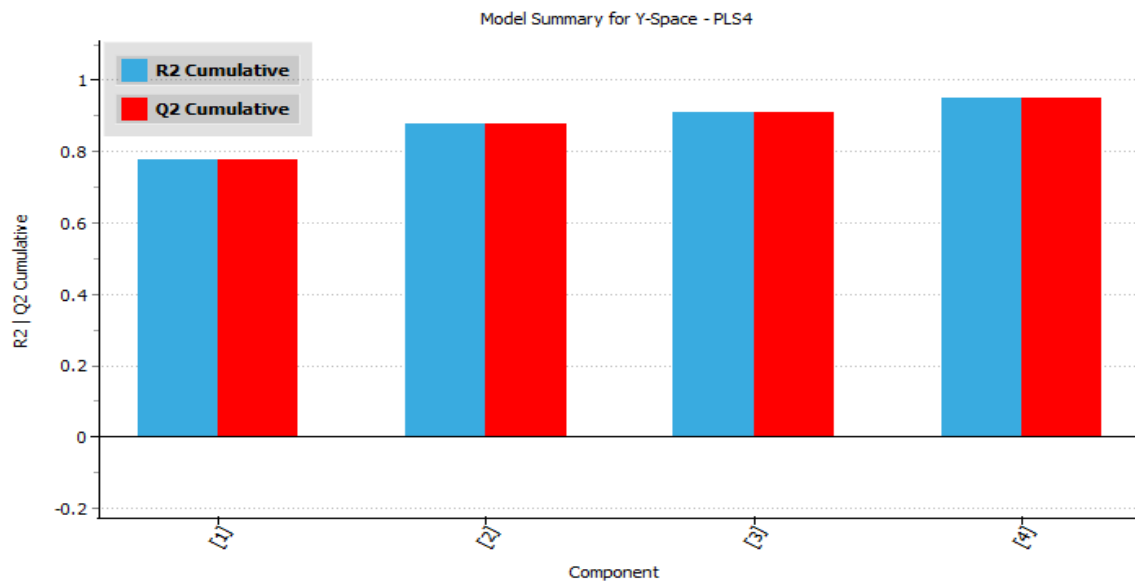


Figure 4.7. Principal Component R2 score for PLS model without lag

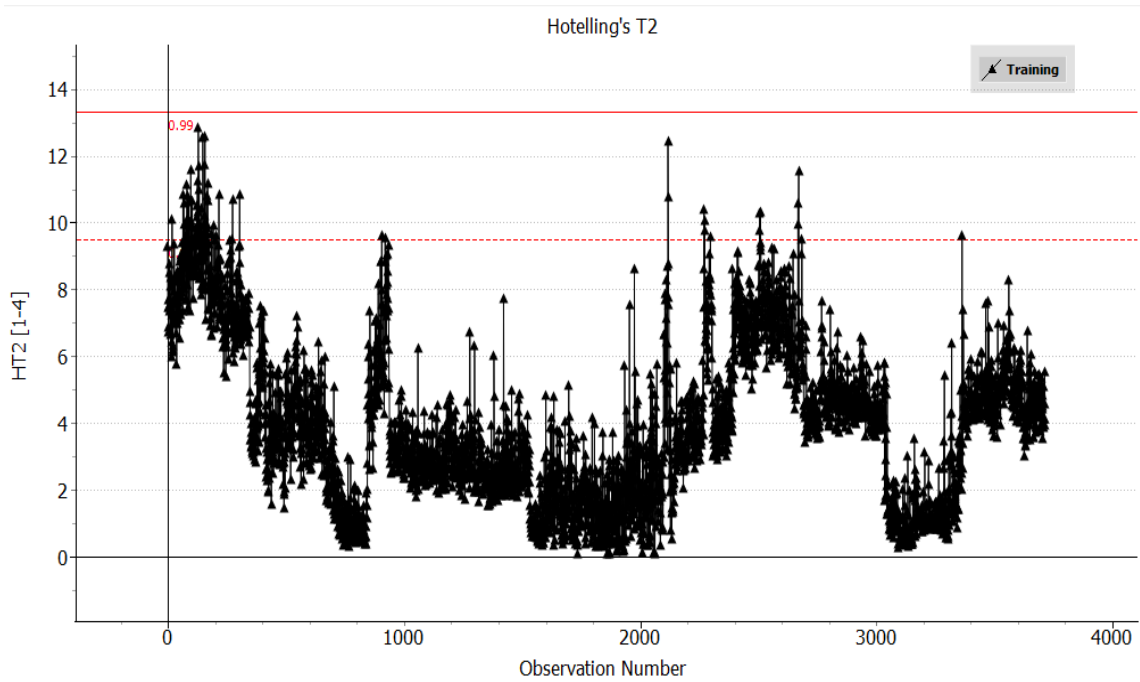


Figure 4.8. T2 plot of the data after removing the process outliers

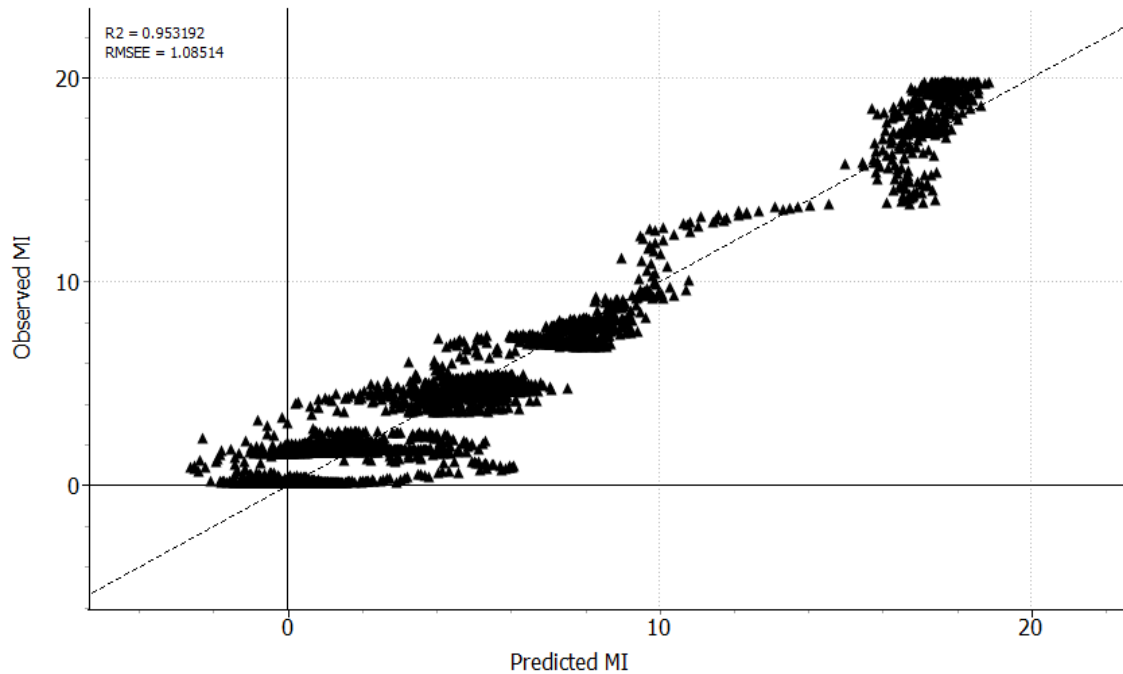


Figure 4.9. Prediction plot for PLS model without lag

The Root Mean Squared Error (RMSE) plot for the PLS model without lag is 1.08 for test data and the plot of the observed v/s predicted values is shown in Figure 4.9. The variable importance of each variable in defining the variance of the PLS model is shown

in Figure 4.8. The loading plot is shown in Figure 4.11 which defines the correlation of the variables which signify that MI is highly correlated with H2, H2/C2 and CAT (since they lie nearer to each other). The bar plot gives a quantitative dependence of each variable for MI prediction.

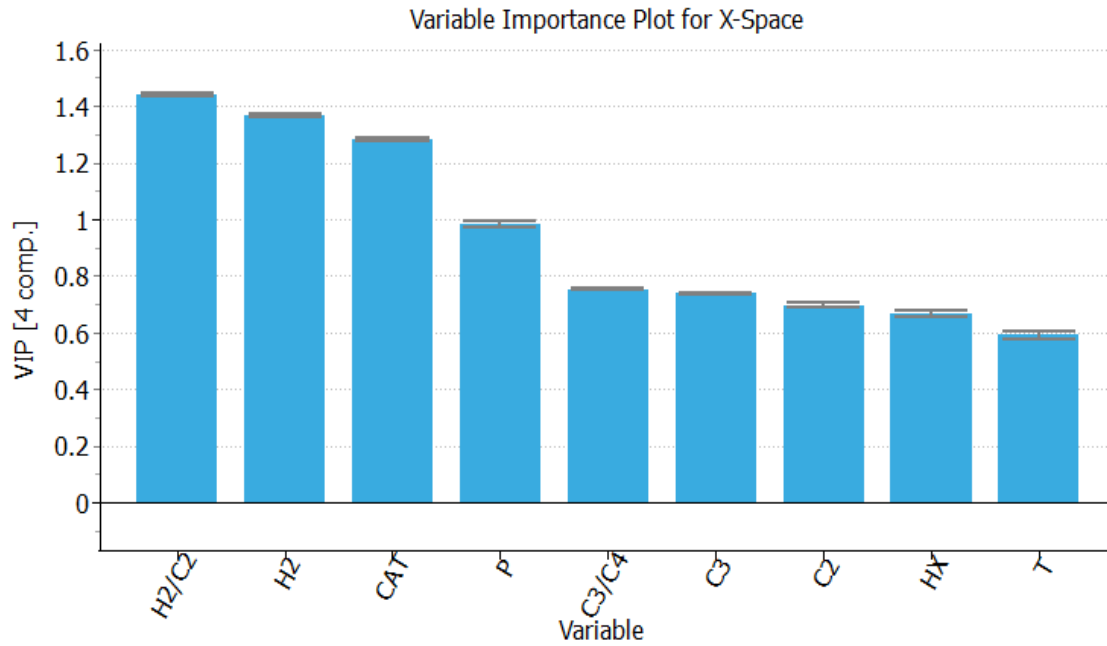


Figure 4.10. Variable importance plot for PLS model without lag

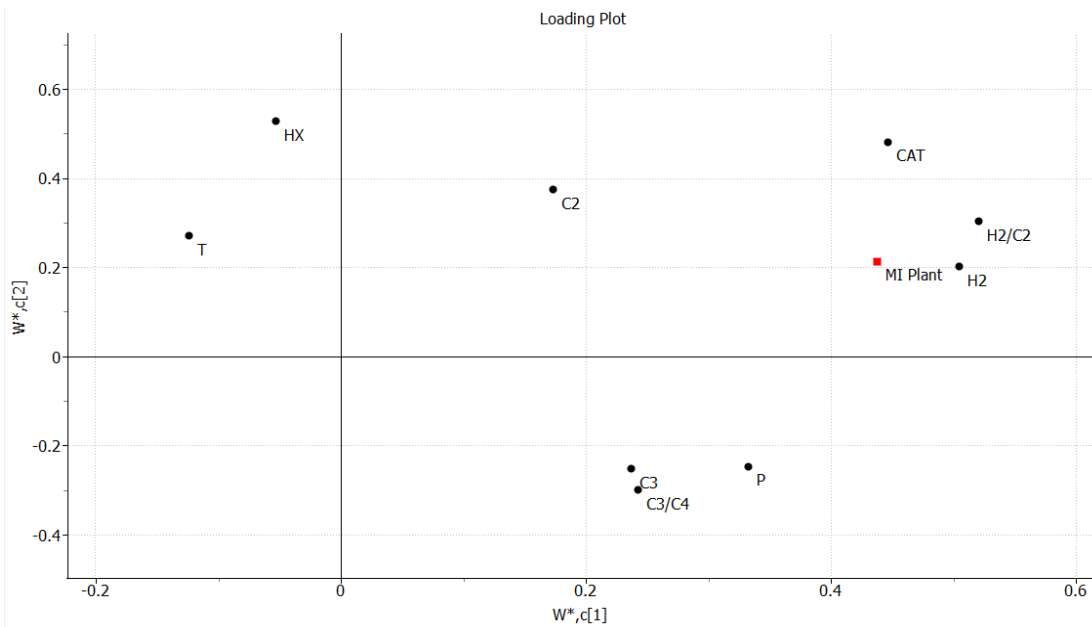


Figure 4.11. Loading plot for PLS model without lag

Now since this is a **dynamic process** there is some lag between the time when the MI at reactor outlet is measured and the process variable. So the output in a dynamic process is related to the past process variable inputs and past outputs as well. In order to handle the autocorrelation data we mimic the concept of auto-regressive moving average exogenous (ARMAX) time series models by forming the data matrix with previous observation in each observation vector. The time series model which relates independent variable Y at present time to past independent variable Ys and dependent variable Xs.

The model equation is represented below:

$$y_t = \beta_1 y_{t-1} + \beta_2 y_{t-2} + \dots + \gamma_1 x_{t-1} + \gamma_2 x_{t-2} + e_t$$

This eventually means that we need to use a lagged value of the variable to account for the dynamic analysis. Thus, we consider the autocorrelation in the data in Pro MV by introduction of the lag of variable order. This time series modeling technique is also referred as **Dynamic PLS** ⁷³.

In this case we introduce a lag of order 1 in both the input process variables and the process output MI, so that the MI at the current time is function of the historical value of process variables and past MI value. By introducing the process lag the R2 value of the PLS model increases to 0.98, the R2 value is shown in figure 4.12. The RMSE value of the model improves significantly to 0.58. The prediction values are shown in figure 4.13.

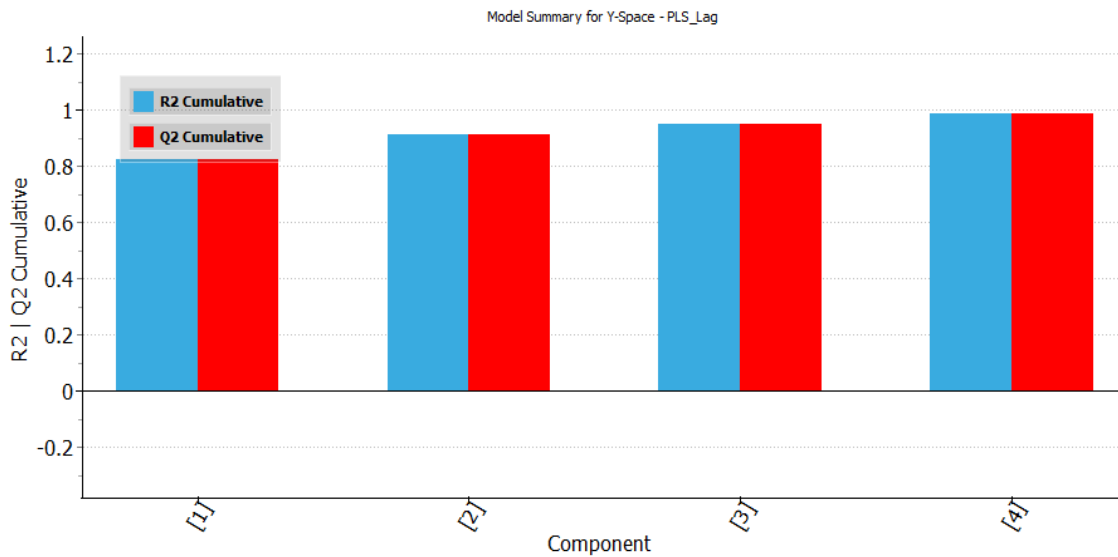


Figure 4.12. Principal component of dynamic PLS model with lag

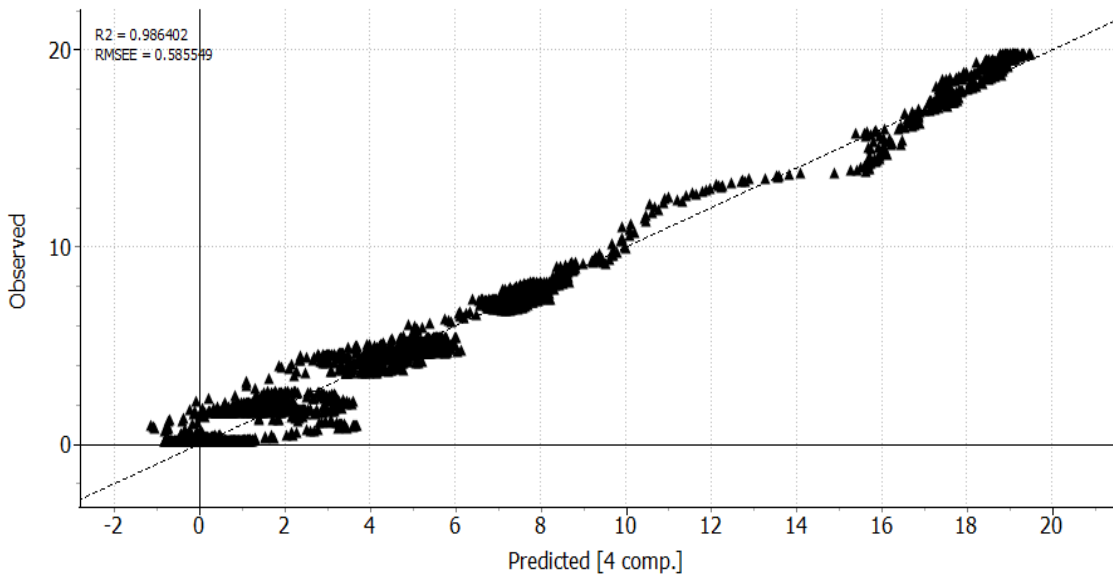


Figure 4.13. Prediction plot of dynamic PLS model with lag

In the VIP plot, we can see that the lagged variables become more important and the MI lagged value becomes the most important variable for the dynamic PLS model as shown in Figure 4.14.

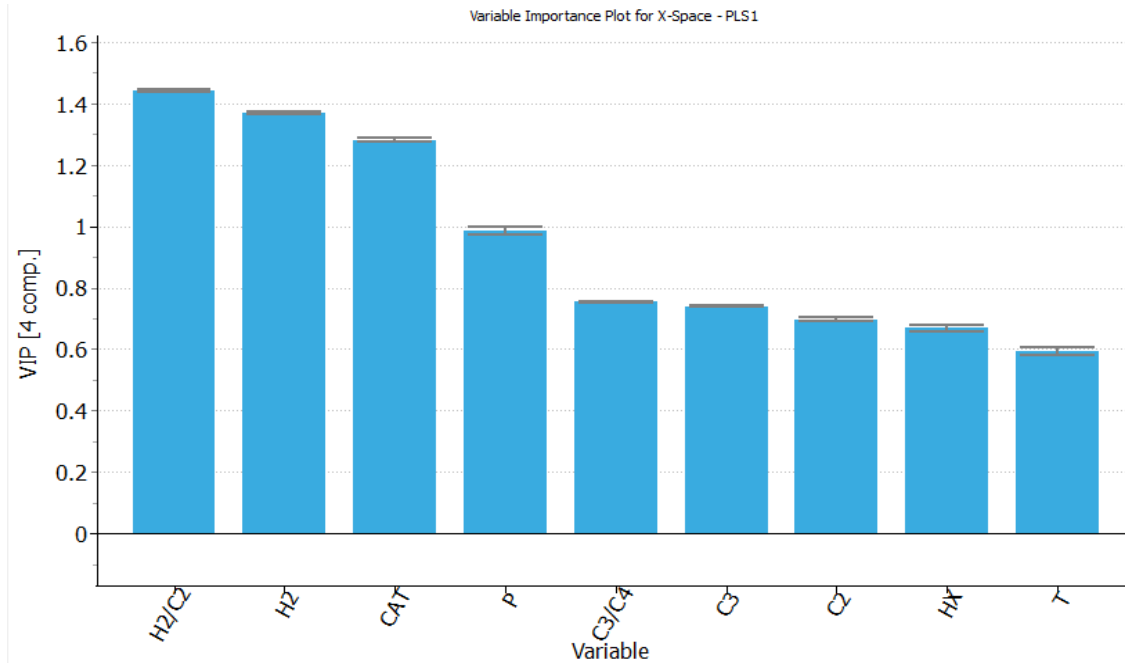


Figure 4.14. Variable Importance Plot for Dynamic PLS model including lag

Figure 4.15 compares the measured time-dependent MI data for the slurry HPDE process from with grade transitions to the predictions from a regressed model based on the multivariate statistical analysis with partial least squares (PLS). Now, we will compare the same time -dependent grade transitions for predictive ML models

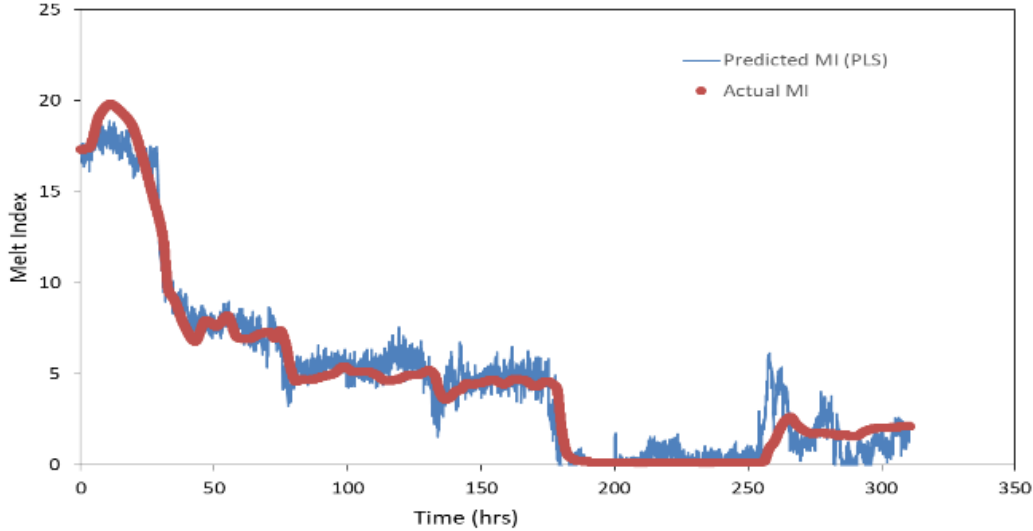


Figure 4.15. Development of a soft sensor of MI based on Causal PLS model

4.4.2. Predictive Machine Learning Models

We use different predictive machine learning (ML) models to predict the MI index values.

In general, we evaluate the relative accuracy of different regression models using the root mean square error (RMSE). Regression methods like support vector regression performed worst for this dataset. The other regression models like linear/ridge, Bayesian, lasso regression has RMSE values around the same range as PLS model in the range of 0.8 to 1.3, but still lower than Dynamic PLS models with RMSE of 0.58.

Deep Neural Network model with 3 hidden layers and 100 neurons in each layer gives slightly better RMSE of 0.4 which can be further improved by hyper parameter estimation. The Neural Network architecture with 9 inputs, 3 hidden layers and 1 output is represented in Figure 4.16.

In neural networks or any ML model we define an error function which calculates the difference between the current model output and the expected value called as loss function. The loss curve of the deep learning model for training and validation is shown in Figure 4.17, which shows how the loss decreases with the increasing epochs.

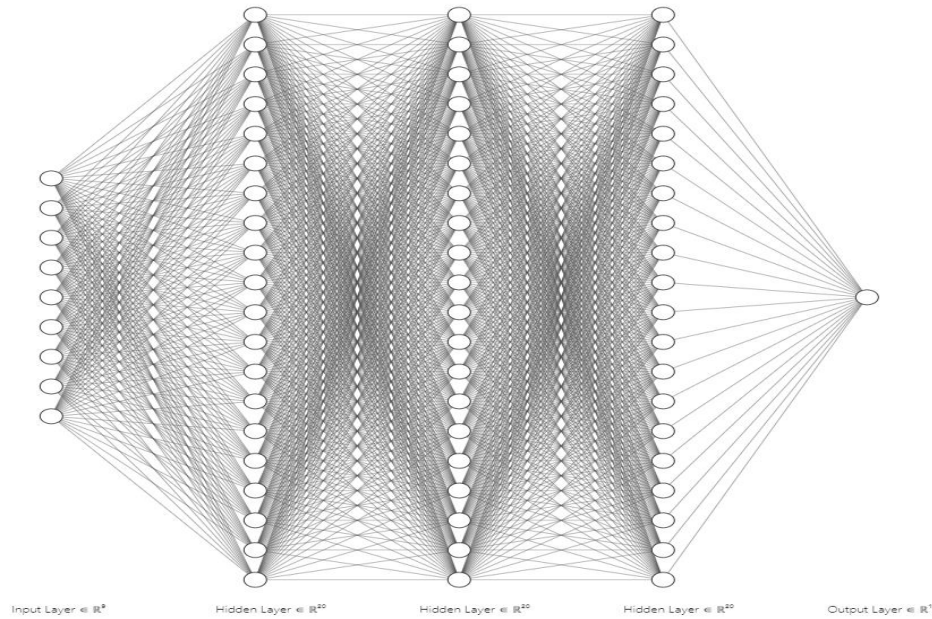


Figure 4.16. Deep Neural Network Architecture with three hidden layers

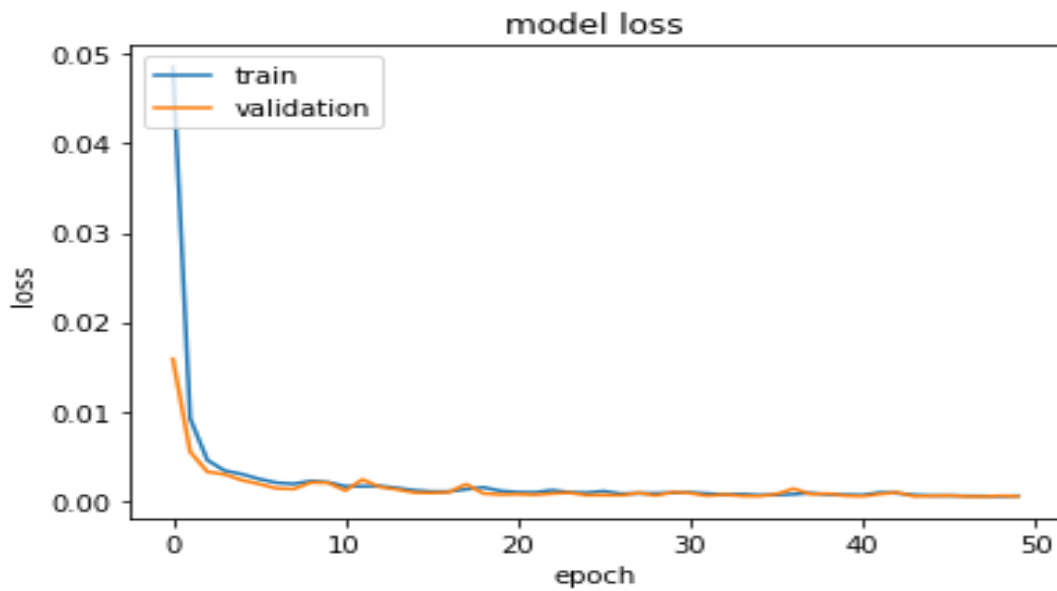


Figure 4.17. Loss curve of Deep Learning model for MI prediction

Ensemble models perform best for this dataset with Gradient Boosting/Xgboost regression model with an RMSE of 0.2 and Random Forest model with a RMSE of 0.12. We use grid search 5-fold cross validation to obtain the best hyper parameters for both the initial and meta-regressors. 5-fold cross-validation means that the data set is split into 5 number of sections/folds where each fold is used for testing while rest use for training

iteratively. For each regressor we choose a range of values of some hyperparameters and finally choose the parameter values that gives the best prediction using the cross validation. For instance, in the random forest model - number of trees is one of the important hyperparameter model that can be varied to improve the validation accuracy. The Figure 4.18 shows the accuracy scores (R2) for Random Forest model, we can see how the cross-validation score varies by changing the number of tree estimators in the model.

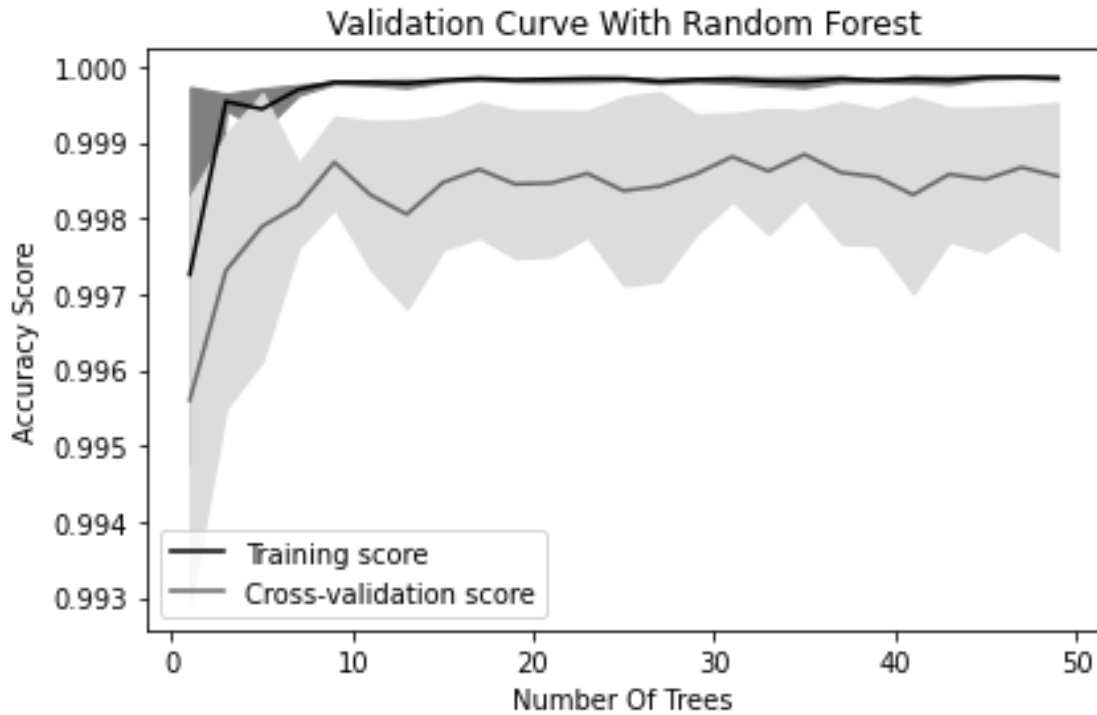


Figure 4.18. The variation of hyperparameter in a Random Forest Model

We plot a sub model of the random forest model of a single tree and max depth =3 to visualize the tree model in figure 4. We visualize the recursive tree model as the tree splits in a way so that overall sum of squares of error are minimized. Figure 4.29 shows the same comparison of the plant MI values with the random forest model predictions.

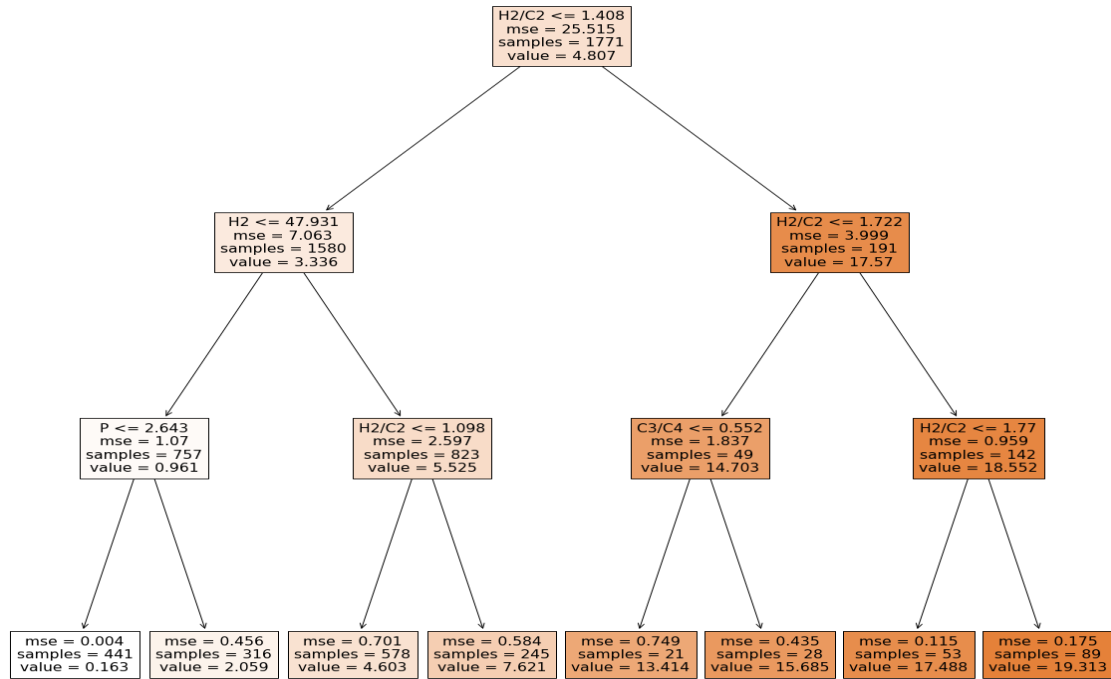


Figure 4.19. Visualization of a tree from the Random Forest Model

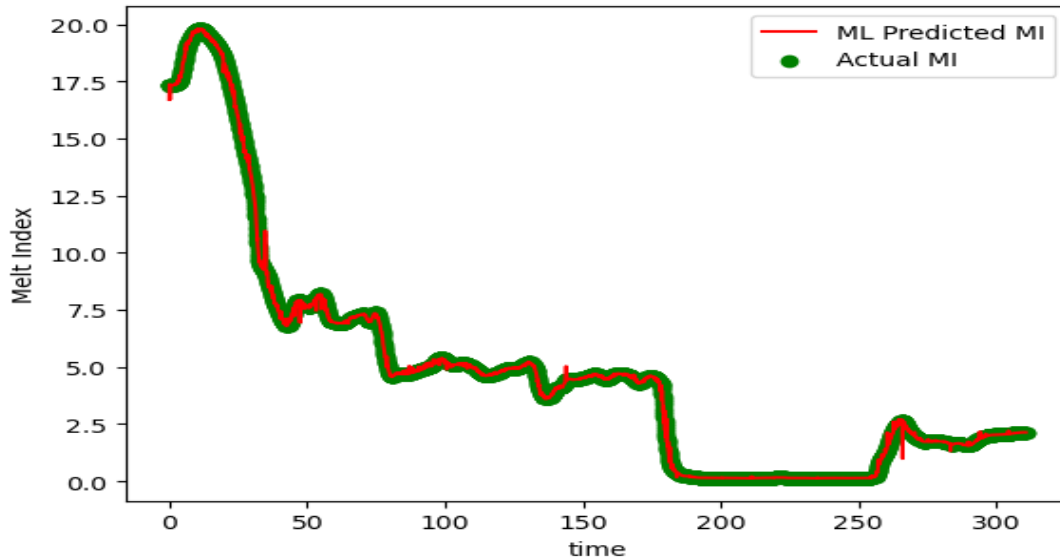


Figure 4.20. Development of a soft sensor of ML based on Predictive random forest model

Table 4.2 and Figure 4.21 summarizes the comparison of each of the ML models

Table 4.2. Comparison of different ML models for MI prediction

Model	RMSE (test) MI
Random Forest	0.12
Xgboost/Gradient Boosting/Stacking reg	0.2
Deep Neural Network	0.42
Dynamic PLS	0.58
Ada-boost Regression	0.64
Linear/Ridge Regression	0.77
Bayesian Regression	0.8
PLS	1.08
Lasso Regression	1.3
Support Vector Regression	4.44

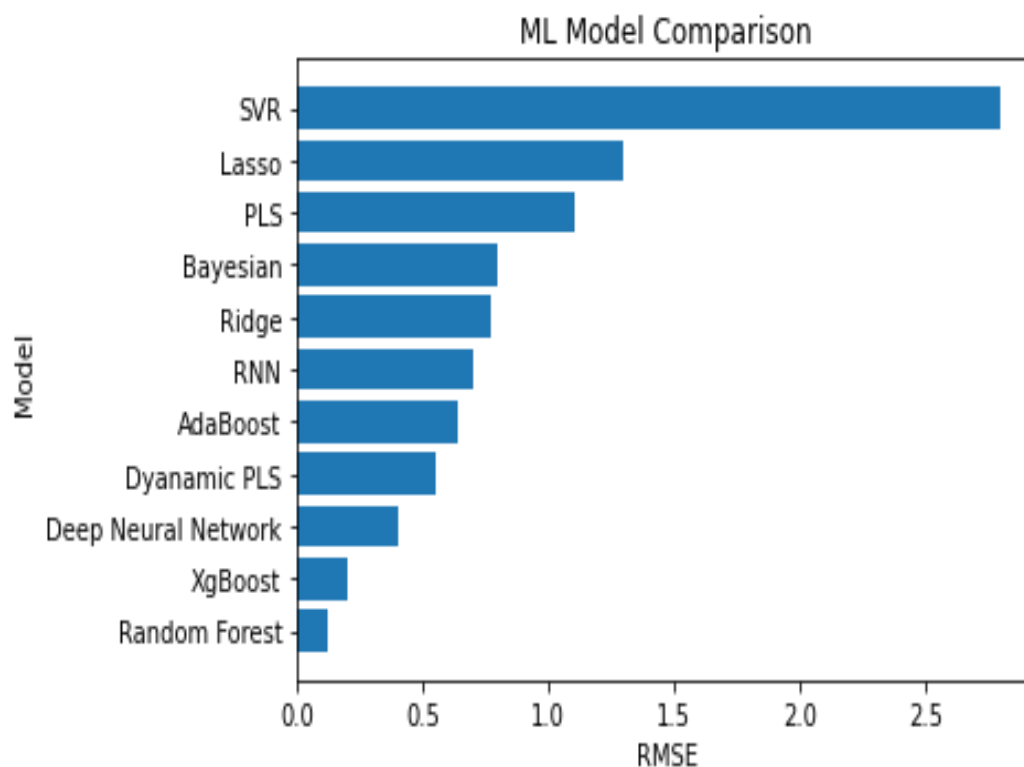


Figure 4.21. Comparison of different ML models for MI prediction

4.5. Disadvantages of Stand-alone Data-Based Models

The predictive ML models are not able to identify the important features correctly, hence they are not able to identify the model sensitivities accurately. Based on the knowledge of polyolefin reaction kinetics, we know that melt index (MI) is highly

dependent on the hydrogen flow rate and a small change in hydrogen flow leads to a significant change in MI. So, the variation of MI with hydrogen flow for a first principle model and ML model is shown in table, as we can see the accurate predictive model like is not able to identify accurate process sensitivities. By doubling the hydrogen flow rate, there is much less change in ML model compared to a first-principle model or latent variable causal model, which is scientifically inconsistent since MI is highly dependent on H2 flow. Now we start with an observation with H2 = 60 m3/hr with all values of process variables same as those of the data and use it to predict MI from each of the models and compare the result with plant data. We increase H2 flow to 95 m3/hr above the operating flow range keeping other process variables as same. For the actual plant data, we write the corresponding value of H2 when H2 flow is 95 m3/hr, even though other variables are different since it is the most important factor. We find that the first principle model is better able to predict the change since it is built on accurate reaction kinetics. The ML model is not able to capture the individual effect of the features, it is more accurate only if given the same combination of features that the model was trained on (all features when H2 flow is 90 m3/hr for accurate prediction when H2 flow is 95 m3/hr). The causal PLS model is better able to capture the effect of individual features. Still for a more accurate prediction beyond the operating range we will need a hybrid combination of first-principle and ML models.

Table 4.3. Model comparison based on MI values at varying hydrogen flow

Model	MI (H2 = 60 m3/hr)	MI (H2 = 95 m3/hr) (beyond operating range)
Plant Actual value	5	22
First principle	6.1	17
Causal ML model	4.7	15
Predictive ML model	4.9	12

4.6. Semi-supervised Learning for Polymer Process Data Analysis

We demonstrate the application of semi-supervised learning techniques for polyolefin data analysis. In many polyolefin plants, the product quality variables are not measured online and they are usually measured in lab sample analysis at much longer time intervals compared to the process data measurements. The quality data, also referred as labelled data, are expensive and difficult to get while unlabeled is abundant and cheap.

4.6.1. Self-Training

We can use self-training semi-supervised techniques like pseudo-labeling to utilize unlabeled data. It improves the model robustness by more precise decision boundary. We simulate real plant scenario by reducing the frequency of product quality measurement to much lower values compared to the process variables. Thus, we consider the same polyolefin process as mentioned previously with the feed process variables and the MI as

the quality variable. We consider only 1% MI values for the y data. For 5000 observations of process data (X), only 50 values of MI data (Y) are available.

For the analysis of these data we use semi-supervised learning techniques called pseudo-labeling. This method utilizes both the labelled and unlabeled process data. We refer the data which have MI measurements as labelled, while the data which do not have MI values as unlabeled. We first train labelled data by a regressor model. We use random forest regressor for this data. Then, we use the model to predict labels on the unlabeled data, creating the pseudo labels or predictions. We combine the labelled and the unlabeled data, giving an augmented dataset which is again used to train the random forest regressor model. The model predicts much higher accuracy when we used the unlabeled data set along with the labeled data compared to just using the labeled data set alone. The prediction accuracy is much higher than using only labelled data. In Figure 4.22 we see the RMSE value of the Pseudo-labelled regression prediction is 0.8 compared to 1.8 considering only the labelled data. Sample rate denotes the percentage of unlabeled data to be used as the pseudo labelled for the modelling purpose.

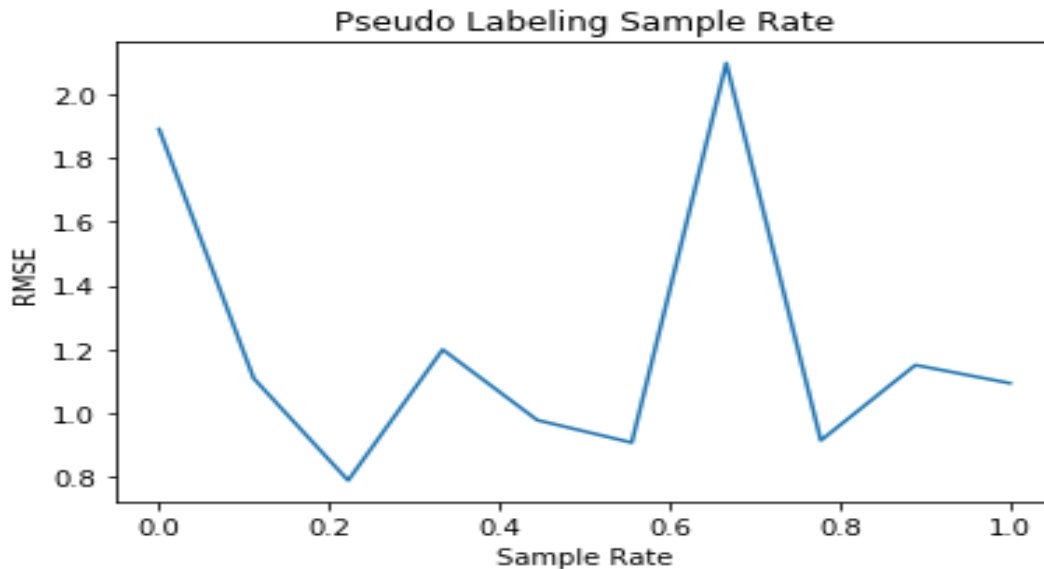


Figure 4.22. Accuracy v/s the sampling rate for Semi-Supervised Learning MI prediction

4.6.2 Generative Model - GAN

Another approach when less data is available can be used to generate more data. GAN models explained previously are useful for generating more data. The generative model generates data with some noise and the discriminator model detects from the real data from the generated/fake data in the form of a loss function. With each iterative process the generative model becomes better at generating fake data. So that finally when the model converges the discriminator is not able to distinguish real from fake data.

We use the same HDPE dataset and consider only 50 available observations. We showcase how to generate 1000 more data points from these 50 available observations using the GAN models. We use the Condition GAN model by Xu et. al.⁷⁴ where they showcase the methodology of generating tabular data like our dataset. They model the probability distributions of each of the rows in dataset and generate realistic synthetic data dealing with both discrete and continuous dataset. Figure 4.23 compares the the absolute log mean of the actual data (real) and generated data (fake) and the comparison of each feature is shown in Figure 4.24. Probability Density Distribution of each feature comparison of of the real and generated data is shown in figure 4.25.

These plots show that the generated dataset represents the original dataset quite well. The original dataset with 50 data points is used to fit a gradient boosting regression model for the MI prediction which gives a higher RMSE value of 1.14. Now the augmented dataset with 1050 data-points is again used to fit the regression model which results in improvement in prediction with RMSE Of 0.85.

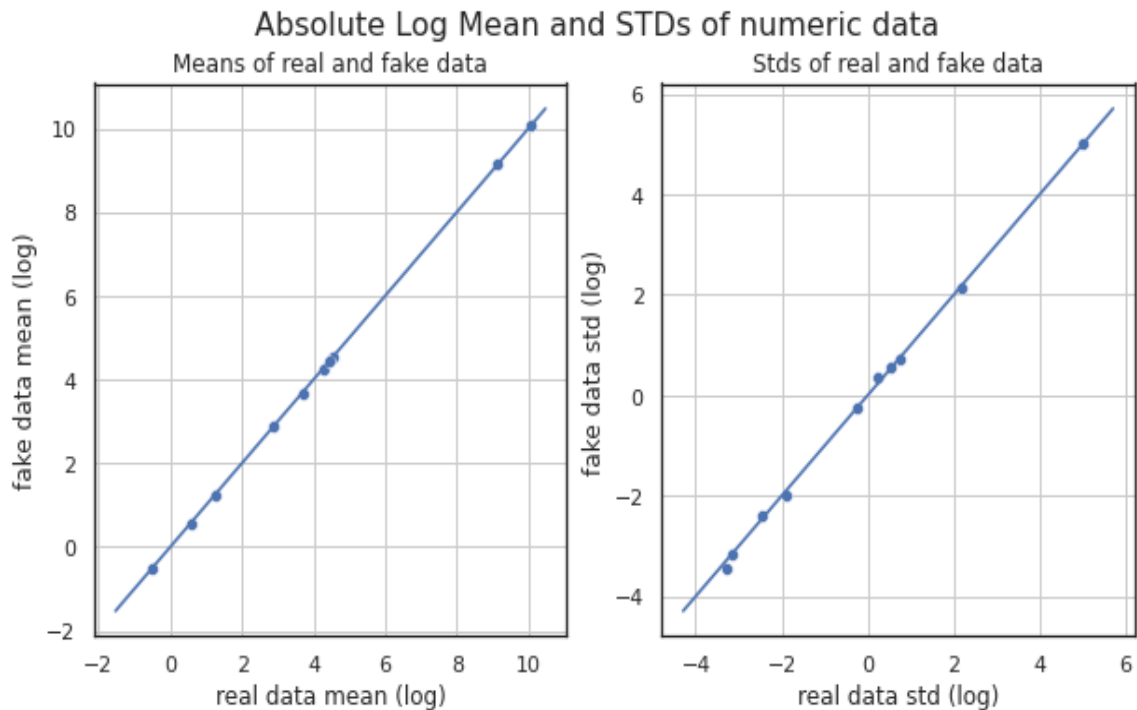


Figure 4.23. The comparison of the real and fake(generated data) in terms of means and stdev.

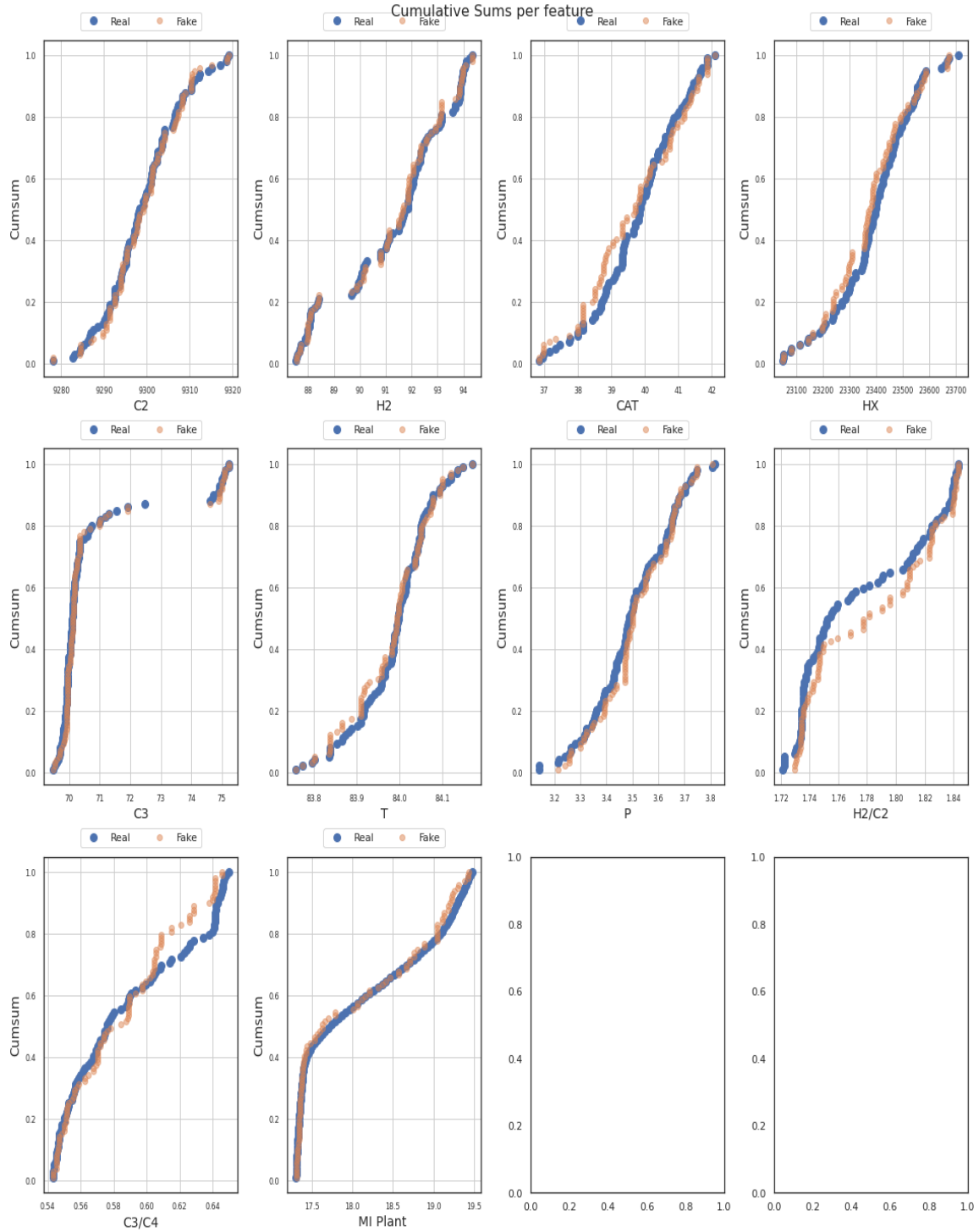


Figure 4.24. Comparison of each of the real and generated data for each of the features using the GAN model

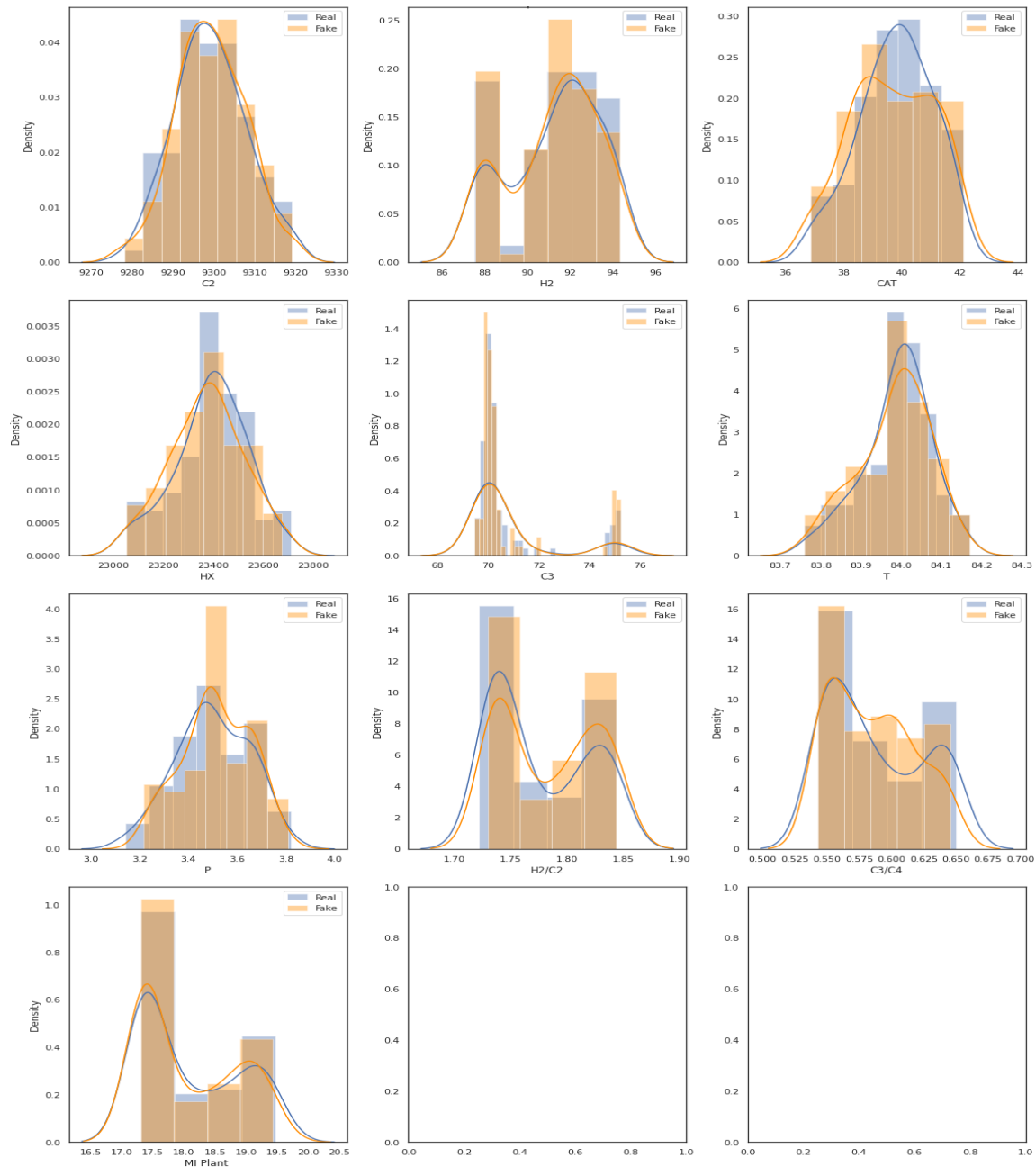


Figure 4.25. Comparison of each feature b/w real and fake data with Probability Density Distribution of each feature comparison

4.7. Batch Data Analysis

Most of the data analysis till now has been for continuous processes. For data analysis of batch process we require a different approach. An industrial batch process data with multiple batches has a three-dimensional structure with the three data dimensions, namely, process variables, time and number of batches. Thus we need to apply data unfolding techniques along with the PLS models for analysis. Batch data analysis requires the The

Batch Wise Unfolding (BWU) approach was first established by Nomikos and Macgregor⁷⁵, it examines the variation among batches since the different batches may have different disturbance. In BWU, the batch observation are extracted horizontally in a time-wise fashion. Each batch becomes a single row of data as shown in Figure 4.26. Thus, BWU score predicts the final state of each batch based on all the time history of that batch to current time.

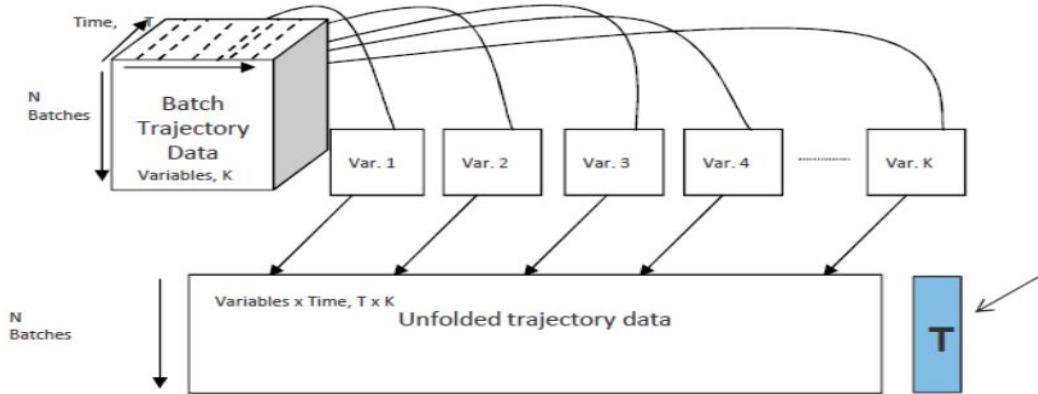


Figure 4.26. Batch wise unfolding methodology

In contrast if we use a similar data analysis methodology as we used for the continuous processes it can be termed as the Observation Wise Unfolding (OWU), where the data for each batch is stacked on top of one another and the analysis will summarize the instantaneous condition of each batch using the measured values at the current time.

We consider a polymer batch data provided by Kevin Dunn¹⁰ consisting of only the process variables (10) X of the 55 batches. Thus, we use PCA along with the BWU analysis to identify the bad batches using Aspen Pro-MV. The R^2 score for the PCA model for the Batch model is 0.66. By plotting the score plot shown in Figure 4.27 we identified the abnormal batches (50-55)

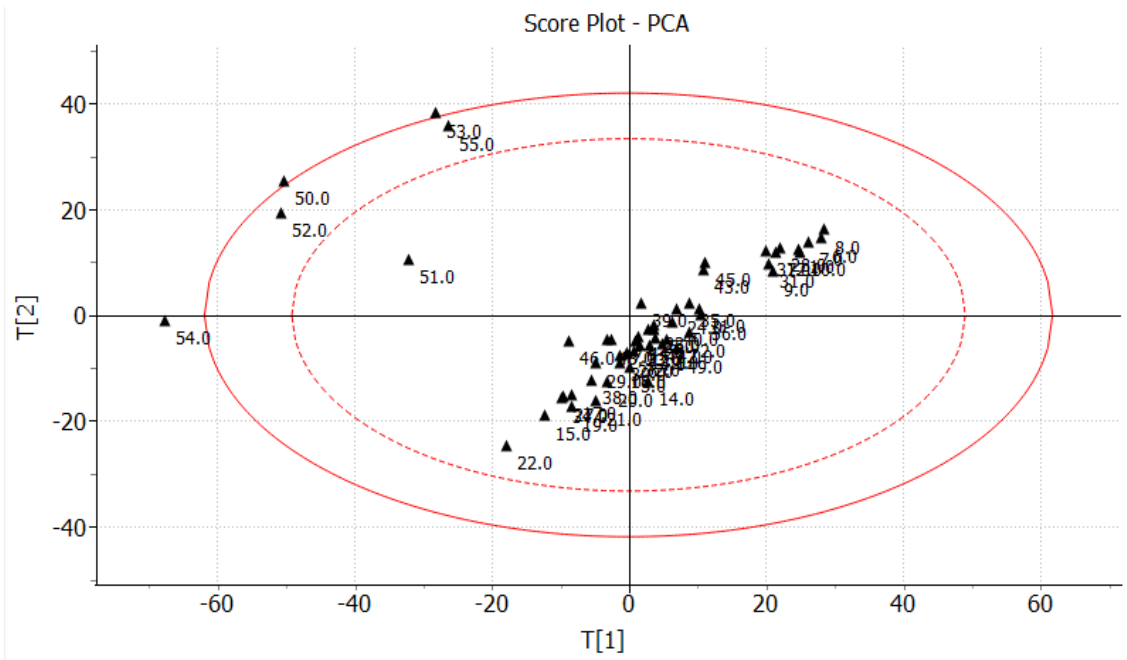


Figure 4.27. Score plot of PCA polymer batches

Then we also try to identify the causes for the batches to be abnormal by plotting the contribution plot for the scores from 50 to 55 as shown in Figure 4.28.

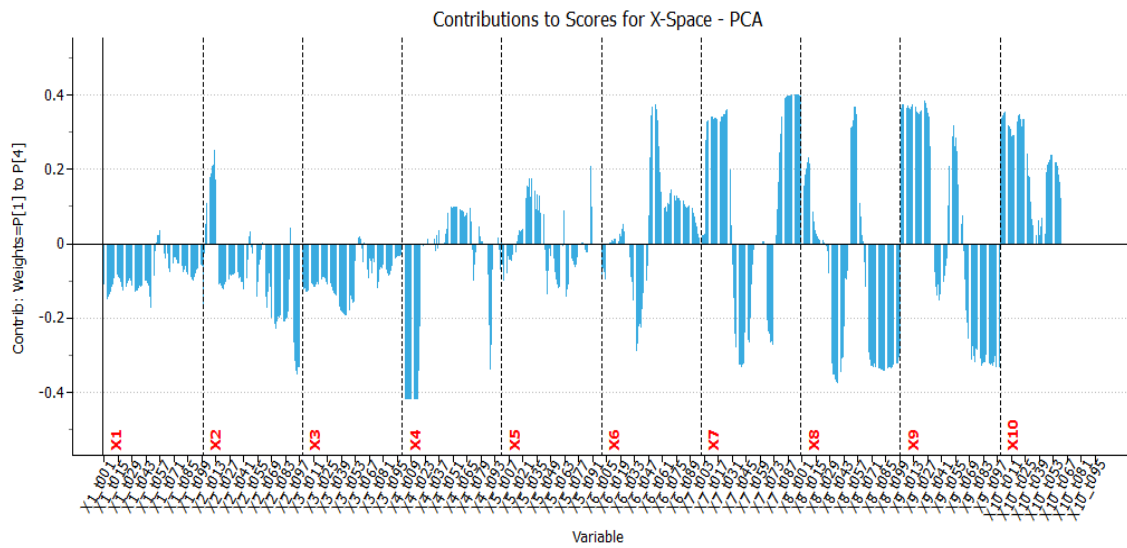


Figure 4.28. Contribution to scores of bad batches

If we use the OWU for the same dataset, the score plot for the PCA model does not provide any interpretable results to identify outliers shown in figure 4.29.

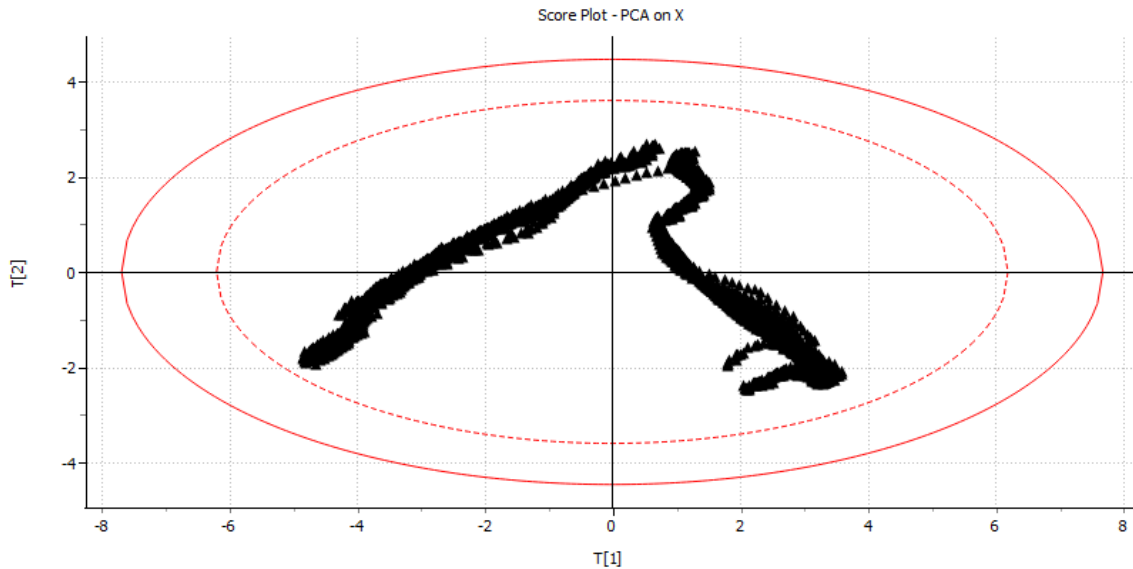


Figure 4.29. Observation wise Analysis of Batch data

Thus, BWU approach is more suitable than OWU for any batch data analysis.

4.8. Industrial Case study of Extrusion Process Monitoring

In a extrusion process by Universal Fibers, Virginia they had an issue of high modification ratio (MR) for one of their fiber product which is not good for their process quality specification. We analyze industrial data for a month with more than 10000 observations. The process variables/features were mainly the extruder variables, pump variables and spinning variables like: RPM, pressure, amp, temperature etc. with a total of 50 features.

We first use PCA on the data set we reduce the 50 features to 7 principle components with R2 of 0.65. Then we identify process outliers using Hotelling T2 method and plot the score plot as shown in Figure 4.30. We find that the process outliers lie in the same period when the MR was high b/w the range 4-5. Thus, we analyze the reason for the process faults to be high value of pump amp and the low value of extruder RPM using contribution scores. The contribution plot for the outliers is shown in Figure 4.31. We also use the MR data (Y) to fit a PLS model and analyze the relationship between MR and process variables. The loading plot in Figure 4.32 shows the variables highly correlated with the MR values like Extruder (RPM), Pump AMP.

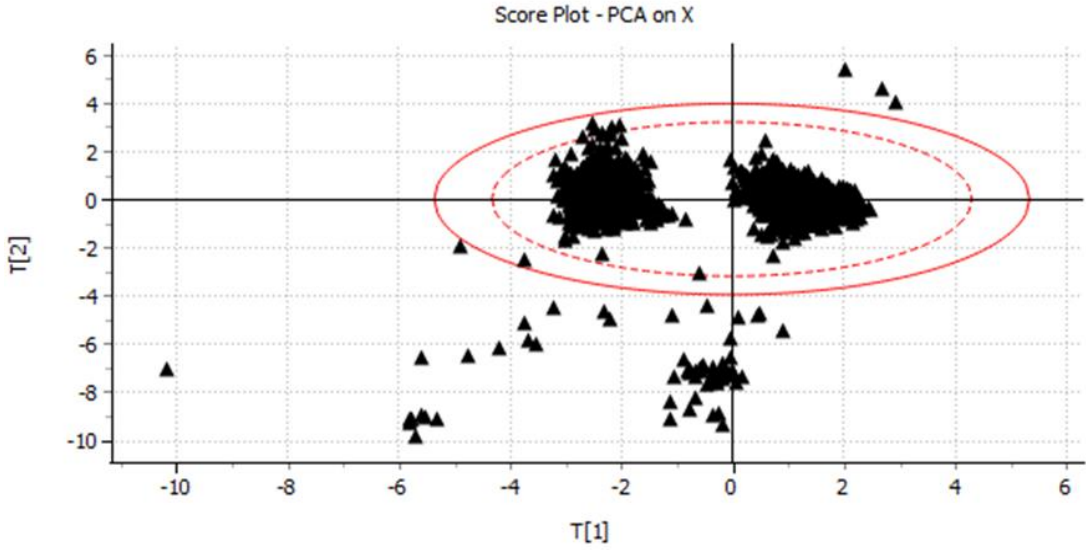


Figure 4.30. Score plot of the extruder process data

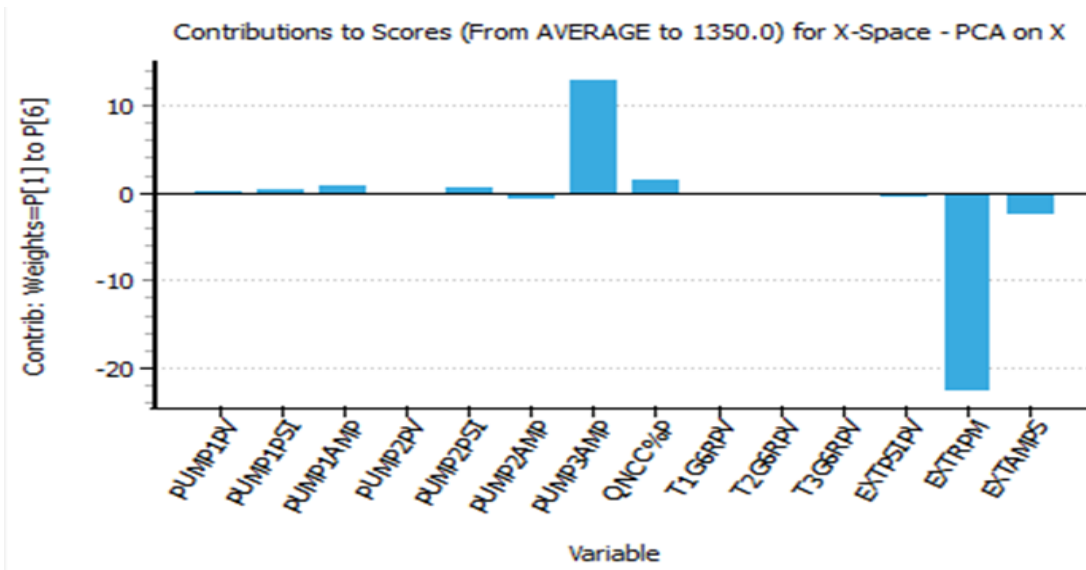


Figure 4.31. Contribution to score plot of process anomaly in an industrial extrusion process

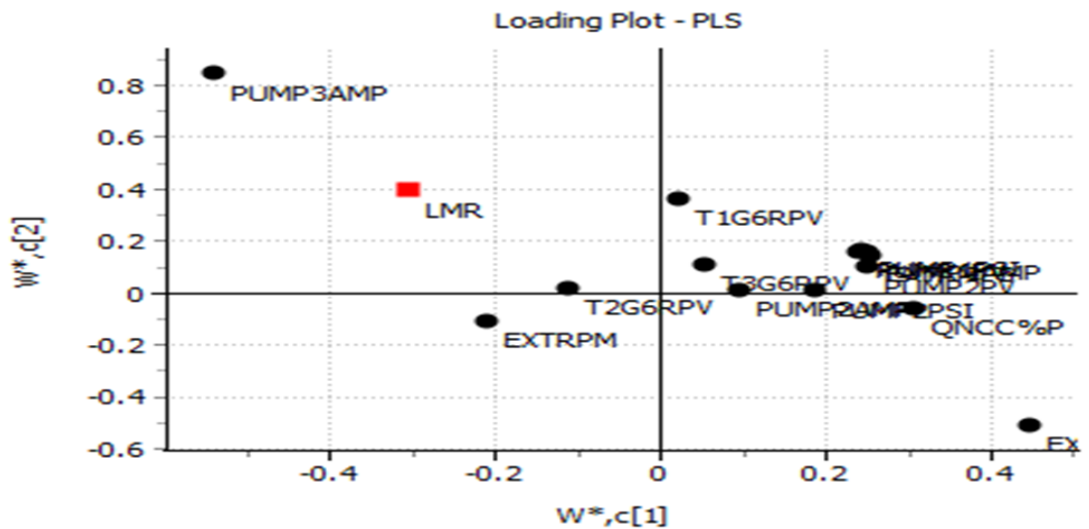


Figure 4.32. Loading plot for the PLS analysis of the extruder data

4.9. Conclusion

We have showcased the utility of latent variable models like PLS for causal analysis to identify correct correlations between input and outputs using the polymer process application. We also showcase the utility of predictive models like ensemble random forest for predicting the process outputs, predicting the MI with lowest RMSE. We identify the Dynamic PLS model utility in dynamic time series process data by considering the measurement lags. We conclude that a data-based model alone has a high accuracy, but it may give scientifically inconsistent results for predictions beyond process operating data which the model uses and also not able to accurately simulate individual feature importance. Hence, we advocate the integration of first principle process model with data-based ML models in hybrid modeling strategy in following chapters. We showcase the applications of semi-supervised learning methods like self-training and generative models. We also show the methodology for analysis of batch data. We also showcase the fault diagnosis in an industrial extrusion process.

References

1. Quantrille, T. E.; Liu, Y. A., *Artificial intelligence in chemical engineering*. Elsevier: 2012.
2. Baughman, D. R.; Liu, Y. A., *Neural networks in bioprocessing and chemical engineering*. Academic press: 2014.
3. Qin, S. J., Process data analytics in the era of big data. *AIChE Journal* **2014**, *60* (9), 3092-3100.
4. Chiang, L.; Lu, B.; Castillo, I., Big data analytics in chemical engineering. *Annual review of chemical and biomolecular engineering* **2017**, *8*, 63-85.
5. Ge, Z.; Song, Z.; Ding, S. X.; Huang, B., Data mining and analytics in the process industry: The role of machine learning. *Ieee Access* **2017**, *5*, 20590-20616.

6. MacGregor, J. F., Using on-line process data to improve quality: challenges for statisticians. *International Statistical Review* **1997**, *65* (3), 309-323.
7. Skagerberg, B.; MacGregor, J. F.; Kiparissides, C., Multivariate data analysis applied to low-density polyethylene reactors. *Chemometrics and intelligent laboratory systems* **1992**, *14* (1-3), 341-356.
8. Haykin, S., *Neural Networks and Learning Machines* 3rd Ed. NY: NYL Pearson Prentice Hall. 2009.
9. Johnson, R. A.; Wichern, D. W., *Applied multivariate statistical analysis*. Pearson London, UK:: 2014; Vol. 6.
10. Dunn, K., Process improvement using data. *Experimentation for Improvement. Hamilton, Ontario, Canada. Creative Commons Attribution-ShareAlike* **2019**, *4*, 325-404.
11. MacGregor, J. F.; Kourti, T., Statistical process control of multivariate processes. *Control engineering practice* **1995**, *3* (3), 403-414.
12. Qin, S. J.; Chiang, L. H., Advances and opportunities in machine learning for process data analytics. *Computers & Chemical Engineering* **2019**, *126*, 465-473.
13. Shang, C.; You, F., Data analytics and machine learning for smart process manufacturing: recent advances and perspectives in the big data era. *Engineering* **2019**, *5* (6), 1010-1016.
14. Haghghatlari, M.; Hachmann, J., Advances of machine learning in molecular modeling and simulation. *Current Opinion in Chemical Engineering* **2019**, *23*, 51-57.
15. Goldsmith, B. R.; Esterhuizen, J.; Liu, J. X.; Bartel, C. J.; Sutton, C., Machine learning for heterogeneous catalyst design and discovery. **2018**.
16. Ning, C.; You, F., Data-driven stochastic robust optimization: General computational framework and algorithm leveraging machine learning for optimization under uncertainty in the big data era. *Computers & Chemical Engineering* **2018**, *111*, 115-133.
17. Sharma, N. In *Polyolefin Process Modeling and Monitoring*, 2019 AIChE Annual Meeting, AIChE: 2019.
18. LeCun, Y.; Bengio, Y.; Hinton, G., Deep learning. *nature* **2015**, *521* (7553), 436-444.
19. Tibshirani, R., Regression shrinkage and selection via the lasso. *Journal of the Royal Statistical Society: Series B (Methodological)* **1996**, *58* (1), 267-288.
20. Smola, A. J.; Schölkopf, B., A tutorial on support vector regression. *Statistics and computing* **2004**, *14* (3), 199-222.
21. Lewis, R. J. In *An introduction to classification and regression tree (CART) analysis*, Annual meeting of the society for academic emergency medicine in San Francisco, California, Citeseer: 2000.
22. Schapire, R. E., The strength of weak learnability. *Machine learning* **1990**, *5* (2), 197-227.
23. Breiman, L., Random forests. *Machine learning* **2001**, *45* (1), 5-32.
24. Friedman, J. H., Greedy function approximation: a gradient boosting machine. *Annals of statistics* **2001**, 1189-1232.

25. Chen, T.; Guestrin, C. In *Xgboost: A scalable tree boosting system*, Proceedings of the 22nd acm sigkdd international conference on knowledge discovery and data mining, 2016; pp 785-794.
26. Breiman, L., Stacked regressions. *Machine learning* **1996**, *24* (1), 49-64.
27. Geladi, P.; Kowalski, B. R., Partial least-squares regression: a tutorial. *Analytica chimica acta* **1986**, *185*, 1-17.
28. Ellis, B.; Wong, W. H., Learning causal Bayesian network structures from experimental data. *Journal of the American Statistical Association* **2008**, *103* (482), 778-789.
29. Wold, S.; Esbensen, K.; Geladi, P., Principal component analysis. *Chemometrics and intelligent laboratory systems* **1987**, *2* (1-3), 37-52.
30. Grandvalet, Y.; Bengio, Y., Semi-supervised learning by entropy minimization. *CAP* **2005**, *367*, 281-296.
31. Goodfellow, I.; Pouget-Abadie, J.; Mirza, M.; Xu, B.; Warde-Farley, D.; Ozair, S.; Courville, A.; Bengio, Y., Generative adversarial nets. *Advances in neural information processing systems* **2014**, *27*.
32. Kaelbling, L. P.; Littman, M. L.; Moore, A. W., Reinforcement learning: A survey. *Journal of artificial intelligence research* **1996**, *4*, 237-285.
33. Hoskins, J.; Himmelblau, D., Process control via artificial neural networks and reinforcement learning. *Computers & chemical engineering* **1992**, *16* (4), 241-251.
34. Pedregosa, F.; Varoquaux, G.; Gramfort, A.; Michel, V.; Thirion, B.; Grisel, O.; Blondel, M.; Prettenhofer, P.; Weiss, R.; Dubourg, V., Scikit-learn: Machine learning in Python. *the Journal of machine Learning research* **2011**, *12*, 2825-2830.
35. Abadi, M.; Barham, P.; Chen, J.; Chen, Z.; Davis, A.; Dean, J.; Devin, M.; Ghemawat, S.; Irving, G.; Isard, M. In *Tensorflow: A system for large-scale machine learning*, 12th {USENIX} symposium on operating systems design and implementation ({OSDI} 16), 2016; pp 265-283.
36. Lou, S.; Wu, P.; Guo, L.; Duan, Y.; Zhang, X.; Gao, J., Sparse principal component analysis using particle swarm optimization. *Journal of Chemical Engineering of Japan* **2020**, *53* (7), 327-336.
37. Ning, C.; You, F., Data-driven decision making under uncertainty integrating robust optimization with principal component analysis and kernel smoothing methods. *Computers & Chemical Engineering* **2018**, *112*, 190-210.
38. He, X.; Liu, Y.; Huang, S.; Liu, Y.; Pu, X.; Xu, T., Raman spectroscopy coupled with principal component analysis to quantitatively analyze four crystallographic phases of explosive CL-20. *RSC advances* **2018**, *8* (41), 23348-23352.
39. Fezai, R.; Mansouri, M.; Taouali, O.; Harkat, M. F.; Bouguila, N., Online reduced kernel principal component analysis for process monitoring. *Journal of Process Control* **2018**, *61*, 1-11.

40. Harrou, F.; Kadri, F.; Chaabane, S.; Tahon, C.; Sun, Y., Improved principal component analysis for anomaly detection: Application to an emergency department. *Computers & Industrial Engineering* **2015**, *88*, 63-77.
41. Brestrich, N.; Ruedt, M.; Buechler, D.; Hubbuch, J., Selective protein quantification for preparative chromatography using variable pathlength UV/Vis spectroscopy and partial least squares regression. *Chemical Engineering Science* **2018**, *176*, 157-164.
42. Kocevskaja, S.; Maggioni, G. M.; Rousseau, R. W.; Grover, M. A., Spectroscopic Quantification of Target Species in a Complex Mixture Using Blind Source Separation and Partial Least-Squares Regression: A Case Study on Hanford Waste. *Industrial & Engineering Chemistry Research* **2021**, *60* (27), 9885-9896.
43. Zhang, X.; Kano, M.; Li, Y., Locally weighted kernel partial least squares regression based on sparse nonlinear features for virtual sensing of nonlinear time-varying processes. *Computers & Chemical Engineering* **2017**, *104*, 164-171.
44. Jiang, Q.; Yan, X.; Yi, H.; Gao, F., Data-driven batch-end quality modeling and monitoring based on optimized sparse partial least squares. *IEEE Transactions on Industrial Electronics* **2019**, *67* (5), 4098-4107.
45. Hattori, Y.; Otsuka, M., Modeling of feed-forward control using the partial least squares regression method in the tablet compression process. *International journal of pharmaceutics* **2017**, *524* (1-2), 407-413.
46. Willis, M. J.; Montague, G. A.; Di Massimo, C.; Tham, M. T.; Morris, A. J., Artificial neural networks in process estimation and control. *Automatica* **1992**, *28* (6), 1181-1187.
47. Iliyas, S. A.; Elshafei, M.; Habib, M. A.; Adeniran, A. A., RBF neural network inferential sensor for process emission monitoring. *Control Engineering Practice* **2013**, *21* (7), 962-970.
48. Sun, K.; Liu, J.; Kang, J.-L.; Jang, S.-S.; Wong, D. S.-H.; Chen, D.-S., Development of a variable selection method for soft sensor using artificial neural network and nonnegative garrote. *Journal of Process Control* **2014**, *24* (7), 1068-1075.
49. Hough, B. R.; Beck, D. A.; Schwartz, D. T.; Pfaendtner, J., Application of machine learning to pyrolysis reaction networks: Reducing model solution time to enable process optimization. *Computers & Chemical Engineering* **2017**, *104*, 56-63.
50. Shang, C.; Yang, F.; Huang, D.; Lyu, W., Data-driven soft sensor development based on deep learning technique. *Journal of Process Control* **2014**, *24* (3), 223-233.
51. Gao, X.; Shang, C.; Jiang, Y.; Huang, D.; Chen, T., Refinery scheduling with varying crude: A deep belief network classification and multimodel approach. *AIChE Journal* **2014**, *60* (7), 2525-2532.
52. Li, F.; Zhang, J.; Shang, C.; Huang, D.; Oko, E.; Wang, M., Modelling of a post-combustion CO₂ capture process using deep belief network. *Applied Thermal Engineering* **2018**, *130*, 997-1003.
53. Zhang, Z.; Zhao, J., A deep belief network based fault diagnosis model for complex chemical processes. *Computers & chemical engineering* **2017**, *107*, 395-407.

54. Namdari, M.; Jazayeri-Rad, H., Incipient fault diagnosis using support vector machines based on monitoring continuous decision functions. *Engineering Applications of Artificial Intelligence* **2014**, *28*, 22-35.
55. Pani, A. K.; Mohanta, H. K., Online monitoring and control of particle size in the grinding process using least square support vector regression and resilient back propagation neural network. *ISA transactions* **2015**, *56*, 206-221.
56. Gholami, A. R.; Shahbazian, M., Soft sensor design based on fuzzy C-Means and RFN_SVR for a stripper column. *Journal of Natural Gas Science and Engineering* **2015**, *25*, 23-29.
57. Zio, E.; Baraldi, P.; Popescu, I. C., A fuzzy decision tree method for fault classification in the steam generator of a pressurized water reactor. *Annals of Nuclear Energy* **2009**, *36* (8), 1159-1169.
58. Ge, Z., Process data analytics via probabilistic latent variable models: A tutorial review. *Industrial & Engineering Chemistry Research* **2018**, *57* (38), 12646-12661.
59. Zhou, L.; Chen, J.; Song, Z., Recursive Gaussian process regression model for adaptive quality monitoring in batch processes. *Mathematical Problems in Engineering* **2015**, *2015*.
60. MacGregor, J. F.; Jaeckle, C.; Kiparissides, C.; Koutoudi, M., Process monitoring and diagnosis by multiblock PLS methods. *AIChE Journal* **1994**, *40* (5), 826-838.
61. Gonzaga, J.; Meleiro, L. A. C.; Kiang, C.; Maciel Filho, R., ANN-based soft-sensor for real-time process monitoring and control of an industrial polymerization process. *Computers & chemical engineering* **2009**, *33* (1), 43-49.
62. Shi, J.; Liu, X.; Sun, Y., Melt index prediction by neural networks based on independent component analysis and multi-scale analysis. *Neurocomputing* **2006**, *70* (1-3), 280-287.
63. Han, I. S.; Han, C.; Chung, C. B., Melt index modeling with support vector machines, partial least squares, and artificial neural networks. *Journal of Applied Polymer Science* **2005**, *95* (4), 967-974.
64. Sharmin, R.; Sundararaj, U.; Shah, S.; Griend, L. V.; Sun, Y.-J., Inferential sensors for estimation of polymer quality parameters: Industrial application of a PLS-based soft sensor for a LDPE plant. *Chemical Engineering Science* **2006**, *61* (19), 6372-6384.
65. Ao, T.; Dong, X.; Zhizhong, M., Batch-to-batch iterative learning control of a batch polymerization process based on online sequential extreme learning machine. *Industrial & Engineering Chemistry Research* **2009**, *48* (24), 11108-11114.
66. Kaneko, H.; Arakawa, M.; Funatsu, K., Novel soft sensor method for detecting completion of transition in industrial polymer processes. *Computers & chemical engineering* **2011**, *35* (6), 1135-1142.
67. Ge, Z.; Chen, T.; Song, Z., Quality prediction for polypropylene production process based on CLGPR model. *Control Engineering Practice* **2011**, *19* (5), 423-432.

68. Liu, Y.; Chen, J., Integrated soft sensor using just-in-time support vector regression and probabilistic analysis for quality prediction of multi-grade processes. *Journal of Process control* **2013**, *23* (6), 793-804.
69. Xu, S.; Liu, X., Melt index prediction by fuzzy functions with dynamic fuzzy neural networks. *Neurocomputing* **2014**, *142*, 291-298.
70. Wang, W.; Liu, X., Melt index prediction by least squares support vector machines with an adaptive mutation fruit fly optimization algorithm. *Chemometrics and Intelligent Laboratory Systems* **2015**, *141*, 79-87.
71. Liu, Y.; Yang, C.; Gao, Z.; Yao, Y., Ensemble deep kernel learning with application to quality prediction in industrial polymerization processes. *Chemometrics and Intelligent Laboratory Systems* **2018**, *174*, 15-21.
72. Park, T. C.; Kim, T. Y.; Yeo, Y. K., Prediction of the melt flow index using partial least squares and support vector regression in high-density polyethylene (HDPE) process. *Korean Journal of Chemical Engineering* **2010**, *27* (6), 1662-1668.
73. Chen, J.; Liu, K.-C., On-line batch process monitoring using dynamic PCA and dynamic PLS models. *Chemical Engineering Science* **2002**, *57* (1), 63-75.
74. Xu, L.; Skoularidou, M.; Cuesta-Infante, A.; Veeramachaneni, K., Modeling tabular data using conditional gan. *arXiv preprint arXiv:1907.00503* **2019**.
75. Nomikos, P.; MacGregor, J. F., Monitoring batch processes using multiway principal component analysis. *AIChE Journal* **1994**, *40* (8), 1361-1375.

Chapter 5: A Hybrid Science-Guided Machine Learning Approach for Modeling and Optimizing Chemical Processes: A Review

5.1. Introduction

Modeling of many physiochemical systems requires detailed scientific knowledge of the system which is not always feasible for complex processes. We make some assumptions when modeling the system with first principles that ultimately leads to some knowledge gaps in describing the original system. Even for the systems where the scientific knowledge is sufficient to model the system, there are too many model parameters to estimate. We often apply data-based models to study the systems where scientific data are available since they are more accurate in prediction. However, data-based/machine learning models are black-box models which can over-fit the data and also produce scientifically inconsistent results. For better accuracy, ML models also require more data which is not always feasible for many problems. Therefore, it is important to integrate science-based knowledge and data-based knowledge for an accurate and scientifically consistent prediction, which we will refer to as *hybrid science- guided machine learning (SGML) approach*.

The most popular hybrid SGML approach that is being practiced in different fields of science is to combine a data-based ML model with a science-based first-principle model. However, there are more ways to combine scientific knowledge and data-based knowledge. In this work, we focus on both aspects of science complementing ML, and ML complementing science.

In our development of the hybrid SGML approach, we have benefited from two latest references. In their 2017 article, Karpatne et. al.¹ suggest the theory-guided data science as a new paradigm for scientific discovery from data. They classify the theory-guided data science methods into different categories, such as theory-guided design of models, initialization, theory-guided refinement of data science outputs, hybrid models of theory of data science, and augmenting theory-based models using data science. In their 2020 article, Willard et. al.² classify the integration of physics-based modeling with ML methodology according to the modeling objectives. The latter include, for example, improving the predictions beyond physical models, downscaling the complexity of physics-based models, generating data, quantifying uncertainty, and discovering governing equations of the data-based model.

This study presents a broad perspective of hybrid process modeling and optimization combining the scientific knowledge and data analytics in bioprocessing and chemical engineering with a science-guided machine learning (SGML) approach. We divide the approach into two major categories. The first refers to the case where a data-based ML model compliments and makes the first-principle science-based model more accurate in prediction, and the second corresponds to the case where scientific knowledge helps make the ML model more scientifically consistent. We present a detailed review of scientific and engineering literature relating to the hybrid SGML approach, and propose a systematic

classification of hybrid SGML models. For applying ML to improve science-based models, we present expositions of the sub-categories of direct serial and parallel hybrid modeling and their combinations, inverse modeling, reduced-order modeling, quantifying uncertainty in the process and even discovering governing equations of the process model. For applying scientific principles to improve ML models, we discuss the sub-categories of science-guided design, learning and refinement. For each sub-category, we identify its requirements, strengths and limitations, together with their published and potential areas of applications in bioprocessing and chemical engineering.

This work differentiates itself from several recent reviews of hybrid modeling in bioprocessing and chemical engineering through the following contributions: (1) presentation of a broader hybrid SGML methodology of integrating science-guided and data-based models, and not just the direct combinations of first-principle and ML models; (2) classification of the hybrid model applications according to their methodology and objectives, instead of their areas of applications; (3) identification of the themes and methodologies which have not been explored much in chemical engineering applications, like the use of scientific knowledge to help improve the ML model architecture and learning process for more scientifically consistent solutions; and (4) illustrations of the use of these hybrid SGML methodologies applied to industrial polymer processes, such as inverse modeling, and science-guided loss which have not been applied previously in such applications.

The objective of this paper is to present a comprehensive review and exposition of scientific and engineering literature relating to the hybrid SGML approach, and propose a systematic classification of hybrid SGML models focusing on both sciences complementing ML models, and ML complementing science-based models. Section 5.2 gives a review of the broad applications of hybrid SGML approach in bioprocessing and chemical engineering. As the number of reported methodologies and applications continues to rise significantly, it is hard for a person unfamiliar with the subject to identify the appropriate approach for a specific application. This leads to our key focus in Sections 3 and 4, presenting a systematic classification and exposition of hybrid SGML methodologies. Section 5.3-5.5 explains different categories of applying ML to complement science-based models, discuss their requirements, strengths and limitations, suggest potential areas of applications, and present illustrative examples from chemical manufacturing. Section 4 focuses on different categories of applying scientific principles to complement ML models, together with their requirements, strengths and limitations, as well as their potential applications and illustrative examples. Section 5.6 summarizes our conclusions.

5.2. Applications of Hybrid SGML Approach in Bioprocessing and Chemical Engineering

The integration of science-based models with data-based models has appeared in various fields like fluid mechanics³, turbulence modeling⁴, quantum physics⁵, climate science⁶, geology⁷ and biological sciences.⁸

This study focuses on applications of hybrid SGML methodologies in bioprocessing and chemical engineering. Among the earliest applications is *the direct hybrid modeling* involving the integration of first-principle model with data-based neural networks⁹. Psychogios and Unger¹⁰ combine a partial first-principle model based on prior process knowledge with a neural network, which serves as an estimator of unmeasured process parameters that are difficult to model from first principle. They apply the hybrid model to a fed-batch bioreactor, and the integrated model has better properties than the standard “black-box” neural network models in that it is able to interpolate and extrapolate much more accurately, is easier to analyze and interpret, and requires significantly fewer training examples. Thompson and Kramer¹¹ later demonstrate how to integrate simple process model and first-principle equations to improve the neural network predictions of cell biomass and secondary metabolite in a fed-batch penicillin fermentation reactor when trained on sparse and noisy process data.

Agarwal¹² develops a general qualitative framework for identifying the possible ways of combining neural networks with the prior knowledge and experience embedded in the available first-principle models, and discusses *the direct hybrid modeling with series or parallel configuration* to combine the outputs of the science-based model and the ML model. Asprion, et al.¹³ present the term, *grey-box modeling*, for optimization of chemical processes. They consider the case where a predictive model is missing for a process unit within a larger process flowsheet, and use measured operating data to set up hybrid models combining physical knowledge and process data. They report results of optimization using different gray-box models for process simulators applied to a cumene process. Actually, in a number of earlier studies, Bohlin and his coworkers have explored in details the concepts of gray-box identification for process control and optimization, and Bohlin has summarized the concepts, tools and applications of grey-box hybrid modeling in an excellent book.¹⁴

Over the years, we have seen a growing number of applications of hybrid modeling in bioprocessing and chemical engineering as part of the advances in smart manufacturing¹⁵⁻¹⁷.

In their 2021 paper, Sansana et al.¹⁶ discuss mechanistic modeling, data-based modeling, hybrid modeling structures, system identification methodologies, and applications. They classify their hybrid model into parallel, series, surrogate models (which are simpler mathematical representations of more complex models and similar to reduced-order models that we discuss below), and alternate structures (which include gray-box modeling mentioned above). In the alternate structures, they refer to some applications of semi-mechanistic model structures where the best hybrid model is selected using optimization

concepts. They also classify the hybrid models based on some of the chemical industry applications into analysis of model-plant mismatch¹⁷, model transfer, feasibility analysis and predictive maintenance, apart from the previous mentioned applications like process control, monitoring and optimization.

Von Stosch et. al.¹⁸ have used the term, *hybrid semi-parametric modeling*, in their 2014 review, and have summarized applications in biochemical engineering for process monitoring, control, optimization, scale-up and model reduction. They emphasize that the application of hybrid semi-parametric techniques does not automatically lead to better results, but that rational knowledge integration has potential to significantly improve model-based process design and operation.

Qin and Chiang¹⁹ review the advances in statistical machine learning and process data analytics that can provide efficient tools in developing future hybrid models. In a latest paper, Qin et. al.²⁰ propose a statistical learning procedure integrating with process knowledge to handle a challenging problem of developing a predictive model for process impurity levels from more than 40 process variables in an industrial distillation system. Both studies highlight the power of statistical machine learning for developing future hybrid process models.

A survey of the literature has shown applications of hybrid modeling in bioprocesses²¹⁻²⁷, chemical and oil and gas process industries²⁸⁻³², and polymer processes^{33,34} for more accurate and scientifically consistent predictions. This survey has also shown many topical focuses of applications in bioprocessing and chemical engineering, including process control³⁵⁻³⁸, design of experiments^{39,40}, process development and scale-up^{41,42}, process design⁴³ and optimization^{13,44,45}.

In a recent study, Zhou et al.⁴⁶ present *a hybrid approach for integrating material and process design* that holds much promise in process and product design. Cardillo et. al.⁴⁷ demonstrate the importance of hybrid models in silico production of vaccines to accelerate the manufacturing process. Chopda et. al.²³ apply integrated process analytical techniques, and modeling and control strategies to enable the continuous manufacturing of monoclonal antibodies. McBride et. al.⁴⁸ classify the hybrid modeling applications in different separation processes in chemical industry, namely, distillation⁴⁹⁻⁵¹, crystallization^{52,53}, extraction⁵⁴⁻⁵⁶, floatation^{57,58}, filtration^{59,60} and drying^{61,61}. Venkatasubramanian⁶³ gives an excellent exposition of the current state of development and applications of artificial intelligence in chemical engineering. The author highlights the intellectual challenges and rewards for developing the conceptual frameworks for hybrid models, mechanism-based causal explanations, domain-specific knowledge discovery engines, and analytical theories of emergence, and presents examples from optimizing material design and process operations.

In an excellent edited volume, Glassey and Stosch⁶⁴ discuss some of the key strengths of hybrid modeling in chemical processes, particularly in the prediction of scientifically consistent results beyond the experimentally tested process conditions, which is crucial for

process development, scale-up, control and optimization. They also identify some challenges. For example, incorrect fundamental knowledge in a science-based model could impose bias on predictions, thus the underlying assumptions used in a model are important for analysis. Also, time and accuracy of parameter estimation is critical when deciding on a hybrid modeling strategy. Kahrs and Marquardt⁶⁵ discuss the approach of simplifying the complex hybrid models into sequence of simpler problems, such as data preprocessing, solving nonlinear equations, parameter estimation and building empirical models using ML.

A recent patent by Chan et al.⁶⁶ presents Aspen Technology's approach on asset optimization using integrated modeling, optimization and artificial intelligence. In a later white paper, Beck and Munoz⁶⁷ describe Aspen Technology's current focus on hybrid modeling, combining AI and domain expertise to optimize assts. In particular, based on their application experience in in chemical industries, Aspen Tech have classified hybrid models into three categories: AI-driven, first-principle driven and reduced-order models⁶⁷. They define *an AI-driven hybrid model* as an empirical model based on plant or experimental data and use first principles, constraints and domain knowledge to create a more accurate model. Examples of AI-driven models are inferential sensors or online equipment models. They define *a first-principle driven hybrid model* as an existing first-principle model augmented with data and AI to improve model's accuracy and predictability, which has seen many applications in bioprocessing and chemical engineering. Lastly, they define *a reduced-order model* where we use ML to create an empirical data-based model based on data from numerous first-principle process simulation runs, augmented with constraints and domain expertise, in order to build a fit-for-purpose low-dimensional model that can run more quickly. With reduced-order models, we can extend the scale of modeling from units to the plant-wide models that can be deployed faster.

5.3. A Classification and Exposition of Hybrid Science-Guided Machine Learning Models

As we have seen thus far, the majority of work in hybrid model applications in bioprocessing and chemical engineering focuses on the direct combination of science-based and data-based models. In this article, we portray a broad perspective of the combination of scientific knowledge and data analysis in bioprocessing and chemical engineering as inspired by some of the applications in physics and other areas^{1,2}. We categorize these hybrid SGML applications in chemical process industry into two major categories, namely, ML compliments science and science compliments ML, together with their subcategories based on the methodologies and objectives of hybrid modeling as illustrated in Figure 5.1. We also classify the applications in bioprocessing and chemical engineering according to our hybrid SGML approach. We present examples in several areas of SGML which have not been explored much thus far, and which have great potential for process improvement and optimization.

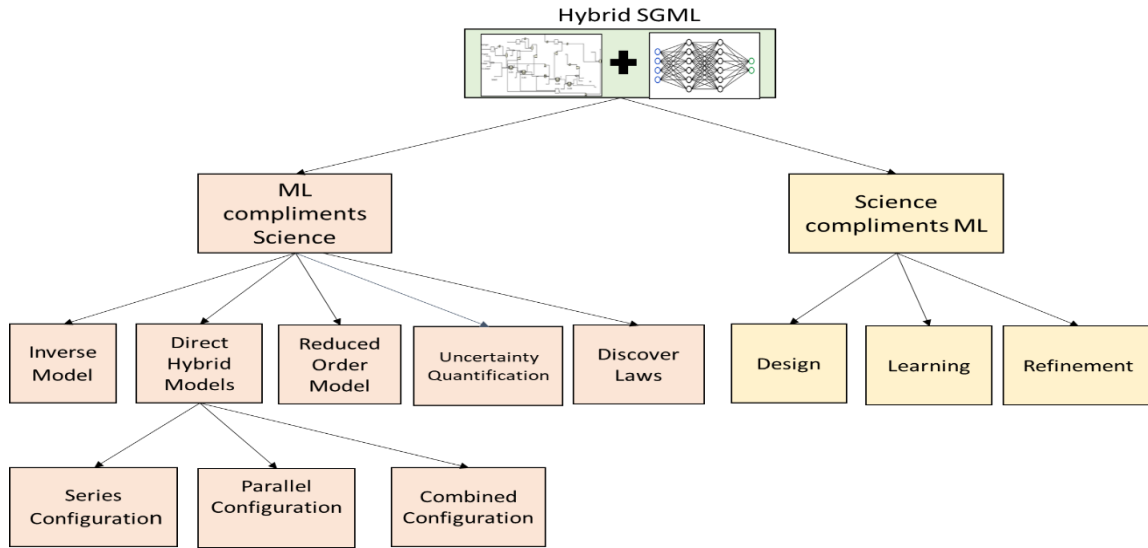


Figure 5.1. Classification of hybrid SGML models

5.4. ML Compliments Science

We can integrate a first-principle scientific model with a data-based model to improve the model accuracy and consistency. In the following, we introduce the subcategories of direct hybrid modeling, inverse modeling approach, reducing model complexity, quantifying uncertainty in the process, and discovering governing equations.

5.4.1 Direct Hybrid Modeling

A direct hybrid model combines the output of a first-principle or science-based model with the output of a data-based ML model to improve the prediction accuracy of dependent variables. These combinations could occur in a series configuration, a parallel configuration, or a series-parallel configuration. The direct hybrid modeling strategy is the most widely used approach in hybrid modeling in bioprocessing and chemical engineering.

5.4.1.1 Parallel Direct Hybrid Model

Figure 5.2 illustrates the concept of a parallel direct hybrid model. The science-based model may use the initial conditions and boundary conditions as inputs to make a prediction (Y_m), while the ML model uses dynamic time-varying data to make the predictions (Y_{ml}). We then combine both outputs directly or with assigned weights (w_1 , w_2) to achieve higher prediction accuracy.

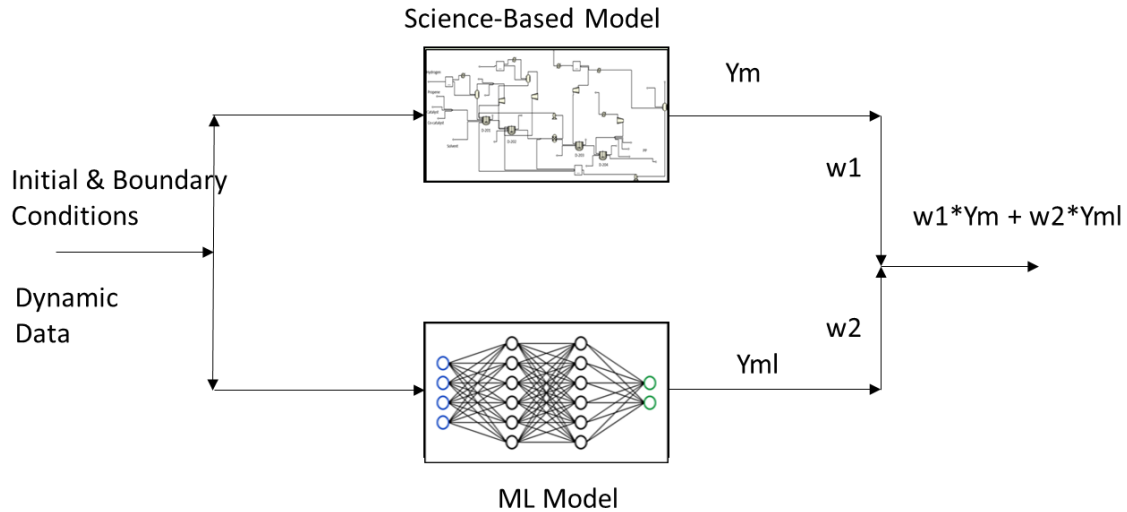


Figure 5.2. Parallel direct hybrid model: Y_m and Y_{ml} are model predictions, and w_1 and w_2 are weights.

Galvanauskas et. al.⁶⁸ combine directly the data-based neural networks for kinetics and viscosity predictions with the first-principle mass balance ordinary differential equations to optimize the production rate of an industrial penicillin process. Chang et. al.³³ showcase a parallel hybrid model for the dynamic simulation of a batch free-radical polymerization of methyl methacrylate. They combine an approximate rate function for the concentration of the immeasurable initiator concentration with a black-box time-dependent or recurrent neural network model⁹ of the dependent variables representing the mass and moment balance equations of the polymerization reactor. They use the resulting hybrid neural network and rate function (HNNRF) model to optimize the batch polymerization system, identifying the optimal recipe or operating conditions of the batch polymerization system.

Hybrid residual modeling or parallel direct hybrid residual model is a class of the parallel direct hybrid model, where we use a first-principle or science-based process model to quantify the time-dependent prediction error or residual, Y_{res} , between plant data $Y(t)$ and science-based model prediction Y_m as a function of process variables^{41,69-71}. Figure 3 illustrates the concept of the parallel direct hybrid residual model. The correction to the model output taking care of the prediction error or residual of the ML model in the hybrid residual configuration improves the model accuracy over the non-residual configuration of Figure 5.2.

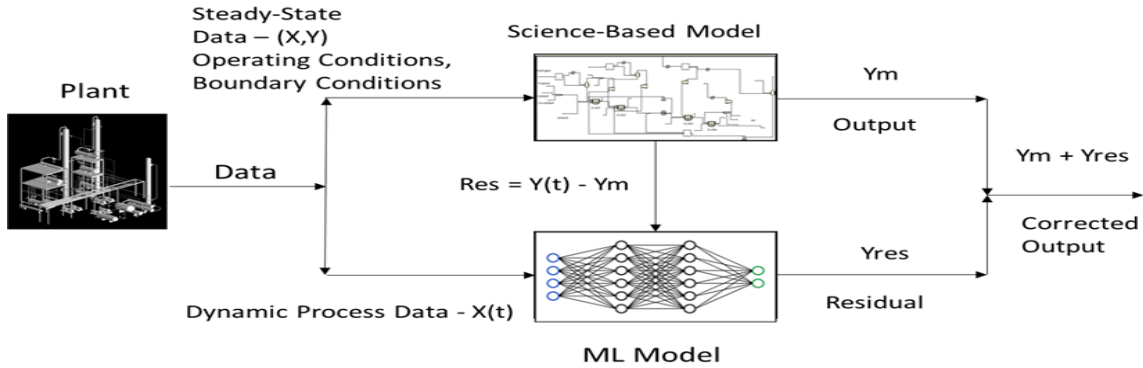


Figure 5.3. Parallel direct hybrid residual model: Y_m represents model outputs, Res are the time-dependent prediction errors or residues between plant data $Y(t)$ and science-based model outputs Y_m , and $Y_m + Y_{res}$ are the corrected model outputs

Tian et al.⁶⁹ develop a hybrid residual model for a batch polymerization reactor. First, they develop a simplified process model based on polymerization kinetics, and mass and energy balances to predict the monomer conversion, number-average molecular weight M_{WN} , and weight-average molecular weight M_{WW} . This first-principle process model cannot predict these product quality targets accurately because of its neglect of the gel effect at high monomer conversion and other factors. Next, the authors develop a parallel configuration of three data-based, time-dependent or recurrent neural networks⁹ trained by process data to predict the residuals of monomer conversion, M_{WN} and M_{WW} of the simplified first-principle process model. The predicted residuals are added to the predictions from the simplified process model to form the final hybrid model predictions. Because of focus in batch process control is on the end-of-batch product quality targets, the use of time-dependent or recurrent neural networks can usually offer good long-range predictions. Therefore, the resulting hybrid residual model performs well in many batch process control and optimization applications^{41,43,69-71}.

Simutis and Lubnert³⁶ present another application of the direct hybrid modeling methodology to state estimation for bioprocess control. This work combines a first-principle state Kalman filter based on mass balances of biomass, substrate and product, and an ML-based observation model for quantifying relationship between less established variables and measurements. Recently, Ghosh et. al.⁷²⁻⁷³ apply the parallel hybrid modeling framework in process control, where they combine first-principle models with data-based model built by applying subspace identification for better prediction of batch polymer manufacturing and seed crystallization system. Hanachi et. al.⁷⁴ showcase the application of direct hybrid modeling methodology for predictive maintenance. They combine a physics-based model with a data-based inferential model in an iterative parallel combination for predicting manufacturing tool wear.

5.4.1.2. Series Direct Hybrid Model

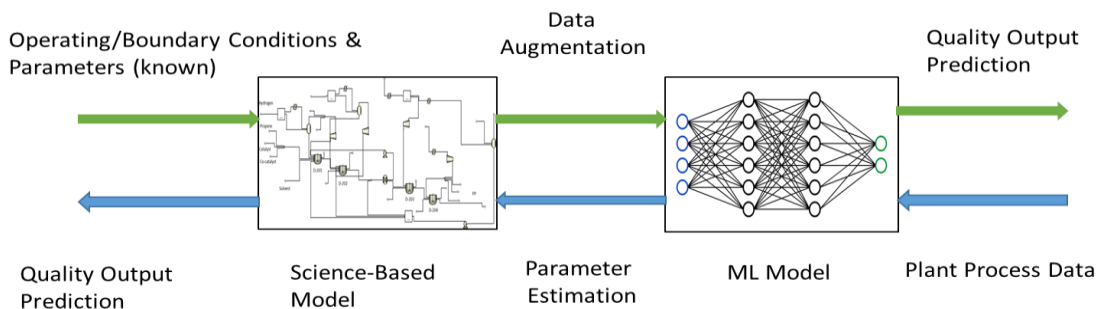


Figure 5.4. Serial direct hybrid model

Figure 5.4 illustrates the serial direct hybrid model. The science-based process model serves to augment the data needs of the ML model, while the ML model can help in estimating the parameters of the science-based model. Babanezhad et al.⁷⁵ consider the computational fluid dynamics (CFD) for two-phase flows in chemical reactors, and couple science-based CFD results to a ML model based on an adaptive network-based fuzzy inference system (ANFIS). Once the ML model captures the pattern of the CFD results, they use the hybrid model for process simulation and optimization. Some features calculated from a science-based CFD model can *augment the data* as inputs to a ML model. Chan et. al.⁶⁶ have discussed the advantages of data augmentation by combining simulation and plant data to generate a more accurate data-based analysis. In an application to crude distillation in petroleum refining, Mahalec and Sanchez⁵¹ use a science-based model to calculate the internal reflux to augment other plant data as inputs to a ML model, in order to calculate the relationship to the product true boiling point curves for quality analysis.

Krippel et. al.⁷⁶ present the hybrid modeling of an ultrafiltration process where they calculate the flux using a ML model to act as an input to a science-based model. Similarly, Luo et al.²⁹ develop a hybrid model for a fixed-bed reactor for ethylene oxidation, integrating first-principle reaction kinetics and reactor model with a ML catalyst deactivation model. The latter is developed with support vector regression from operating data, assuming the deactivation property decreasing monotonically with time. With the hybrid model, the prediction error is less than 5% for the prediction of an industrial reactor. The approach can predict the production more accurately and have more reliable extrapolation.

Figure 4 shows that a ML model can also help in *estimating the parameters* of the science-based model. Mantovanelli et al.⁷⁷ develop a hybrid model for an industrial alcoholic fermentation process, combining first-principle mass and energy balance equations for a series of five fermenters with a data-based, functional link network⁷⁵ to identify the kinetic parameters of the fermentation reactors trained by plant data. The hybrid model includes the effect of temperature on the fermentation kinetics and show good nonlinear approximation capability. Sharma and Liu⁷⁸ show how to use plant data to estimate kinetic parameters of first-principle models for industrial polyolefin processes.

Finally, we note that as illustrated in Figure 5.4, we can interchangeably use a science-based model or a ML model first in the hybrid framework, depending on we require to add more features to augment the data set or to estimate model parameters.

5.4.1.3. Serial-Parallel or Combined Direct Hybrid Model

Figure 5.5 shows a combined direct hybrid model, where we use the steady-state data from the plant to estimate the unknown parameters of a science-based process model and then uses the hybrid residual modeling strategy of Figure 5.3 for prediction. This serial-parallel combination or feedback system can improve model predictions depending on the application.

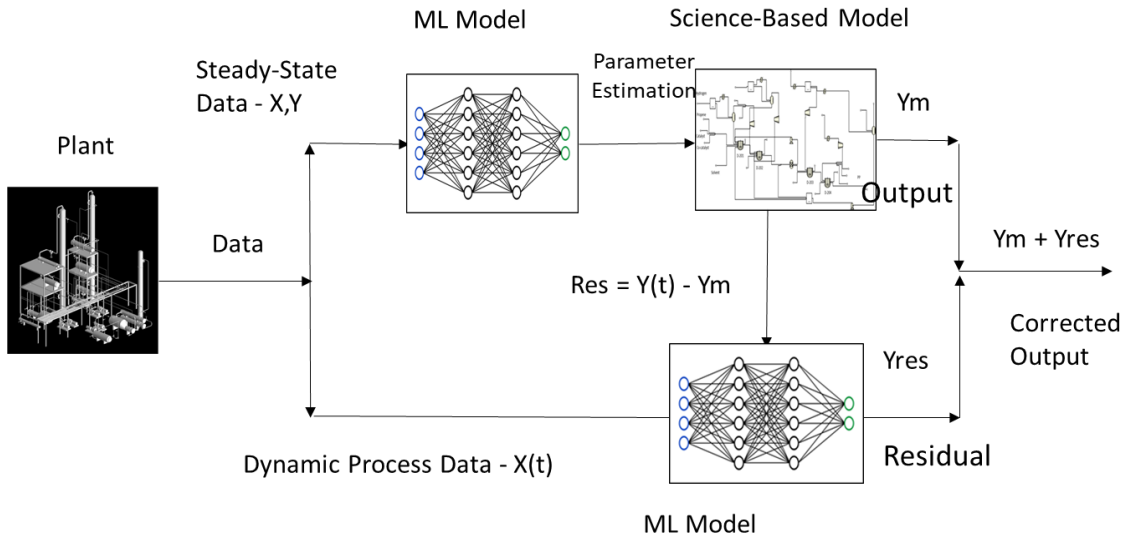


Figure 5.5. Combined Direct Hybrid Model: Y_m are outputs, Y_{res} are residuals, and $Y_m + Y_{res}$ are corrected outputs

Bhutani et. al.⁷⁹ present a definitive study comparing first-principle, data-based and hybrid models applied to an industrial hydrocracking process. In particular, they couple a first-principle hydrocracking model based on pseudocomponents with data-based neural network models of different configurations of Figures 5.3 to 5.5 that quantify the variations in operating conditions, feed quality and catalyst deactivation. The neural network component of the hybrid model either provides updated model parameters in the first-principle process model connected in series or correct predictions of the first-principle process models. The hybrid models are able to represent the behavior of an industrial hydrocracking unit to provide accurate and consistent predictions in the presence of process variations and changing operating scenarios.

Song et. al.⁸⁰ also apply the direct hybrid model configurations of Figure 5.3 to 5.5 to an industrial hydrocracking process and analyze the strengths and weaknesses of these configurations. They call a model *a mechanism-dominated model* if the accuracy of its outputs is mainly dominated by the available theoretical knowledge used to develop the model; and they also call a model *a data-dominated model* if the accuracy of its outputs is mainly dominated by the quality of the training data and the performance of the resulting

data-based model. In particular, they give both the first-principle model and the serial direct hybrid model of Figure 4 as examples of mechanism-dominated models, and cite the data-based model, parallel direct residual model of Figure 3, and the combined direct hybrid model of Figure 5 as examples of data-dominated models.

In their work, Song et al.⁸⁰ combine a mechanism-dominated model with a data-dominated model as a hybrid direct model of Figure 2, with the weighting factors for the outputs of two individual models being determined in an adaptive fashion. For their application, Song et al. work with a mechanism-dominated model of an industrial hydrocracking process based on kinetic lumping^{79,80}, and with a data-dominated model based on a self-organizing map (SOM) followed by a convolutional neural network (CNN), with both being trained by simulated process data based on Aspen HYSYS⁸⁰. They evaluate the performance of the hybrid model for operational optimization of the hydrocracking producing different product scenarios. While this study includes new conceptual development, it needs much simplification of its relatively complex methodology to make it readily applicable by data scientists and practicing engineers.

In a recent study, Chen and Lerapetritou¹⁷ demonstrate how to use partial correlation analysis from multivariate statistics and mutual information analysis from information theory to identify and improve the plant-model mismatch in using a direct combined hybrid model for a pharmaceutical manufacturing process. As the authors state, implementing this plant-model mismatch strategy requires active excitation of variables online in order to capture the corresponding response data from the plant, which is often difficult to perform in manufacturing plants and in experimental settings, and could benefit from new development in computing and information technology.

Lima et al.⁸¹ propose a semi-mechanistic model building framework based on selective and localized model extensions. They use a symbolic reformulation of a set of first-principle model equations in order to derive hybrid mechanistic–empirical models. The symbolic reformation permits the addition of empirical elements selectively and locally to the model. They apply the approach to the identification of a non-ideal reactor and to the optimization of the Otto–Williams benchmark reactor.

5.4.2 Inverse Modeling

In *inverse modeling*, we use the output of a system to infer its corresponding input or independent variables; this is different from the *forward modeling* where we use the known independent variables to predict the output of the system². Figure 5.6 illustrates the inverse modeling framework. We see that in the traditional data-based approach, we use process variable data (X) and quality target data (Y) to train and test a ML model. Because the plant does not measure most quality targets continuously, we can apply a science-based process model, developed by first principles and validated by plant data, to predict and augment the quality target data (Y) for given process variable (X).

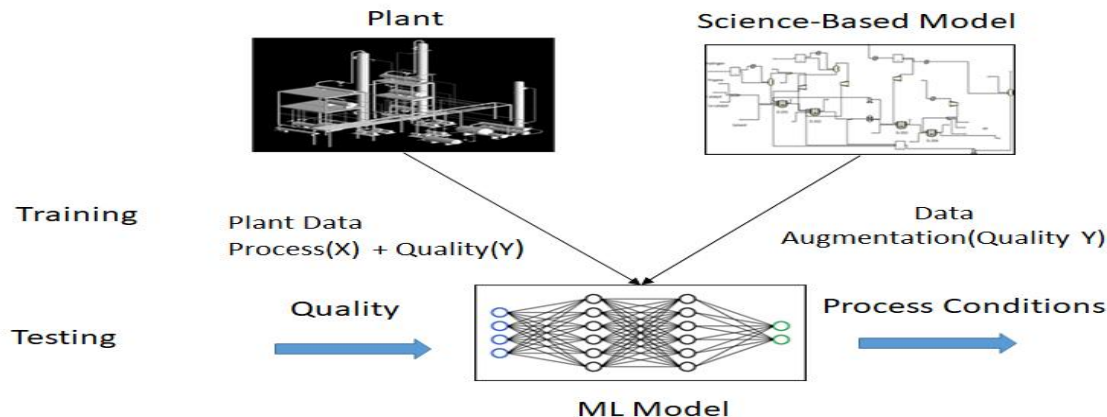


Figure 5.6. Inverse Modeling Framework

One of the earliest applications of inverse modeling for chemical process was by Savkovic-Stevanovic et. al.⁸³ They use a neural network controller for product composition control of a distillation plant based on the process inverse dynamic model relating the product composition to the reflux flow rate. The results illustrate the feasibility of using neural network for learning nonlinear dynamic model of the distillation column from plant input-output data. Their results also demonstrate the importance to take the time-delay of the plant into account.

Pharmaceutical product design and development typically uses the design of experiments (DOE) and response surface modeling (RSM) for steady-state process modeling, while neglecting the process dynamics and time delays. Tomba et. al.^{84,85} demonstrate how to use the inverse modeling concept to generate process understanding with dynamic process models, quantifying the impact of temporal deviations and production dynamics. Specifically, they perform data-based, latent variable regression model inversion to find the best combination of raw materials and process variables to achieve the desired quality targets. The authors propose to combine design-of-experiments studies with hybrid modeling for process characterization.

Recently, Bayer al.⁸⁶ apply the inverse modeling approach to *Escherichia coli* fed-batch cultivations, evaluating the impact of three critical process variables. They compare the performance of a hybrid model to a pure data-driven model and the widely adopted RSM of the process endpoints, and show the superior behavior of the hybrid model compared to the pure black-box approaches for process characterization. The inverse modeling methodology makes the decision-making process in pharmaceutical product development faster, while minimizing the number of experiments and reducing the raw material consumption.

Raccuglia et.al.⁸⁷ train the ML learning model using reaction data to predict reaction outcomes for the crystallization of templated vanadium selenites. They demonstrate the use of ML to assist material discovery using data from previously unsuccessful or failed material synthesis experiments. The resulting ML model outperforms traditional human strategies, and successfully predicts conditions for new organically templated, inorganic

product formation with a success rate of nearly 90%. Significantly, they show that inverting the machine-learning model reveals new hypotheses regarding the conditions for successful product formation.

There is a growing interest in the inverse approach to material design, in which the desired target properties are used as input to identify the atomic identity, composition and structure (ACS) that exhibit such properties. Liao et al.⁸⁸ present a metaheuristic approach to material design that incorporates the inverse modeling framework. Vankatasunramanian⁶¹ also mentions the importance of inverse problem being solved by the application of artificial intelligence in chemical engineering processes.

5.4.3 Reduced-Order Models

Reduced-order models (ROMs) are simplified models that represent a complex process in a computationally inexpensive manner, but also maintain high degree of accuracy of prediction in simulating the process. In bioprocessing and chemical engineering, we can apply the ROM methodology to simulate complex processes and then use ML models to optimize the processes. See Figure 5.7. We can use ROMs to simulate different scenarios and sensitivities in order to generate process data, which in turn can be combined with ML models to build accurate soft sensors to predict quality variables. This approach helps to make sure that the ML model is trained on process data with multiple variations which is not possible in a steady plant run. Hence, data-based sensors will be accurate for any future process optimization, scale up etc. and it is also easier to deploy such models online.

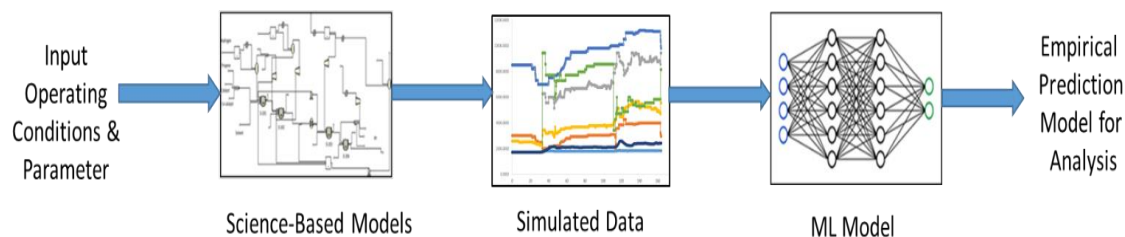


Figure 5.7. Reduced order process modeling framework

The concept of *Digital Twin*⁸⁹ in chemical process industry is also based on the concept of Reduced Order Models of combining multiple models so that they can run multiple processes simultaneously to simulate a virtual plant.

In one of the earliest applications of ROM, MacGregor et. al.⁹⁰ apply a PLS (projection to latent squares or partial least squares) ML model of a polyethylene using process data simulated from a process model to develop inferential prediction models for polymer properties. This application involves a high-pressure tubular reactor system producing low-density polyethylene, in which all the fundamental polymer properties are extremely difficult to measure and are usually unavailable, and some on-line measurements such as the temperature profile down the reactor and the solvent flow rate are available on a frequent basis. The dimensionality reduction aspects of PLS facilitates the development of

a multivariate statistical control plot for monitoring the operating performance of the reactors.

Reduced-order models have also been called *surrogate models* in the context of grey-box modeling techniques where first-principle models are combined with data-based optimization techniques. Rogers and Lerapetritou^{91,92} propose the use of surrogate models as reduced-order models that approximate the feasibility function for a process in order to evaluate the flexibility and operability of a science-based process model, since it is difficult to directly evaluate the feasibility due to black-box constraints.

In a recent study, Abdullah et. al.⁹³ showcase a data-based reduced-order modeling of non-linear processes that have time-scale multiplicity to identify the slow process state variables that can be used in a dynamic model. Agarwal et. al.⁹⁴ use ROM for modeling pressure swing adsorption process where they use a low-dimensional approximation of a dynamic partial differential equation model, which is more computationally efficient. In another study, Kumar et. al.⁴⁵ use a reduced-order steam methane reformer model to optimize furnace temperature distribution. In a recent study, Shafer et al.⁹⁵ use a reduced-dimensional dynamic model for the optimal control of air separation unit. The model combines compartmentalization to reduce the number of differential equations with artificial neural networks to quantify the nonlinear input–output relations within compartments. This work reduces the size of the differential equation system by 90%, while limiting the additional error in product purities to below 1 ppm compared to a full-order stage-by-stage model.

Our focus on ROM is more towards using the science-based model to simulate process data that can be used by ML models to derive empirical correlations for process optimization. ROM are particularly useful in chemical processes for dynamic optimization of a complex large-scale process.

5.4.4 Hybrid SGML Modeling for Uncertainty Quantification

A science-based model can produce results with some uncertainties which can be quantified by some ML-based techniques. The uncertainties in science-based models arise from uncertainty in model parameters, and boundary and initial conditions. In some cases, the model bias and assumptions can be a source of uncertainty as well. We can use the predictions from a calibrated model to quantify uncertainties. Data-based ML models like Gaussian process, neural networks etc. are used to help build a surrogate model that defines a relation between model inputs and outputs which can then be used to quantify the uncertainty. This surrogate data-based ML modeling reduces the computational expense of Monte Carlo methods, which are traditionally used for uncertainty quantification (UQ)⁹⁶.

Because of uncertainty in process inputs and process states in a chemical process model, the uncertainty propagates to the process outputs as well. The uncertainty in a science-based model due to any of the parameters or any of the prior knowledge can be used by a ML model to quantify uncertainty in a chemical process as shown in figure 5.8. Duong et. al.⁹⁷ uses UQ for process design and sensitivity analysis of complex chemical processes

using the polynomial chaos theory. Fenila et. al.⁹⁸ utilize UQ for electrochemical synthesis, where they calculate simulation uncertainties and global parameter sensitivities for the hybrid model. UQ has also been applied to understand complex reaction mechanisms.

Proppe et. al.⁹⁹ showcase kinetic simulations in discrete-time space considering the uncertainty in free energy and detecting regions of uncertainty in reaction networks. UQ techniques are popular in the field of catalysis and material science as they are used to quantify the uncertainty of models based on density functional theory^{100,101}. In another study, Boukouval and Lerapetritou¹⁰² demonstrate the feasibility analysis of a science-based process model over a multivariate factor space. They use a stochastic data-based model for feasibility evaluation, referred to as Kriging and develop an adaptive sampling strategy to minimize sampling cost while maintaining feasibility.

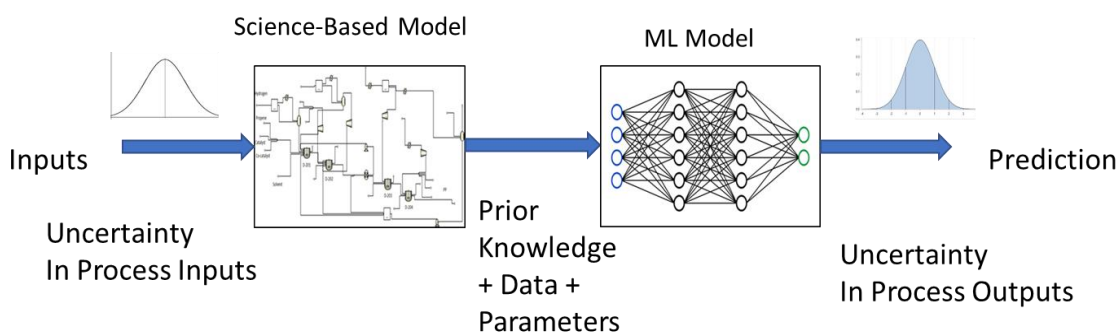


Figure 5.8. Uncertainty quantification modeling framework

5.4.5 Hybrid HGML Modeling to Aid in Discovering Scientific Laws using ML

One way in which ML can help science-based modeling is by discovering new scientific laws which governs the system. There is a growing application of ML in physics to rediscover or discover physical laws mainly by data-driven discovery of partial differential equations (PDE). ML can be used to develop an empirical correlation which can be used as a scientific law in a science-based model or ML can be used to solve the PDE defining scientific laws as illustrated in figure 5.9.

Rudy et. al.¹⁰³ showcase the discovery of physical laws like the Navier-Stokes equation and the reaction-diffusion equation in chemical processes by a sparse regression method governing the PDE by using a system of time series measurements. Langley et. al.¹⁰⁵ present the applications of ML in rediscovering some of the chemistry laws, such as the law of definite proportions, law of combining volumes, determination of atomic weights and many others.

Another important application of ML is to discover some of the thermodynamic laws which can be useful in defining the phase equilibrium and critical for an accurate science-based process model. Nentwich et. al.¹⁰⁷ use data-based mixed adaptive sampling strategy to calculate the phase composition, instead of the complex equation-of-state models. In another novel approach. In another novel approach Hoffmann et. al.¹⁰⁸ discovers governing reactions from concentration data. They use a sparse tensor regression method for identification of non-linear dynamics to estimate a complex reaction networks.

Thus, ML application can have promising use in discovering more accurate physical and chemistry laws that govern the chemical process. These scientific laws calculated by ML-based models can then be utilized in first-principle model to improve accuracy as well as reduce model complexity.

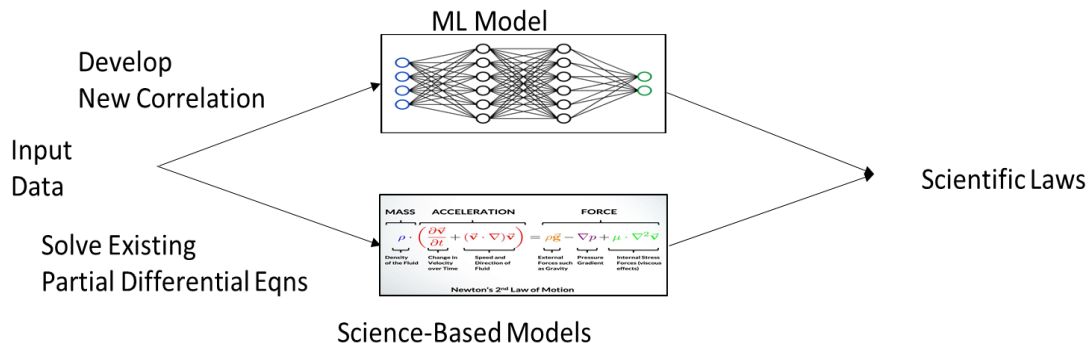


Figure 5.9. Discovering scientific laws

5.5. Science Compliments ML

Referring to Figure 5.1, we can also improve ML models using scientific knowledge. We can improve the generalization or extrapolation capability and reduce the scientific inconsistency of ML models by using scientific knowledge in designing the ML models. The scientific knowledge can also help in improving the architecture of the data-based ML model or the learning process of the ML model and even with the final post-processing of the ML model results.

5.5.1 Science-Guided Design

In science-guided design, we choose the model architecture based on scientific knowledge. For a neural network, we can decide the intermediate variables expressed as hidden layers based on scientific knowledge of the system. This helps in improving the interpretative ability of the models. Figure 5.10 illustrates a neural network model whose architecture like the number of neurons, hidden layers, activation layers etc. can be decided by prior scientific knowledge. In a bioprocess application, Rodriguez-Granrose et. al.³⁹ use the design of experiments (DOE) to create and evaluate a neural network architecture. They use DOE to evaluate activation functions and neurons on each layer to optimize the neural network. In their recent study, Wang et al.¹⁰⁷ design their theory-infused neural networks based on adsorption energy principles for interpretable reactivity prediction.

The use of the novel neural differential equation¹⁰⁸ to solve a first-principle dynamic system represents a hybrid SGML approach, where the architecture of ML model is influenced by the system and finds applications in continuous time series models and scalable normalizing flows. The derivative of hidden state is parameterized using a neural network and the output of the network is computed using a differential equation solver. In a recent study, Jaegher et. al.¹⁰⁹ use the neural differential equation to predict the dynamic behavior of electro-dialysis fouling under varying process conditions. In a recent application of this theme in chemical process for model predictive control, Wu et. al.¹¹⁰ use

prior process knowledge to design the recurrent neural network structure⁹. They showcase a methodology to design the RNN structure using prior scientific knowledge of the system and also employ weight constraints in the optimization problem of the RNN training process. Reis et. al.¹¹¹ discuss the concept of incorporation of process-specific structure to improve process fault detection and diagnosis.

Fuzzy Artificial Neural Networks(ANN) is a class of Neural Networks which utilize prior scientific knowledge of the system is used to formulate rules mapped on to the structure of the ANN¹¹². The weights of the ANN connecting the process input to output can be connected to physical process variables⁶⁴. Apart from making the models more scientifically consistent with prior knowledge they also reduce computational complexity and provides interpretable results. The use of prior knowledge also makes them suitable for extrapolation. Fuzzy ANN have been particularly useful for applications in process control¹¹³. Simutis et. al. have used fuzzy ANN system for industrial bioprocess monitoring and control¹¹⁴⁻¹¹⁵. Simutis et. al. have showcased the application of fuzzy ANN process control expert to perform appropriate control actions based on process trends for bioprocess optimization and control¹¹⁶.

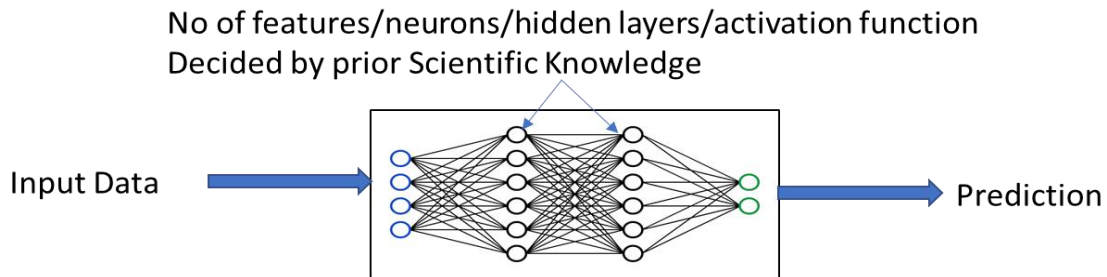


Figure 5.10. Science-guided design framework of neural network architecture

5.5.2 Science-Guided Learning

Here, we make use of the scientific principles to improve the scientific consistency of data-based models by modifying the machine learning process. We do this by modifying the loss function, constraints and even the initialization of ML models based on scientific laws.

Specifically, in order to make the ML models physically consistent we make the loss function of NN model incorporate physical constraints². A loss function in ML measures how far an estimated value is from its true value. A loss function maps decisions to their associated costs. Loss functions are not fixed, they change depending on the task in hand and the goal to be met. Figure 5.11 illustrates the science-guided loss framework.

We can define a loss function of the ML model ($Loss_M$) for regression to calculate the difference between the true value (Y_{true}) and the model predicted value (Y_{pred}). Likewise, we can define a loss function for a science-based model ($Loss_{SC}$), which is a function of the model predicted value (Y_{pred}) consistent with science-based loss. We include a weighting factor λ to express the relative importance of both loss terms. We write the overall loss function ($Loss$) as:

$$Loss = Loss_M(Y_{true} - Y_{pred}) + \lambda Loss_{SC}(Y_{pred}) \quad (5.1.)$$

Figure 5.8 illustrates the concept of science-guided loss function.

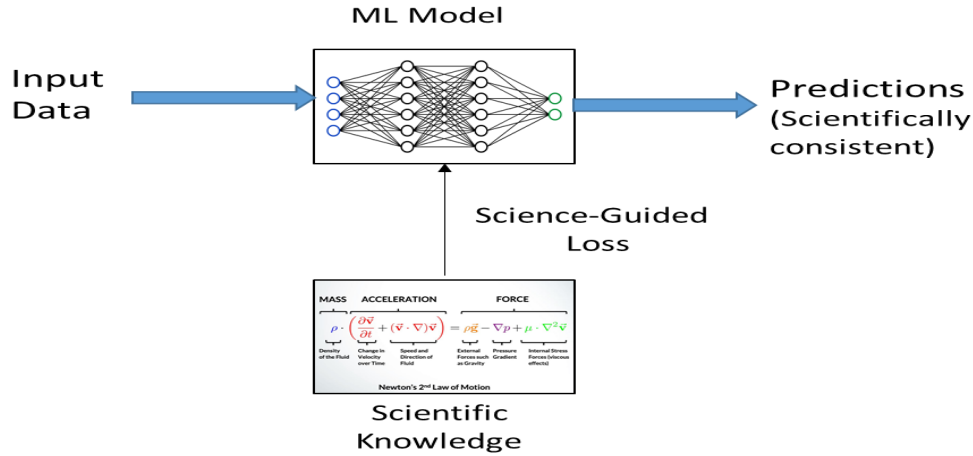


Figure 5.11. Science-guided loss function representation

A science-guided initialization helps in deriving an initial choice of parameters before a model is trained so that it improves model training and also prevents from reaching a local minimum, which is the concept of transfer learning. Thus, we can use the data from a science-based model to pre-train a ML model based on this concept of initialization^{1,2,7}. This concept has been utilized in chemical process model in the form of process similarity and developing new process models through migration. In particular, Lu et. al.¹¹⁷ introduce the concept of process similarity, and classify it into attribute-based and model-based similarities. They present a model migration strategy to develop a new process model by taking advantage of an existing base model, and process attribute information. Adapting existing process models can allow using fewer experiments for the development of a new process model, resulting in a saving of time, cost, and effort. They apply the concept to predict the melt-flow-length in injection molding and obtain satisfactory results.

In another study on the similar concept, Yan et al.¹¹⁸ use a Bayesian method for migrating a ML Gaussian process regression model. They showcased an approach of an iterative model migration and process optimization for an epoxy catalytic reaction process.

Recently, Kumar et. al.¹¹⁹ try to optimize the Non-Newtonian fluid flow for industrial processes like crude oil transportation using a physics- based loss function for the shear stress calculation for more accurate flow predictions. In another study on the similar principle, Pun et. al.¹²⁰ apply physics-informed neural networks for more accurate and transferable atomistic modeling of materials.

5.5.3. Science-Guided Refinement

By science-guided refinement, we mean the post-processing of ML model results based on scientific principle. The raw data without any feature engineering can be used as input to a ML model for prediction and then the science-based model can be used to test the scientific consistency of ML predictions. Figure 5.12. illustrates the science-guided refinement framework This post-processing of results of the ML model using science-

based models can be useful to the design and prediction of material structure¹¹³. Thus, the discovery of materials forms the basis of chemical process development from which the manufacturing process of any compound can be designed. This is different than the serial direct hybrid model discussed in Section 5.3.1.2. In particular, we use the science-based model to merely test the scientific consistency of the ML model results. Hautier et. al.¹¹⁴ use first-principle models based on density functional model to refine the results of probabilistic ML models to discovery ternary oxides.

Another application for science-guided learning is for data generation. ML techniques like generalized adversarial networks (GAN) are useful for generating data in an unsupervised data. GANs do have a problem of high sample complexity² which can be reduced by incorporating some science-based constraints and prior knowledge. Cang et al.¹¹⁵ apply ML models to predict the structure and properties of materials and use the results of the ab initio calculations to refine the ML model results. They generate more imaging data for property prediction using a convolution neural network and introduce a morphology constraint form scientific principles, while training of the generative models so that it improves the prediction of the structure- property model.

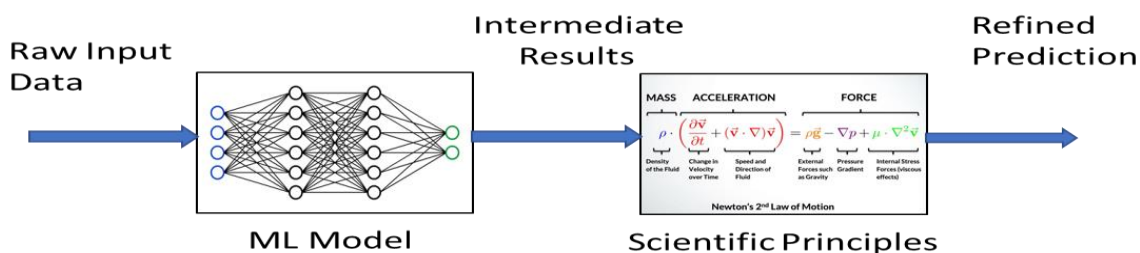


Figure 5.12. Science-guided refinement framework

Thus, some of these methodologies of having science complimenting ML have much potential for future applications to bioprocessing and chemical engineering.

5.6. Conclusion

Table 5.1 summarizes all the hybrid SGML models and their advantages, limitations and potential applications.

We present a broad perspective of hybrid modeling with a science-guided machine learning (SGML) approach and its application in bioprocessing and chemical engineering. We give a detailed review and exposition of the hybrid SGML modeling approach and its applications, and classify the approach into two categories. The first refers to the case where a data-based ML model compliments and makes the first-principle science-based model more accurate in prediction, and the second corresponds to the case where scientific knowledge helps make the ML model more scientifically consistent. We point out some of the areas of SGML which have not been explored much in chemical process modeling and have potential for further use like in the areas where Science can help improve the data-based model by improving the model design, learning and refinement. We have recently submitted a modified version of this chapter in AIChE journal and it is under review¹²⁴.

Table 5.1. Summary of hybrid SGML approach

Hybrid Modeling	SGML	Science-based model /knowledge	ML model	Advantages	Limitations	Potential applications
ML compliments Science (base model: Science Based)						
Direct Hybrid modeling	Series	Science-based model (SBM)	Regression	Parameter estimation, data augmentation	Limited by data for parameter estimation	Kinetic estimation ⁷⁸ soft sensor ^{51,86} process modeling ^{29,75} process scale-up ⁴¹
	Parallel	SBM	Regression	Improved accuracy of prediction	Scientific consistency depends on SBM	Process control ^{36,43,72} softSensor ³³ process monitoring ⁶⁸ predictive maintenance ^{66,74}
	Series-parallel	SBM	Regression	Higher Accuracy	Increased Model complexity	Process monitoring and control ⁵⁸ plant-model mismatch ¹⁷
Inverse modeling		SBM	Probabilistic, Regression	Computationally cheaper inverse problem	Lower generality of the model	Product design and development ^{84,85} polymer grade change, material design ⁸⁷
Reduced-order models		SBM	Regression	Fast online deployment,	Higher Bias,	Process Optimization

			reduce model complexity	limited by SBM accuracy	at plant scale ^{84,85} , dynamic modeling ^{93,95} soft Sensor ⁹⁴ feasibility Analysis ^{91,92}
Uncertainty quantification	SBM	Probabilistic	Gives real error estimate and solution space	Limited by SBM assumptions, parameters	Process design and development ⁹⁷ feasibility Analysis ¹⁰²
Discovering scientific law	SBM	Regression, probabilistic	System stability interpretability	Limited by data size/availability	Thermodynamics phase equilibrium ¹⁰⁵ Reaction Network ¹⁰⁶
Science Compliments ML (base model : ML)					
Science-guided design	- Laws or SBM	Deep neural network (DNN) Neural Diff. Eqn.	Scientifically consistent and interpretable	Requires deep scientific knowledge of system	Dynamic time-dependent systems ¹⁰⁹ process control ^{110,111}
Science-guided learning	- Laws	DNN	Scientifically consistent and interpretable	Possible lower prediction accuracy	Process design and development ¹⁰⁰ , process Monitoring,
Science-guided refinement	- SBM	Probabilistic	Less effort in feature selection	Limited by SBM assumptions, parameters	Process design, discovery of materials ¹⁰⁶

Acknowledgement

We gratefully acknowledge Aspen Technology, Inc., for their support of the Center of Excellence in Process System Engineering in the Department of Chemical Engineering at Virginia Tech since 2002. We would like to thank Dr. Anuj Karpatne for sharing his knowledge of theory-guided data science through his course, physics-guided machine learning, at Virginia Tech.

References

1. Karpatne, A.; Atluri, G.; Faghmous, J. H.; Steinbach, M.; Banerjee, A.; Ganguly, A.; Shekhar, S.; Samatova, N.; Kumar, V., Theory-Guided Data Science: A New Paradigm for Scientific Discovery from Data. *IEEE Transactions on Knowledge and Data Engineering*. **2017**, *29*, 2318.
2. Willard, J.; Jia, X.; Xu, S.; Steinbach, M.; Kumar, V., Integrating Physics-Based Modeling with Machine Learning: A Survey. **2020**, *arXiv preprint arXiv:2003.04919v4 [physics.comp-ph]*.
3. Muralidhar, N.; Bu, J.; Cao, Z.; He, L.; Ramakrishnan, N.; Tafti, D.; Karpatne, A. PhyNet: Physics Guided Neural Networks for Particle Drag Force Prediction in Assembly, *Proceedings of the 2020 SIAM International Conference on Data Mining*, SIAM: **2020**, 559.
4. Bode, M.; Gauding, M.; Lian, Z.; Denker, D.; Davidovic, M.; Kleinheinz, K.; Jitsev, J.; Pitsch, H., Using Physics-Informed Super-Resolution Generative Adversarial Networks for Subgrid Modeling in Turbulent Reactive Flows. **2019**, *arXiv preprint arXiv:1911.11380*.
5. Schütt, K. T.; Kindermans, P.-J.; Sauceda, H. E.; Chmiela, S.; Tkatchenko, A.; Müller, K.-R., Schnet: A Continuous-Filter Convolutional Neural Network for Modeling Quantum Interactions. **2017**, *arXiv preprint arXiv:1706.08566*.
6. Faghmous, J. H.; Kumar, V., A Big Data Guide to Understanding Climate Change: The Case for Theory-Guided Data Science. *Big Data*. **2014**, *2*, 155.
7. Karpatne, A.; Watkins, W.; Read, J.; Kumar, V. Physics-Guided Neural Networks : An Application in Lake Temperature Modeling., <https://arxiv.org/abs/1710.11431> [cs.LG], accessed August 1, 2021.
8. Yazdani, A.; Lu, L.; Raissi, M.; Karniadakis, G. E., Systems Biology Informed Deep Learning for Inferring Parameters and Hidden Dynamics. *PLoS Computational Biology*. **2020**, *16*, e1007575.
9. Baughman, D. R.; Liu, Y. A. *Neural Networks in Bioprocessing and Chemical Engineering*. Academic Press, San Didgo, CA, **1995**.
10. Psychogios, D. C.; Ungar, L. H., A Hybrid Neural Network-First Principles Approach to Process Modeling. *AIChE Journal*. **1992**, *38*, 1499.

11. Thompson, M. L.; Kramer, M. A., Modeling Chemical Processes Using Prior Knowledge and Neural Networks. *AIChE Journal*. **1994**, *40*, 1328.
12. Agarwal, M., Combining Neural and Conventional Paradigms for Modelling, Prediction and Control. *International Journal of Systems Science* **1997**, *28*, 65.
13. Asprión, N.; Böttcher, R.; Pack, R.; Stavrou, M. E.; Höller, J.; Schwientek, J.; Bortz, M., Gray-Box Modeling for the Optimization of Chemical Processes. *Chemie Ingenieur Technik* **2019**, *91*, 305.
14. Bohlin, T., *Practical Grey-Box Process Identification*. Springer-Verlag, London, United Kingdom, **2006**.
15. Yang, S.; Navarathna, P.; Ghosh, S.; Bequette, B. W., Hybrid Modeling in the Era of Smart Manufacturing. *Computers and Chemical Engineering*. **2020**, *140*, 106874.
16. Sansana, J.; Joswiak, M. N.; Castillo, I.; Wang, Z.; Rendall, R.; Chiang, L. H.; Reis, M. S., Recent Trends on Hybrid Modeling for Industry 4.0. *Computers and Chemical Engineering* **2021**, *151*, 107365.
17. Chen, Y.; Ierapetritou, M., A Framework of Hybrid Model Development with Identification of Plant-Model Mismatch, *AIChE J.* **2020**, *66*, e16996.
18. Von Stosch, M.; Oliveira, R.; Peres, J.; de Azevedo, S. F., Hybrid Semi-Parametric Modeling in Process Systems Engineering: Past, Present and Future. *Computers and Chemical Engineering*. **2014**, *60*, 86.
19. Qin, S. J.; Chiang, L. H. Advances and Opportunities in Machine Learning for Process Data Analytics. *Computers and Chemical Engineering*. **2019**, *125*, 465.
20. Qin, S. J.; Guo, S.; Li, Z.; Chiang, L. H.; Castillo, I.; Braun, B.; Wang, Z., Integration of Process Knowledge and Statistical Learning for the Dow Data Challenge Problem, *Computers and Chemical Engineering* **2021**, 107451.
21. O'Brien, C. M.; Zhang, Q.; Daoutidis, P.; Hu, W.-S., A Hybrid Mechanistic-Empirical Model for in silico Mammalian Cell Bioprocess Simulation. *Metabolic Engineering* **2021**, *66*, 31.
22. Pinto, J.; de Azevedo, C. R.; Oliveira, R.; von Stosch, M., A Bootstrap-Aggregated Hybrid Semi-Parametric Modeling Framework for Bioprocess Development. *Bioprocess and biosystems engineering* **2019**, *42*, 1853.
23. Chopda, V.; Gyorgypal, A.; Yang, O.; Singh, R.; Ramachandran, R.; Zhang, H.; Tsilomelekis, G.; Chundawat, S. P.; Ierapetritou, M. G., Recent Advances in Integrated Process Analytical Techniques, Modeling, and Control Strategies to Enable Continuous Biomanufacturing of Monoclonal Antibodies. *Journal of Chemical Technology and Biotechnology*. **2021**. <https://doi.org/10.1002/jctb.6765>, accessed July 23, 2021.

24. Zhang, D.; Del Rio-Chanona, E. A.; Petsagkourakis, P.; Wagner, J., Hybrid Physics-Based and Data-Driven Modeling for Bioprocess Online Simulation and Optimization. *Biotechnology and Bioengineering*. **2019**, *116*, 2919.
25. Al-Yemni, M.; Yang, R. Y., Hybrid Neural-Networks Modeling of an Enzymatic Membrane Reactor. *Journal of the Chinese Institute of Engineers*. **2005**, *28*, 1061.
26. Chabbi, C.; Taibi, M.; Khier, B., Neural and Hybrid Neural Modeling of a Yeast Fermentation Process. *International Journal of Computational Cognition*. **2008**, *6*, 42.
27. Zanin, G., Determination of Inhibition in the Enzymatic Hydrolysis of Cellobiose Using Hybrid Neural Modelling. *Brazilian Journal of Chemical Engineering*. **2005**, *22*, 19.
28. Azarpour, A.; Borhani, T. N.; Alwi, S. R. W.; Manan, Z. A.; Mutalib, M. I. A., A Generic Hybrid Model Development for Process Analysis of Industrial Fixed-Bed Catalytic Reactors. *Chemical Engineering Research and Design*. **2017**, *117*, 149.
29. Luo, N.; Du, W.; Ye, Z.; Qian, F., Development of a Hybrid Model for Industrial Ethylene Oxide Reactor. *Industrial and Engineering Chemistry Research* **2012**, *51*, 6926.
30. Zahedi, G.; Lohi, A.; Mahdi, K., Hybrid Modeling of Ethylene to Ethylene Oxide Heterogeneous Reactor. *Fuel Processing Technology* **2011**, *92*, 1725.
31. Simon, L. L.; Fischer, U.; Hungerbühler, K., Modeling of a Three-Phase Industrial Batch Reactor Using a Hybrid First-Principles Neural-Network Model. *Industrial and Engineering Chemistry Research*. **2006**, *45*, 7336.
32. Bellos, G.; Kallinikos, L.; Gounaris, C.; Papayannakos, N., Modelling of the Performance of Industrial HDS Reactors using a Hybrid Neural Network Approach. *Chemical Engineering and Processing: Process Intensification*. **2005**, *44*, 505.
33. Chang, J.-S.; Lu, S.-C.; Chiu, Y.-L., Dynamic Modeling of Batch Polymerization Reactors via the Hybrid Neural-Network Rate-Function Approach. *Chemical Engineering Journal* **2007**, *130*, 19.
34. Hinchliffe, M.; Montague, G.; Willis, M.; Burke, A., Hybrid Approach to Modeling an Industrial Polyethylene Process. *AIChE journal*. **2003**, *49*, 3127.
35. Madar, J.; Abonyi, J.; Szeifert, F., Feedback Linearizing Control Using Hybrid Neural Networks Identified by Sensitivity Approach. *Engineering Applications of Artificial Intelligence*. **2005**, *18*, 343.
36. Simutis, R.; Lübbert, A., Hybrid Approach to State Estimation for Bioprocess Control. *Bioengineering*. **2017**, *4*, 21.
37. Cubillos, F.; Callejas, H.; Lima, E.; Vega, M., Adaptive Control Using a Hybrid-Neural Model: Application to a Polymerisation Reactor. *Brazilian Journal of Chemical Engineering*. **2001**, *18*, 113.

38. Doyle III, F. J.; Harrison, C. A.; Crowley, T. J., Hybrid Model-Based Approach to Batch-to-Batch Control of Particle Size Distribution in Emulsion Polymerization. *Computers and Chemical Engineering*. **2003**, *27*, 1153.
39. Rodriguez-Granose, D.; Jones, A.; Loftus, H.; Tandeski, T.; Heaton, W.; Foley, K. T.; Silverman, L., Design of Experiment (DOE) Applied to Artificial Neural Network Architecture Enables Rapid Bioprocess Improvement. *Bioprocess and Biosystems Engineering*. **2021**, *44*, 1301.
40. Brendel, M.; Marquardt, W., Experimental Design for the identification of hybrid reaction models from transient data. *Chemical Engineering Journal*. **2008**, *141*, 264.
41. Bollas, G.; Papadokonstadakis, S.; Michalopoulos, J.; Arampatzis, G.; Lappas, A.; Vasalos, I.; Lygeros, A., Using Hybrid Neural Networks in Scaling up an FCC Model from a Pilot Plant to an Industrial Unit. *Chemical Engineering and Processing: Process Intensification*. **2003**, *42*, 697.
42. von Stosch, M.; Hamelink, J.-M.; Oliveira, R., Hybrid Modeling as a QbD/PAT Tool in Process Development: An Industrial E. coli Case Study. *Bioprocess and Biosystems Engineering*. **2016**, *39*, 773.
43. Iwama, R.; Kaneko, H., Design of Ethylene Oxide Production Process Based on Adaptive Design of Experiments and Bayesian Optimization. *AIChE J.*, **2021**, *3*, e10085.
44. Zhang, S.; Wang, F.; He, D.; Jia, R., Batch-to-Batch Control of Particle Size Distribution in Cobalt Oxalate Synthesis Process Based on Hybrid Model. *Powder Technology*. **2012**, *224*, 253.45.
45. Kumar, A.; Baldea, M.; Edgar, T. F., Real-Time Optimization of an Industrial Steam-Methane Reformer under Distributed Sensing. *Control Engineering Practice*. **2016**, *54*, 140.
46. Zhou, T.; Gani, R.; Sundmacher, K., Hybrid Data-Driven and Mechanistic Modeling Approaches for Multiscale Material and Process Design. *Engineering* **2021**. <https://doi.org/10.1016/j.eng.2020.12.022>, accessed July 23, 2021.
47. Cardillo, A. G.; Castellanos, M. M.; Desailly, B.; Dessoy, S.; Mariti, M.; Portela, R. M.; Scutella, B.; von Stosch, M.; Tomba, E.; Varsakelis, C., Towards *in silico* Process Modeling for Vaccines. *Trends in Biotechnology* **2021**. <https://doi.org/10.1016/j.tibtech.2021.02.004>, accessed July 23, 2021.
48. McBride, K.; Sanchez Medina, E. I.; Sundmacher, K., Hybrid Semi-Parametric Modeling in Separation Processes: A Review. *Chemie Ingenieur Technik*. **2020**, *92*, 842.
49. Safavi, A.; Nooraii, A.; Romagnoli, J., A Hybrid Model Formulation for a Distillation Column and the On-line Optimisation Study. *Journal of Process Control* **1999**, *9*, 125.

50. Mahalec, V. Hybrid Modeling of Petrochemical Processes. In *Hybrid Modeling in Process Industries*, Glassey, J. and Von Stosch, M., editor, CRC Press, Boca Raton, FL, pp.130-165.
51. Mahalec, V.; Sanchez, Y., Inferential Monitoring and Optimization of Crude Separation Units via Hybrid Models. *Computers and Chemical Engineering*, **2012**, *45*, 15.
52. Peroni, C. V.; Parisi, M.; Chianese, A., Hybrid Modelling and Self-Learning System for Dextrose Crystallization Process. *Chemical Engineering Research and Design* **2010**, *88*, 1653.
53. Xiong, Z.; Zhang, J., A Batch-to-Batch Iterative Optimal Control Strategy Based on Recurrent Neural Network Models. *Journal of Process Control* **2005**, *15*, 11.
54. Zhang, S.; Chu, F.; Deng, G.; Wang, F., Soft Sensor Model Development for Cobalt Oxalate Synthesis Process Based on Adaptive Gaussian Mixture Regression. *IEEE Access* **2019**, *7*, 118749.
55. Nentwich, C.; Winz, J.; Engell, S., Surrogate Modeling of Fugacity Coefficients Using Adaptive Sampling. *Industrial & Engineering Chemistry Research* **2019**, *58*, 18703.
56. Kunde, C.; Keßler, T.; Linke, S.; McBride, K.; Sundmacher, K.; Kienle, A., Surrogate Modeling for Liquid–Liquid Equilibria Using a Parameterization of the Binodal Curve. *Processes* **2019**, *7*, 753.
57. Côte, M.; Grandjean, B. P.; Lessard, P.; Thibault, J., Dynamic Modelling of the Activated Sludge Process: Improving Prediction Using Neural Networks. *Water Research* **1995**, *29*, 995.
58. Dong, Z.; Wang, R.; Fan, M.; Fu, X., Switching and Optimizing Control for Coal Flotation Process Based on a Hybrid Model. *PLoS ONE* **2017**, *12*, e0186553. 12(10): e0186553. <https://doi.org/10.1371/journal.pone.0186553>. Accessed July 25, 2021.
59. Hwang, T.-M.; Oh, H.; Choi, Y.-J.; Nam, S.-H.; Lee, S.; Choung, Y.-K., Development of a Statistical and Mathematical Hybrid Model to Predict Membrane Fouling and Performance. *Desalination* **2009**, *247*, 210.
60. Piron, E.; Latrille, E.; Rene, F., Application of Artificial Neural Networks for Crossflow Microfiltration Modelling: “Black-Box” and Semi-Physical Approaches. *Computers and Chemical Engineering* **1997**, *21*, 1021.
61. Zbiciński, I.; Strumiłło, P.; Kamiński, W., Hybrid Neural Model of Thermal Drying in a Fluidized Bed. *Computers and Chemical Engineering* **1996**, *20*, S695.
62. Cubillos, F. A.; Alvarez, P. I.; Pinto, J. C.; Lima, E. L., Hybrid-Neural Modeling for Particulate Solid Drying Processes. *Powder Technology* **1996**, *87*, 153.
63. Venkatasubramanian, V., The Promise of Artificial intelligence in Chemical Engineering: Is it Here, Finally? *AIChE Journal* **2019**, *65*, 466.

64. Glassey, J.; Von Stosch, M., editors, *Hybrid Modeling in Process Industries*. CRC Press, Boca Raton, FL, **2018**.
65. Kahrs, O.; Marquardt, W., Incremental Identification of Hybrid Process Models. *Computers and Chemical Engineering* **2008**, *32*, 694.
66. Chan, W. K. C.; Fischer, B.; Varvarezos, D.; Rao, A.; Zhao, H., Asset Optimization Using Integrated Modeling, Optimization, and Artificial Intelligence. U.S. patent 20200287818A1, Dec. 10, **2020**.
67. Beck, R.; Munoz, G. Hybrid Modeling: AI and Domain Expertise Combine to Optimize Assets., **2020**. <https://www.aspentech.com/en/resources/white-papers/hybrid-modeling-ai-and-domain-expertise-combine-to-optimize-assets/?src=blog-global-wpt.>, accessed June 18, 2021.
68. Galvanauskas, V.; Simutis, R.; Lübbert, A., Hybrid Process Models for Process Optimization, Monitoring and Control. *Bioprocess and Biosystems Engineering* **2004**, *26*, 393.
69. Tian, Y.; Zhang, J.; Morris, J., Modeling and Optimal Control of a Batch Polymerization Reactor Using a Hybrid Stacked Recurrent Neural Network Model. *Industrial and Engineering Chemistry Research* **2001**, *40*, 4525.
70. Su, H. T.; McAvoy, T. J.; Werbos, P., Long-Term Predictions of Chemical Processes Using Recurrent Neural Networks: A Parallel Training Approach. *Industrial and Engineering Chemistry Research* **1992**, *31*, 1338.
71. Hermanto, M. W.; Braatz, R. D.; Chiu, M. S., Integrated Batch-to-Batch and Nonlinear Model Predictive Control for Polymorphic Transformation in Pharmaceutical Crystallization. *AIChE journal* **2011**, *57*, 1008.
72. Ghosh, D.; Hermonat, E.; Mhaskar, P.; Snowling, S.; Goel, R., Hybrid Modeling Approach Integrating First-Principles Models with Subspace Identification. *Industrial and Engineering Chemistry Research* **2019**, *58*, 13533.
73. Ghosh, D.; Moreira, J. S.; Mhaskar, P., Model Predictive Control Embedding a Parallel Hybrid Modeling Strategy. *Industrial and Engineering Chemistry Research* **2021**, *60*, 2547.
74. Hanachi, H.; Yu, W.; Kim, I.Y.; Liu, J.; Mechefske, C.K. Hybrid Data-Driven Physics-Based Model Fusion Framework for Tool Wear Prediction. *The International Journal of Advanced Manufacturing Technology*, **2019**, *101*, 2861.
75. Babanezhad, M.; Behroyan, I.; Nakhjiri, A. T.; Marjani, A.; Rezakazemi, M.; Shirazian, S., High-Performance Hybrid Modeling Chemical Reactors Using Differential Evolution Based Fuzzy Inference System. *Scientific Reports* **2020**, *10*, 1.
76. Krippel, M.; Dürauer, A.; Duerkop, M., Hybrid Modeling of Cross-Flow Filtration: Predicting the Flux Evolution and Duration of Ultrafiltration Processes. *Separation and Purification Technology* **2020**, *248*, 117064.

77. Mantovanelli, I. C.; Rivera, E. C.; Da Costa, A. C.; Maciel Filho, R., Hybrid Neural Network Model of an Industrial Ethanol Fermentation Process Considering the Effect of Temperature. *Applied Biochemistry and Biotechnology* **2007**, *137*, 817.
78. Sharma, N.; Liu, Y. A., 110th Anniversary: An Effective Methodology for Kinetic Parameter Estimation for Modeling Commercial Polyolefin Processes from Plant Data Using Efficient Simulation Software Tools. *Industrial and Engineering Chemistry Research* **2019**, *58*, 14209.
79. Bhutani, N.; Rangaiah, G.; Ray, A., First-Principles, Data-Based, and Hybrid Modeling and Optimization of an Industrial Hydrocracking Unit. *Industrial and Engineering Chemistry Research* **2006**, *45*, 7807.
80. Song, W.; Du, W.; Fan, C.; Yang, M.; Qian, F., Adaptive Weighted Hybrid Modeling of Hydrocracking Process and Its Operational Optimization. *Industrial and Engineering Chemistry Research* **2021**, *60*, 3617.
81. Lima, P.V.; Saraiva, P.M.; and Group, G.P. A Semi-Mechanistic Model Building Framework Based on Selective and Localized Model Extensions. *Computers and Chemical Engineering*. **2007**, *31*, 361.
82. Breiman, L. Random Forests. *Machine Learning*. **2001**. *45*, 5.
83. Savkovic-Stevanovic, J., Neural Net Controller by Inverse Modeling for a Distillation Plant. *Computers and Chemical Engineering* **1996**, *20*, S925.
84. Tomba, E., Barolo, M. and García-Muñoz, S., General Framework for Latent Variable Model Inversion for the Design and Manufacturing of New Products. *Industrial and Engineering Chemistry Research* **2012**, *51*, 12886.
85. Tomba, E., Barolo, M. and García-Muñoz, S., In-Silico Product Formulation Design through Latent Variable Model Inversion. *Chemical Engineering Research and Design*. **2014**, *92*, 534.
86. Bayer, B.; Von Stosch, M.; Striedner, G.; Duerkop., M., Comparison of Modeling Methods for DoE-Based Holistic Upstream Process Characterization., *Biotechnology journal*. **2020**, *15*, 1900551.
87. Raccuglia, P.; Elbert, K. C.; Adler, P. D.; Falk, C.; Wenny, M. B.; Mollo, A.; Zeller, M.; Friedler, S. A.; Schrier, J.; Norquist, A. J., Machine-Learning-Assisted Materials Discovery Using Failed Experiments. *Nature* **2016**, *533*, 73.
88. Liao, T. W.; Li, G., Metaheuristic-Based Inverse Design of Materials—A Survey. *Journal of Materiomics* **2020**, *6*, 414.
89. Bamberg, A., Urbas, L., Bröcker, S., Bortz, M. and Kockmann, N., The Digital Twin—Your Ingenious Companion for Process Engineering and Smart Production. *Chemical Engineering & Technology* **2021**, *44*, 954.
90. MacGregor, J.; Skagerberg, B.; Kiparissides, C., Multivariate Statistical Process Control and Property Inference Applied to Low Density Polyethylene Reactors. In

- Advanced Control of Chemical Processes 1991*, Elsevier, Amsterdam, Netherlands, **1992**; pp 155-159.
- 91.** Rogers, A.; Ierapetritou, M. Feasibility and Flexibility Analysis of Black-Box Processes Part 1: Surrogate-based Feasibility Analysis. *Chemical Engineering Science*. **2015**, *137*, 986.
 - 92.** Rogers, A. and Ierapetritou, M., Feasibility and Flexibility Analysis of Black-Box Processes Part 2: Surrogate-based Feasibility Analysis. *Chemical Engineering Science*. 2015, *137*, pp.1005-1013.
 - 93.** Abdullah, F.; Wu, Z.; Christofides, P. D., Data-Based Reduced-Order Modeling of Nonlinear Two-Time-Scale Processes. *Chemical Engineering Research and Design* **2021**, *166*, 1-9.
 - 94.** Agarwal, A.; Biegler, L. T.; Zitney, S. E., Simulation and Optimization of Pressure Swing Adsorption Systems Using Reduced-Order Modeling. *Industrial and Engineering Chemistry Research*. **2009**, *48*, 2327.
 - 95.** Schäfer, P.; Caspari, A.; Kleinhans, K.; Mhamdi, A.; Mitsos, A., Reduced Dynamic Modeling Approach for Rectification Columns Based on Compartmentalization and Artificial Neural Networks. *AIChE Journal*. **2019**, *65*, e16568.
 - 96.** Zhang, J.; Yin, J.; Wang, R., Basic Framework and Main Methods of Uncertainty Quantification. *Mathematical Problems in Engineering* 2020, Article ID 6068203, <https://doi.org/10.1155/2020/6068203>.
 - 97.** Duong, P. L. T.; Ali, W.; Kwok, E.; Lee, M., Uncertainty Quantification and Global Sensitivity Analysis of Complex Chemical Process Using a Generalized Polynomial Chaos Approach. *Computers and Chemical Engineering* **2016**, *90*, 23.
 - 98.** Francis-Xavier, F.; Kubanek, F.; Schenkendorf, R., Hybrid Process Models in Electrochemical Syntheses under Deep Uncertainty. *Processes* **2021**, *9*, 704.
 - 99.** Proppe, J.; Husch, T.; Simm, G. N.; Reiher, M., Uncertainty Quantification for Quantum Chemical Models of Complex Reaction Networks. *Faraday discussions* **2017**, *195*, 497.
 - 100.** Parks, H. L.; McGaughey, A. J.; Viswanathan, V., Uncertainty Quantification in First-Principles Predictions of Harmonic Vibrational Frequencies of Molecules and Molecular Complexes. *Journal of Physical Chemistry C* **2019**, *123*, 4072.
 - 101.** Wang, S.; Pillai, H. S.; Xin, H., Bayesian Learning of Chemisorption for Bridging the Complexity of Electronic Descriptors. *Nature communications* **2020**, *11*, 1.
 - 102.** Boukouvala, F.; Ierapetritou, M. G., Feasibility analysis of Black-Box Processes using an Adaptive Sampling Kriging-based Method. *Computers and Chemical Engineering* **2012**, *36*, 358.
 - 103.** Rudy, S. H.; Brunton, S. L.; Proctor, J. L.; Kutz, J. N., Data-Driven Discovery of Partial Differential equations. *Science Advances* **2017**, *3*, e1602614.

- 104.** Langley, P.; Bradshaw, G. L.; Simon, H. A., Rediscovering Chemistry with the Bacon System. In *Machine Learning: An Artificial Intelligence Approach*, Michalski, R. S.; Carbonell, J. G.; Mitchell, T. M., Eds. Springer, Berlin Heidelberg **1983**; pp 307-329.
- 105.** Nentwich, C.; Engell, S., Surrogate Modeling of Phase Equilibrium Calculations Using Adaptive Sampling. *Computers and Chemical Engineering* **2019**, *126*, 204
- 106.** Hoffmann, M., Fröhner, C. and Noé, F., Reactive SINDy: Discovering Governing Reactions from Concentration Data. *The Journal of chemical physics* **2019**, *150*, 025101
- 107.** Wang, S.-H.; Pillai, H. S.; Wang, S.; Achenie, L. E.; Xin, H., Infusing Theory into Machine Learning for Interpretable Reactivity Prediction. *arXiv:2103.15210v2[physics,chem-ph]* . **2021**. <https://arxiv.org/abs/2103.15210>. Accessed August 5, 2021.
- 108.** Chen, R. T.; Rubanova, Y.; Bettencourt, J.; Duvenaud, D., Neural Ordinary Differential Equations. *arXiv:1806.07366v5[cs.LG]*, **2018**. <https://arxiv.org/abs/1806.07366>. Accessed August 5, 2021.
- 109.** De Jaegher, B.; Larumbe, E.; De Schepper, W.; Verliefde, A.; Nopens, I., Colloidal Fouling in Electrodialysis: A Neural Differential Equations model. *Separation and Purification Technology* **2020**, *249*, 116939
- 110.** Wu, Zhe, David Rincon, and Panagiotis D. Christofides., Process Structure-Based Recurrent Neural Network Modeling for Model Predictive Control of Nonlinear Processes. *Journal of Process Control* **2020**, *89*, 74.
- 111.** Reis, Marco S., Geert Gins, and Tiago J. Rato., Incorporation of Process-Specific Structure in Statistical Process Monitoring: A Review., *Journal of Quality Technology* , **2019**, *51*, , 407.
- 112.** Hayashi, Y., Buckley, J.J. and Czogala, E., Fuzzy Neural Network with Fuzzy Signals and Weights., *International Journal of Intelligent Systems* **1993**., *8*, 527.
- 113.** Brown, M. and Harris, C.J., Neurofuzzy Adaptive Modelling and Control **1994**.
- 114.** Simutis, R., Havlik, I., Schneider, F., Dors, M. and Lübbert, A., 1995. Artificial Neural Networks of Improved Reliability for Industrial Process Supervision. *IFAC Proceedings Volumes*, *28*, pp.59.
- 115.** Simutis, R. and Lübbert, A., 2015. Bioreactor Control Improves Bioprocess Performance. *Biotechnology journal*, *10*, pp.1115.
- 116.** Schubert, J., Simutis, R., Dors, M., Havlik, I. and Lübbert, A., 1994. Bioprocess Optimization and Control: Application of Hybrid Modelling. *Journal of biotechnology*, *35*, pp.51.
- 117.** Lu, J.; Yao, K.; Gao, F., Process Similarity and Developing New Process Models through Migration. *AIChE journal* **2009**, *55*, 2318.

118. Yan, W.; Hu, S.; Yang, Y.; Gao, F.; Chen, T., Bayesian Migration of Gaussian Process Regression for Rapid Process Modeling and Optimization. *Chemical Engineering Journal* **2011**, *166*, 1095.
119. Kumar, A.; Ridha, S.; Narahari, M.; Ilyas, S. U., Physics-Guided Deep Neural Network to Characterize Non-Newtonian Fluid Flow for Optimal Use of Energy Resources. *Expert Systems with Applications* **2021**, *183*, 115409.
120. Pun, G. P.; Batra, R.; Ramprasad, R.; Mishin, Y., Physically Informed Artificial Neural Networks for Atomistic Modeling of Materials. *Nature communications* **2019**, *10*, 1.
121. Fischer, C. C.; Tibbetts, K. J.; Morgan, D.; Ceder, G., Predicting Crystal Structure by Merging Data Mining with Quantum Mechanics. *Nature Materials* **2006**, *5*, 641.
122. Hautier, G.; Fischer, C. C.; Jain, A.; Mueller, T.; Ceder, G., Finding Nature's Missing Ternary Oxide Compounds Using Machine Learning and Density Functional Theory. *Chemistry of Materials* **2010**, *22*, 3762.
123. Cang, R.; Li, H.; Yao, H.; Jiao, Y.; Ren, Y., Improving Direct Physical Properties Prediction of Heterogeneous Materials from Imaging Data via Convolutional Neural Network and a Morphology-Aware Generative Model. *Computational Materials Science* **2018**, *150*, 212.
124. Sharma, N.; Liu, Y. A., A Hybrid Science-Guided Machine Learning Approach for Modeling and Optimizing Chemical Processes: A Review. *AIChE Journal*, 2021 (In review)

Chapter 6: Application of Hybrid Science-Guided Machine Learning for Polymer Processes Improvement

6.1. Introduction

The hybrid science-guided machine learning techniques (SGML) integrate science-based knowledge and data-based knowledge for an accurate and scientifically consistent prediction as showcased by Sharma and Liu ¹ and chapter 5 as well. Polymer processes such as Ziegler Natta Polyolefin process which is a multi-site catalytic process there are many unknown reaction kinetic parameters which needs to be estimated with limited information. The thermodynamic parameters like phase equilibrium/interaction parameters of some polymers are also uncertain. The process is highly exothermic and heat transfer is important to defining process physics, the parameters of which may be based on certain assumptions. Thus, the first-principle-based polymer process models are built on many assumptions which lead to less accurate predictions. Similarly, for data-based analysis of polymer processes, the lesser frequency of quality measurements in certain cases becomes a limitation. Also, data-based models may tend to give scientifically consistent results beyond the process operating range on which the models are trained. Thus, hybrid models combining science-based models and machine learning models are quite useful for polymer process modeling.

There have been limited applications of hybrid modeling on polymer processes over the years. Tsen et. al. ² showcase one of the earliest applications of hybrid modeling for predictive control of a batch polymerization process. They used a hybrid model combining the physics model and a neural network model to control polymer quality parameters like dispersity and molecular weight. They have trained a data-based neural network model using an augmented data set combining results from a chemical process model and experimental data. They have shown their hybrid model performing better than a theoretical model built only on experimental data.

Tian et. al. ³ work on a hybrid residual model to accurately predict the gel effect in the batch polymerization process. They use the hybrid model for optimal temperature control of reactor temperature. First, they develop a simplified process model based on polymerization kinetics, and mass and energy balances to predict the monomer conversion, number-average molecular weight MWN, and weight-average molecular weight MWW. This first-principle process model cannot predict these product quality targets accurately because of its neglect of the gel effect at high monomer conversion and other factors. Next, the authors develop a parallel configuration of three data-based, time-dependent or recurrent neural networks trained by process data to predict the residuals of monomer conversion, MWN and MWW of the simplified first-principle process model. The predicted residuals are added to the predictions from the simplified process model to form the final hybrid model predictions. Because of focus in batch process control is on the end-

of-batch product quality targets, the use of time-dependent or recurrent neural networks can usually offer good long-range predictions.

Hinchliffe et. al. ⁴ apply the hybrid modeling approach for modeling an industrial polyethylene process for accurate prediction of the Molecular Weight Distribution(MWD) of the polymer. They use Neural Network to predict some of the multipliers to some important features that affect the MWD in the mechanistic model like the mass fraction of polymer produced at each sites and degree of polymerization.

Doyle et. al. ⁵ apply the hybrid modeling strategy for batch-to-batch control of particle size distribution in an emulsion polymerization process. They combine the first-principle population balance model with a data-based partial least squares model for controlling the particle size for batch-to-batch optimization. Chang et. al. ⁶ use a hybrid modeling approach for dynamic modeling of a batch polymerization process. They include some of the state variables which could not be measured by mechanistic models and then combine the model results with the measurements in a neural network rate function model for better prediction. In this chapter, we showcase some more applications of the hybrid SGML methodologies for industrial polyolefin process improvements.

6.2. Polyolefin Process and Data Description

6.2.1. Industrial parallel/single reactor HDPE process

For most of the applications, we consider an industrial HDPE process using actual plant data from LG Petrochemicals in South Korea by Park et. al ⁷. The industrial process is a slurry single reactor (parallel process) Ziegler Natta process. We first estimate the polymerization kinetic parameters from plant production targets in a steady-state model using Aspen Polymers based on our reported methodology ⁸. This results in a validated Aspen Polymers steady-state simulation model. Next, we convert the steady-state model to a dynamic model using Aspen Plus Dynamics. We use the dynamic model to simulate the product quality data for different process operating conditions, which include the data characterizing the polymer grade transitions. Figure 6.1 shows the process flowsheet of the parallel HDPE process.

The data consist of the input stream flow rates and product quality targets varying with time at the two reactor outlets. The dataset consists of about 5000 observations. Table 6.1 summarizes the process variables and quality targets for the parallel HDPE process

Table 6.1. Process variables and quality targets for the parallel HDPE process

Process variable	Description
C2	Ethylene feed flow rate (kg/hr)
H2	Hydrogen feed flow rate (kg/hr)
CAT	Catalyst feed flow rate (kg/hr)
HX	Hexane solvent feed flow rate (kg/hr)
C3	Comonomer feed flow rate (kg/hr)
T	Temperature of the reactor (C)

P	Pressure in the reactor (Bar)
H2/C2	Feed concentration ratio in the reactor of ethylene to hydrogen
C3/C4	Feed concentration ratio of Propylene to Butylene monomer
MI	Melt Index of polymer

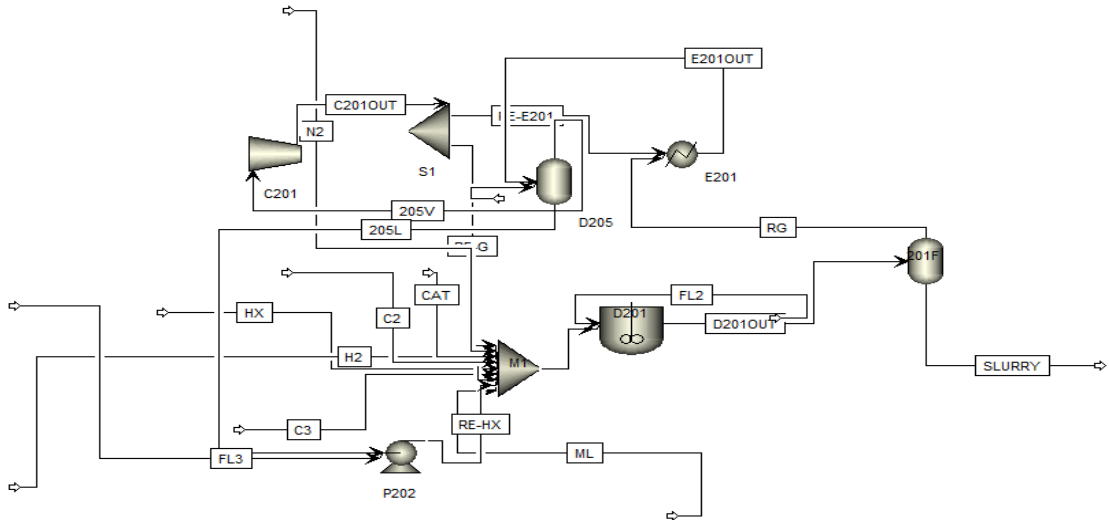


Figure 6.1. Process flowsheet of industrial parallel HDPE process

6.2.2. Industrial series reactors slurry HDPE process

We also simulate a two-reactor slurry HDPE process by Mitsui. Ethylene is the monomer for the process and propylene or butylene is comonomer. Hexane is used as a diluent to dissolve the monomer, co-monomer and hydrogen. The process variables are shown in figure. Figure 6.2 shows the flowsheet for the process made in Aspen Polymers and Table 6.2 summarizes the process variables.

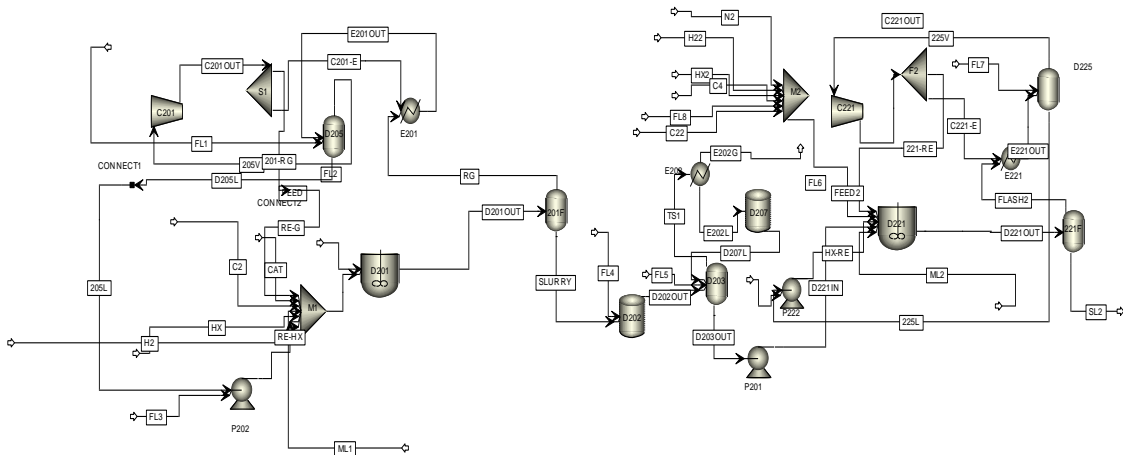


Figure 6.2. Process flowsheet for industrial series HDPE process

Table 6.2. Process variables for the series reactor HDPE process

	Process Variable
C21	Ethylene monomer flow in the feed to the first reactor (kg/hr)
H21	Hydrogen flow in the feed to the first reactor (kg/hr)
CAT	Catalyst flow in the first reactor (kg/hr)
HX1	Solvent flow in the first reactor (kg/hr)
C42	1-Butene co-monomer flow in the second reactor (kg/hr)
C22	Ethylene monomer flow in the second reactor (kg/hr)
H22	Hydrogen flow in the second reactor (kg/hr)
HX2	Solvent flow in the second reactor (kg/hr)
	Quality Target
MI	Melt index
Rho	Polymer density (kg/ m ³)
PDI	Polydispersity index
P	Polymer flow rate (kg/hr)

We simulate grade change for the process to simulate dynamic data. Figure 6.3 shows the grade change simulated for 4 grades with different Melt Index and Density values.

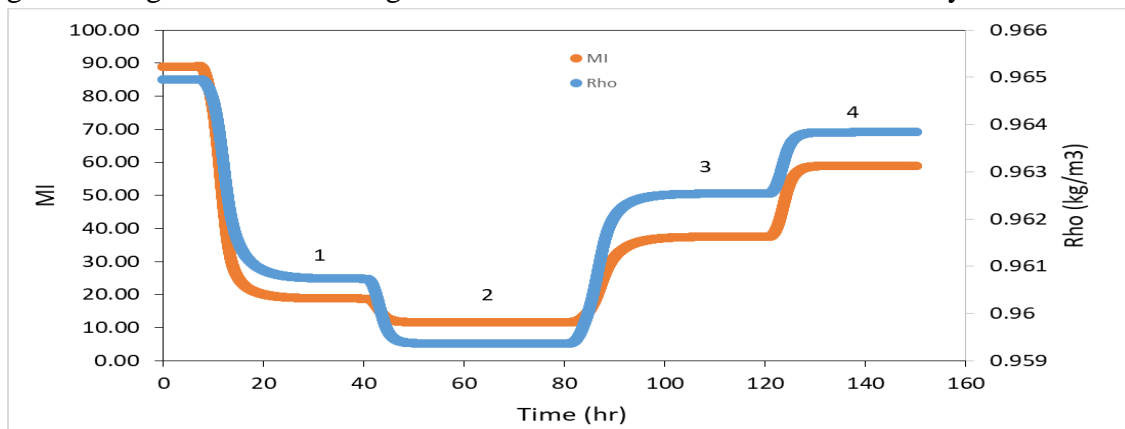


Figure 6.3. The variation of the quality data (MI and Rho) with time for different HDPE grades

6.2.3. Industrial Hypol PP process

We also simulate the Hypol PP process. Mitsui Hypol process is used for making polypropylene (PP) homopolymers and propylene-ethylene impact copolymer. The process consists of two autoclave reactors in series followed by two fluidized-bed reactors (FBR). It is a mixed-phase process with the fluid phase in the autoclave reactors and gas phase in the FBR. The FBRs have scrapers to eliminate fouling for making high-rubber-content impact copolymers. Figure 6.4 shows the flowsheet for the and the table 6.3 lists the process variables.

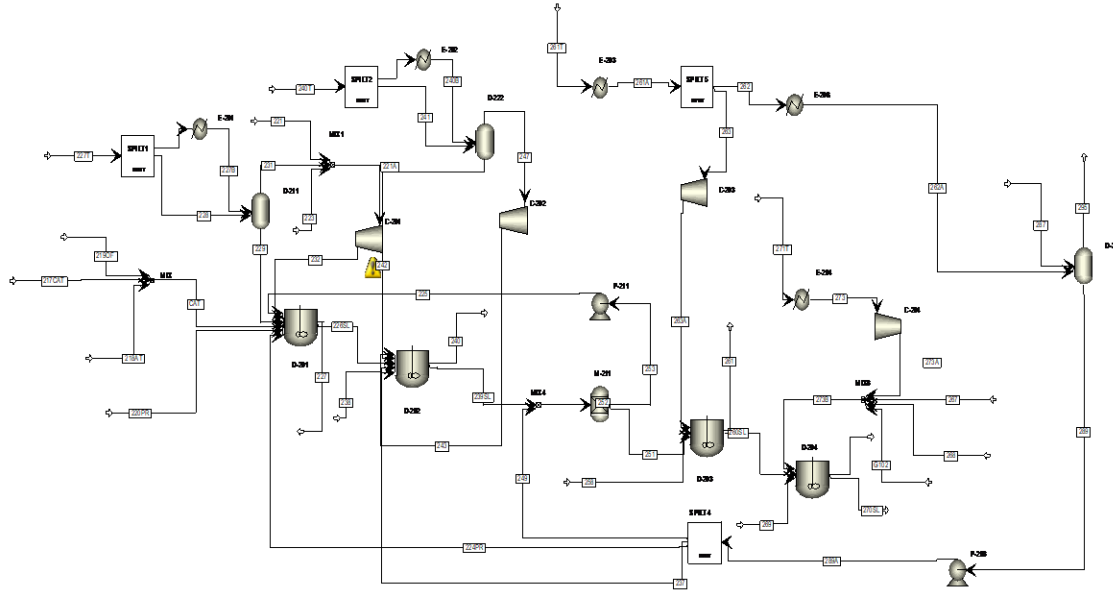


Figure 6.4. Process flowsheet for industrial Hypol process
 For this process, we simulate steady-state sensitivity data by varying the independent process variables. The simulated dataset for the two processes have 200 observations.

Table 6.3: Process and quality variables of Hypol process

	Process Variable
C31, C32, C33, C34	Propylene monomer flow in each of the reactors (R1, R2,R3,R4)(kg/hr)
H21, H22, H23, H24	Hydrogen flow in each of the reactors (R1,R2,R3,R4) (kg/hr)
CAT	Catalyst flow in the first reactor (kg/hr)
HX1	Solvent flow in the first reactor (kg/hr)
C24	Ethylene co-monomer flow in the 4 th reactor (kg/hr)
T1, T2, T3, T4	Temperature in each of the reactors (R1, R2, R3, R4) C
P1, P2, P3, P4	Pressure in each of the reactors (R1, R2, R3, R4) Bar
MI	Melt Index (QualityTarget)

6.2.4. Industrial LDPE process

We model a high-pressure industrial LDPE process which follows the free radical polymerization mechanism and consists of high-pressure tubular reactors in series/parallel arrangement as shown in the flowsheet in figure 6.5. Table 6.4 lists the independent process variables and product quality for the LDPE process. Due to free radical kinetics both long chain and short chain branching also need to be tracked to determine the LDPE polymer properties. The feed to the process is ethylene monomer (E2) and two initiators are benzoyl peroxide (INI1) and di-t-butyl-peroxide (INI2)

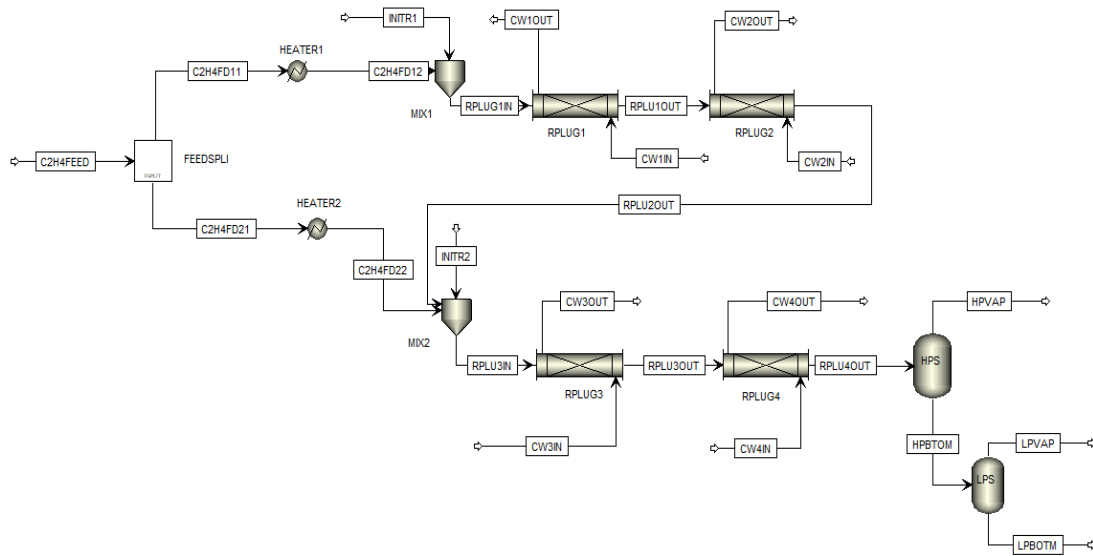


Figure 6.5. Process flowsheet of the industrial LDPE process

Table 6.4. Process variables and Quality for LDPE process

	Process Variable
E2	Ethylene feed flow (kg/hr)
INITF1	Flow of initiator into the mixer(M1) INITR1 (kg/hr)
INI1M1	Mass frac of INI1 (stream INITR1)
INI2M1	Mass Frac of INI2 (stream INITR1)
CW1	Cooling water flow rate to 1st reactor RPLUG1 (kg/hr)
TCW1	Temperature of cooling water in 1 ST reactor RPLUG1 (C)
CW2	Cooling water flow rate to 2nd reactor RPLUG2(kg/hr)
TCW2	Temperature of cooling water in 2 nd reactor RPLUG1 (C)
INITF2	Flow of initiator into the mixer(M2) INITR2(kg/hr)
INI1M2	INI1 Mass frac (INITR2) flow
INI2M2	INI2 Mass Frac (INITR2) flow
CW3	Cooling water flow rate to 3 rd reactor RPLUG3 (kg/hr)
TCW3	Temperature of cooling water in 3 rd reactor RPLUG3 (C)
CW4	Cooling water flow rate to 4 th reactor RPLUG4 (kg/hr)
TCW4	Temperature of cooling water in 4 th reactor RPLUG4 (C)
	Product Quality Target
LCB	Long Chain Branching in LDPE polymer (kmol/hr)
SCB	Short Chain Branching in LDPE product (kmol/hr)
MWW	Weight Average Molecular Weight of LDPE polymer
MWN	Number Average Molecular Weight of LDPE polymer
POLYF	Mass flow rate of LDPE polymer

6.3. An Application of Combined Direct Hybrid Modeling to Polyolefin Manufacturing

We apply the combined direct modeling strategy to an industrial polyethylene process for the prediction of melt index. We build a first-principle steady-state model of a Mitsui slurry high-density polyethylene (HDPE) process by following the methodology and kinetic parameters presented in Sharma and Liu⁸. We convert the steady-state simulation model based on Aspen Plus to a dynamic simulation model using Aspen Plus Dynamics. The resulting dynamic simulation model has similar independent process variables, including the feed flow and compositions and the reactor operating conditions. We use the hybrid residual modeling strategy where we use a first-principle or science-based process model to quantify the time-dependent prediction error or residual between plant data and science-based model prediction as a function of process variables.

$$MI_{Plant} - MI_{Model} = Res = f(X_{Process}) \quad (1)$$

$$MI_{Hybrid} = MI_{Model} + Res \quad (2)$$

Figure 6.6 compares the predictions of the first-principle dynamic simulation model (in red) with the plant data with grade transitions (in green). We see much deviation between the model predictions (MI_{Model}) and the plant data (MI_{Plant}). We compare the MI values from the model with the plant data and calculate the error residuals (Res). *The root-mean-squares-error (RMSE) values of the model residual is to 1.5 for the actual MI data with a standard deviation of 5.1.*

To improve the accuracy of model predictions, we develop a regression model to predict the error residues as a function of independent process variables ($X_{Process}$) using a random forest ML algorithm with Python. This leads to a hybrid model that predicts the MI value as a sum of the dynamic simulation model prediction (first-principle-based) and the predicted error residual (data-based) corresponding to a give set of independent process variable values, as shown in Equations 1-2. Figure 6.6 shows that the hybrid model predictions (*with a RMSE value of 0.21*) match the plant data much better than a first-principle dynamic simulation model alone. We note that a data-based model alone has also a similar accuracy, but it may give scientifically inconsistent results for predictions beyond the range of process operating data which the model uses. Thus, the hybrid model is not only accurate, but also gives scientifically consistent results beyond current operating range.

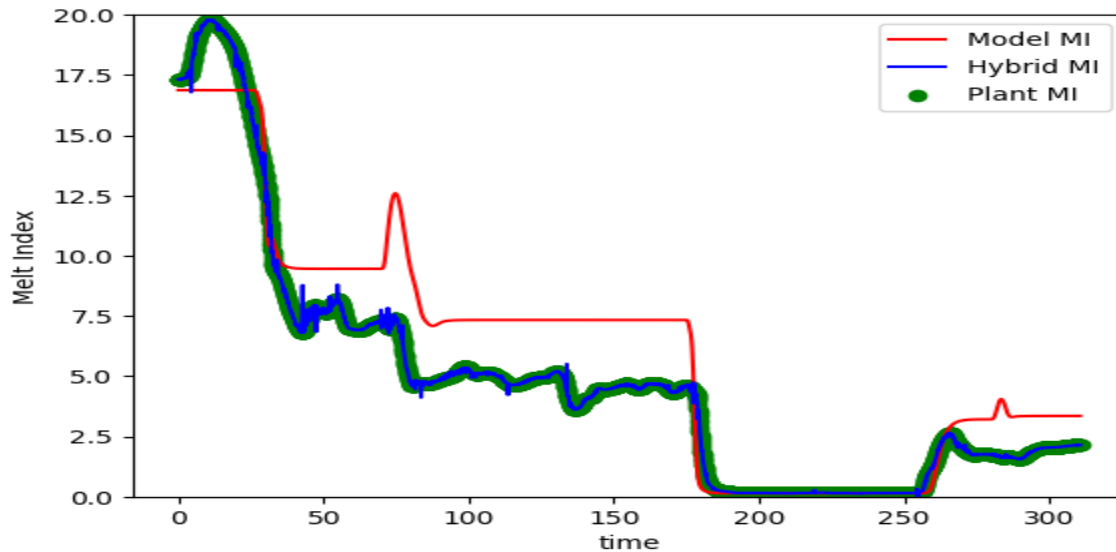


Figure 6.6. Melt index prediction of a combined direct hybrid model compared to the first-principle model and plant data

As a test of the scientific consistency of the hybrid model we use the same conditions of testing hybrid models beyond operating range at $H_2 = 95 \text{ m}^3/\text{hr}$ as in table 4.3. We compare the hybrid model results with first principle and ML results in table 6. From the results we can see hybrid SGML models are more accurate and scientifically consistent in extrapolation of results beyond operating range compared to the first-principle and ML models.

Table 6.5. Model comparison based on MI values at varying hydrogen flow

Model	MI ($H_2 = 60 \text{ m}^3/\text{hr}$)	MI ($H_2 = 95 \text{ m}^3/\text{hr}$) (beyond operating range)
Plant Actual value	5	22
First principle	6.1	17
Causal ML model	4.7	15
Predictive ML model	4.9	12
Hybrid Model	5.3	21.5

6.4. An Application of Inverse Modeling to Polymer Manufacturing

6.4.1. Predicting Operating Conditions of Different Polymer Grades

We illustrate the application of an inverse modeling approach that integrates steady-state and dynamic simulation models of a Mitsui slurry HDPE process, developed from first principles and validated by plant data, with a data-based ML model. The goal is to predict the operating conditions for producing new polymer grades, given the desired product quality targets, such as melt index (MI), polymer density (ρ), polydispersity index (PDI) and polymer production rate (P).

We first use the single-reactor industrial HDPE process to predict the operating conditions. We with the simulated product quality data as input, and the process operating conditions (flow rates of all input streams) as the output. We use an ensemble machine learning regression model to regress the simulated data.

We apply the gradient boosting regressor model for predictions and also determine the uncertainty in prediction using prediction intervals as shown in figure 6.7. The RMSE for the hydrogen feed flow rate prediction comes to be 2.2 (uncertainty range 1 – 5) with actual standard deviation of H2 flow being 22 kg/hr. We further use the stacked regression models⁹ with combination of ensemble models which predicts the operating conditions/feed flow rates with a high accuracy.

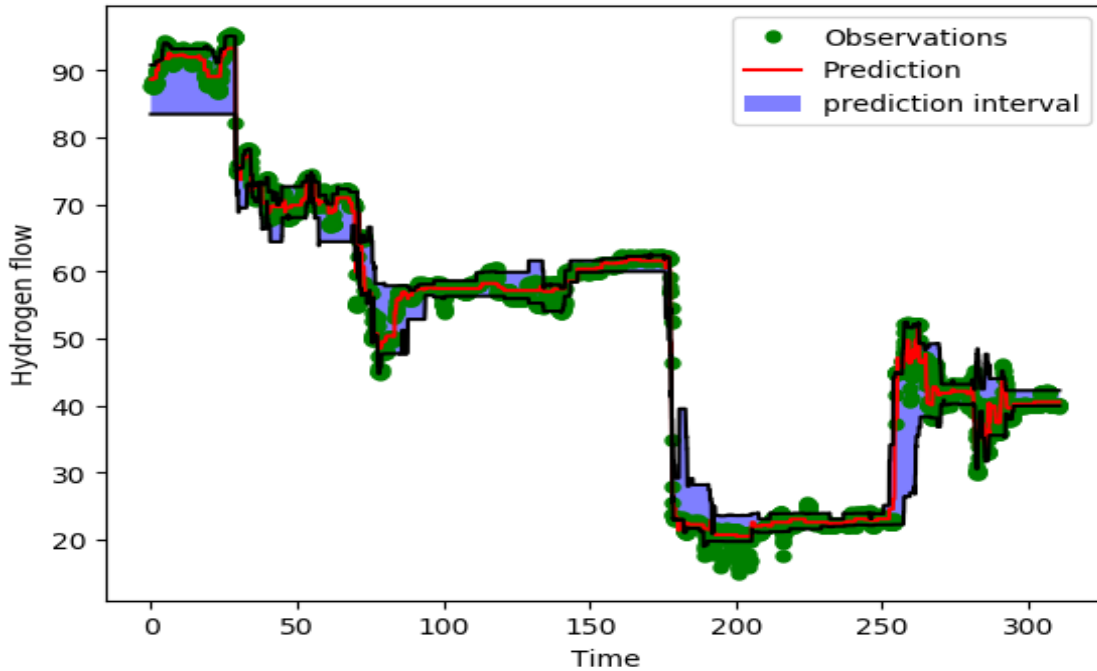


Figure 6.7. Hydrogen feed predictions for single reactor HDPE process using inverse modeling including the uncertainty of predictions using gradient boosting regression.

We used tree regression models like the gradient boosting, ada boosting, Random forest and Xgboost regression model for the stacked regression algorithm. We combine regression models by first individually fitting the regression models and then the regressor which performs best is chosen as the Meta regressor while the other three regressors are chosen as the Initial regressors. We compared the prediction of the stacked regressor with the individual ensemble regressors to come up with our stacking regressor. The RMSE values for the prediction of some of the process variables are compared for each of the individual regressors – gradient boosting, adaboost, xgboost and random forest regressors, xgboost¹⁰ has lower RMSE value as compared to other regressors, thus we chose it as meta regressor while using other ensemble regressors as initial regressor. Figure 6.8 shows the stacked regression algorithm for prediction of the inverse model.

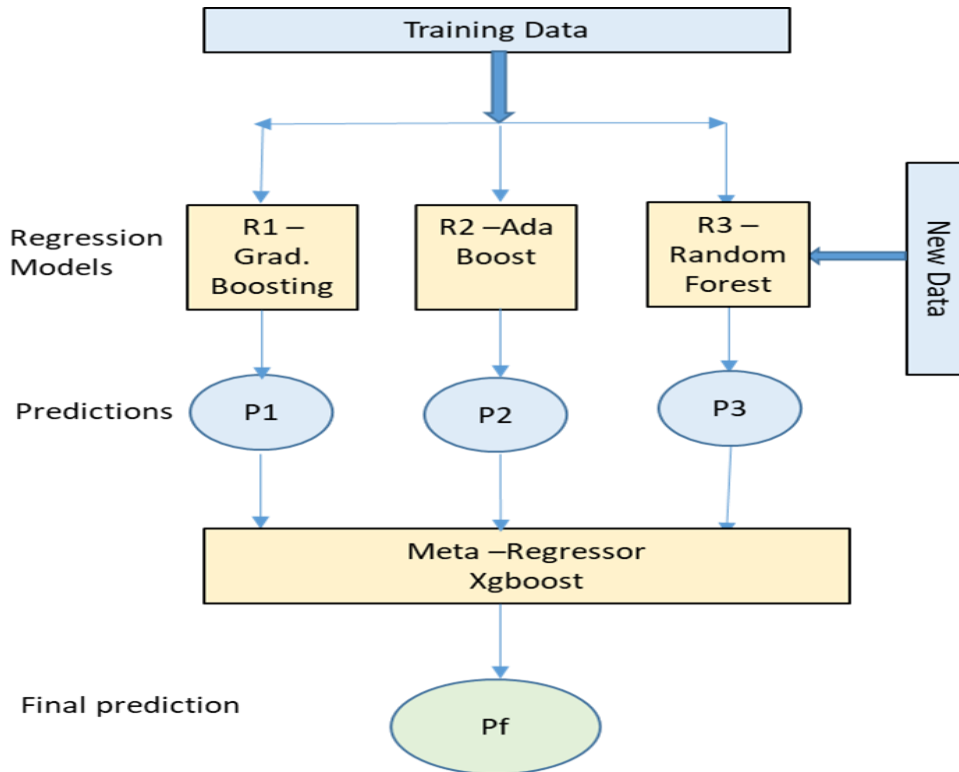


Figure 6.8. Stacked Regression Algorithm

The stacked ML model predictions gave a low RMSE of 0.9 when compared to actual plant data for a standard deviation of 20. We predict all process variables for the parallel HDPE process using the stacked regression model as shown in table 6.6. The table consists of the mean and standard deviation of each of the process variables from the actual data and the RMSE and NRMSE predictions.

Table 6.6. Process variable prediction for parallel HDPE process using inverse modeling

Predicted variable (kg/hr)	Data Mean (kg/hr)	Data Stdev (kg/hr)	RMSE (test) kg/hr	NRMSE (%)
H2	52	21	1.04	2
C2	8873	569	68.5	0.772005
CAT	26	5.6	1.03	3.961538
HX	22356	2734	219	0.979603
C3	51	44	2.83	5.54902
T	84	0.3	0.11	0.130952
P	3.1	0.7	0.2	6.451613
H2/C2	0.95	0.4	0.01	1.052632
C3/C4	0.4	0.37	0.014	3.5

Now we also test the inverse modeling methodology on the HDPE series reactor process and predict more process variables for the two-reactor process. We use the same stacking regression model for prediction. Table 6.7 and figure 6.9 A-D showcase the predictions of the process variables for the series HDPE process using the inverse modeling methodology.

Table 6.7. Prediction of operating conditions for series HDPE process

Predicted variable (kg/hr)	Data Mean (kg/hr)	Data Stdev (kg/hr)	RMSE (test) kg/hr	NRMSE (test) %
H21	5	0.98	0.04	0.8
C21	5750	49	0.4	0.006957
CAT1	255	0.54	0.003	0.001176
HX1	14980	186	1.1	0.007343
C22	5450	49	0.35	0.006422
C4	1030	76	0.43	0.041748
HX2	2020	35	0.93	0.04604
H22	0.75	0.24	0.0011	0.146667

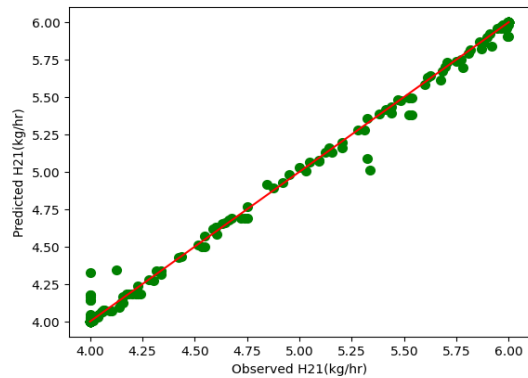


Figure 6.9a.

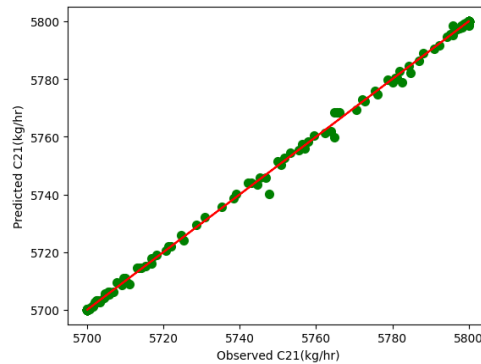


Figure 6.9b.

Figure 6.9a. Inverse ML model prediction v/s the observed data for hydrogen flow(H21)

Figure 6.9b. Inverse ML model prediction v/s the observed data for ethylene monomer flow (C21)

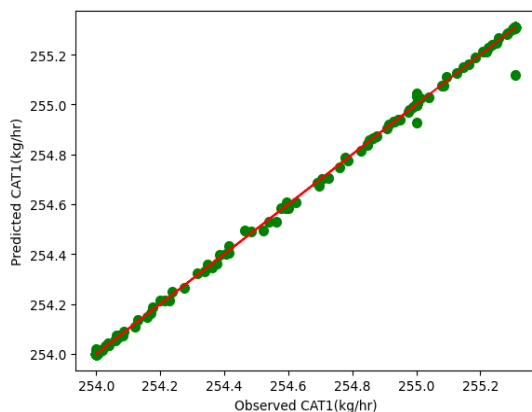


Figure 6.9c.

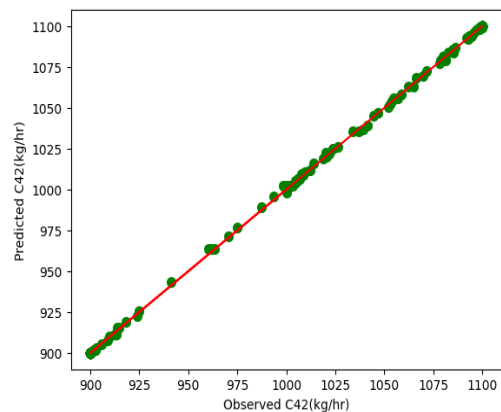


Figure 6.9d.

Figure 6.9c. Inverse ML model prediction v/s the observed data for catalyst flow (CAT1)
 Figure 6.9d. Inverse ML model prediction v/s the observed data for butlene comonomer flow(C42)

The %RMSE on predictions are less than 2.5% on the average for both the examples. Hence, we are able to accurately predict the operating conditions using inverse modeling methodology. Thus, if we want to produce a new polymer grade given its quality targets, we can predict the operating conditions required to produce that polymer grade using the inverse modeling approach.

6.4.2. Kinetic Estimation Using Inverse Modeling

Another application of inverse modeling can be for parameter estimation as well as better model calibration. We showcase the inverse model approach for estimation of kinetic model parameter for the HDPE process. We use the methodology to estimate the catalyst site concentration which is one of the assumed parameters that we use for modeling the Ziegler Natta process as even mentioned in the kinetic estimation study by Sharma and Liu⁸. The ultimate aim of this inverse model application is to showcase that given the polymer quality characteristics we can estimate some assumed model parameters for more accurate predictions. We calculate a multiplication factor to the rate constants to account for the assumed model parameters for their better estimate.

We use the dynamic process model of the HDPE process to generate data for different values of the multiplying factor to the rate constant. We simulate the grade change dynamic data with different values of the rate constant keeping the grade change process same. The process variable changes in hydrogen flow, ethylene flow rate etc. are same for each of the values of the rate constant and collate the polymer quality data mainly the Molecular Weight, Polydispersity and Polymer flow with time. Thus, we consider the polymer quality data as the features and use it to predict the multiplying factor deciding the model assumed parameters for catalyst concentrations. Figure 6.10 illustrates the kinetic estimation methodology.

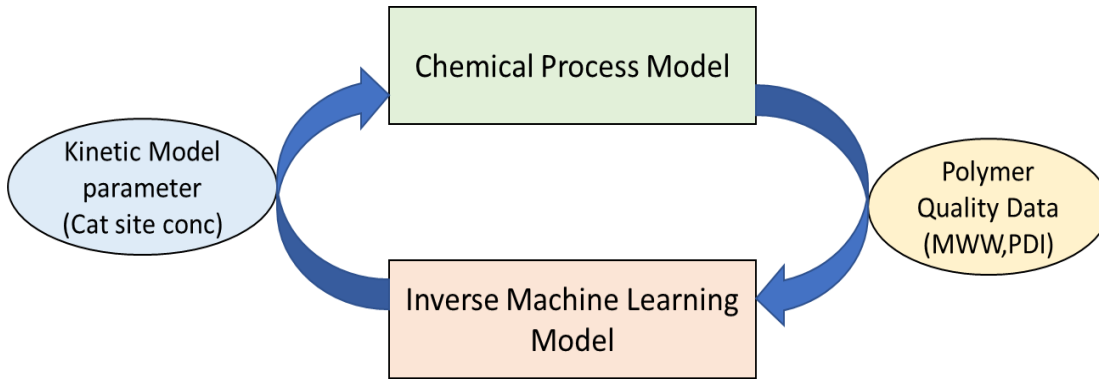


Figure 6.10. Inverse Modeling modelling framework for kinetic parameter estimation

We use a Neural Network model with 2 hidden layers with 512 and 256 neuron and Rectified Linear Unit as activation function. A loss function in ML measures how far the model estimated value is from the actual value. The loss curve for the training and validation of the model is shown in figure 6.11. The RMSE value for prediction of multiplying factor is 0.1. Thus, given any new set of quality parameter we can infer the multiplication factor of the kinetic rate constant that will lead to a more accurate assumption and better kinetic estimation and prediction.

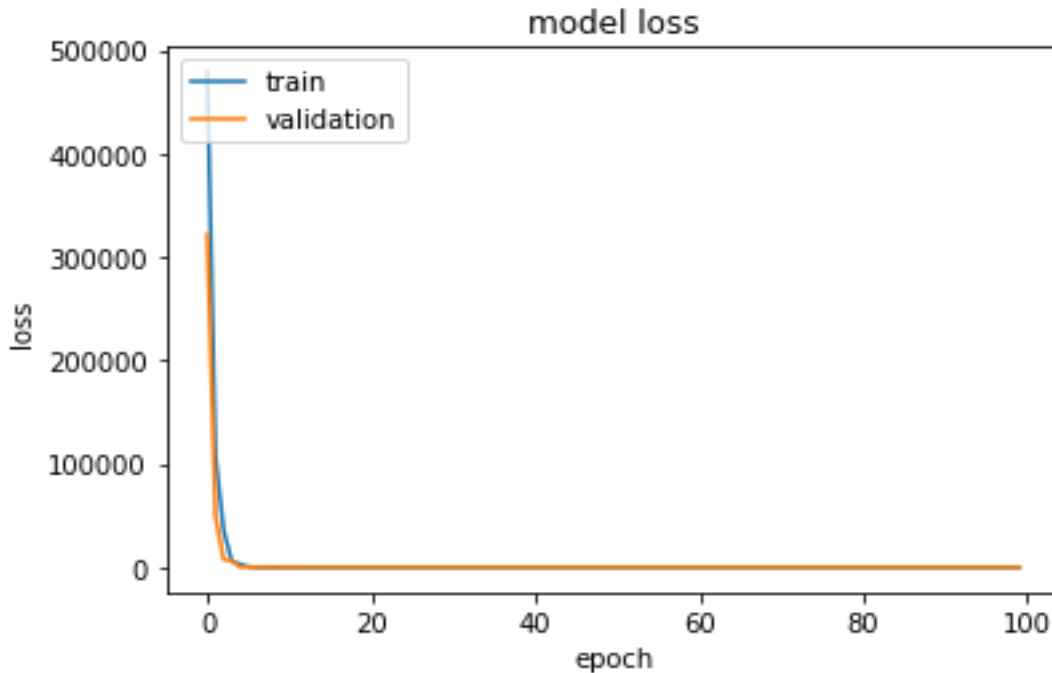


Figure 6.11. Loss curve for prediction of inverse modeling kinetic parameter estimation

6.5. An Application of Reduced-Order Modeling to Polymer Manufacturing

6.5.1. Reduced-Order Modeling of Hypol PP process

We illustrate the ROM methodology in a HYPOL polypropylene production process. The Hypol process is complex with series of reactors, separators and recycle loops. The process has many operating variables, such as feed flow rates of propylene, hydrogen to

each reactor, and temperature and pressure in each reactor. We consider 19 critical independent process variables for the Hypol process as shown in table 6.3. It is critical to quantify the effects of operating variables on the polymer quality targets, particularly melt index, in order to design or optimize the process. To achieve this, we need multivariate process data which are not usually available in a steady running plant. Hence, we use the ROM methodology. We build a simpler model with reduced complexity and build a digital twin of the whole process and then we use the model to simulate the multivariate data.

We model the HYPOL polypropylene production process and then run multiple steady-state simulations to generate multivariate data with varying operating variables and the corresponding melt index predictions. We use a random forest ML model to train the simulated data to predict the melt index as a function of the process variables and also understand the causality of important features affecting the polymer quality. We can use the empirical ML model of melt index can be used to predict the melt index at varying process variables and can act as an approximate quality sensor. The RMSE for prediction is 0.5 for the data with standard deviation 2.5. Thus, the multivariate complex process can be approximated using this ROM for process design and optimization a shown in figure

The ML model also decides the relative importance of different operating variables based on the mean decrease in “node impurity”, which is a measure of how much each operating variable feature reduces the variance in the model. Figure 6.12 (B) illustrates that the model calculates the important features like hydrogen flow rate (H24) and the temperature to the fourth reactor (R4T) as the most important variables affecting the melt index, which can then be used to find the optimum conditions to produce polymer of certain melt index and to improve the process design for a new process.

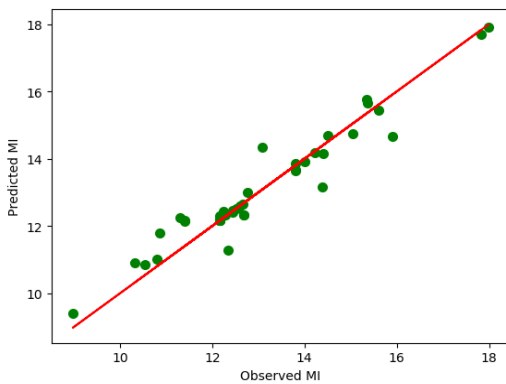


Figure 6.12a.

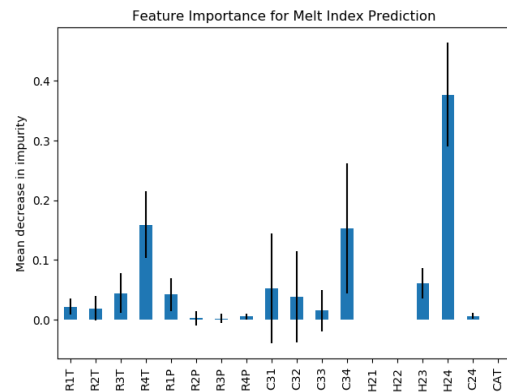


Figure 6.12b.

Figure 6.12a. Melt Index comparison of observed v/s prediction

Figure 6.12b. Feature importance for melt Index prediction:

6.5.2. Reduced-Order Modeling of Industrial LDPE process

The high-pressure LDPE process is a complex process with many reactors in series/parallel operations. It has 15 critical independent process variables and also has multiple polymer product quality characteristics like branching apart from the Molecular Weights that affect the final polymer quality. We use the concept of the ROM to build empirical data-based model to predict LDPE quality variables based on the input process variables. We generate multivariate data by sensitivity analysis of the independent process variables and then build a machine learning model to predict the LCB/SCB and MWW/MWN. Branching LCB and SCB determine the polymer properties like morphology and rheology. Hence, it is critical to predict the branching for different grades based on different applications. Hence, we build empirical ML based models for branching prediction of LDPE apart from the Molecular Weights.

We use the Xgboost model for prediction of branching, which gives a good fit with a very low RMSE of 0.0002. The prediction of SCB and LCB (kmol/hr) for the test data is shown in figure 6.13 A-B. We also find that the most important feature based on the node impurity decrease for prediction of branching both (SCB, LCB) is ethylene mass flow (E2).

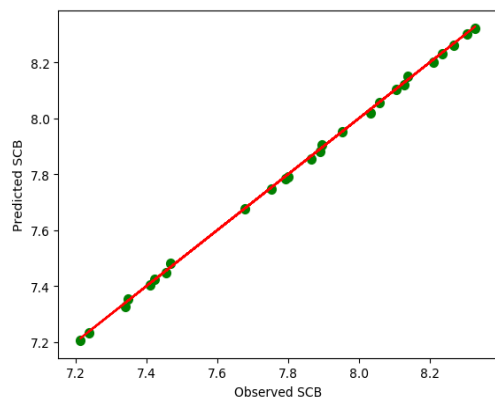


Figure 6.13a.

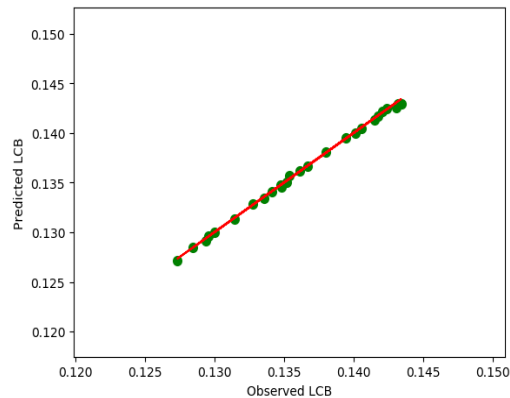


Figure 6.13b.

Figure 6.13a. Prediction v/s Observed values of branching SCB

Figure 6.13b. Prediction v/s Observed values of branching LCB

6.6. An Application of HGML Modeling to Uncertainty Quantification in Polymer Manufacturing

We quantify the uncertainty of the chemical process model in predicting the melt index for the industrial HDPE process described in Section. This uncertainty in prediction may result from the estimated kinetic parameters of the process, which propagates to the quality output as well. Uncertainty in a process can be classified into two main types.

Aleatoric Uncertainty: This is the Inherent Uncertainty in the process/data also refers to the irreducible noise

Epistemic Uncertainty: This is the uncertainty due to the model which has parameters whose values are uncertain due to limited data. This is reducible uncertainty as can be reduced by adding more data.

Bayesian Neural Networks ¹¹ are particularly useful for Uncertainty Quantification as they are able to capture both the irreducible noise/inherent uncertainty in the data as well as the due to uncertainty about the model parameters due to limited training data. The Bayesian NN learns weight distributions instead of specific weight values. We use Monte Carlo methods to sample the output for the weight distributions to calculate the uncertainty given the prior and posterior distribution of weights. We refer to Keras tutorial for this analysis ¹².

We generate the data from the process model and showcase the use of bayesian neural network for predicting the uncertainty in predicting normalized melt index as shown in figure 6.14. The uncertainty lies between 0.25 for the normalized predictions.

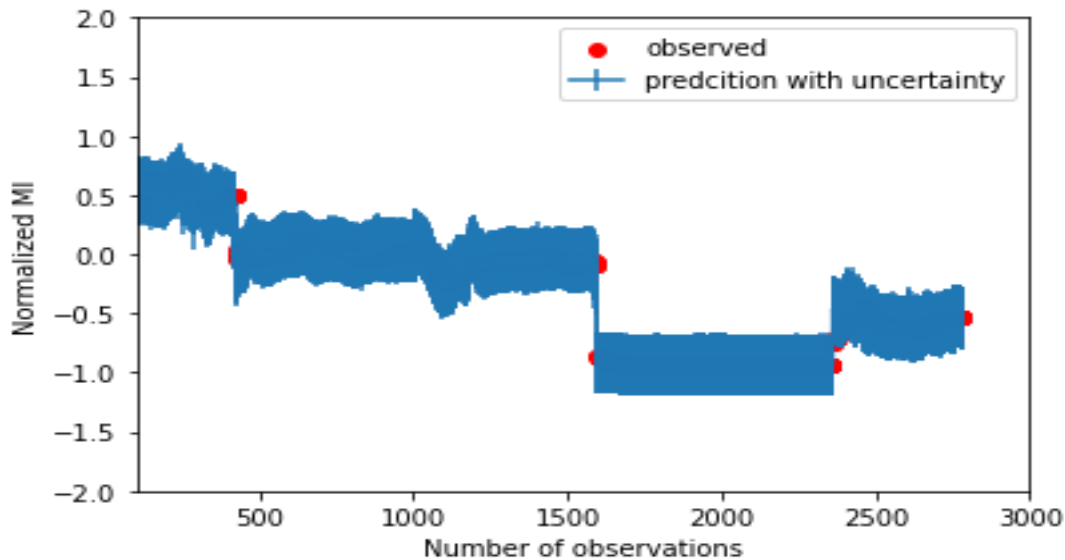


Figure 6.14. Uncertainty prediction of Melt Index using Bayesian Neural Networks

Since deep learning models are more computationally expensive for a smaller dataset and for this case we are more interested in deterministic results. The probabilistic Bayesian neural network are more useful for prediction of output distribution in processes where are stochastic in nature, which is not the case for this polymer process problem. Also, ensemble learning model seems more accurate for prediction of this medium-sized process data we will recommend the calculation of deterministic prediction intervals using ensemble methods.

For this case, we use a gradient boosting ¹³ ML model for Melt prediction. We make use of the concept of quantile regression ¹⁴ loss to create prediction interval. Quantile regression estimates conditional quantile (percentile like medians) of the response variables by minimizing the quantile loss to predict a quantile. Quantile regression is suitable to model uncertainty of a regression model with increasing variance of residuals. For example, if we calculate the 0.977 and 0.023 percentiles/quantiles, the prediction interval between them has 95% probability of values within the interval.

We can use the quantile regression loss in any regression model to estimate prediction intervals. The gradient boosting model uses the quantile loss to predict the 10th and 90th quantile and use the predictions as an interval. Figure 6.15 illustrates the uncertainty in the prediction of melt index given by the range of the prediction interval which lies between the 10% and 90% confidence intervals. The resulting RMSE value lies within 0.94 to 1.1, with the standard deviation of melt index data equals 5.1. From the figure, we see a higher uncertainty in prediction for time less than 100 hours compared to the later stage. Thus, UQ helps in making better process decisions after knowing the error estimate of the model.

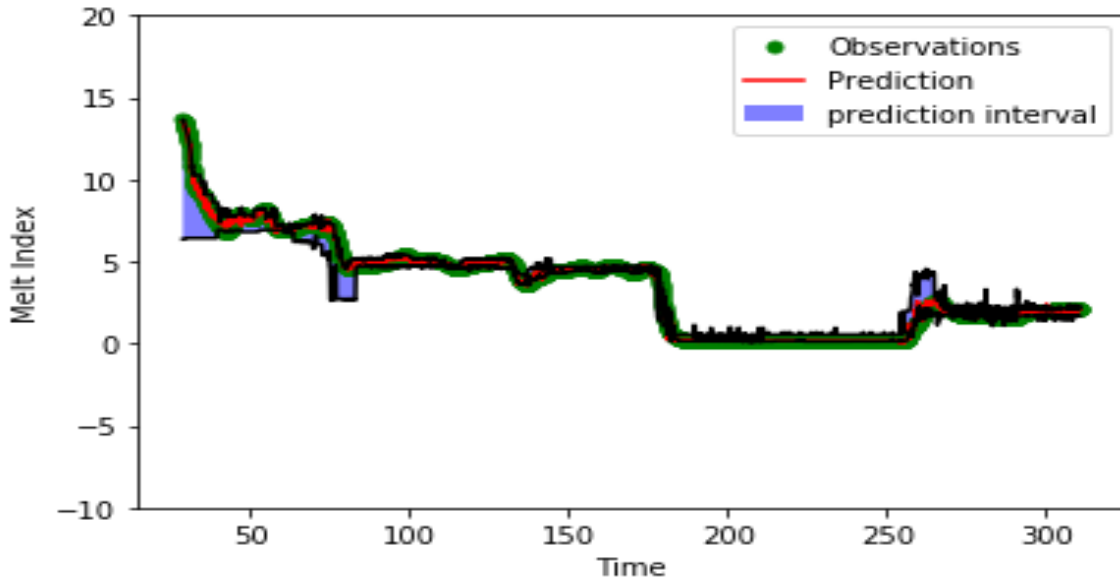


Figure 6.15. Uncertainty quantification of melt Index prediction of a slurry HDPE process

6.7. An illustrative Example of Science-Guided Learning

Physics-based loss functions in neural networks have been used to make more scientifically consistent and accurate predictions¹⁵. We showcase the application of the science-guided loss function in the slurry HDPE process for the industrial HDPE process described in Section 2.1.4. The goal is to predict the melt index of the polymer. The plant data only measure the polymer melt index as the quality output, but we also want the data-based ML model to predict the scientifically consistent polymer density values.

We express polymer density as a function of the melt index using some empirical correlations and replace Y_{pred} in Eq. (1) by $\rho(MI_{pred})$, that is, density as an empirical function of the melt index. See Eq. (3) below. We then train a deep learning neural network model to predict the melt index of the polymer. Figure 6.16. illustrates that the SGML hybrid model calculates the melt index, resulting in a RMSE of the melt Index that is slightly higher (RMSE = 0.8) (standard deviation of data= 5) compared to a standalone ML model. However, in addition to predicting the melt index values, the hybrid SGML model is simultaneously predicting the polymer density correctly within the physically consistent range of 0.94-0.97 g/c. By contrast, the density estimates by the ML model alone result in density values greater than 1, which is physically inconsistent.

$$Loss = Loss_M(MI_{true} - MI_{pred}) + \lambda Loss_{SC}(\rho(MI_{pred})) \quad (3)$$

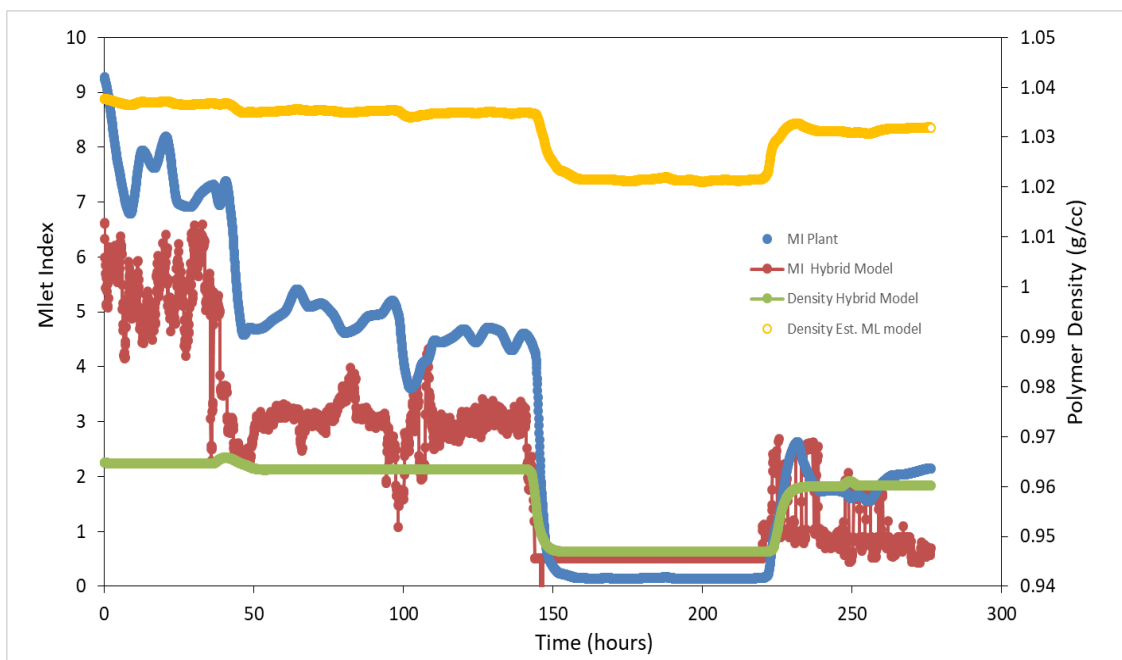


Figure 6.16. Melt index and polymer density prediction with a ML model with a science-guided loss function

6.8. Conclusion

We showcase the application of the Science Guided Machine Learning techniques for polymer processes for scientifically consistent and accurate predictions. These techniques can be useful for building soft sensors for polymer quality, polymer process design and development and help in polymer grade change.

References

1. Sharma Niket, L. Y.-A., A Hybrid Science-Guided Machine Learning Approach for Modeling and Optimizing Chemical Processes: A Review *AIChE Journal* **2021**.
2. Tsen, A. Y. D.; Jang, S. S.; Wong, D. S. H.; Joseph, B., Predictive control of quality in batch polymerization using hybrid ANN models. *AIChE Journal* **1996**, *42* (2), 455-465.
3. Tian, Y.; Zhang, J.; Morris, J., Modeling and optimal control of a batch polymerization reactor using a hybrid stacked recurrent neural network model. *Industrial & engineering chemistry research* **2001**, *40* (21), 4525-4535.
4. Hinchliffe, M.; Montague, G.; Willis, M.; Burke, A., Hybrid approach to modeling an industrial polyethylene process. *AIChE journal* **2003**, *49* (12), 3127-3137.
5. Doyle III, F. J.; Harrison, C. A.; Crowley, T. J., Hybrid model-based approach to batch-to-batch control of particle size distribution in emulsion polymerization. *Computers & Chemical Engineering* **2003**, *27* (8-9), 1153-1163.

6. Chang, J.-S.; Lu, S.-C.; Chiu, Y.-L., Dynamic modeling of batch polymerization reactors via the hybrid neural-network rate-function approach. *Chemical Engineering Journal* **2007**, *130* (1), 19-28.
7. Park, T. C.; Kim, T. Y.; Yeo, Y. K., Prediction of the melt flow index using partial least squares and support vector regression in high-density polyethylene (HDPE) process. *Korean Journal of Chemical Engineering* **2010**, *27* (6), 1662-1668.
8. Sharma, N.; Liu, Y., 110th Anniversary: An Effective Methodology for Kinetic Parameter Estimation for Modeling Commercial Polyolefin Processes from Plant Data Using Efficient Simulation Software Tools. *Industrial & Engineering Chemistry Research* **2019**, *58* (31), 14209-14226.
9. Breiman, L., Stacked regressions. *Machine learning* **1996**, *24* (1), 49-64.
10. Chen, T.; Guestrin, C. In *Xgboost: A scalable tree boosting system*, Proceedings of the 22nd acm sigkdd international conference on knowledge discovery and data mining, 2016; pp 785-794.
11. Kononenko, I., Bayesian neural networks. *Biological Cybernetics* **1989**, *61* (5), 361-370.
12. https://keras.io/examples/keras_recipes/bayesian_neural_networks
13. Friedman, J. H., Stochastic gradient boosting. *Computational statistics & data analysis* **2002**, *38* (4), 367-378.
14. Koenker, R.; Hallock, K. F., Quantile regression. *Journal of economic perspectives* **2001**, *15* (4), 143-156.
15. Karpatne, A.; Watkins, W.; Read, J.; Kumar, V., Physics-guided neural networks (pgnn): An application in lake temperature modeling. *arXiv preprint arXiv:1710.11431* **2017**.

Chapter 7: Conclusion and Future Work

7.1. Conclusion

In this work, we have demonstrated an effective methodology for estimating kinetic parameters for Ziegler-Natta polymerization for commercial processes producing polyolefins, such as HDPE, PP and LLPDE. We consider the catalyst activation, initiation, propagation, chain transfer, deactivation and other polymer-specific reactions. We have identified the reaction rate constants in Ziegler-Natta polymerization kinetics that have most significant impacts on common production targets. This greatly simplifies the kinetic parameter estimation for simulation and optimization models for polyolefin processes from plant data. We showcase the utility of dynamic models for efficient grade transition in polyolefin processes. We also use the dynamic models for inferential control of polymer processes. Thus, we showcase the methodology for making first-principle polyolefin process models which are scientifically consistent, but tend to be less accurate due to many modeling assumptions in a complex system.

We have illustrated the utility of multivariate statistical methods, such as partial least squares (PLS) for causal analysis to identify correct correlations between input and outputs in polymer process application. We also showcase the utility of data-based machine learning (ML) methods such as ensemble random forest for predicting the process outputs e.g. the melt index (MI). We also identify the Dynamic PLS model utility in dynamic time series process data by considering the measurement lags. We conclude that a data-based model alone has a high accuracy, but it may give scientifically inconsistent results for predictions beyond process operating data which the model uses and also not able to accurately simulate individual feature importance.

We present a broad perspective of hybrid modeling with a science-guided machine learning (SGML) approach and its application in bioprocessing and chemical engineering. We give a detailed review and exposition of the hybrid SGML modeling approach and its applications, and classify the approach into two categories. The first refers to the case where a data-based ML model compliments and makes the first-principle science-based model more accurate in prediction, and the second corresponds to the case where scientific knowledge helps make the ML model more scientifically consistent. We point out some of the areas of SGML which have not been explored much in chemical process modeling and have potential for further use like in the areas where science can help improve the data-based model by improving the model design, learning and refinement. We also illustrate some of these applications of the hybrid SGML methodologies for industrial polymer/chemical process improvement.

Based on our analysis, we recommend the use of stand-alone machine learning models for data analytics of chemical and polymer processes for interpolation applications like quality predictions in an established process with fixed operating conditions and model is trained on the data of the given operating range. For applications requiring extrapolation like new process and product development, we recommend the use of the hybrid science-

guided machine learning models since they also focus on the scientific consistency of predictions and not just accuracy.

7.2. Future Work

In this section, we suggest some of the research directions and ideas in which the current research can move forward.

There is opportunity in utilizing more of process operating knowledge in designing machine learning architecture which will yield practically relevant predictions. We can integrate multiple first-principle models at different stages along with the machine learning (ML) models. For example, for the polymer processes, molecular simulation can be used to estimate some of the thermodynamic phase-equilibrium parameters that can be used in the macro-scale process model. Similarly, for certain parts of the process model which require deeper insights into mixing, mass and heat transfer as in modeling the fluidized-bed reactor in polyolefin process, we can utilize computational fluid dynamics for modeling the system. ML can be used in any of the first-principle models for estimation of parameters.

In current times, we have seen the growing use of reinforcement learning (RL) in many artificial intelligence applications like robotics where an agent learns behavior through trial error interactions in a dynamic environment using a reward policy. For process analytics, RL can be particularly useful for process control and monitoring, hence can be utilized for polymer process control as well. Computer vision along with deep learning has many applications like self-driving cars can also be useful for chemical/polymer manufacturing as well. For instance, computer vision can be used to detect final polymer quality based on its color and structure. Similarly, the image data from different spectroscopic methods which yield molecular weight distribution curves can be trained using a convolution neural network to predict some polymer quality parameters.

Currently in ML field, researchers are also working on the interpretability of machine learning/deep learning models to make the black-box models more interpretable. The interpretability of models can be in the form of feature summary statistics/visualizations or model internal like learned weights. The methods of interpretation can be model-specific or model agnostic. Thus, using these techniques for chemical/polymer process data analytics, we can simultaneously make interpretable and accurate predictions

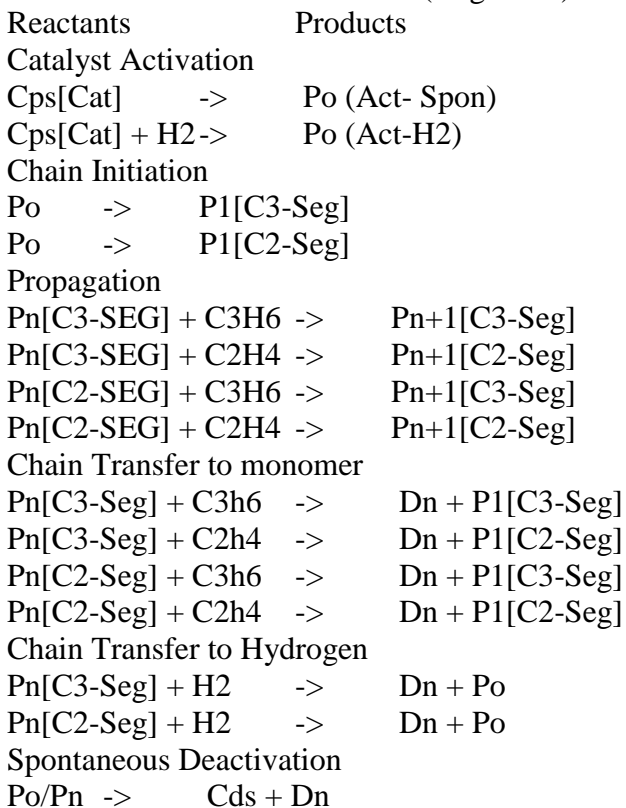
Appendix A (Chapter 2)

A.1. Hypol PP Process

Mitsui Hypol process is used for making polypropylene (PP) homopolymers and propylene- ethylene impact copolymer. The process consists of two autoclave reactors in series followed by two fluidized-bed reactors (FBR). It is a mixed-phase process with the fluid phase in the autoclave reactors and gas phase in the FBR. The FBRs have scrapers to eliminate fouling for making high rubber content impact copolymers. We have developed a steady-state model of the Hypol process using Aspen Polymers for estimating the kinetic parameters using plant data. The process consists of four continuously stirred tank reactors (CSTR) in series. The first three CSTRs are used to make the PP homo-polymers, while the fourth reactor makes the PP impact copolymer. Figure S1 shows the Aspen flowsheet of the process.

A.1.1 Reactions

The main reactions we consider (single site) for the Hypol process are as follows.



* where Cps is an activated catalyst site, Po is the empty site, P1[Ci-seg] is the site with polymer segment from propylene or ethylene, Cds is a dead catalyst site, and Dn is a dead polymer.

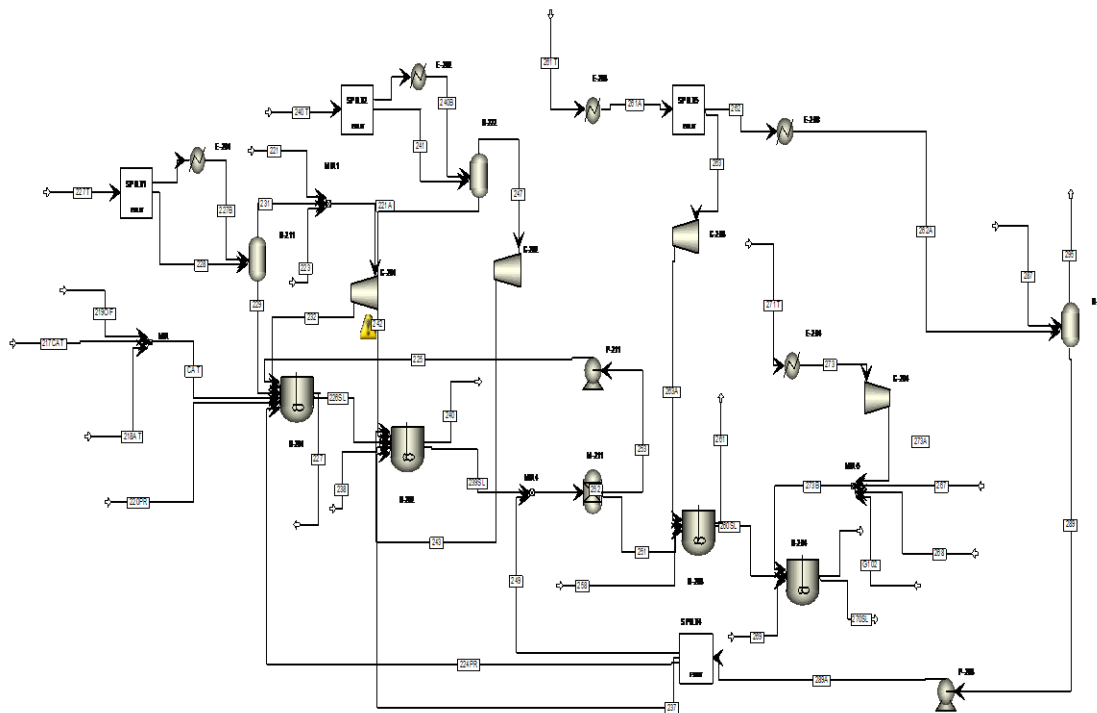


Figure A1. Flowsheet for Hypol simulation

A.1.2. Targets

Based on the available plant data, the targets we use for estimation and validation of kinetics are:

Single-site Targets

- Production rate
- Number-average molecular weight (MWN)
- Co-monomer content - (ratio of C2/C3 segments)-ethylene content (Copolymer)

Multiple-site targets

- Polymer polydispersity index (PDI) of polymer
- MWN total and produced at each site
- Production rate total and produced at each site
- Co-monomer content - (ratio of C2/C3 segments)-ethylene content (Copolymer)

Note: In this case, we do not have data for atactic fraction and melt index so we cannot consider those reactions.

A.1.3 Deconvolution

We use the GPC data for the final polypropylene to deduce the number of sites of the Ziegler- Natta catalyst (assuming a similar distribution for homo-polymer and copolymer since the fraction of ethylene is low in the final polymer). The resulting number of catalyst sites from deconvolution is 4. The fraction of polymer molecular weight in each site appears below:

Site	1	2	3	4
Frac. Area	0.249	0.086	0.511	0.154

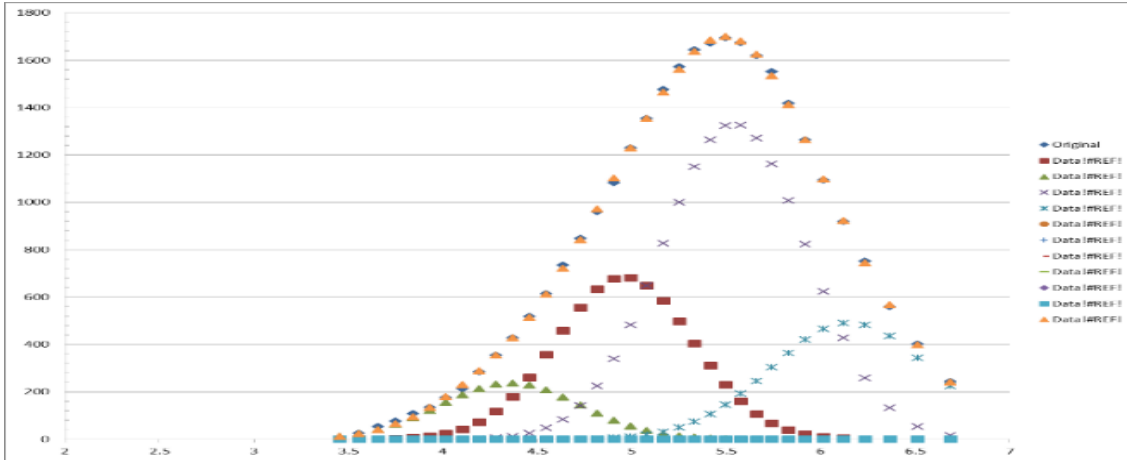


Figure A2. Deconvolution Curve for PP made from catalyst with 4 active sites

A.1.4. Kinetic Estimation Algorithm

We divide the modeling strategy into single site and multiple sites. We make a closed-loop steady-state model for the two grades. The two grades have different reactor operating conditions, mainly the residence time and pressure. We simultaneously make the Hypol model for the two grades. We have the plant data in the form of polymer flow rate, molecular weight, co-monomer content and PDI. We use the plant data for both the grades simultaneously and estimate different parameters using the Aspen Polymers Data Fit tool based on our estimation methodology.

A.1.5. Single Site (Multiple Grades)

- We use the production rate in the first three reactors to estimate the catalyst activation and deactivation reactions and propagation reaction for propylene (set the maximum sites concentration to a general observed value – 0.001 moles of sites per g of catalyst) to match the same.
- We use the MWN in first three reactors to regress the chain transfer to hydrogen and chain transfer to monomer for propylene.
- Lastly, we use the MWN, production rate and SFRAC in the last reactor to estimate the propagation and chain transfer reaction for ethylene

The rate constants estimated for single-site kinetics are (Reference temperature = 69C:

Type	Site No.	Comp 1	Comp 2	Pre-Exp 1/sec	Act-Energy cal/mol
ACT-SPON	1	CAT		0.000182	1000
ACT-H2	1	CAT	H2	1.00E-05	1000
CHAIN-INI	1	C3H6		97	9000
CHAIN-INI	1	C2H4		600	9000
PROPAGATION	1	C3-SEG	C3H6	97	9000
PROPAGATION	1	C3-SEG	C2H4	600	9000
PROPAGATION	1	C2-SEG	C3H6	97	9000
PROPAGATION	1	C2-SEG	C2H4	600	9000

CHAT-MON	1	C3-SEG	C3H6	0.04	9100
CHAT-MON	1	C3-SEG	C2H4	0.0014	9100
CHAT-MON	1	C2-SEG	C3H6	0.04	9100
CHAT-MON	1	C2-SEG	C2H4	0.0014	9100
CHAT-H2	1	C3-SEG	H2	0.22	9100
CHAT-H2	1	C2-SEG	H2	0.01	9100
DEACT-SPON	1			3.76E-05	1000

A.1.6. Multiple Sites (Multiple Grades)

- After tuning for single polymer grade and single catalyst active site, we use the deconvolution GPC data to estimate the number of active catalyst sites and the active surface area for each active catalyst. We use the GPC data to estimate the multisite kinetic parameters as follows.
- The estimate for pre-exponential factor of the catalyst activation reaction (ACT-SPON and ACT-H2) at each active site is: $k_{ai} = k_a / N_{site}$
- The estimate of pre-exponential factor for the chain initiation reaction (CHAIN-INI) at each active site is: $k_{ii} = k_i * Frac.AreaSi / 100 * N_{site}$
- The estimate of pre-exponential factor for the chain propagation reaction (PROPAGATION) at each active site is: $k_{pi} = k_p * Frac.AreaSi / 100 * N_{site}$
- The estimate of pre-exponential factor for the chain transfer reaction (CHAT-MON and CHAT-H2) at each active site is: $k_{ci} = k_c * Frac.AreaSi / 100 * N_{site}$
- The pre-exponential factor for catalyst deactivation reaction at each active site is the same as that for the single active site.
- Now by using the above rate constants in the model, we validate that the fraction of polymer molecular weight in each site matches the GPC data.
- In order to match the polymer plant PDI from the outlet of each reactor, we regress the reaction rate constant for each of the chain transfer reactions involving monomer and hydrogen using the PDI data. We also use the MWN data along with the PDI for regressing the reaction rate constants so that we match both the PDI and MWN as well.

The multiple-site rate constants obtained are:

Type	Site No.	Comp 1	Comp 2	Pre-Exp 1/sec	Act-Energy cal/mol
------	----------	--------	--------	---------------	--------------------

ACT-SPON	1	CAT		4.54E-05	1000
ACT-SPON	2	CAT		4.54E-05	1000
ACT-SPON	3	CAT		4.54E-05	1000
ACT-SPON	4	CAT		4.54E-05	1000
ACT-H2	1	CAT	H2	2.50E-06	1000
ACT-H2	2	CAT	H2	2.50E-06	1000
ACT-H2	3	CAT	H2	2.50E-06	1000
ACT-H2	4	CAT	H2	2.50E-06	1000
CHAIN-INI	1	C3H6		96.6	9000
CHAIN-INI	1	C2H4		598	9000
CHAIN-INI	2	C3H6		33.368	9000
CHAIN-INI	2	C2H4		206.4	9000
CHAIN-INI	3	C3H6		198.268	9000
CHAIN-INI	3	C2H4		1226.4	9000
CHAIN-INI	4	C3H6		59.752	9000
CHAIN-INI	4	C2H4		369.6	9000
PROPAGATION	1	C3-SEG	C3H6	96.612	9000
PROPAGATION	1	C3-SEG	C2H4	597.6	9000
PROPAGATION	1	C2-SEG	C3H6	96.612	9000
PROPAGATION	1	C2-SEG	C2H4	597.6	9000
PROPAGATION	2	C3-SEG	C3H6	33.368	9000
PROPAGATION	2	C3-SEG	C2H4	206.4	9000
PROPAGATION	2	C2-SEG	C3H6	33.368	9000
PROPAGATION	2	C2-SEG	C2H4	206.4	9000
PROPAGATION	3	C3-SEG	C3H6	198.268	9000
PROPAGATION	3	C3-SEG	C2H4	1226.4	9000
PROPAGATION	3	C2-SEG	C3H6	198.268	9000
PROPAGATION	3	C2-SEG	C2H4	1226.4	9000
PROPAGATION	4	C3-SEG	C3H6	59.752	9000
PROPAGATION	4	C3-SEG	C2H4	369.6	9000
PROPAGATION	4	C2-SEG	C3H6	59.752	9000
PROPAGATION	4	C2-SEG	C2H4	369.6	9000
CHAT-MON	1	C3-SEG	C3H6	0.15343	9100
CHAT-MON	1	C3-SEG	C2H4	0.013083	9100
CHAT-MON	1	C2-SEG	C3H6	0.15343	9100
CHAT-MON	1	C2-SEG	C2H4	0.013083	9100
CHAT-MON	2	C3-SEG	C3H6	0.002748	9100
CHAT-MON	2	C3-SEG	C2H4	4.72E-05	9100
CHAT-MON	2	C2-SEG	C3H6	0.002748	9100
CHAT-MON	2	C2-SEG	C2H4	4.72E-05	9100
CHAT-MON	3	C3-SEG	C3H6	0.047955	9100
CHAT-MON	3	C3-SEG	C2H4	1.11E-05	9100
CHAT-MON	3	C2-SEG	C3H6	0.047955	9100

CHAT-MON	3	C2-SEG	C2H4	1.11E-05	9100
CHAT-MON	4	C3-SEG	C3H6	0.003439	9100
CHAT-MON	4	C3-SEG	C2H4	0.000665	9100
CHAT-MON	4	C2-SEG	C3H6	0.003439	9100
CHAT-MON	4	C2-SEG	C2H4	0.000665	9100
CHAT-H2	1	C3-SEG	H2	0.031767	9100
CHAT-H2	1	C2-SEG	H2	0.001444	9100
CHAT-H2	2	C3-SEG	H2	0.09753	9100
CHAT-H2	2	C2-SEG	H2	0.004433	9100
CHAT-H2	3	C3-SEG	H2	2.70E-06	9100
CHAT-H2	3	C2-SEG	H2	1.23E-07	9100
CHAT-H2	4	C3-SEG	H2	0.002903	9100
CHAT-H2	4	C2-SEG	H2	0.000132	9100

DEACT-SPON	1			3.76E-05	1000
DEACT-SPON	2			3.76E-05	1000
DEACT-SPON	3			3.76E-05	1000
DEACT-SPON	4			3.76E-05	1000

A.1.7. Sensitivity Analysis

Figure A3 illustrates that varying the reaction rate constant for chain transfer to monomer, $k_{tm,i}$ results in similar trends of change in PDI, SMWN and MWN, as with the chain transfer to hydrogen.

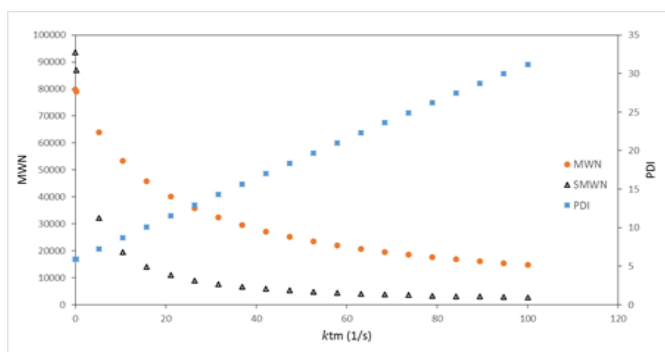


Figure A3. Sensitivity of the PDI, MWN and SMWN for the HYPOL PP process on the pre-exponential factor of the reaction rate constant for chain transfer to monomer.

A.1.8. Model Validation

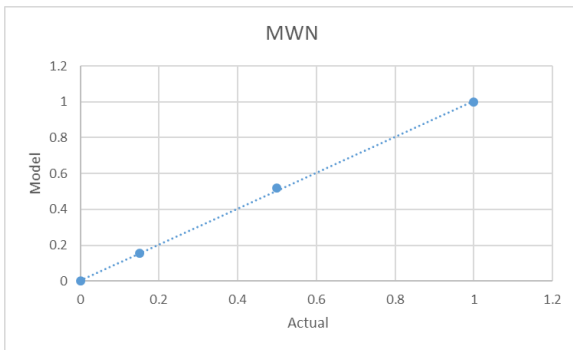


Figure A4. Comparison of model molecular weight with actual molecular weight

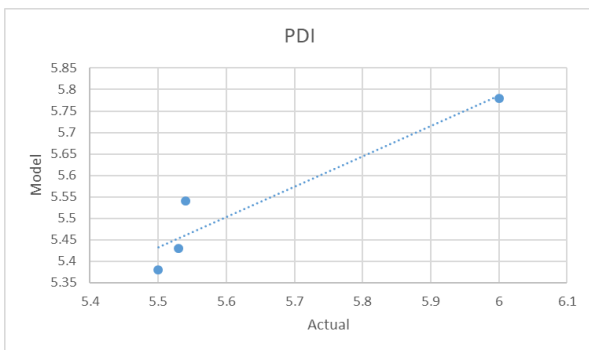


Figure A5. Comparison of model PDI with actual PDI

A.2. Mitsui Slurry HDPE process

A.2.1. Process Description

The Mitsui process for manufacturing HDPE is a slurry-phase process. Ethylene is the monomer for the process and propylene or butylene is comonomer. Hexane is used as a diluent to dissolve the monomer, co-monomer and hydrogen. The process usually consists of two autoclave reactors in series or in parallel configuration. Figure A6 shows the flowsheet for the process made in Aspen Polymers.

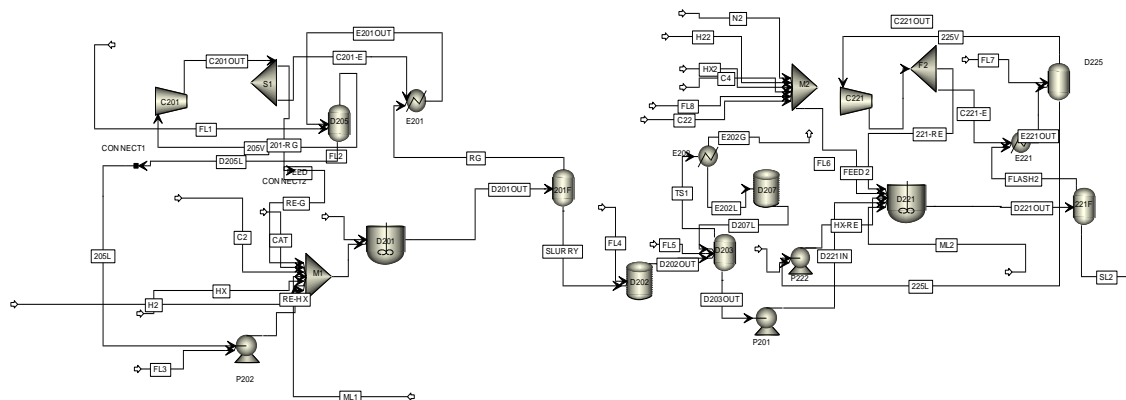


Figure A6. Flowsheet for the slurry HDPE process with reactor in series.

A.2.2. Kinetics

The main reactions considered for the HDPE slurry process are with a comonomer of C3H6 or C4H8 for single site:

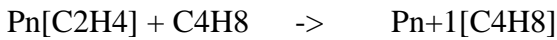
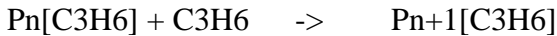
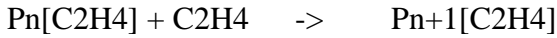
Catalyst Activation



Chain Initiation



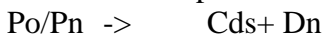
Propagation



Chain Transfer to Hydrogen



Deactivation Spontaneous



Inhibition reactions



* where Cps is an activated catalyst site, Po is the empty site, P1[Ci-seg] is the site with polymer segment from propylene or ethylene, Cds is a dead catalyst site, and Dn is a dead polymer.

A.2.3. Production Targets

The production targets used for kinetic estimation are:

- Production rate
- Number-average molecular weight (MWN/MI)
- Conversion of monomer-comonomer
- PDI
- H2/C ratio
- SMWN & SPFRAC (Site based)
- Residence time
- CISFRAC

A.2.4. Estimated Rate Constants

The GPC deconvolution gives 5 minimum active catalyst sites. The reference temperature for rate constants is very high ($1e^{35}$ C)

The final set of multisite estimated rate constants for 5 active catalyst sites are:

Type	Site No.	Comp 1	Comp 2	Pre-Exp	Act-Energy	Order
------	----------	--------	--------	---------	------------	-------

				1/sec	J/kmol	
ACT-COCAT	1	PZ	AT	900000	33494000	1
ACT-COCAT	2	PZ	AT	900000	33494000	1
ACT-COCAT	3	PZ	AT	900000	33494000	1
ACT-COCAT	4	PZ	AT	900000	33494000	1
ACT-COCAT	5	PZ	AT	900000	33494000	1
CHAIN-INI	1	C2H4		82000000	29308000	1
CHAIN-INI	1	C3H6		3300000	29308000	1
CHAIN-INI	1	C4H8		1100000	29308000	1
CHAIN-INI	2	C2H4		82000000	29308000	1
CHAIN-INI	2	C3H6		3300000	29308000	1
CHAIN-INI	2	C4H8		1100000	29308000	1
CHAIN-INI	3	C2H4		82000000	29308000	1
CHAIN-INI	3	C3H6		3300000	29308000	1
CHAIN-INI	3	C4H8		1100000	29308000	1
CHAIN-INI	4	C2H4		82000000	29308000	1
CHAIN-INI	4	C3H6		3300000	29308000	1
CHAIN-INI	4	C4H8		1100000	29308000	1
CHAIN-INI	5	C2H4		82000000	29308000	1
CHAIN-INI	5	C3H6		3300000	29308000	1
CHAIN-INI	5	C4H8		1100000	29308000	1
PROPAGATION	1	C2H4	C2H4	21703760	29308000	1
PROPAGATION	1	C2H4	C3H6	873444	29308000	1
PROPAGATION	1	C3H6	C2H4	1164592	29308000	1
PROPAGATION	1	C3H6	C3H6	185276	29308000	1
PROPAGATION	1	C2H4	C4H8	291148	29308000	1
PROPAGATION	1	C4H8	C2H4	397020	29308000	1
PROPAGATION	1	C4H8	C4H8	174688.8	29308000	1
PROPAGATION	2	C2H4	C2H4	1.21E+08	29308000	1
PROPAGATION	2	C2H4	C3H6	4873770	29308000	1
PROPAGATION	2	C3H6	C2H4	6498360	29308000	1
PROPAGATION	2	C3H6	C3H6	1033830	29308000	1
PROPAGATION	2	C2H4	C4H8	1624590	29308000	1
PROPAGATION	2	C4H8	C2H4	2215350	29308000	1
PROPAGATION	2	C4H8	C4H8	974754	29308000	1
PROPAGATION	3	C2H4	C2H4	1.11E+08	29308000	1
PROPAGATION	3	C2H4	C3H6	4451535	29308000	1
PROPAGATION	3	C3H6	C2H4	5935380	29308000	1
PROPAGATION	3	C3H6	C3H6	944265	29308000	1
PROPAGATION	3	C2H4	C4H8	1483845	29308000	1
PROPAGATION	3	C4H8	C2H4	2023425	29308000	1
PROPAGATION	3	C4H8	C4H8	890307	29308000	1
PROPAGATION	4	C2H4	C2H4	1.05E+08	29308000	1

PROPAGATION	4	C2H4	C3H6	4238025	29308000	1
PROPAGATION	4	C3H6	C2H4	5650700	29308000	1
PROPAGATION	4	C3H6	C3H6	898975	29308000	1
PROPAGATION	4	C2H4	C4H8	1412675	29308000	1
PROPAGATION	4	C4H8	C2H4	1926375	29308000	1
PROPAGATION	4	C4H8	C4H8	847605	29308000	1
PROPAGATION	5	C2H4	C2H4	51266400	29308000	1
PROPAGATION	5	C2H4	C3H6	2063160	29308000	1
PROPAGATION	5	C3H6	C2H4	2750880	29308000	1
PROPAGATION	5	C3H6	C3H6	437640	29308000	1
PROPAGATION	5	C2H4	C4H8	687720	29308000	1
PROPAGATION	5	C4H8	C2H4	937800	29308000	1
PROPAGATION	5	C4H8	C4H8	412632	29308000	1
CHAT-H2	1	C2H4	H2	2.38E+27	1.76E+08	0.85
CHAT-H2	1	C3H6	H2	2.38E+27	1.76E+08	0.85
CHAT-H2	1	C4H8	H2	2.85E+27	1.76E+08	0.85
CHAT-H2	2	C2H4	H2	4.29E+27	1.76E+08	0.85
CHAT-H2	2	C3H6	H2	4.29E+27	1.76E+08	0.85
CHAT-H2	2	C4H8	H2	1.24E+27	1.76E+08	0.85
CHAT-H2	3	C2H4	H2	1.94E+27	1.76E+08	0.85
CHAT-H2	3	C3H6	H2	1.94E+27	1.76E+08	0.85
CHAT-H2	3	C4H8	H2	2.85E+27	1.76E+08	0.85
CHAT-H2	4	C2H4	H2	9.08E+26	1.76E+08	0.85
CHAT-H2	4	C3H6	H2	9.08E+26	1.76E+08	0.85
CHAT-H2	4	C4H8	H2	3.85E+27	1.76E+08	0.85
CHAT-H2	5	C2H4	H2	3.87E+25	1.76E+08	0.85
CHAT-H2	5	C3H6	H2	3.87E+25	1.76E+08	0.85
CHAT-H2	5	C4H8	H2	2.87E+25	1.76E+08	0.85
DEACT-SPON	1			0.002	4186800	1
DEACT-SPON	2			0.002	4186800	1
DEACT-SPON	3			0.002	4186800	1
DEACT-SPON	4			0.002	4186800	1
DEACT-SPON	5			0.002	4186800	1
FSINH-H2	1	H2		5141.333	8373600	0.5
FSINH-H2	2	H2		2855.22	8373600	0.5
FSINH-H2	3	H2		6.29E+03	8373600	0.5
FSINH-H2	4	H2		1.34E+04	8373600	0.5
FSINH-H2	5	H2		8.16E+04	8373600	0.5
RSINH-H2	1	H2		6.00E-01	8373600	1
RSINH-H2	2	H2		6.00E-01	8373600	1
RSINH-H2	3	H2		6.00E-01	8373600	1
RSINH-H2	4	H2		6.00E-01	8373600	1
RSINH-H2	5	H2		6.00E-01	8373600	1

CHAT-AGENT	5	C2H4	C2H4	1.10E+25	1.76E+08	1
CHAT-AGENT	5	C2H4	C3H6	1.10E+25	1.76E+08	1
CHAT-AGENT	5	C3H6	C2H4	1.10E+25	1.76E+08	1
CHAT-AGENT	5	C3H6	C3H6	1.10E+25	1.76E+08	1

A.2.5. Results

The GPC curve for the polymer results in a bimodal curve in the outlet of the first reactor itself and the model results also confirm the same, because of different site-inhibition reactions.

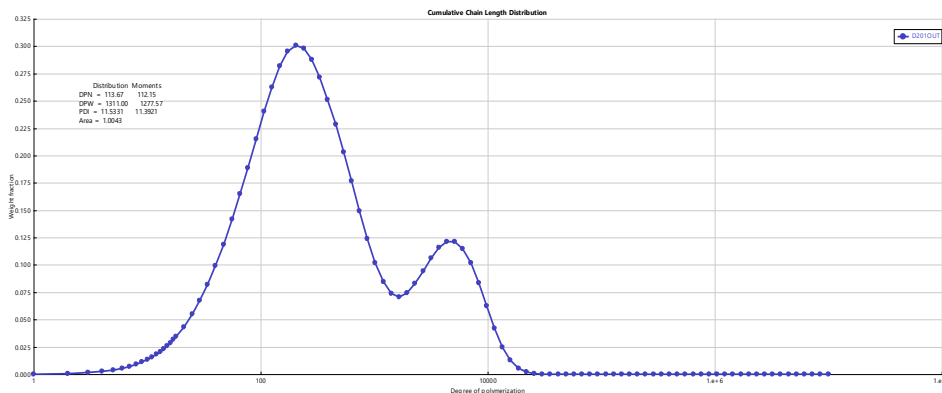


Figure A7. MWD of the product in the outlet of the first reactor

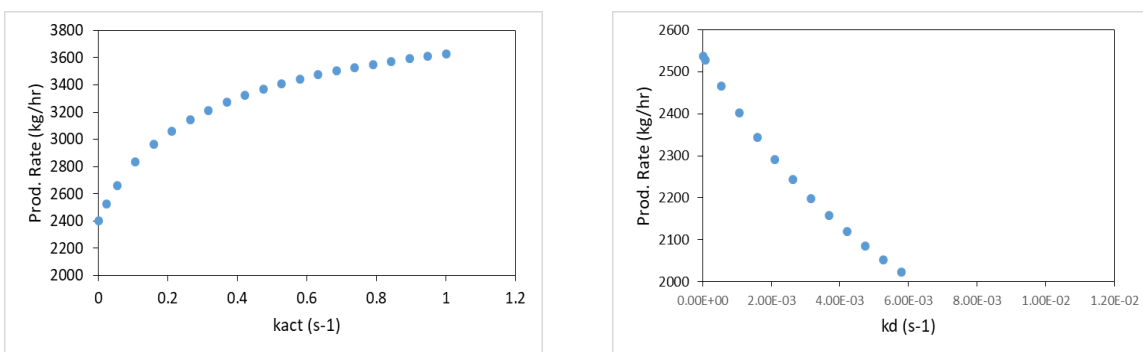


Figure A8. The effect of the sensitivity of the activation reactions on production rate for Mitsui HDPE process

A.2.6. Sensitivity Analysis

We study the effect of the catalyst inhibition reaction for the Mitsui slurry HDPE process. Figure A9 shows that varying the rate constants for the catalyst inhibition by hydrogen reaction (k_{inh}) for a particular site, the MWD of the polyolefin produced from a single reactor can change from unimodal to bimodal. This happens since the difference in the rate of inhibition for different catalyst sites.

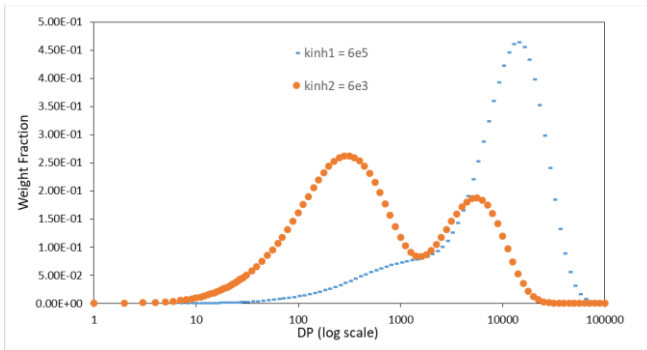


Figure A9. The effect on the MWD by varying the catalyst inhibition reaction rate for the Mitsui HDPE process

A.3. Innovene and Horizone PP process

Japan Polypropylene Corporation developed the Horizone process and INEOS developed the Innovene process for manufacturing PP. This is a gas-phase process and consists of two horizontal stirred bed reactors (HSBR) which are stirred powder beds in series. The catalyst and co-catalyst are injected at separate points in the initial section of the first reactor. The reactor is cooled by spraying liquid PP over the powder in the bed. The residence times will be different in the two reactors which helps in speeding up grade transitions. We model each HSBR as four CSTR in series [2]. The plug flow like characteristics enhance the polymer properties [5]. Figure A10 shows the flowsheet of the process made in Aspen Polymers.

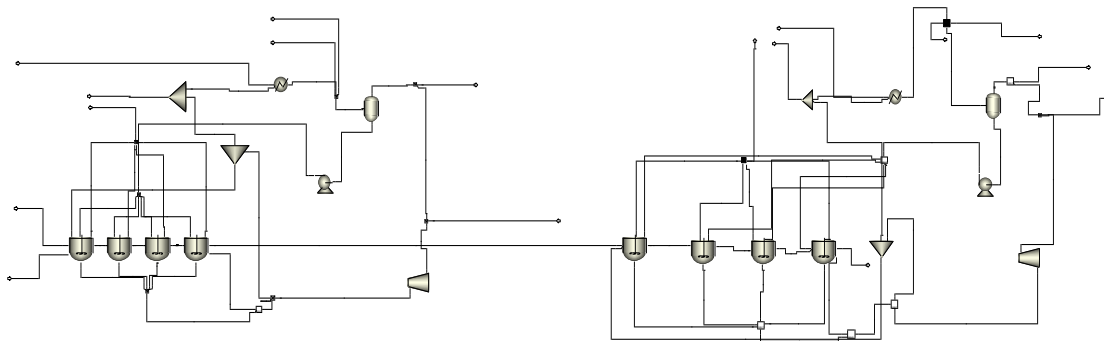
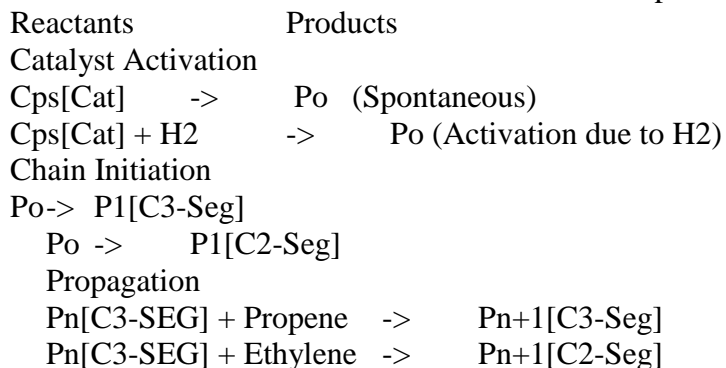
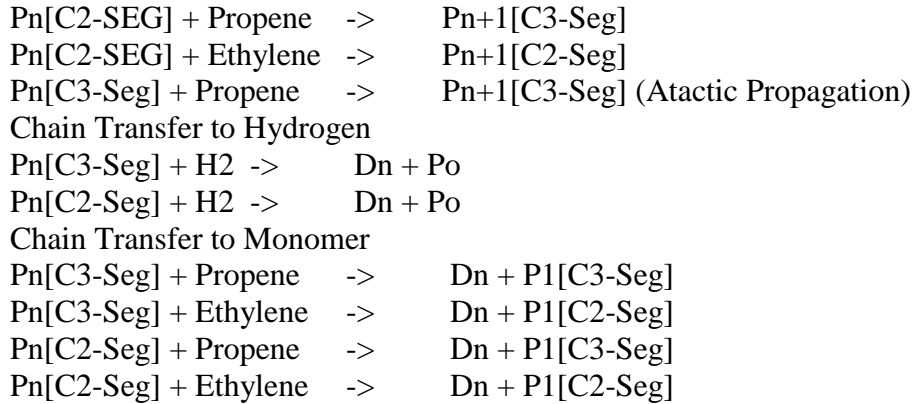


Figure A10. Flow-sheet of Innovene process

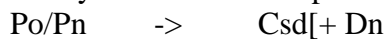
A.3.1. Kinetics

The main reactions for the Innovene/Horizone PP process are shown below:

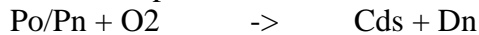
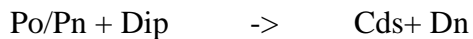
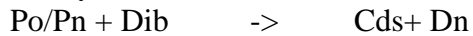




Catalyst Deactivation Spontaneous



Catalyst Deactivation due to Poison



A.3.2. Production Targets

The production targets used for kinetic estimation are:

- Production rate
- Number-average molecular wt. (MWN/MI)
- Conversion of monomer-comonomer
- PDI
- H₂/C ratio
- SMWN & SPFRAC (Site-based)
- Residence time
- ATFRAC

A.3.3. Estimated Rate Constants

The GPC deconvolution predicts 4 minimum active catalyst sites.

The reference temperature is (66 C):

The final set of estimated rate constants for 4 active catalyst sites:

Type	Site No.	Comp 1	Comp 2	Pre-Exp 1/sec	Act- Energy cal/mol	Order
ACT-SPON	1	CAT		0.00017 5	2000	1
ACT-SPON	2	CAT		0.00017 5	2000	1
ACT-SPON	3	CAT		0.00017 5	2000	1
ACT-SPON	4	CAT		0.00017 5	2000	1

ACT-H2	1	CAT	H2	0.00203	9	4557	0.5
				0.00203			
ACT-H2	2	CAT	H2	9	4557	0.5	
				0.00203			
ACT-H2	3	CAT	H2	9	4557	0.5	
				0.00203			
ACT-H2	4	CAT	H2	9	4557	0.5	
				8.62403			
CHAIN-INI	1	PROPENE		3	9000	1	
				63.0317			
CHAIN-INI	1	ETHYLENE		2	9000	1	
				45.6045			
CHAIN-INI	2	PROPENE		6	9000	1	
				333.316			
CHAIN-INI	2	ETHYLENE		7	9000	1	
				76.4643			
CHAIN-INI	3	PROPENE		8	9000	1	
				558.866			
CHAIN-INI	3	ETHYLENE		3	9000	1	
				52.9980			
CHAIN-INI	4	PROPENE		6	9000	1	
				387.354			
CHAIN-INI	4	ETHYLENE		6	9000	1	
PROPAGATIO				8.62403			
N	1	PROPENE	PROPENE	3	9000	1	
PROPAGATIO			ETHYLEN	63.0317			
N	1	PROPENE	E	2	9000	1	
PROPAGATIO		ETHYLEN		8.62403			
N	1	E	PROPENE	3	9000	1	
PROPAGATIO		ETHYLEN	ETHYLEN	63.0317			
N	1	E	E	2	9000	1	
PROPAGATIO				45.6045			
N	2	PROPENE	PROPENE	6	9000	1	
PROPAGATIO			ETHYLEN	333.316			
N	2	PROPENE	E	7	9000	1	
PROPAGATIO		ETHYLEN		45.6045			
N	2	E	PROPENE	6	9000	1	
PROPAGATIO		ETHYLEN	ETHYLEN	333.316			
N	2	E	E	7	9000	1	
PROPAGATIO				76.4643			
N	3	PROPENE	PROPENE	8	9000	1	
PROPAGATIO			ETHYLEN	558.866			
N	3	PROPENE	E	3	9000	1	
PROPAGATIO		ETHYLEN		76.4643			
N	3	E	PROPENE	8	9000	1	

PROPAGATIO N	3	ETHYLEN E	ETHYLEN E	558.866 3	9000	1
PROPAGATIO N	4	PROPENE	PROPENE	52.9980 6	9000	1
PROPAGATIO N	4	PROPENE	ETHYLEN E	387.354 6	9000	1
PROPAGATIO N	4	ETHYLEN E	PROPENE	52.9980 6	9000	1
PROPAGATIO N	4	ETHYLEN E	ETHYLEN E	387.354 6	9000	1
CHAT-MON	1	PROPENE	PROPENE ETHYLEN	0.00159	24500	1
CHAT-MON	1	PROPENE ETHYLEN	E	0.00159	24500	1
CHAT-MON	1	E ETHYLEN	PROPENE ETHYLEN	0	24000	1
CHAT-MON	1	E	E	0 0.00169	24000	1
CHAT-MON	2	PROPENE	PROPENE ETHYLEN	4 0.00169	24500	1
CHAT-MON	2	PROPENE ETHYLEN	E	4	24500	1
CHAT-MON	2	E ETHYLEN	PROPENE ETHYLEN	0	24000	1
CHAT-MON	2	E	E	0	24000	1
CHAT-MON	3	PROPENE	PROPENE ETHYLEN	0.0009	24500	1
CHAT-MON	3	PROPENE ETHYLEN	E	0.0009	24500	1
CHAT-MON	3	E ETHYLEN	PROPENE ETHYLEN	0	24000	1
CHAT-MON	3	E	E	0 0.00019	24000	1
CHAT-MON	4	PROPENE	PROPENE ETHYLEN	8 0.00019	24500	1
CHAT-MON	4	PROPENE ETHYLEN	E	8	24500	1
CHAT-MON	4	E ETHYLEN	PROPENE ETHYLEN	0	24000	1
CHAT-MON	4	E	E	0 2.66810	24000	1
CHAT-H2	1	PROPENE ETHYLEN	H2	6 2.66810	24500	0.5
CHAT-H2	1	E	H2	6 2.83102	24500	0.5
CHAT-H2	2	PROPENE	H2	9	24500	0.5

		ETHYLEN		2.83102		
CHAT-H2	2	E	H2	9	24500	0.5
CHAT-H2	3	PROPENE	H2	1.50637	24500	0.5
		ETHYLEN				
CHAT-H2	3	E	H2	1.50637	24500	0.5
				0.33490		
CHAT-H2	4	PROPENE	H2	8	24500	0.5
		ETHYLEN		0.33490		
CHAT-H2	4	E	H2	8	24500	0.5
DEACT-POISON	1	DIB		6.12613		
				9	1000	1
DEACT-POISON	1	DIP		0.00010		
				3	1000	1
DEACT-POISON	1	O2		0.88261		
				7	5000	0.5
DEACT-POISON	2	DIB		0.00010		
				3	1000	1
DEACT-POISON	2	DIP		0.00010		
				3	1000	1
DEACT-POISON	2	O2		0.88261		
				7	5000	0.5
DEACT-POISON	3	DIB		0.00010		
				3	1000	1
DEACT-POISON	3	DIP		0.00010		
				3	1000	1
DEACT-POISON	3	O2		0.88261		
				7	5000	0.5
DEACT-POISON	4	DIB		0.00010		
				3	1000	1
DEACT-POISON	4	DIP		0.00010		
				3	1000	1
DEACT-POISON	4	O2		0.88261		
				7	5000	0.5
DEACT-SPON	1			0.00029		
				9	10000	1
DEACT-SPON	2			0.00029		
				9	10000	1
DEACT-SPON	3			0.00029		
				9	10000	1
DEACT-SPON	4			0.00029		
				9	10000	1
ATACT-PROP	1	C3-SEG	PROPENE	8.4	9000	1
ATACT-PROP	2	C3-SEG	PROPENE	0.042	9000	1
ATACT-PROP	3	C3-SEG	PROPENE	0.042	9000	1
ATACT-PROP	4	C3-SEG	PROPENE	0.042	9000	1

A.3.4. Sensitivity Analysis

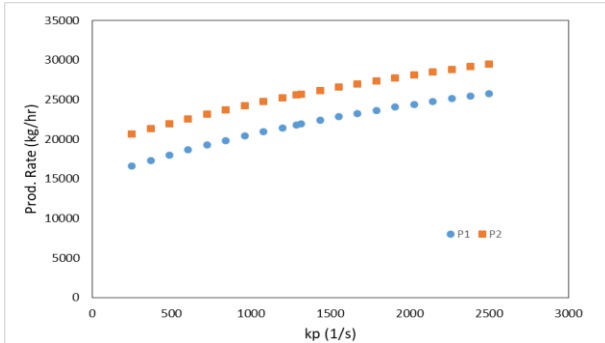


Figure A11. The sensitivity of the production rate from an Innovene gas-phase PP process to changes in the propagation reaction rate constant.

Figure A11 shows the effect on the production rates for the two horizontal bed reactors (represented as P1, P2 in Figure A10) in the Innovene gas-phase PP process by varying the pre-exponential factor of propagation reaction rate constant for a particular active site.

A.4. Spheripol PP process

The Spheripol PP process by Basel is a mixed-phase process used for producing PP. The process consists of a prepolymerizer followed by two loop reactors in series, and by a fluidized-bed reactor (FBR). The loop reactors are slurry-phase, while the FBR is gas-phase required for the impact copolymer production because of the limited solubility of ethylene in liquid propylene. The process is modeled by using 4 CSTR's in series. Figure A12 shows a flowsheet of the process taken (with permission) from an example file within Aspen Polymers.

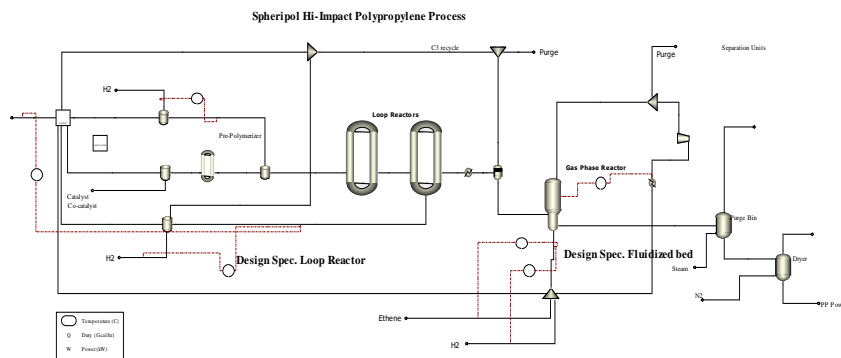
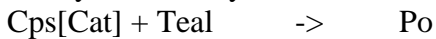


Figure A12. Flowsheet of Spheripol PP process

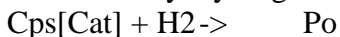
A.4.1. Kinetics

The reaction kinetics for the Spheripol PP process are defined below:

Catalyst Co-catalyst Activation



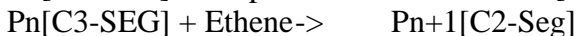
Activation by Hydrogen



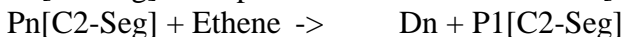
Chain Initiation



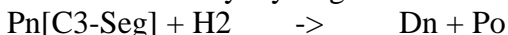
Propagation



Chain Transfer by monomer



Chain Transfer by Hydrogen



Chain Transfer by Co-catalyst



Spontaneous Deactivation



A.4.2. Production Targets

The production targets used for kinetic estimation are:

- Production rate
- Number-average molecular wt. (MWN/MI)
- Conversion of monomer-comonomer
- PDI
- H₂/C ratio
- SMWN & SPFRAC (Site based)
- Residence time
- ATFRAC

A.4.3. Kinetic Estimation

The GPC deconvolution predicts 4 minimum active catalyst sites. The reference temperature is very high $1e^{35}$ C:

The final set of estimated reaction rate constants for 4 active catalyst sites are:

Type	Site No.	Comp 1	Comp 2	Pre-Exp 1/hr	Act-Energy kcal/mol
ACT-COCAT	1	CAT	TEAL	1155	10
ACT-COCAT	2	CAT	TEAL	1155	10
ACT-COCAT	3	CAT	TEAL	1155	10
ACT-COCAT	4	CAT	TEAL	1155	10
ACT-H2	1	CAT	H2	150	15
ACT-H2	2	CAT	H2	150	15
ACT-H2	3	CAT	H2	150	15

ACT-H2	4	CAT	H2	150	15
CHAIN-INI	1	PROPENE		1065561	10
CHAIN-INI	1	ETHENE		85337130	10
CHAIN-INI	2	PROPENE		6181176	10
CHAIN-INI	2	ETHENE		4.94E+08	10
CHAIN-INI	3	PROPENE		6481009	10
CHAIN-INI	3	ETHENE		5.19E+08	10
CHAIN-INI	4	PROPENE		2675434	10
CHAIN-INI	4	ETHENE		2.14E+08	10
PROPAGATION	1	C3-SEG	PROPENE	1065561	10
PROPAGATION	1	C3-SEG	ETHENE	1314653	10
PROPAGATION	1	C2-SEG	PROPENE	7103739	10
PROPAGATION	1	C2-SEG	ETHENE	41515360	10
PROPAGATION	2	C3-SEG	PROPENE	6181176	10
PROPAGATION	2	C3-SEG	ETHENE	9225636	10
PROPAGATION	2	C2-SEG	PROPENE	38517029	10
PROPAGATION	2	C2-SEG	ETHENE	2.27E+08	10
PROPAGATION	3	C3-SEG	PROPENE	6942291	10
PROPAGATION	3	C3-SEG	ETHENE	9225636	10
PROPAGATION	3	C2-SEG	PROPENE	44974974	10
PROPAGATION	3	C2-SEG	ETHENE	2.79E+08	10
PROPAGATION	4	C3-SEG	PROPENE	2675434	10
PROPAGATION	4	C3-SEG	ETHENE	4382177	10
PROPAGATION	4	C2-SEG	PROPENE	17159682	10
PROPAGATION	4	C2-SEG	ETHENE	1.01E+08	10
CHAT-MON	1	C3-SEG	PROPENE	33.97478	14
CHAT-MON	1	C3-SEG	ETHENE	33.97478	14
CHAT-MON	1	C2-SEG	PROPENE	33.97478	14
CHAT-MON	1	C2-SEG	ETHENE	33.97478	14
CHAT-MON	2	C3-SEG	PROPENE	33.97478	14
CHAT-MON	2	C3-SEG	ETHENE	33.97478	14
CHAT-MON	2	C2-SEG	PROPENE	33.97478	14
CHAT-MON	2	C2-SEG	ETHENE	33.97478	14
CHAT-MON	3	C3-SEG	PROPENE	33.97478	14
CHAT-MON	3	C3-SEG	ETHENE	33.97478	14
CHAT-MON	3	C2-SEG	PROPENE	33.97478	14
CHAT-MON	3	C2-SEG	ETHENE	33.97478	14
CHAT-MON	4	C3-SEG	PROPENE	33.97478	14
CHAT-MON	4	C3-SEG	ETHENE	33.97478	14
CHAT-MON	4	C2-SEG	PROPENE	33.97478	14
CHAT-MON	4	C2-SEG	ETHENE	33.97478	14
CHAT-H2	1	C3-SEG	H2	133219.1	13
CHAT-H2	1	C2-SEG	H2	159863.8	13

CHAT-H2	2	C3-SEG	H2	188500.4	13
CHAT-H2	2	C2-SEG	H2	226563	13
CHAT-H2	3	C3-SEG	H2	66156.41	13
CHAT-H2	3	C2-SEG	H2	79387.53	13
CHAT-H2	4	C3-SEG	H2	8573.13	13
CHAT-H2	4	C2-SEG	H2	10295.01	13
CHAT-SPON	1	C3-SEG		900	15
CHAT-SPON	1	C2-SEG		900	15
CHAT-SPON	2	C3-SEG		900	15
CHAT-SPON	2	C2-SEG		900	15
CHAT-SPON	3	C3-SEG		900	15
CHAT-SPON	3	C2-SEG		900	15
CHAT-SPON	4	C3-SEG		900	15
CHAT-SPON	4	C2-SEG		900	15
DEACT-SPON	1			0.24	2
DEACT-SPON	2			0.24	2
DEACT-SPON	3			0.24	2
DEACT-SPON	4			0.24	2
ATACT-PROP	1	C3-SEG	PROPENE	161448.6	10
ATACT-PROP	2	C3-SEG	PROPENE	161448.6	10
ATACT-PROP	3	C3-SEG	PROPENE	4318.289	10
ATACT-PROP	4	C3-SEG	PROPENE	178.1978	10

A.4.4. Sensitivity Analysis

Figure A12 shows how increasing the atactic propagation rate constant increases the atactic fraction, ATFRAC, for the SPHERIPOL PP process

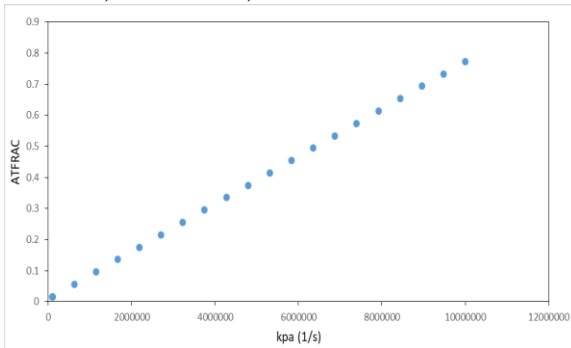


Figure A13. The sensitivity of the atactic fraction ATFRAC to changes in the atactic propagation reaction rate constant for the Spheripol PP process.

A.5. Unipol LLDPE process

This is a process for manufacturing linear low-density polyethylene (LLDPE) and high-density polyethylene (HDPE) developed by Union Carbide (Now part of Dow Chemical). It is a gas phase process consisting of a fluidized-bed reactor (FBR) where the unreacted monomer is removed from the product by flashing. The process consists of a FBR, a

product discharge system to get the polymer out of the system and flash off the monomer, and a purge column to remove any residual monomer. Figure A13 shows a flowsheet of the Aspen Polymers model for the process.

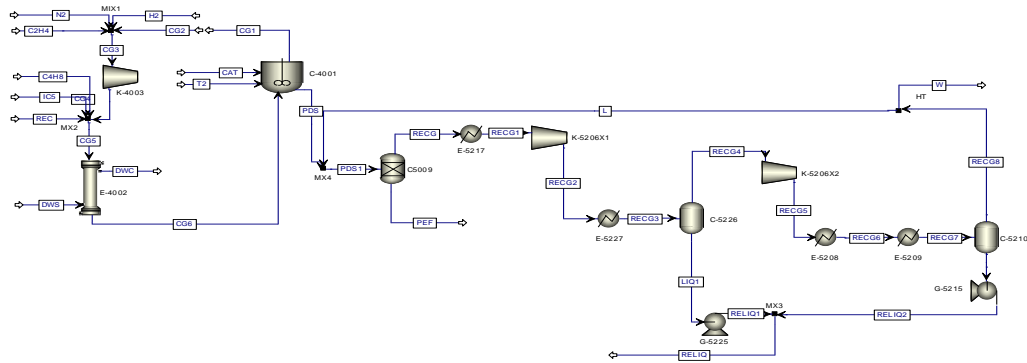


Figure A14. Flowsheet of the Unipol process

A.5.1. Kinetics

The reaction kinetics of the Unipol LLDPE process are:

Catalyst Activation

Activation Spontaneous



Activation By Co-catalyst



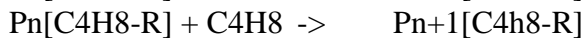
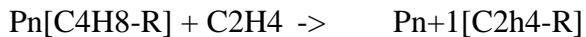
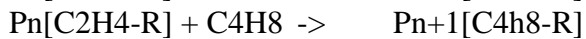
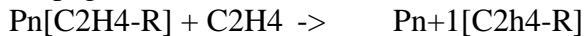
Activation By monomer



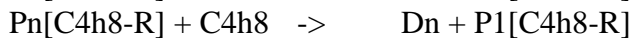
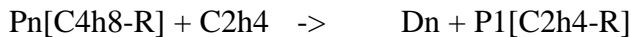
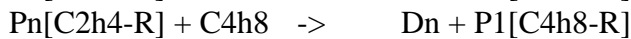
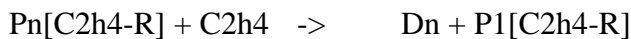
Chain Initiation



Propagation



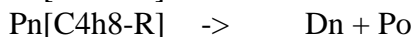
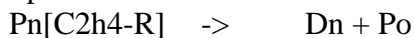
Chain Transfer to Monomer



Chain Transfer to Hydrogen



Spontaneous Chain Transfer



Catalyst Deactivation

Deactivation due to poison

Po/Pn + Co -> Cds+ Dn
 Spontaneous Deactivation
 Po/Pn -> Csd [+ Dn

A.5.2. Production Targets

The production targets used for kinetic estimation are:

- Production rate
- Number-average molecular wt. (MWN/MI)
- Conversion of monomer-comonomer
- PDI
- H2/C ratio
- SMWN & SPFRAC (Site-based)
- Residence time

A.5.3. Estimated Rate Constants

The GPC deconvolution predicts 3 minimum active catalyst sites.

The reference temperature is very high $1e^{35}$ C

The final set of estimated reaction rate constants for 3 active catalyst sites are:

Type	Site No.	Comp 1	Comp 2	Pre-Exp 1/sec	Act-Energy cal/mol
ACT-SPON	1	TICL3		0.001	900
ACT-SPON	2	TICL3		0.001	900
ACT-SPON	3	TICL3		0.001	900
ACT-COCAT	1	TICL3	TEAL	0.023333	900
ACT-COCAT	2	TICL3	TEAL	0.023333	900
ACT-COCAT	3	TICL3	TEAL	0.023333	900
ACT-MON	1	TICL3	C2H4	0.000167	900
ACT-MON	1	TICL3	C4H8	3.33E-05	900
ACT-MON	2	TICL3	C2H4	0.000167	900
ACT-MON	2	TICL3	C4H8	3.33E-05	900
ACT-MON	3	TICL3	C2H4	0.000167	900
ACT-MON	3	TICL3	C4H8	3.33E-05	900
CHAIN-INI	1	C2H4		27661.58	500
CHAIN-INI	1	C4H8		546.6832	500
CHAIN-INI	2	C2H4		16576.61	500
CHAIN-INI	2	C4H8		327.6079	500
CHAIN-INI	3	C2H4		6610.303	500
CHAIN-INI	3	C4H8		130.6412	500
PROPAGATION	1	C2H4-R	C2H4	27661.58	500
PROPAGATION	1	C2H4-R	C4H8	546.6832	500
PROPAGATION	1	C4H8-R	C2H4	546.6832	500
PROPAGATION	1	C4H8-R	C4H8	5.044209	500

PROPAGATION	2	C2H4-R	C2H4	16576.61	500
PROPAGATION	2	C2H4-R	C4H8	327.6079	500
PROPAGATION	2	C4H8-R	C2H4	327.6079	500
PROPAGATION	2	C4H8-R	C4H8	3.022816	500
PROPAGATION	3	C2H4-R	C2H4	6610.303	500
PROPAGATION	3	C2H4-R	C4H8	130.6412	500
PROPAGATION	3	C4H8-R	C2H4	130.6412	500
PROPAGATION	3	C4H8-R	C4H8	1.205418	500
CHAT-MON	1	C2H4-R	C2H4	0.001253	850
CHAT-MON	1	C2H4-R	C4H8	2.92E-05	850
CHAT-MON	1	C4H8-R	C2H4	2.92E-05	850
CHAT-MON	1	C4H8-R	C4H8	2.92E-07	850
CHAT-MON	2	C2H4-R	C2H4	2.07E-05	850
CHAT-MON	2	C2H4-R	C4H8	4.82E-07	850
CHAT-MON	2	C4H8-R	C2H4	4.82E-07	850
CHAT-MON	2	C4H8-R	C4H8	4.82E-09	850
CHAT-MON	3	C2H4-R	C2H4	0.001273	850
CHAT-MON	3	C2H4-R	C4H8	2.97E-05	850
CHAT-MON	3	C4H8-R	C2H4	2.97E-05	850
CHAT-MON	3	C4H8-R	C4H8	2.97E-07	850
CHAT-H2	1	C2H4-R	H2	85.9114	850
CHAT-H2	1	C4H8-R	H2	85.9114	850
CHAT-H2	2	C2H4-R	H2	14.6419	850
CHAT-H2	2	C4H8-R	H2	14.6419	850
CHAT-H2	3	C2H4-R	H2	92.07744	850
CHAT-H2	3	C4H8-R	H2	92.07744	850
CHAT-SPON	1	C2H4-R		8.36E-05	850
CHAT-SPON	1	C4H8-R		2.01E-06	850
CHAT-SPON	2	C2H4-R		1.38E-06	850
CHAT-SPON	2	C4H8-R		3.30E-08	850
CHAT-SPON	3	C2H4-R		8.49E-05	850
CHAT-SPON	3	C4H8-R		2.04E-06	850
DEACT- POISON	1	CO		10	1000
DEACT- POISON	2	CO		10	1000
DEACT- POISON	3	CO		10	1000
DEACT-SPON	1			8.00E-05	1000
DEACT-SPON	2			8.00E-05	1000
DEACT-SPON	3			8.00E-05	1000
DEACT-H2	1	H2		0.001	1000
DEACT-H2	2	H2		0.001	1000

A.5.4. Sensitivity Analysis

Figure 4a how varying the reaction rate constant for chain transfer to hydrogen, $k_{th,i}$ of just one of the three active site affects the final LLPDE polymer properties, including the polydispersity index PDI, the number-average molecular weight at the chosen catalyst site SMWN, and the overall MWN. As we increase the reaction rate constant for chain transfer to hydrogen, both the SMWN and MWN decreases, while the PDI increases gradually. In other words, we can vary the hydrogen flow rate to change the rate of chain transfer reaction in order to achieve desired MWN and PDI.

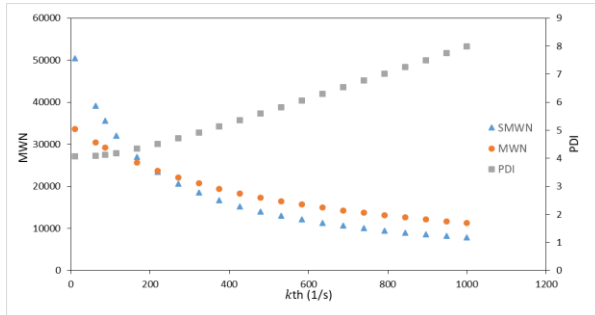


Figure A15. Sensitivity of the PDI, MWN and SMWN for the UNIPOL LLDPE process on the pre-exponential factor of the reaction rate constant for chain transfer to hydrogen

Appendix B (Chapter 3)

B.1. Configuring a PID Controller

Table B1 describes the ideal, series and parallel algorithms. See AD online help for vendor algorithms.

We choose the Ideal algorithm for the current example.

Table B1. Typical PID controller algorithms

PID algorithm	Model equation
1. Ideal	$OP = Bias + K_c \times \{E_p + (1/T_I) \int E_I dt + T_D dE_D/dt\}$
2. Series (interacting form)	$OP = Bias + K_c \times \{E_p + (1/T_I) \int E_I dt\} \times \{1 + T_D dE_D/dt\}$
3. Parallel (standard , ISA, or non- interacting form)	$OP = Bias + K_c \times E_p + (1/T_I) \int E_I dt + T_D dE_D/dt$
<p>OP = controller output; Bias =the value of the manipulated variable when the process is at steady state; Gain = proportional gain K_c; E = error = setpoint – process variable; E_p = proportional mode error; E_I = integral mode error; E_D = Derivative mode error; T_I = integral time; T_D = derivative error</p>	

We give some observations on the PID controller tuning parameters below:

- (1) The proportional gain, K_c , is typically expressed as $100/(\text{proportional band, PB})$. The PB is the error (expressed in percentage of the range of the measured variable) required to move the control valve (the final control element) from fully closed to fully open. Typically, PB has a value between 30 and 300.
- (2) The larger the proportional gain, K_c , the smaller the difference between the setpoint value and the process variable value at steady state (called steady-state error or offset). P(proportional) control corrects the present error between the setpoint and the process variable.
- (3) The integral time or the reset time, T_I , is the time it takes the controller to give an output that is twice the output from a proportional controller, following a step change

in error. In other words, the integral time is the time it takes for the controller to “repeat” the proportional controller action.

- (4) The integral controller acts to eliminate the steady-state error (offset) that is present in applying the proportional controller action alone. A large integral or reset time essentially minimizes the integral controller action. PI(proportional-integral) control corrects the past and present errors between the setpoint and process variable.
- (5) The derivative action increases the stability of the controlled system, and permits either a higher controller gain K_c , or a lower integral or reset time, T_I , to be used. The latter speeds up the dynamic response of the controlled system. If the derivative time T_D is large enough, the controlled system would be theoretically stable for all the controller gains. PID(proportional-integral-derivative) control corrects the past, present and future errors between setpoint and process variable, considering the positive or negative rate of change of the error in the output variable in affecting the future error.

Table B2 gives the heuristic PID controller tuning parameters for different types of controllers [1,2].

Table B2. Initial PID controller tuning parameters

Controller type	Proportional gain, K_c	Integral time, T_I , min	Derivative time, T_D , min
Flow	0.1	0.2	0
Level	2	10	0
Pressure	2	2	0
Temperature	1	20	0
Composition	0.1	0.2	0

We follow these initial values for our temperature controller, as illustrated in FigureB2. We also choose **Reverse** controller action for this temperature controller, because we need to decrease the HEATER heat duty when the temperature increases. Table B3 summarizes the other options for controller action.

Table B3. PID controller actions

When the action is	And the measured variable (controlled variable) or process variable	Then the manipulated variable

Direct	Increases	Increases
Direct	Decreases	Decreases
Reverse	Increases	Decreases
Reverse	Decreases	Increases

Lastly, we mention that AD automatically generates pressure, level and temperature according to the guidelines of Table B4 .

Table B4. Guidelines for AD default controllers

Controller added	When	Measured variable (controlled variable or process variable)	Manipulated variable	PID tuning parameters
Pressure	Vapor holdup is modeled	Pressure in vessel	Vapor outlet flow rate	$K_c = 0.2$, $T_1 = 12$ min
Level	Liquid holdup is modeled	Liquid level	Liquid outlet flow rate	$K_c = 0.2$
Temperature	Stirred reactor block	Vessel temperature	Heat duty	$K_c = 0.2$, $T_1 = 12$ min

B.2. Controller tuning for HDPE slurry process dynamics and control.

In the following, we want to learn how to use the tuning tool within the PID controller and check if these tuning parameters are optimum. We use the model in 3.4. for the HDPE control using H2/C2 ratio. We use the H2C2 PID controller which takes input the H2/C2 ration from ratio block and outputs specifies the mass fraction split of the purge stream.

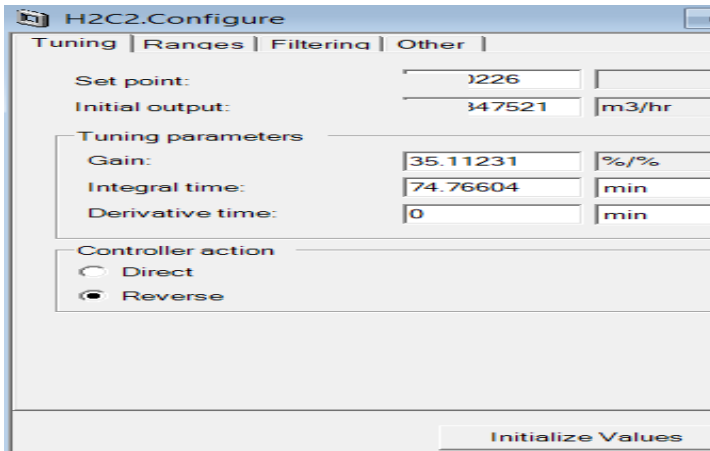




Figure B1. Gain and integral time for the H2C2 controller.

Next, we follow the heuristic gain and integral time for a composition controller given in, and change the gain displayed in Figure B1 to 0.1, and the integral time to 0.2 min, and initialize values. We then follow the following procedure to tune the controller parameters.

1. **Run** the simulation in **Dynamic** run mode for a few steps.
2. **Pause** the simulation.
3. Open the controller **Faceplate**.
4. Display the result plot. 
5. Click the tune button.  See the resulting Figure B2 .
6. Click the <Start Test> button, as seen in Figure B2.
7. Run the simulation and you should observe that the OP of the controller is stepped up, and the ratio on the stage PV increases., **Pause** the simulation when it reaches steady state. Click **Finish Test** on the controller tuning sheet.
8. Click the **Tuning parameters** tab.

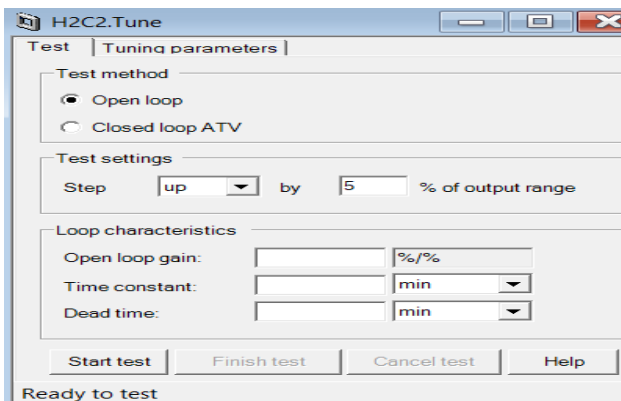


Figure B2. Controller “Tune” interface

9. Select the tuning method (PI controller and Cohen-Coon tuning rule). Click the <Calculate> button. See Figure B3 The reader may search Aspen Dynamics online help for “Cohen-Coon” about explanations of different tuning rules.

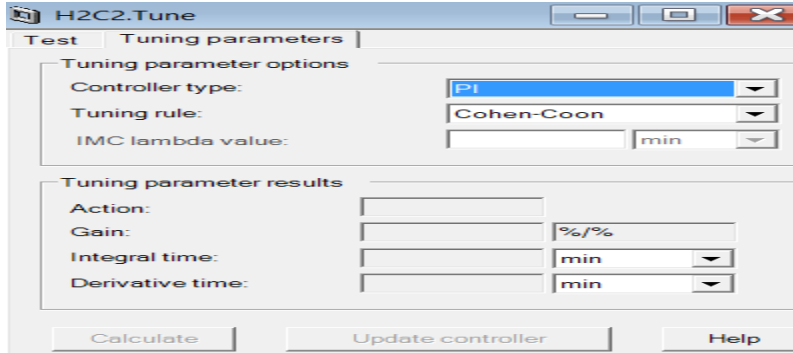


Figure B3. Choosing tuning rule.

10. You click <Update Controller> the new settings are applied. **Restart** the simulation. Click **Update controller** button. We see the updated tuning parameters in Figure B4, and the continually decaying controller response in Figure B5 . This concludes the current workshop. We save the simulation file as

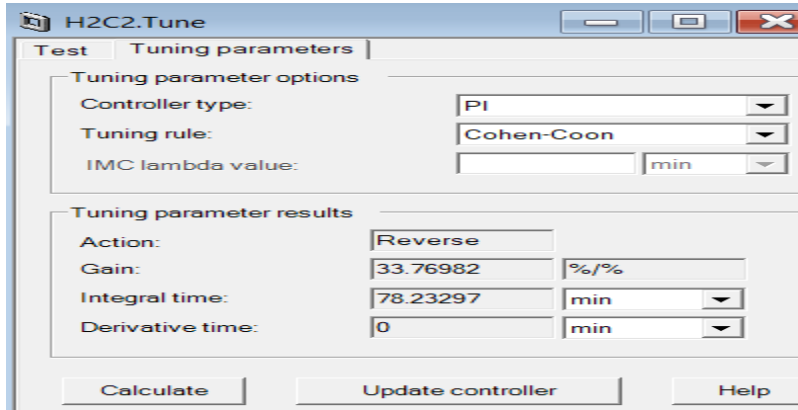


Figure B4. Updated tuning parameters.

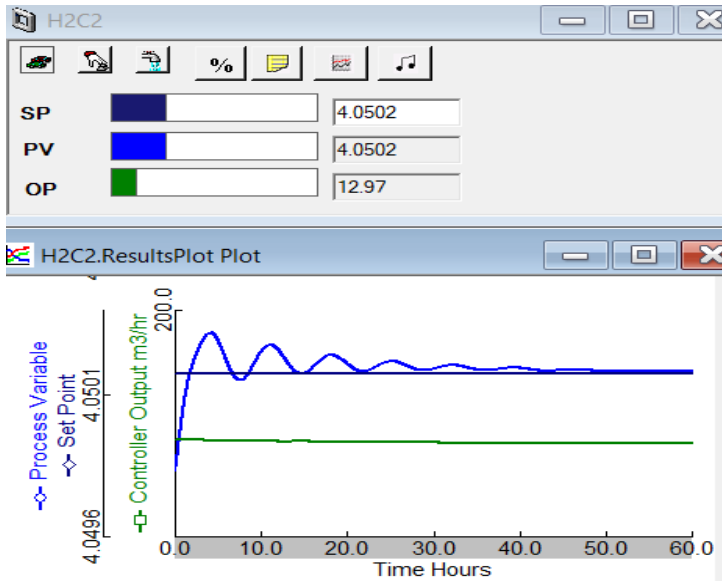


Figure B5. Continually decaying response resulting from the updated tuning parameters

